Polymer Treatment of Oil Sands Tailings: Experimental and Modeling Investigations

by

Vahid Vajihinejad

A thesis submitted in partial fulfillment of the requirements for the degree of

Doctor of Philosophy

in

Chemical Engineering

Department of Chemical and Materials Engineering
University of Alberta

Abstract

Near 10^9 m^3 tailings have been released to the environment as the result of oil sands mining operations in Canada. These fluid fine tailings are alkaline slurries of water, clays, and residual bitumen that after 3 to 5 years of gradual sedimentation form a thick mud-like slurry (30-40% by weight solid) called mature fine tailing (MFT). MFT clays do not settle by gravity even after decades. Polymer flocculants are used to dewater tailings by aggregating these micron-sized particles. Typical flocculants are high molecular weight anionic polyacrylamides, A-poly(AAm). A-poly(AAm) can capture micron-sized clay particles in aggregates having characteristic dimensions up to several hundred micrometers. However, residual bitumen and process water ions in oil sands tailings affect the interactions between this flocculant and clays, and reduce the flocculant performance. Calcium ions are often used in combination with A-poly(AAm) to reduce the charge density of the MFT clays. This combination forms aggregates that settle fast and generates a reasonably clean supernatant, but it also produces a gel-like sediment that is hard to dewater to the required solids content levels. Copolymers of acrylamide and partially hydrophobic or cationic comonomers have also been used to treat MFT, some with promising dewatering performance. However, what is missing in the field of oil sand tailings treatment is a more fundamental understanding on how the microstructure of the polymer flocculant affects its flocculation and dewatering performance. In this thesis, a combination of polymer reaction engineering tools and design of experiments were used to synthesize polymer flocculants to investigate the impact of flocculant microstructure in dewatering MFT.

The results of this thesis comprise three studies:

1- Synthesis of acrylamide and diallyl dimethyl ammonium chloride (DAD-

MAC) copolymer flocculants with different properties. The results showed that the dewatering capacity of aggregates, as measured by capillary suction time (CST) and specific resistance to filtration (SRF), was not a strong function of molecular weight of the copolymers, but was substantially influenced by their chemical composition. The settling rate of the aggregates and the clarity of the supernatant, on the other hand, depended on both average molecular weight and chemical composition of the copolymer flocculant. A similar cationic copolymer was also used to examine the effect of its chemical composition distribution (CCD) on MFT dewatering. The results showed that the performance of flocculants with narrow and broad CCD is dependent on copolymer dosage: at low dosages, polymers with broad CCD form larger aggregates that settle faster and dewater more quickly, while at higher dosages a shift in performance was observed, where polymers with narrow CCD produced larger aggregates.

2- Synthesis of a novel homopolymer flocculant that met the required metrics of tailings dewatering and to address the challenges associated with the production of copolymer flocculants. The high molecular weight cationic homopolymer of (vinylbenzyl) trimethylammonium chloride, poly(VBTMAC) showed excellent performance in dewatering of high solids MFT as measured by filtration tests. The modes of flocculation of poly(VBTMAC) were found to be a combination of charge neutralization and bridging, strongly influenced by chain relaxation on the surface of particles. We also tested the ultimate potential of poly(VBTMAC) in dewatering undiluted MFT. Poly(VBTMAC) showed to be a superior flocculant compared to the industry standard, high molecular weight A-poly(AAm), consistently producing more compact aggregate network with improved dewatering rate and sediments of higher shear strength.

3- To further investigate the flocculation and kinetics of MFT aggregate formation by poly(VBTMAC), population balance models were developed using ex-

perimental data obtained by focused beam reflectance measurement (FBRM) to describe the flocculation kinetics and predict the MFT aggregate sizes obtained in different conditions. A time-varying function was defined to account for the aggregate size evolution trends observed during flocculation. The validity of the model was tested by varying shear rates, mixing time, and polymer dosage using FBRM measurements. The proposed model is the first of its kind towards a more rational and quantitative approach to control treatment processes for oil sands tailings.

Preface

Chapter 2 of this thesis has been partially published in V. Vajihinejad, S. Gumfekar, B. Bazoubandi, Z. Rostami, J. B. P. Soares, Water Soluble Polymer Flocculants: Synthesis, Characterization, and Performance Assessment, *Macromolecular Materials and Engineering* 2019, 304, 1800528. This is a literature review paper; I was the lead author responsible for writing the largest part of the article, coordinating the different sections with the several co-authors, and writing the final version of the manuscript.

Part of Chapter 3 of this thesis has been published in V. Vajihinejad, R. Guillermo, J. B. P. Soares, Dewatering Oil Sands Mature Fine Tailings (MFTs) with Poly(acrylamide-*co*-diallyldimethylammonium chloride): Effect of Average Molecular Weight and Copolymer Composition, *Industrial & Engineering Chemistry Research* 2017, 56, 1256-1266. Another part of this chapter has been submitted for publication as V. Vajihinejad, D. Dixon, M. da Silva, J. B. P. Soares, Effect of Polymer Chemical Composition Distribution on Flocculation: The Case of Composition Drift in Batch Reactors". These results were also presented in V. Vajihinejad, J. B. P. Soares, Impact of Polymer Microstructure on Flocculation and Dewatering: The Case of the Canadian Oil Sands Tailings, *ACS Fall 2019 National Meeting & Expo*, San Diego, CA, USA, August 25-29, 2019. I designed the experiments, synthesized the polymers, analyzed the data, performed most of the flocculation experiments, and wrote the manuscripts and presentation. Ms. R. Guillermo helped me conduct some of flocculation experiments, Mr. D. Dixon provided technical assistance with the NMR analysis, and Dr. M. da Silva measured the copolymer molecular weight distributions.

Chapter 4 of this thesis has been submitted for publication as V. Vajihinejad, S. Gumfekar, J. B. P. Soares, Enhanced Dewatering of Oil Sands Tailings by a Novel Water-Soluble Cationic Polymer, *Environmental Science: Water Research & Technology*. I designed the experiments, produced the polymers, analyzed the data, and wrote the manuscript composition. Dr. S. Gumfekar

also contributed to the manuscript composition.

Chapter 5 of this thesis has been published in V. Vajihinejad, J. B. P. Soares, Monitoring Polymer Flocculation in Oil Sands Tailings: A Population Balance Model Approach, *Chemical Engineering Journal* 2018, 346, 447-457. I was responsible for the design of experiments, data analysis and model development, as well for the manuscript composition.

The paper presented in Appendix A has been published in V. Vajihinejad, J. B. P. Soares, Can We Make Better Polyurethane Composite Foams with Oil Sands Mature Fine Tailing?, *Macromolecular Materials and Engineering*, 2016, vol. 301, pp 383-389. I was responsible for the design of experiment, polymer synthesis and data analysis, as well the manuscript composition.

The paper presented in Appendix B has been published in R. Hripko, V. Vajihinejad, J. B. P. Soares, Enhanced Flocculation of Oil Sands Mature Fine Tailings using Hydrophobically Modified Polyacrylamide Copolymers, *Global Challenges* 2018, 2, 1700135. I was responsible for the design of experiments, part of data analysis, and manuscript composition. Mr. R. Hripko contributed to the polymer synthesis, flocculation experiments, as well as manuscript composition.

In all the aforementioned papers, Dr. J. Soares contributed to the manuscript composition and edits.

Acknowledgements

I would like to express my greatest acknowledgment to my supervisor, Professor João B. P. Soares, who gave me support, encouragement and inspiration throughout my PhD - a true leader, in my opinion – I will remain in his debt forever. I also would like to thank my peers and colleagues who have helped me in accomplishing this thesis. My thanks goes to Dr. Marco Antonio Silva for his patience and sincere help with the GPC measurements, Mr. Louis Kabwe for the sincere help with the rheology measurements, Dr. Linda Botha for discussions and her help with NMR analysis, Ms. Arlene Oatway for her help with SEM analysis, Mr. Mark Labbe for his help with clay sample preparation, Dr. Saeid Mehdiabadi and Dr. Mirjavad Geramian for their constructive scientific discussions.

I am grateful to my parents for their love and support throughout my life, without them I never would have been able to unleash my potentials. Lastly, and most importantly, I am grateful to my wife, Shabnam, without her this journey may have not been possible - I am grateful for all the support and love you gave me!

Table of Contents

List of Tables

List of Figures

Nomenclature

Acronym

A-poly(AAm)	anionic poly(acrylamide)
AAm	acrylamide
AAS	atomic absorption spectroscopy
AFM	atomic force microscopy
Al-poly(AAm)	$Al(OH)_3$-polyacrylamide
ANOVA	analysis of variance
AP-g-poly(AAm)	amylopectin-grafted polyacrylamide
CCD	chemical composition distribution
CRP	Controlled radical polymerization
CST	capillary suction time
DADMAC	diallyldimethylammonium Chloride
EDL	electric double layer
FBRM	focused beam reflectance measurement
FFF	field flow fractionation
FFT	fluid fine tailings

FTIR	Fourier-transform infrared spectroscopy
GPC	gel permeation chromatography
HBfPE	hyperbranched functional polyethylene
KPS	potassium persulfate
LCST	lower critical solution temperature
MFT	mature fine tailings
MMT	montmorrillonite
MWD	molecular weight distribution
PDI	polydispersity index
PEO	polyethylene oxide
PEOMA	poly(ethylene oxide) methyl ether methacrylate
Poly(AAm)	poly(acrylamide)
poly(AAm)-*graft*-PPO	polyacrylamide-g-poly(propylene oxide)
Poly(AAm)-*g*-PEOMA	poly(acrylamide)-*g*-poly(ethylene oxide) methyl ether methacrylate
Poly(AAm-*co*-AAc)	poly(acrylamide-*co*-acrylic acid)
Poly(AAm-*co*-DADMAC)	poly(AAm-*co*-diallyldimethylammonium Chloride
Poly(AAm-*co*-VBTMAC)	poly(acrylamide-*co*-vinylbenzyl trimethylammonium chloride)
Poly(NIPAM)	poly(N-isopropylacrylamide)
Poly(VBTMAC)	poly(vinylbenzyl trimethylammonium chloride)
pphp	parts per hundred parts of polyol by weight
ppm	parts per million (weight)
PPO	poly(propylene oxide)

PSD	particle size distribution
RAFT	reversible additionfragmentation chain-transfer
Ref-PAM	reference anionic polyacrylamide
SEM	scanning electron microscope
SMFS	single molecule force spectroscopy
SRF	specific resistance to filtration
TEM	transmission electron microscope
V-50	2,2′-azobis(2-methylpropionamidine) dihydrochloride
VBTMAC	(vinylbenzyl) trimethylammonium chloride

Symbol

$[M_1]$	concentration of monomer 1
$[M_2]$	concentration of monomer 2
$[P_r]$	concentration of dead polymer chains of length r
$[R^o]$	total concentration of polymer radicals in the system
$[R^o_r]$	concentration of polymer radicals of length r
$[R^o_1]$	total concentration of polymer radicals ending with monomer 1
$[R^o_2]$	total concentration of polymer radicals ending with monomer 1
$[R^o_{r,1}]$	concentration of polymer radicals of length r ending with monomer 1
$[R^o_{r,2}]$	concentration of polymer radicals of length r ending with monomer 2

$\alpha_{i,j}$	capture efficiency between aggregates from the i^{th} channel and the j^{th} channel
α_{max}	maximum capture efficiency
α_{min}	minimum capture efficiency
$\bar{d_s}$	average size of primary particles
$\bar{d_{agg}}$	average size of aggregates
$\beta_{i,j}$	collision frequency between aggregates from the i^{th} channel and the j^{th} channel
ϵ	average energy dissipation rate in a stirred vessel
$\Gamma(v, v')$	breakage distribution function
κ	Debye length
μ_f	filtrate viscosity
μ_0	viscosity of the suspending liquid
μ_{sus}	slurry viscosity
Ω	impeller rotation speed
$\overline{F}_1$	cumulative molar fraction of monomer 1 in the copolymer
$\overline{F}_{AAm}$	cumulative molar fraction of acrylamide in the copolymer
$\overline{K_p}$	pseudo-propagation rate constant
$\overline{K}_t$	pseudo-termination rate constant
$\overline{K}_{fm}$	pseudo-transfer to monomer rate constant
$\overline{K}_{tc}$	pseudo-termination by combination rate constant
$\overline{K}_{td}$	pseudo-termination by disproportionation rate constant

$\overline{r}_n$	instantaneous number-average chain length of the polymer
$\overline{W}(r,t)$	cumulative molecular weight distribution of the copolymer
$\overline{W}(r,y,t)$	cumulative bivariate distribution of chain length and composition
Φ_i^o	molar fraction of polymer radicals ending with monomer i
ϕ_{eff}	effective volume fraction of the aggregates
ϕ_{max}	maximum solid fraction
ψ	fraction of polymer chains needed to adsorb onto the surface of particles for the flocculation to begin
ρ_s	primary solid particles density
ρ_w	water density
ρ_{sus}	slurry density
τ_{ads}	characteristic adsorption time
τ_{agg}	characteristic aggregation time
ε	medium permittivity
b_i	coefficient for linear term in regression model
b_{ii}	coefficient for quadratic term in regression model
b_{ij}	coefficient for interaction term in regression model
C_i	molar concentration of ions of type i
d_i	diameter of particle i
$d_{exp.}$	experimental average aggregate size
d_F	(mass) fractal dimension

d_{model}	model average aggregate size
d_{PF}	perimeter fractal dimension
e	charge of an electron
f	fractional initiator efficiency
F_1	instantaneous molar fraction of monomer 1 in the copolymer
f_i	molar fraction of monomer i
f_{10}	initial molar fraction of monomer 1 in the reactor
f_1	instantaneous molar fraction of monomer 1 in the reactor
$f_{AAm,0}$	initial molar fraction of AAm in the reactor
G	average shear rate or fluid velocity gradient
k_B	Boltzmann constant
k_I	rate constant for initiator decomposition
k_p	rate constant for propagation
k_t	rate constant for termination
k_{11}	propagation rate constant of radical ending with monomer 1 propagating with monomer 1
k_{12}	propagation rate constant of radical ending with monomer 1 propagating with monomer 2
k_{21}	propagation rate constant of radical ending with monomer 2 propagating with monomer 1
k_{22}	propagation rate constant of radical ending with monomer 2 propagating with monomer 2
k_{ads}	adsorption rate constant

k_d	capture efficiency decay constant
k_{f11}	transfer-to-monomer rate constant of radical ending with monomer 1 transferring to monomer 1
k_{f12}	transfer-to-monomer rate constant of radical ending with monomer 1 transferring to monomer 2
k_{f21}	transfer-to-monomer rate constant of radical ending with monomer 2 transferring to monomer 1
k_{f22}	transfer-to-monomer rate constant of radical ending with monomer 2 transferring to monomer 2
k_f	rate constant for transfer to monomer
k_{ij}	collision rate coefficient between particles i and j
k_{tc11}	termination by combination rate constant of radical ending with monomer 1 terminating with monomer 1
k_{tc12}	termination by combination rate constant of radical ending with monomer 1 terminating with monomer 2
k_{tc21}	termination by combination rate constant of radical ending with monomer 2 terminating with monomer 1
k_{tc22}	termination by combination rate constant of radical ending with monomer 2 terminating with monomer 2
k_{td11}	termination by disproportionation rate constant of radical ending with monomer 1 terminating with monomer 1
k_{td12}	termination by disproportionation rate constant of radical ending with monomer 1 terminating with monomer 2

k_{td21}	termination by disproportionation rate constant of radical ending with monomer 2 terminating with monomer 1
k_{td22}	termination by disproportionation rate constant of radical ending with monomer 2 terminating with monomer 2
M_1	monomer 1
M_2	monomer 2
M_n	polymer number-average molecular weight
M_w	polymer weight-average molecular weight
$MAPE$	Mean absolute percentage error
mw_1	molecular weight of monomer 1
mw_2	molecular weight of monomer 2
mw_{ave}	average molecular weight of monomer 1 and monomer 2
$n(v,t)$	number of aggregates of size v in unit volume at time t
$n(v',t)$	number of aggregates of size v' in unit volume at time t
N_A	Avogadro's number
n_p	number density of polymer chains in the suspension
n_s	number density of particles in suspension
$N_{0,i}$	number concentration primary particles registered in the i^{th} channel
N_i	number concentration of aggregates with size v_i

N_p	impeller power number
P_{1+1}	dead polymer chain as a result of combination with two polymer radicals ending with monomer 1 and monomer 1
P_{1+2}	dead polymer chain as a result of combination with two polymer radicals ending with monomer 1 and monomer 2
P_1	dead polymer chain ending with monomer 1
P_{2+2}	dead polymer chain as a result of combination with two polymer radicals ending with monomer 2 and monomer 2
P_2	dead polymer chain ending with monomer 2
$P_{m,n}$	dead polymer chain with m units of monomer 1 and n units of monomer 2
PCC	Pearson correlation coefficient
$Q(v, v')$	aggregation kernel between aggregates of size v and v'
Q_1	the first moment of dead copolymer chain distribution
Q_i	the $\mathrm{ith} moment of dead copolymer chain distribution$
R^2	coefficient of determination
R_i^o	primary radicals formed by decomposition of initiator
R_1^o	polymer radical ending with monomer 1
R_2^o	polymer radical ending with monomer 2
$R_{m,n,1}^o$	polymer radical ending with monomer 1 with m units of monomer 1 and n units of monomer 2

$R^o_{m,n,2}$	polymer radical ending with monomer 2 with m units of monomer 1 and n units of monomer 2
$R^o_{r,s,1}$	polymer radical ending with monomer 1 with m units of monomer 1 and n units of monomer 2
$R^o_{r,s,2}$	polymer radical ending with monomer 2 with m units of monomer 1 and n units of monomer 2
r_1	reactivity ratio of monomer 1
r_2	reactivity ratio of monomer 2
R_p	(total) rate of polymerization
R_t	rate of termination
r_{AAc}	reactivity ratio of AAc
r_{AAm}	reactivity ratio of AAm
r_{DADMAC}	reactivity ratio of DADMAC
s	distance between the centers of two particles
$S(v)$	breakage kernel for aggregates of size v
s_1	system-specific constant for breakage kernel
s_2	system-specific constant for breakage kernel
T	temperature
$V_{0,i}$	volume of primary particles registered in the i^{th} channel
W	Fuchs's stability ration
w	solids weight fraction in slurry
$W(r,t)$	instantaneous molecular weight distribution of the copolymer

$W(r, y, t)$	instantaneous bivariate distribution of chain length and composition
x	total molar conversion
y	composition deviation of copolymer
Y_1	the first moment of copolymer radical chain distribution
y_1	composition of monomer 1 in a single given copolymer chain produced instantaneously
Y_2	the second moment of copolymer radical chain distribution
Y_i	the ith$moment of copolymer radical chain distribution$
y_i	i^{th} predicted response in regression model
[I]	initiator concentration
ISR	initial settling rate

Chapter 1

Introduction

1.1 Motivation

With a production rate of about 3 million barrels of bitumen per day, oil sands reserves are vital to the Canadian economy. Surface mining has been a practice for decades, where the bitumen is extracted using a large amount of warm water (estimated to be about 3 barrel of fresh water per each barrel of bitumen produced).[1] Figure 1.1 shows a diagram of the surface mining extraction of bitumen. Oil sands lumps and rocks are crushed and mixed with warm water, air, and caustics. The slurry is sent to the extraction plant and goes to the gravity separation vessels. Flotation cells are used to further liberate and separate the bitumen from sand grains. The aerated bituminous mixture formed on top of the gravity vessel, called froth, normally contains about 60% by weight bitumen, 30% water, and 10% solids. The bottom stream, mostly composed of solids and water, is called tailings and is pumped to tailing ponds. The bitumen froth is further treated with organic solvents to remove water and residual solids from the bitumen, before it can be sent to upgrading plants. Currently, an area in Alberta larger than 1.5 times the size of city of Vancouver has been contaminated with tailings ponds, posing serious environmental challenges to the area.[2]

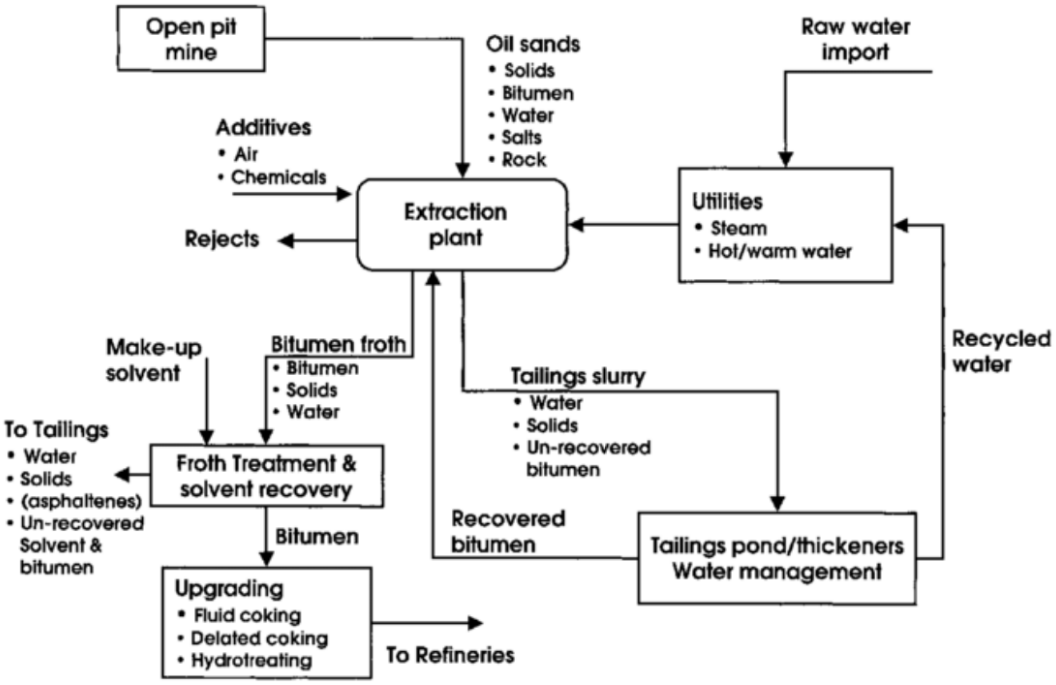

Figure 1.1: A brief diagram of oil sands extraction unit operations.[3]

In the ponds, coarser solids (sands) quickly settle and are used to build containment dikes. The remaining top portion of the pond is called fluid fine tailings (containing mineral particles with characteristic dimensions below 44 μm). They remain in the slurry for about 2-5 years of gradual sedimentation, and eventually form a mud-like slurry (30-40% solids by weight) called mature fine tailings (MFT). The overall volume of MFT generated is approximately 1.5 times the volume of the bitumen extracted from oil sands.[2]

A typical MFT is a thick slurry of fine mineral particles (mostly clays), water (60-70%), and residual bitumen (2-5%). Kaolinite and interlayered kaolinite-smectite (35% by weight, 10-20 $m^2.g^{-1}$), illite and interlayered illite-smectite (60-65%, 65-100 $m^2.g^{-1}$), as well as swelling clays (montmorillonite, 1-2%, 700-840 $m^2.g^{-1}$) form the MFT solids.[4, 5] Due to the use of caustic in the extraction process, MFT water has an alkaline pH (typical about 8). Because the clays are very small and carry charges (mostly negative) on their

surfaces, they constantly repel each other, inhibiting Brownian agglomeration and making it difficult for settling to take place.

Different treatment processes are used to dewater tailings. All of them use chemical additives. The role of these additives, either coagulants such as gypsum, and/or flocculants such as polyacrylamides, is to destabilize the clay dispersion by either changing their surface charges or bridging their particles, allowing gravity to separate the solids from the water. After MFT is treated with these additives, different processes are used to separate the solids and to thicken the tailings: thin lift, rim ditching, consolidated/composite tailings, filtration, and centrifugation. In thin lift drying, for example, the treated MFT is spread over a small slope to facilitate dewatering. The process is inexpensive but needs large areas of land. On the other hand, relatively more expensive processes such as centrifugation or filtration occupy much less space and are effective in dewatering tailings in a shorter period of time.

Most flocculants used in tailings treatment are anionic copolymers of acrylamide, mostly in form of poly(acrylamide-*co*-acrylic acid), poly(AAm-*co*-AAc). This copolymer works well to flocculate low solids suspensions, as those present in mineral processing thickeners, because the long, extended polyacrylamide chains bridge the small clay particles into large aggregates. Larger aggregates are preferable because they increase the separation efficiency while reducing size of the thickeners.[6] There have been many challenges, however, when conventional anionic polyacrylamides are used to treat oil sands tailings:

i) MFT is a high-solids slurry with a gel like texture due to the presence of swelling clays. Conventional flocculants have extremely high molecular weights, making it difficult to disperse them uniformly in the tailings stream, thus lowering the collision efficiency of the clay/polymer particles and creating localized overdosed regions.

ii) Conventional flocculants produce gel-like sediments that are hard to dewater, and unless a coagulant is added together with the polymer, they leave behind a dirty supernatant (low fine capturing capacity). To complicate things further, the accumulation of divalent cations (a typical coagulant) over time in

the recycle water will decrease bitumen extraction efficiency. To mitigate these challenges, researchers have used polymer flocculants with novel chemistries, either alone or in combinations. For instance, cationic copolymer flocculants, cationic/anionic copolymers combinations (dual treatment),[7, 8, 9] or partially hydrophobic polymers chemistry,[10, 11], stimuli-responsive,[12, 13] and natural-based polymers[14, 15] have all been attempted as alternatives to polyacrylamide flocculants. All of these flocculants have shown promising results. However, we lack a systematic understanding of how the polymer flocculant microstructure impacts tailings treatment and specific dewatering metrics. We also need to quantify the flocculation process in tailings to be able to open paths towards a robust control of treatment processes in oil sands operations.

1.2 Research Objectives

This PhD thesis comprised three main themes:

i) Systematic investigation of relationships between polymer flocculant microstructure and MFT dewatering performance.

ii) Synthesis of novel water soluble polymers to replace existing conventional flocculants.

iii) Develop a mathematical model to quantify the flocculation of oil sands tailings.

The specific objectives of this thesis were:

i) Study the relationship between polymer microstructure (average molecular weight and chemical composition) of cationic water-soluble polymers in the flocculation and dewatering of MFT.

ii) Study the effect of composition drift in batch free radical polymerization on the performance of water-soluble copolymers in the flocculation and dewatering of MFT.

iii) Study the performance and model the flocculation kinetics of a novel partially hydrophobic cationic flocculant, poly(VBTMAC), in the dewatering of

MFT.

1.3 Thesis Outline

This thesis has 6 chapters and is written in manuscript-based format.

Chapter 1 (this chapter) discusses the challenges associated with the treatment of oil sands tailings, motivations behind this work, and outlines the objectives of this thesis. **Chapter 2** discusses the fundamentals related to water soluble polymer flocculants, flocculation and dewatering of tailings, and provides a review of the pertinent literature. This chapter has been partially published in V. Vajihinejad, S. Gumfekar, B. Bazoubandi, Z. Rostami, J. B. P. Soares, Water Soluble Polymer Flocculants: Synthesis, Characterization, and Performance Assessment, *Macromolecular Materials and Engineering* 2019, 304, 1800528.

Chapter 3 contains the results of a study on the flocculation and dewatering of oil sands tailings with polymers having different microstructures, specifically discussing the effect of average molecular weight and average chemical composition, as well as chemical composition distribution. The polymers were cationic copolymers of acrylamide, and the performance metrics were settling rate, turbidity of supernatant, solids content, capillary suction time of the aggregates, and aggregate sizes as measured by FBRM. Part of this chapter has been published in V. Vajihinejad, R. Guillermo, J. B. P. Soares, Dewatering Oil Sands Mature Fine Tailings (MFTs) with Poly(acrylamide-*co*-diallyldimethylammonium chloride): Effect of Average Molecular Weight and Copolymer Composition, *Industrial & Engineering Chemistry Research* 2017, 56, 1256-1266. Another part of this chapter has been submitted for publication as V. Vajihinejad, D. Dixon, M. da Silva, J. B. P. Soares, Effect of Polymer Chemical Composition Distribution on Flocculation: The Case of Composition Drift in Batch Reactors". These results were also presented in V. Vajihinejad, J. B. P. Soares, Impact of Polymer Microstructure on Flocculation and Dewatering: The Case of the Canadian Oil Sands Tailings, *ACS Fall 2019 National Meeting & Expo*, San Diego, CA, USA, August 25-29, 2019.

Chapter 4 introduces a novel cationic homopolymer, poly(vinylbenzyl trimethylammonium chloride), poly(VBTMAC), capable of enhancing flocculation and dewatering properties of MFT compared to conventional flocculants. In this chapter, we investigated the modes of flocculation using poly(VBTMAC) and compared its performance to the industrial standard flocculant, a commercially available anionic polyacrylamide, towards dewatering undiluted MFT using filtration. This chapter has been submitted for publication as V. Vajihinejad, S. Gumfekar, J. B. P. Soares, Enhanced Dewatering of Oil Sands Tailings by a Novel Water-Soluble Cationic Polymer, *Environmental Science Water Research & Technology*.

Chapter 5 introduces a mathematical model for the mechanisms and kinetics of MFT flocculation with poly(VBTMAC) that quantifies the laboratory-scale flocculation of MFT under different conditions. This chapter has been published in V. Vajihinejad, J. B. P. Soares, Monitoring Polymer Flocculation in Oil Sands Tailings: A Population Balance Model Approach, *Chemical Engineering Journal* 2018, 346, 447-457.

Chapter 5 summarizes the investigations carried out in this thesis and recommendations for future research work.

Appendix A discusses an unconventional approach to use oil sands tailings in the production of polyurethane foam composites. This appendix has been published in V. Vajihinejad, J. B. P. Soares, Can We Make Better Polyurethane Composite Foams with Oil Sands Mature Fine Tailing?, *Macromolecular Materials and Engineering*, 2016, vol. 301, pp 383-389.

Appendix B discusses polymer flocculants based on hydrophobically-modified copolymers of acrylamide. This appendix has been published in R. Hripko, V. Vajihinejad, J. B. P. Soares, Enhanced Flocculation of Oil Sands Mature Fine Tailings using Hydrophobically Modified Polyacrylamide Copolymers, *Global Challenges* 2018, 2, 1700135.

Appendix C shows a mathematical model for free radical copolymerization in a batch industrial reactor, and explains how the polymer microstructure of industrial flocculant such as anionic polyacrylamides vary as a function of

monomer/comonomer conversion.

Finally, **Appendix D** contains statistical analyses in dewatering design of experiments, NMR spectra of the polymers used in this study and calculations used to estimate monomer conversions and copolymer compositions.

Chapter 2

Background and Literature Review

2.1 Oil Sands Tailings Composition and Colloidal Stability

Oil sands tailings are waste streams of the oil sands extraction process. To extract bitumen form oil sands, water is mixed with oil sands ore. Typically, 2 m^3 of water is needed to produce one barrel of bitumen from 2 tons of oil sands ore.[16] In terms of mineral size, tailings are traditionally divided into coarse tailings (sands, larger than 44 μm), and fine tailings (fines, smaller than 44 μm). The 44 μm is not a magic number, just the opening size of the smallest sieve traditionally used to fractionate oil sands samples.[17] Fines with characteristic dimension lower than 2 μm are made of clay particles. Some investigations have found that the 2 μm limit is a better cut off value to explain properties of tailings streams.[5, 18]

In fresh tailings, the coarser sands rapidly separate from the stream and are used to build containment dikes to store tailings and recycled water. Given sufficient time, the solids settle and release a small portion of water, which is then recycled to the extraction process. The remaining slurry, containing

about 15% solids, is called fluid fine tailings (FFT). After approximately 2 to 5 years of gradual sedimentation, the FFT loses more water until it becomes a thick slurry called mature fine tailings (MFT). MFT still contains about 65-70% by weight of water, some (1-3%) residual bitumen, and traces of organic solvents. MFT is the plateau state for tailings dewatering, after which no further significant consolidation occurs even after decades. The cause for the water retention in MFT is not clear yet. The *organic model* proposed by Scott and Susseault,[19] suggests that bitumen along with water soluble organic surfactants and asphaltenic compounds (from oil sands), attached to the surface of clays, could bring small clays together and restrict the water pathways through the small agglomerates (Figure 2.1). The *mineral model*, contrarily, suggests that the presence of ultrafine clays (below 0.1 μm) and surface charges are responsible for the colloidal stability of MFT.[5] It seems that both the mineral and organic models contribute to water retention in MFT.

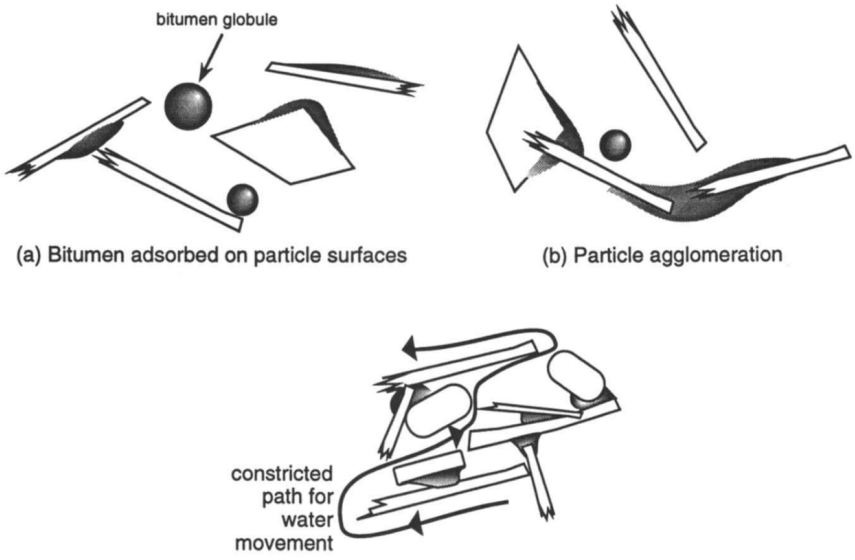

Figure 2.1: Water retention in MFT due to presence of bitumen and soluble organic surfactants (organic model).[5]

Most solids in MFT are fines below 2 μm. They are a mixture of clay minerals containing kaolinite and interlayered kaolinite-smectite (35% by weight, 10-20 $m^2.g^{-1}$), illite and interlayered illite-smectite (60-65%, 65-100 $m^2.g^{-1}$), as well

as swelling clays (such as montmorillonite, 1-2%, 700-840 $m^2.g^{-1}$) form the solids of MFT.[4, 5]

Figure 2.2 shows the mineral structure of some clays. Kaolinite is a non-swelling clay with a two-layer building block, a tetrahedral (T) sheet of silica (SiO_2) and an octahedral (O) sheet of aluminum-oxygen hydroxide (AlOOH). Hydrogen bonds between the –OH groups of O-sheet and –O groups of T-sheet hold the building blocks together. The charge on the T-sheet (base) is permanently negative because of the isomorphic substitution of Si^{4+} by Al^{3+}.[20] The charge on the O-sheet (edge), however, depends on pH. Both surfaces and edges of kaolinite in the pH range found with MFT (approximately 8) are negatively charged. Illite is another non-swelling clay that is present in MFT. Its building blocks are composed of three layers, where the O-sheet is sandwiched between the two T-sheets. The compensating ions, such as K^+ and Na^+, sit on the T-sheet to electrically balance the isomorphic substitution on the basal plane. The compensating ions are hold tight by the six oxygen atoms on the T-sheets, binding the building blocks tightly together and not allowing for significant ion exchange capacity in illite (non-swelling) [21, 22].

A representative of swelling clays is montmorillonite. Montmorillonite is a 3-layered clay similar to illite, but because the degree of isomorphic substitution is large and happens in both T- and O-sheets, the compensating ions on the O-sheet are delocalized (they cannot sit tight near the O-sheet anymore), allowing the clay layers to swell by the penetration of water. The presence of swelling clays in MFT makes the slurry more viscous, and is problematic in bitumen extraction units, and in the treatment and handling of the tailings. Table 2.1 summarizes the characteristics of clays found in oil sands.

The water retained in tailings contains inorganic ions such as Na^+, K^+, Ca^{2+} and Mg^{2+}. Ions in tailings come from connate water (water trapped inside the pores of the oil sands ore), the chemicals additives added to the bitumen extraction process, and HCO_3^- resulting from absorption of atmospheric CO_2 [4]. Because of caustic chemicals, such as NaOH added to the extraction process, tailings water has a basic pH of about 8, and that further impedes solids dewatering due to the formation of negative surface charges on clays.

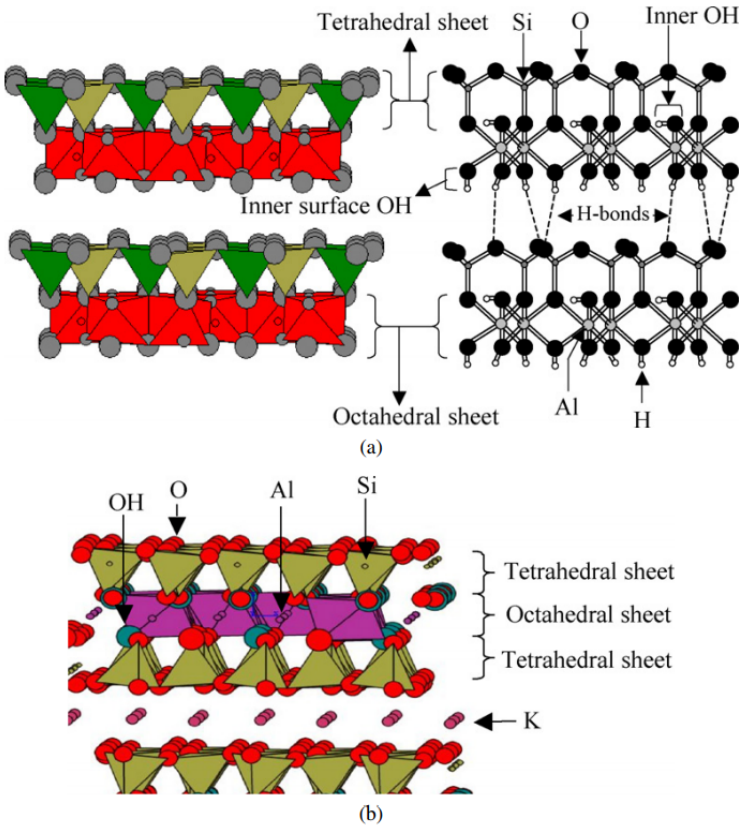

Figure 2.2: Mineral structure of (a) kaolinite and (b) illite.[22]

Table 2.1: Characteristics of clays found in oil sands ore.[21]

Clay type	Kaolinite	Illite	Montmorillonite	Chlorite
Abundance (wt%)	69	28	0.3	1
Structure type	2-layer	3-layer	3-layer	3-layer
Isomorphic substitution	Low in T	High in T	T and O	T and O
Compensating ions	K^+	K^+	Na^+, Ca^{2+}	$Mg(OH)_2(O)$
Specific surface area (m^2g^{-1})	10-20	65-100	700-840	42
Cation exchange capacity (meq/100g)	3-5	10-40	80-150	10-40

2.2 Flocculation and Coagulation: An Overview

Chemicals are used to break apart the colloidal stability of suspension such as MFT and aggregate small particles to sizes large enough so they can settle

by gravity in an acceptable period of time. Aggregation can happen through bridging small particles together with the help of polymer flocculants (flocculation) or by charge manipulation of particle surfaces through the addition of small molecules (coagulation). An example of aggregation by coagulation is the addition of gypsum ($CaSO_4.2H_2O$) to tailings. The coagulant (Ca^{2+} in the case of gypsum) suppress the electrical double layer on the surfaces of the particles and let them aggregate through van der Waals forces upon contact.[23]

Due to the basic pH of tailings water, the clay particles carry negative charges on their surfaces. Cations are attracted to the negatively charged surfaces, forming an electrical double layer (Figure 2.3). The concentration of positive ions adjacent to the particle surface is at maximum while it drops through a diffusion layer to the bulk of the liquid.

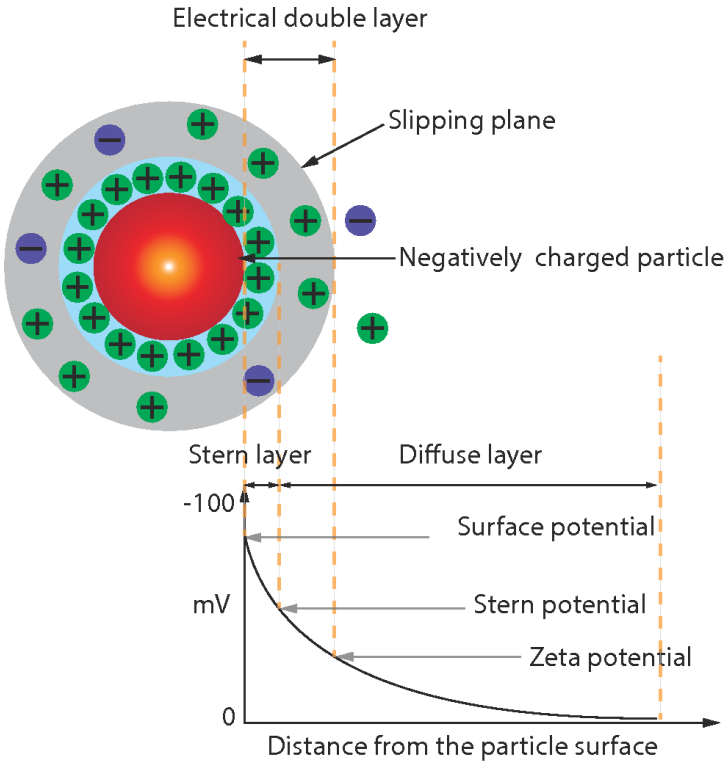

Figure 2.3: Scheme of electric double layer around a particles with negative surface charges.[24]

The size of the electric double layer around a particle is related to a parameter called Debye length (Equation (2.1)) [21].

$$\kappa = (\frac{e^2}{\varepsilon k_B T} \sum_i z_i^2 C_i N_A)^{1/2} \tag{2.1}$$

where C_i is molar concentration of ions of type i, T is temperature, e is the charge of an electron, z_i is the valency number of ions of type i, and ε, k_B and N_A are medium permittivity, Boltzmann constant and Avogadro's number, respectively. The thickness of electric double layer is proportional to the reciprocal of the Debye length, κ^{-1}. According to Equation (2.1), increasing the ionic concentration (for instance, by adding coagulants to the system), decreases the thickness of the electric double layer, making the particles more likely to aggregate upon collision.

When two particles collide in a suspension, the interplay between electrical double layer (repulsive) and van der Waals (attractive) forces determines whether the particles attach together (aggregation) or not. Fuchs defined a parameter that estimates the probability of aggregation upon collision if it happens primarily due to Brownian motion (no shear mixing). The Fuchs's stability ration (W) for two colloidal particles of radius r_i and r_j is defined as[25, 26]

$$W_{i,j} = (r_i + r_j) \int_{r_i+r_j}^{\infty} \frac{exp(V_T/k_B T)}{s^2} ds \tag{2.2}$$

where s is the distance between the centers of the particles, and V_T is the total energy of interaction between the two particles. According to the DLVO theory, V_T is the sum of van der Waals and electrostatic (double layer) energies. The probability of aggregation due to Brownian motion will be proportional to the reciprocal of the Fuchs' stability ratio.

In the case of aggregation by polymers, the adsorbed polymer chains can extend their length from the surface of one particle across, the electrical double layer, and then adsorb to the surface of other particles. Because of the for-

mation of multiple loops and tails on the surface of particles (Figure 2.4), polymer chains can promote the aggregation of more than two particles together through a mechanism called *bridging* flocculation.

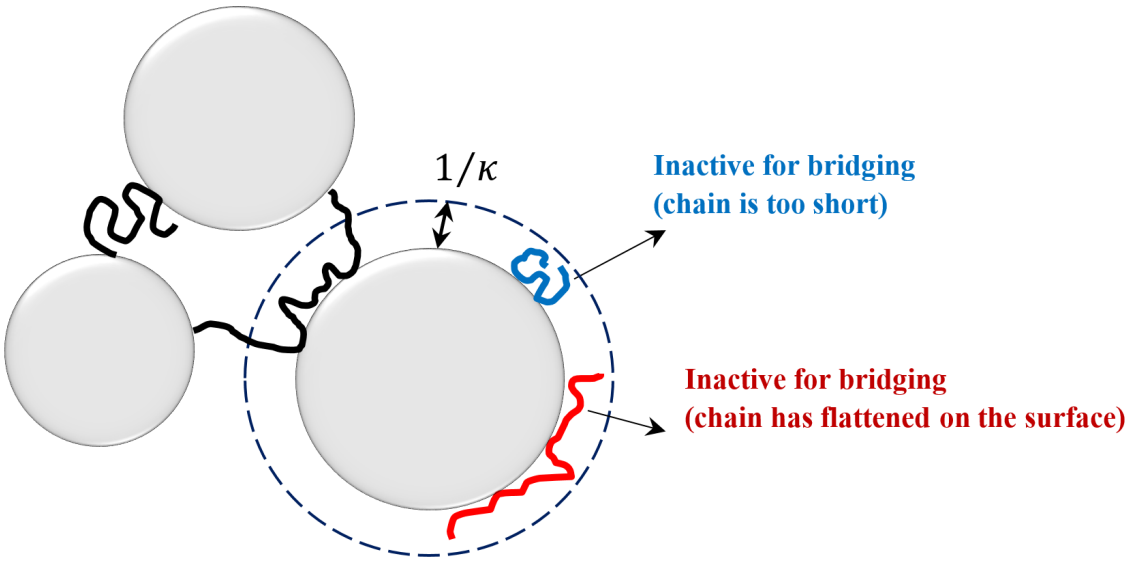

Figure 2.4: Bridging flocculation by polymers. Small chains and those that have flatten on the surface before the contact was made, will lose the chance of bridging.[27]

Polymer adsorption happens via multiple mechanisms, including hydrogen bonding (polyacrylamide on silica silanol groups), electrostatic interactions (cationic polymers on negatively charged sludge), hydrophobic interactions (poly(vinylalcohol) on silver iodide), and ion bridging (anionic polyacrylamide on negatively charged clays with the help of divalent calcium ions).[28]

Most flocculants used in densifying mineral tailings or dewatering oil sands tailings are copolymers of acrylamide and acrylic acid. Figure 2.5 illustrates the adsorption of anionic polyacrylamide on oil sands clays. This process seems counter-intuitive, at the first glance, because both polymer and clays are negatively charged. Such combination, however, has important implications: *i*) charged polymers are generally more extended in solution than neutral polymers. In addition, the polymer chains and clay surfaces repel each other, further extending the loops and tails of the adsorbed polymer away from the clay surface and allowing them contact other particles even at lower polymer

dosage. *ii*) most of adsorption sites are on the edge of the clays (where the most neutral sites exist)[29, 30]. These contribute to the formation of large and porous aggregates with less compact structure compared to cationic polymers [23]. In high solids suspensions containing fine clay particles, such as in MFT, this flocculation mechanism creates large, weak, and gel-like aggregates that are hard to dewater.

The anionic polymer flocculants are often added with a coagulant. The role of adding a coagulant such as Ca^{2+} or a low molecular weight cationic polymer prior to the addition of the polymer flocculant are twofold: *i*) The coagulant compresses the double layer charges and cause some pre-aggregation of the particles in suspension (reducing the required amount of flocculant), and *ii*) The coagulant also creates cation-bridges that allow the negatively-charged polymer to adsorb on the clay surface (Figure 2.5).

Aggregation by coagulation through addition of salts and aggregation by flocculation through addition of high molecular weight polymers differ in some characteristic ways :

i) Because polymer chains form multiple points of contacts with the solid surface, they often form stronger aggregates.
ii) Since the main mechanism in coagulation is charge-neutralization, the breakage of aggregates is reversible. In flocculation, however, the breakage is generally irreversible. The irreversible breakage of aggregates in shear-induced flocculation is likely due to either polymer chain rupture (carbon chain scission)[31, 32, 33, 34] or relaxation (reconformation) of the polymer chains on the particle surfaces.[35, 36, 37]

A minimum amount of polymer needs to adsorb on the particle surface before bridging flocculation may takes place. The free adsorption energy of polymer chains on surfaces is relatively small in the order of 0.3 k_BT per segment; thus, we may assume the rate of polymer adsorption equals the rate of polymer loss from the solution. If the number density of particles in suspension is n_s (m^{-3}), and n_p is the number density of polymer chains in the suspension, then the rate of polymer loss from the suspension (= rate of polymer adsorption) is[28]

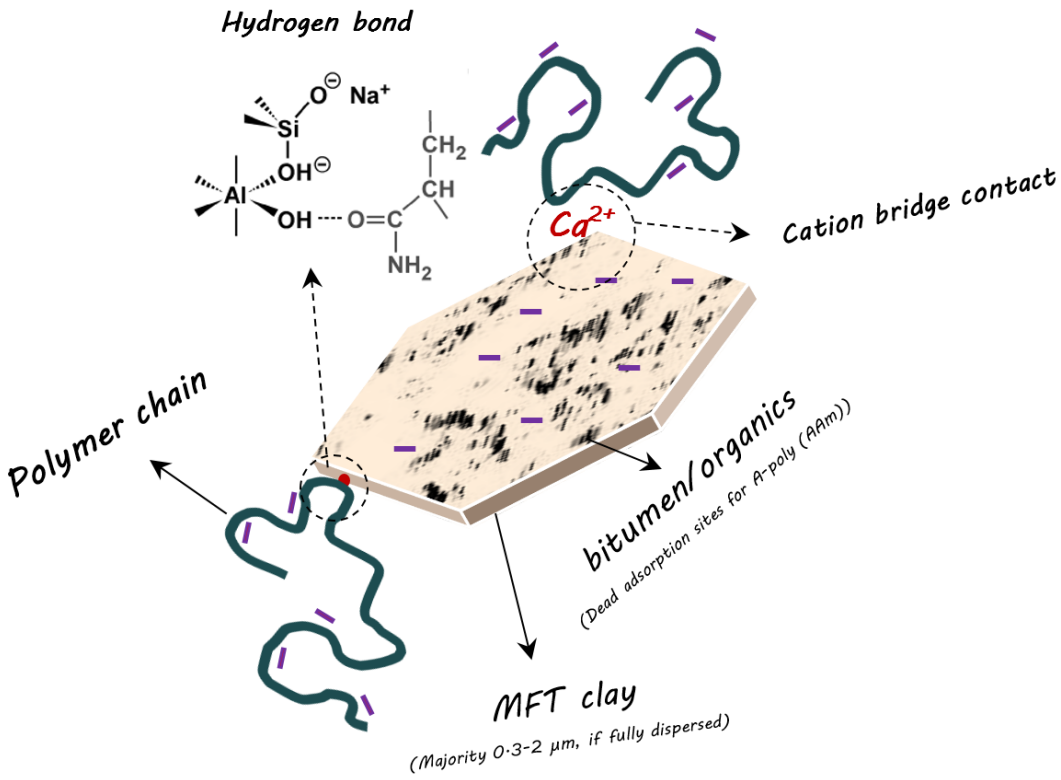

Figure 2.5: Adsorption of anionic polyacrylamide on oil sands clay.

$$-\frac{dn_p}{dt} = k_{ads} n_p n_s \tag{2.3}$$

where k_{ads} is adsorption rate constant. If ψ is the fraction of polymer chains needed to adsorb onto the surface of particles for the flocculation to begin, then solving Equation (2.3) gives the characteristic adsorption time as

$$\tau_{ads} = -\frac{ln(1-\psi)}{k_{ads} n_s} \tag{2.4}$$

In addition to polymer-particle collision (adsorption), particle-particle collision (aggregation) also takes place during flocculation. Similar to τ_{ads}, the characteristic aggregation time, τ_{agg}, or the time it takes for the number of

particles to be reduced by half, may be estimated as[38]

$$\tau_{agg} = \frac{2}{k_{ij} n_s} \tag{2.5}$$

where k_{ij} is the collision rate coefficient between particles i and j. Depending on the hydrodynamic regime of flocculation, k_{ij} may be expressed as[27]

$$k_{ij} = \frac{2k_B T}{3\mu} \frac{(d_i + d_j)^2}{d_i d_j} \text{ Perkinetic aggregation (Brownian diffusion)} \tag{2.6}$$

$$k_{ij} = \frac{1}{6} G (d_i + d_j)^3 \text{ Orthokinetic aggregation (fluid shear)} \tag{2.7}$$

where d_i and d_j are the diameters of particles i and j, and G is the shear rate or fluid velocity gradient. In the case of particle-polymer collision, $k_{ij} = k_{ads}$.

As an example, consider a suspension of 1 wt% negatively-charged monodisperse clay particles ($\rho = 2.65\ gcm^{-3}$) of characteristic size 2 μm that suspended in water containing 1 mM $NaCl$ and 1 mM $CaCl_2$. The following conclusions can be deduced from this example:[27]

i) The electric double layer, estimated using Equation (2.3), is 13.6 nm. For bridging flocculation to take place, the minimum size of the adsorbed polymer chains in solution must be at least twice the size of the electrical double layer. The average size of neutral polymer chains in a theta solvent is estimated to be about 0.06 $MW^{1/2}$, where MW is the molecular weight of the polymer [39, 28]. Thus, the minimum average molecular weight of a polymer to give access to bridging flocculation is about MW = 200 000.

ii) Table 2.2 compares the characteristic adsorption and aggregation times when a non-ionic polyacrylamide with MW= 2×10^6 is used for the flocculation of this suspension at room temperature considering two kinetic mechanisms, and assuming $\psi = 0.7$. As the calculation results suggest, adsorption in the diffusion mode happens long before the particles aggregate, while in the shear mode the adsorption time is the limiting factor in the flocculation process. In

reality, not every collision between particles leads to aggregation, thus adsorption (especially in dilute suspensions such as the case of wastewater treatment) strongly influence the onset and kinetics of flocculation. For concentrated suspensions (more than 10 wt%) such as in oil sands tailings, Equations (2.4) and (2.5) do not work well, because mass transfer (and dispersion) effects could substantially influence both aggregation and the adsorption dynamics [27].

Table 2.2: Relative times of adsorption and aggregation as happened in diffusion and shear flow regimes ($d_s = 2\mu m, d_p = 0.84\mu m$)

	$\tau_{ads}(s)$	$\tau_{agg}(s)$
Diffusion	19	202
Shear (G=100 s^{-1})	9	2.1

2.3 Polymer Flocculation in Oil Sands Tailings

This section reviews the recent literature on the use of polymers for the treatment of oil sands tailings. The focus of the discussion will be on the various chemistries and microstructure of polymer flocculants used to enhance dewatering of oil sands tailings and model tailings.

2.3.1 Stimuli-Responsive Polymers

Stimuli-responsive flocculants are polymers that change their conformation and reverse their solubility when the right stimulus is applied. The stimuli can be temperature, pH, electromagnetic field, ionic strength, redox species, and even light intensity. Among them, thermo-responsive polymers have been tested extensively for solid-liquid separation.[40, 27] Poly(N-isopropylacrylamide), poly(NIPAM), is a common temperature-responsive flocculant, with a lower critical solution temperature (LCST) of about 32 °C. Above this temperature, the polymer is no longer soluble in water: it undergoes a coil-to-globule

transition which causes its coils to decrease by one-third of their original size [41]. Figure **??** shows the phase transition diagram associated with CST. The phase transition around the LCST is mainly driven by hydrophobic interactions, among isopropyl groups, and by the weakening of hydrogen bonds between polymer chains and water molecules, which favors the formation of intra-chain interactions below the LCST.[42, 43, 44, 41] It is worth to note that LCST is the minimum transition temperature in the phase transition diagram that happens at a unique concentration for a given system of polymer and solvent. Any other points on the phase transition diagram curve (at different polymer concentrations) are known as cloud points.[45] In flocculation experiments cloud points are often confused LCST, and readers should be aware of this distinction.

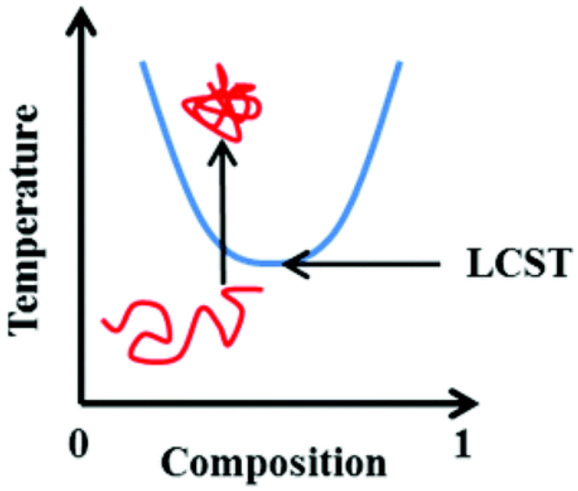

Figure 2.6: Phase transition diagram associated with LCST[46]

Franks showed that switch between attractive and repulsive forces between polymer chains around the cloud point could enhance secondary flocculation by driving water out of the sediment. He added temperature-responsive methylcellulose to a stable suspension of positively-charged zircon particles at room temperature (the LCST of methylcellulose is around 50 °)C. The adsorption of polymer on particles below the cloud point happened through hydrogen bonds and the high dosage of 10000 ppm (10 mg polymer per 1 g solids) ensured excess coverage of the particle surfaces. He then heated up the suspension

to 75° and observed that the particles started to aggregate, mainly due to favorable hydrophobic forces between polymer chains. When he cooled down the sediment, he observed further shrinkage of the sediment volume up to 11%. He attributed this to the rearrangement of particles due to changing attractive to repulsive forces, thus making water escape the pore structure. In other words, the sediments compressive yield stress became lower and that allowed the bed to collapse due to gravitational forces, driving the water out of the aggregated network.[47] Figure 2.7 illustrates the suggested secondary consolidation mechanism induced by thermo-responsive flocculants.

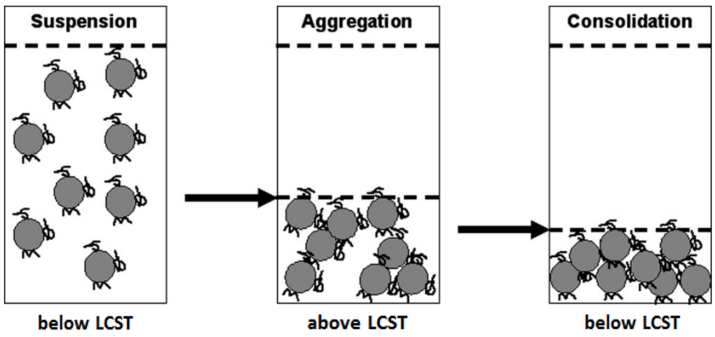

Figure 2.7: Secondary consolidation induced by thermo-responsive polymer flocculants

Secondary consolidation has not been observed with charged thermo-responsive polymers, because the ionic comonomer units can adsorb onto particle surfaces below and above the cloud point, which creates attractive forces in the sediments that hinders secondary consolidation.[12, 47]

In a smart attempt to achieve secondary consolidation with charged copolymers, O'Shea et al. made a series of block cationic and anionic copolymers of poly(NIPAM-*block*-DQA) and poly[NIPAM-*block*-(AAc-*co*-tBA)] (tBA=tertiary butyl acrylate), by reversible addition-fragmentation chain-transfer (RAFT) polymerization. Poly(NIPAM-*block*-DQA) was used to flocculate silica, and poly[NIPAM-block-(AAc-*co*-tBA)] to flocculate alumina.[47] In contrast to random charged copolymers, block copolymers could induce secondary consolidation below LCST (cloud point) because blocks of charged comonomer, adsorbed onto particles above LCST, left the neutral NIPAM chains free to

extend their length into solution and to cause secondary consolidation because of steric repulsion in the sediments below LCST.

Ng et al. showed that further increasing the temperature above the LCST could lead to formation of larger aggregates, as confirmed by focused beam reflectance measurement (FBRM).[48] The authors, however, did not observe this effect in the case of ionic thermo-responsive polymers (Figure 2.8). They hypothesized that, for ionic polymers a greater state of aggregation had already been achieved due to charge-neutralization, which masked the impact of temperature on the average size of the aggregates. The observations of Ng et al. on the impact of temperature was independently supported in a study by Maeda et al., where the authors used FTIR spectroscopy to show that more than 85% of the hydrogen bonds still existed between water molecules and the carbonyl groups of poly(PNIPAM) even above the LCST.[42]

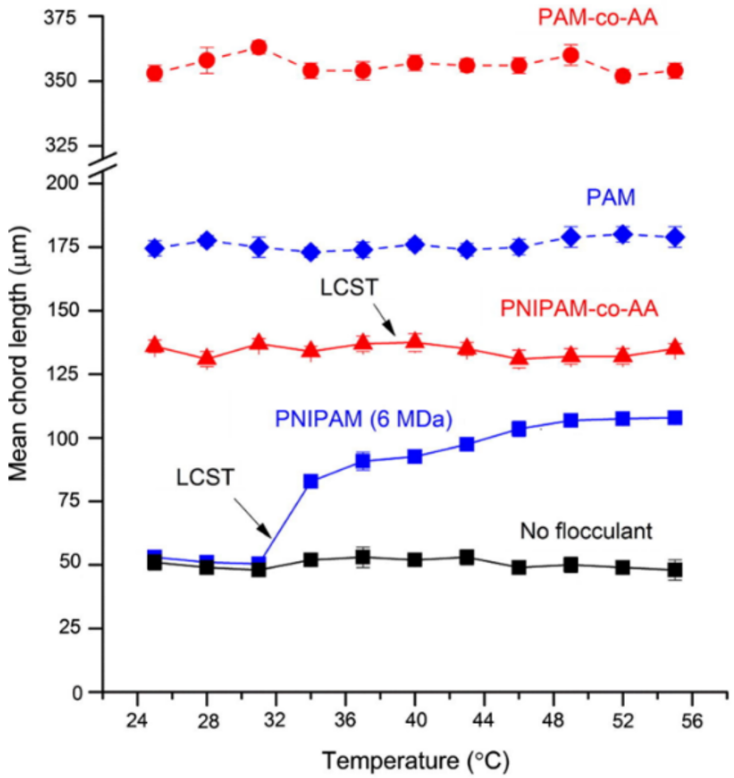

Figure 2.8: Effect of temperature on the iron aggregate sizes obtained by flocculation with thermoresposnive ionic and neutral polymers.

Thermo-responsive polymers have also been used to dewater oil sands tailings.[49, 12] For instance, Li et al. showed that the conformational changes of poly(NIPAM) around the cloud point enhanced the dewatering and geotechnical stability of MFT compared to when the MFT was treated with a commercial anionic polyacrylamide. They observed that the yield stress of the MFT sediments increased by 50% with poly(NIPAM) compared to A-poly(AAm).[50] It is, however, important to note that this higher geotechnical stability required using more than 3 times the dosage of the conventional flocculant. In fact, the inherent drawback of using thermo-responsive polymers for large scale applications, such as MFT treatment, are twofold: 1) the energy required to heat up the slurry above the LCST (or cloud point), and 2) the use of excess polymers to ensure good coverage of particles surfaces to induce aggregation above LCST (or cloud point).

2.3.2 Natural and Bio-Based Polymers

Commonly used bio- or natural polymer flocculants include chitosan, starch, cellulose, alginate and amylopectin. These polymers are attractive because of their wide availability, low prices, non-toxicity, and biodegradability.[27] In this section, we review the use of natural/bio-based polymer flocculants for the treatment of oil sands and model tailings.

In an attempt to partially substitute synthetic flocculants for environmental friendly alternatives, Lu et al. used chitosan in a two-step flocculation process to dewater oil sands tailings.[7] They first added high molecular weight anionic polyacrylamide, followed by cationic chitosan (MW $\approx$ 70 000). Chitosan is a neutral polymer, but becomes positively-charged in acidic medium (the authors dissolved the polymer in 1% acetic acid solution). The cationic chitosan neutralized the fine clays that had not been captured by the A-poly(AAm), and may have also caused some interfloc aggregation.[51] In another study, Bazoubandi and Soares used amylopectin-grafted polyacrylamide (AP-g-poly(AAm)) to dewater MFT. They grafted the polyacrylamide on amylopectin by free radical polymerization, using ceric ammonium nitrate as initiator to generate radicals on the amylopectin backbone. The authors showed

that the amylopectin itself could not significantly flocculate the tailings, due to its relatively small molecular weight. However, the AP-g-poly(AAm) consistently outperformed poly(AAm), achieving higher sediment solids content at slightly larger optimum dosages. The authors confirmed the grafting process had taken place by thermogravimetric analysis of the polymer, as the NMR and FTIR was unable to distinguish the grafted polymers from the mixture of poly(AAm) and amylopectin.[52] In another study, de Oliveira et al. modified chitosan with 3-chloro-2-hydroxypropyltrimethylammonium chloride (Chito-CTA) to increase the solubility of chitosan in water and also grafted polyacrylamide on chitosan by free radical polymerization. They tried different molar ratios of CTA to chitosan and compared it with the graft polymer, concluding that the graft chitosan-g-poly(AAm) performed better than Chito-CTA and cationic polyacrylamide in terms of dewatering metrics, capillary suction time, specific resistance to filtration, and settling rate.[14]

2.3.3 Polymers with Novel Chemistries

Wang et al. synthesized a novel hybrid $Al(OH)_3$-polyacrylamide (Al-poly(AAm)) based on the work of Yang et al., and compared it with the commercial anionic polyacrylamide, Magnafloc 1011 (Percol 727), to treat two types of fresh tailings with low and high fines ores. They synthesized the flocculant in two steps:[53] *i*) $Al(OH)_3$ colloidal particles (about 100 nm) were made by slowly adding an ammonium carbonate solution to an aluminum chloride solution, *ii*) acrylamide was polymerized inside the $Al(OH)_3$ colloidal suspension. The unreacted $Al(OH)_3$ was removed by precipitating the polymer solution in acetone. Figure 2.9 is a schematic of the Al-poly(AAm) structure.

The authors observed that the Al-poly(AAm) could effectively dewater fresh tailings (13.5 wt% solids) to more than 80 wt% solids under 2 psig for 3 minutes, while Magnafloc reached only 30 wt% solids under the same conditions and dosage. The authors performed the filtration test on tailings flocculated under a single dosage. Knowing that the intrinsic viscosity of Magnafloc, as reported by the authors, was about 30 times that of Al-poly(AAm), comparing the two polymers at the same dosage does not seem to be a fair basis for this

comparison.[54]

In another study, Sun et al. used atomic force microscopy (AFM) and single molecule force spectroscopy (SMFS) to prove that Al-poly(AAm) chains had a star-like configuration. They also showed that interactions between silica and Al-poly(AAm) were stronger than those between silica and poly(AAm), and even stronger than interactions between silica and a mixture of poly(AAm) and $AlCl_3$.[55] The authors flocculated a 0.6 wt% clay suspension at alkaline pH and observed that the Al-poly(AAm) produced large (up to a few millimeters in size) pellet-like aggregates with denser structures, in contrast to the loosely-packed aggregates obtained by poly(AAm) or poly(AAm) + $AlCl_3$. The authors proposed a flocculation mechanism where the cores of Al-poly(AAm) attached to the clay particles via charge neutralization and the star-like structure of poly(AAm) chain produced multiple points of bridging with neighboring particles, forming large and dense aggregates.

In another study, Alamgir et al. used Al-poly(AAm) with relatively large molecular weight (2×10^6) to flocculate MFT (diluted to 10 wt%). Their results showed that Al-poly(AAm) could solidify the MFT up to 77 wt% solids after filtration for 10 minutes under 2 psig. Although the polymer was a good filtration aid, the turbidity of the supernatant was Magnafloc was used.[8]

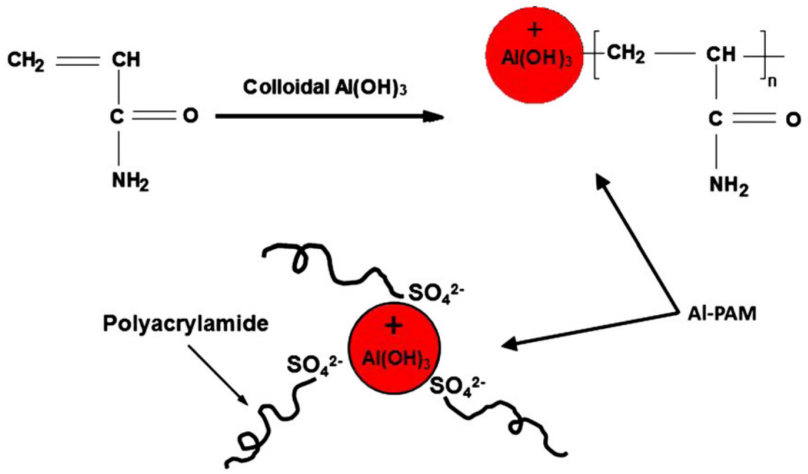

Figure 2.9: Synthesis and structure of Al-PAM. [8]

One of the approaches to enhance the dewatering of MFT has been to synthesize partially hydrophobic polymers that retain less water in the aggregates. In a novel attempt, Botha et al. polymerized anionic hyperbranched functional polyethylene (HBfPE) and used it to treat MFT for the first time.[11] The authors used a late transition metal catalyst that underwent chain walking to synthesize a series of branched polymers with polyethylene as core and methyl acrylate in the branches (Figure 2.10). They used the polymer to treat MFT at 5 wt% and 20 wt% solids, and compared its performance with that of industry standard high molecular weight A-poly(AAm). A-poly(AAm) led to much higher initial settling rates at 5wt% solids, but the situation was reversed for the 20 wt% solids, when HBfPE outperformed A-poly(AAm). The higher settling rate of the A-poly(AAm) in low solids was attributed to the extremely larger molecular weight of the A-poly(AAm) (100 times higher than HBfPE). For the counter-intuitive observation at 20 wt% solids, the authors speculated that since the average distance between the MFT particles were shorter for the high solids MFT, the higher molecular weight of the A-poly(AAm) flocculant played a lesser role in the flocculation. In addition to the authors' hypothesis, an additional explanation for this behavior could be that the formation of large A-poly(AAm) aggregates in the high solids 20 wt% MFT hindered the settling of the aggregates due to strong wall adhesion effects in the relatively small settling cylinders (about 2 inches in diameter) used in their experiments. The effect of wall adhesion and settling rate hindrance is comprehensively discussed in a publication by Benn et al., where the authors performed controlled experiments to study the sedimentation and consolidation of aggregates of various sizes and densities obtained by different flocculants.[56]

Botha et al. also observed that the lowest CST values (which correlates with the highest dewatering rates) at the corresponding optimum dosages was observed when HBfPE was used to treat MFT with both solids contents, supposedly because HBfPE made denser aggregates due to its hyperbranched structure and hydrophobic polyethylene core that repelled more water than when hydrophilic A-poly(AAm) was used. In a subsequent study to further investigate the behavior of this novel polymer, Costine et al. used a floc den-

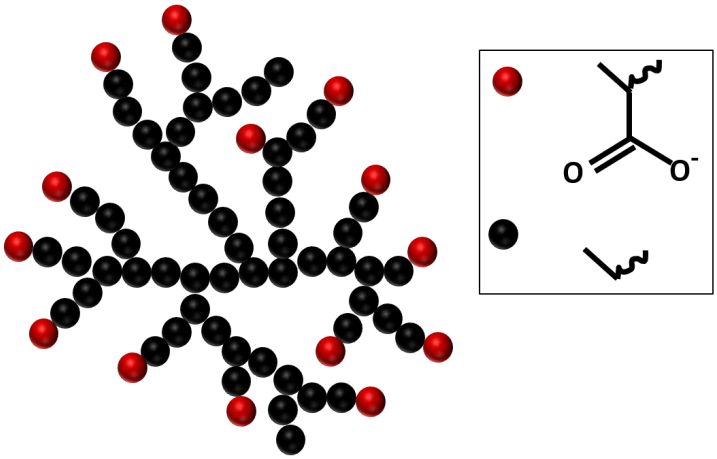

Figure 2.10: Suggested structure for HBfPE.[57]

sity analyzer (FDA) and focused beam reflectance measurement (FBRM) to further characterize the aggregates resulting from the HBfPE treatment of oil sands tailings. They adopted the method of Farrow and Warren[58] to estimate the apparent density of aggregates. In this method, the size and free settling rate (in Stokes regime) of the aggregated are measured using a semi-automated digital camera. Their results confirmed the dewatering observation of Botha et al, showing that the aggregates promoted by the HBfPE treatment indeed had higher densities than those made by A-poly(AAm) (Figure 2.11). Given the large molecular weight difference between the two products, Costine et al. showed that some formulation of HBfPE (i.e. 40 mol% comonomer of methyl acrylate) could produce aggregates of comparable size to those produced by A-poly(AAm) (Figure 2.11). The authors speculated that hydrophobic interactions between polyethylene segments and clay surfaces coated with bitumen and organic compounds could enhance the adsorption of these partially-hydrophobic polymers onto the clays present in MFT.

In another attempt to impart some hydrophobicity to the polyacrylamide chains and to accelerate dewatering, Reis et al. synthesized a series of polyacrylamide-g-poly(propylene oxide) (poly(AAm)-*graft*-PPO) to dewater MFT.[10] In a two-step process, they first synthesized poly(propylene oxide methacrylate) macromonomer by reacting methacryloyl and polypropylene, and then copoly-

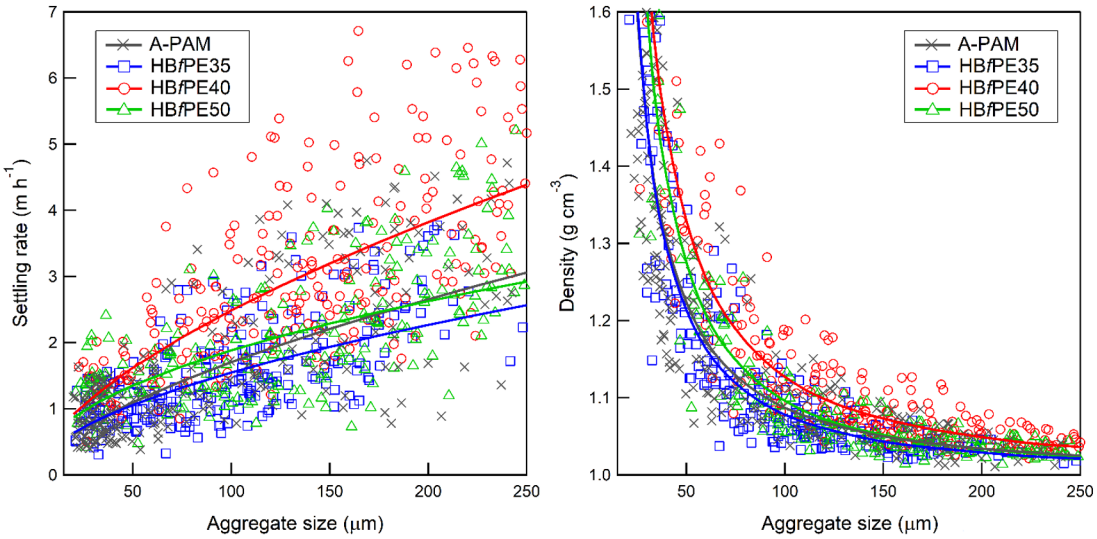

Figure 2.11: Unhindered settling rate and aggregate densities as a function of size obtained for A-poly(AAm) and a series of HB*f*PEs.[59]

merized the macromonomer with acrylamide to produce poly(AAm)-*graft*-PPO (Figure 2.12). When the polymers were tested in low solids MFT (diluted to 2 wt%), commercial A-poly(AAm) (with the addition of calcium) and poly(AAm)-g-PPO (no calcium addition) performed similarly, as quantified by the initial settling rate and CST, with the A-poly(AAm) requiring a much lower dosage than poly(AAm)-g-PPO (optimum performance achieved at about 2 000 ppm for A-poly(AAm) versus 10 000 ppm for poly(AAm)-g-PPO). This significant dosage difference was likely due to the larger molecular weight of the A-poly(AAm) (about 17 millions) compared with that of poly(AAm)-g-PPO (about 1 million). The addition of calcium prior to flocculation with A-poly(AAm) may also have helped reduce the A-poly(AAm) dosage, since it increases the degree of pre-aggregation of the suspended solids. In the high solids MFT (20 wt%), the authors observed that PAP-g-PPO gave much better dewatering than A-poly(AAm) at their respective optimum dosages, as indicated by about 10 times difference in the CST values measured after flocculation. The authors attributed this enhanced dewatering to the hydrophobic segments in poly(AAm)-g-PPO, and not to the lower viscosity (lower molecular weight) of the poly(AAm)-g-PPO solutions. To rule

out the viscosity effect, the authors compared poly(AAm)-g-PPO against neutral poly(AAm) of the same molecular weight (about 1 million) and showed poly(AAm)-g-PPO could still dewater MFT much better than the neutral poly(AAm) (CST of about 40 s vs CST of about 400 s).

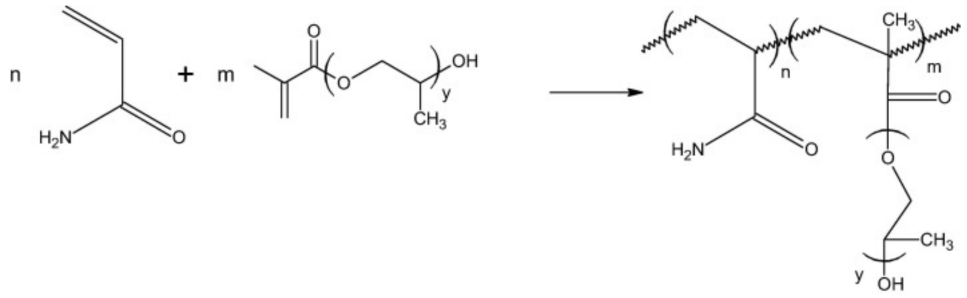

Figure 2.12: Chemical structure of poly(AAm)-g-PPO.[10]

2.3.4 Flocculation and Polymer Microstructure

Polymer microstructure is a generic term that encompasses polymer molecular weight (average chain length), molecular weight distribution (polydispersity), chemical (comonomer) composition and distribution, grafting frequency and density, long chain branching, charge distribution, etc. These properties determine how polymers perform in different applications. For example, polymer molecular weight average and distribution affect polymer processing and mechanical strength, while the short chain branching of polyolefin impacts their crystallinity and impact properties.

In the area of solid-liquid separation, one of the earliest work concerning polymer flocculant microstructure was by Gill and Herrington.[60] In two separate studies, the authors investigated the influence of the flocculant molecular weight and chemical composition for the system of acrylamide compolymerized with [2-(acryloyloxy)ethyl]trimethylammonium chloride for the flocculation of kaolin suspensions. The authors used free radical polymerization to make these polymers: In a first study, they kept the average chemical composition constant and, varied the total average molecular weight from 1×10^6 to 10×10^6,[61] in a second study, they kept the average molecular weight the same 3×10^6, and

changed the average molar fraction of the cationic comonomer from 15 wt% to 44 wt%.[60] They used their polymers to flocculate kaolin suspensions and found that the supernatant clarity and the aggregate settling rate improved with increasing polymer molecular weight. The authors, however, did not find any significant correlation between copolymer composition and settling rate or even between copolymer composition and supernatant turbidity.

Later in subsequent interesting study, Subramanian et al. compared the flocculation performance of graft and random AAm and DADMAC in a dilute model tailing of TiO_2 (concentration of 0.005 wt%, average particle size of 0.4 μm).[62] The authors wanted to test the hypothesis that if the charges on a copolymer were concentrated in a few locations along the backbone (as in the case of block copolymers) rather than being randomly distributed along the chain, the charge neutralization-bridging flocculation would be more effective. In their first study, poly (DADMAC) made by free radical polymerization was grafted onto poly(AAm) through gamma radiation to produce a graft microgel. Gamma radiation extracted hydrogen atoms from the polymer backbones, and the grafted microgel was produced through chain termination by combination. The authors argued that the probability of termination between two poly(DADMAC) chains was low due to electrostatic repulsion between the chains., This hypothesis was confirmed by a controlled experiment showing that the viscosity of the system did not increase substantially after being exposed to gamma radiation for a long time. Chain termination by combination of poly(AAm) with another poly(AAm) chain, however, was favored, but the authors did not attempt to separate any possible homopolymer microgels from the system. In a similar fashion, gamma radiation was applied to a linear random poly(AAm-*co*-DADMAC), made by free radical polymerization, to obtain linear microgels. Figure 2.13 represents the expected structure of the two products. It is important to note that the authors kept the overall concentration of monomers and the intensity of the gamma radiation low enough to avoid formation of macrogels (dense crosslinks) which would otherwise be insoluble in water. Their results on dilute suspensions of TiO_2 showed that grafted microgels performed better than random microgels (at optimum conditions), as

indicated by the size of aggregates and the turbidity of the supernatant. They also showed that both linear and random microgels performed better than linear random copolymer of acrylamide and DADMAC. The authors, however, did not attempt to match the molecular weights of the three products they compared, which may affect the generality of their conclusions.

Xu et al. compared the performance of hyperbranched cationic polyacrylamide and that of linear cationic polyacrylamide in the flocculation of 1wt% kaolinite suspensions. The comonomer used was N-acryloyl-1,2-diaminoethane hydrochloride. They observed that the hyperbranched flocculant had higher settling rate and supernatant clarity. The better performance was attributed to the hyperbranched structure of the polymer giving a more extended chain conformation in solution, which exposed the cationic units more effectively than its linear alternative.[63] The authors reported that their polymer had the same intrinsic viscosity and average molecular weight. This finding, however, is inconsistent with polymer physics: if both polymers had the same intrinsic viscosity, then the hyperbranched flocculant necessarily must have had higher molecular weight than the linear polymer. As stated by the authors, their conclusion seemed to be based on an erroneous interpretation of their experimental results.

O'Shea et al. showed how block thermo-responsive copolymer flocculants could outperform their random counterparts when used to dewater model silica tailings. The authors made a series of cationic random and block copolymers of poly(NIPAM-co-dimethylaminoethyl acrylate quaternary chloride), poly(NIPAM-co-DQA), by free radical and reversible addition-fragmentation chain-transfer (RAFT) polymerization, respectively.[47] They observed, in contrast to random copolymers, that block copolymers induced secondary consolidation below the LCST because the blocks made of the ionic comonomer adsorbed onto silica particles above the LCST, allowing the neutral and thermos-responsive NIPAM blocks extend into solution. When the temperature was lowered below the LCST, intramolecular interactions caused them to expel water and collapse, leading to secondary consolidation . The block copolymers also formed micellar structures above the LCST, promoting more effective

adsorption by charge-neutralization and forming larger aggregates.

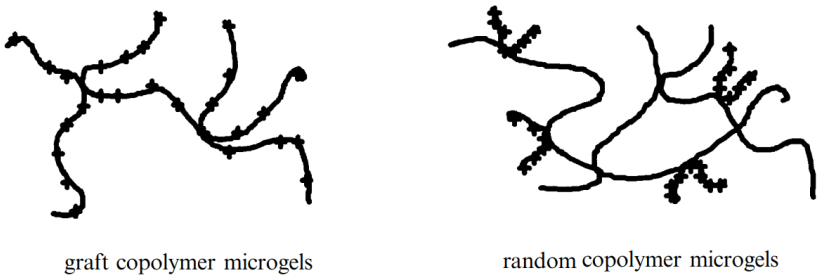

Figure 2.13: Graft and random copolymer microgels. The graft copolymer microgel has been shown to produce more effective flocculation.[62]

Nasser and James used a series of cationic polyacrylamides to find out the effect of charge density and molecular weight on the flocculation and sedimentation of kaolin suspensions. They found that the supernatant turbidity did not improve notably when the copolymer charge density varied from 10% to 35%, but observed that settling rates (at the optimum conditions) decreased when the charge density increased or when the molecular weight decreased, which is a reflection of the effect of polymer microstructure on average size of the aggregates. It is difficult, however, to generalize their results because the authors limited they investigation to a narrow range of molecular weight and charge density.[64]

In the most detailed study of this kind, Costine et al. studied the effect of molecular weight of A-poly(AAm) on flocculation, aggregate properties, and sedimentation behavior of kaolin suspensions under various water chemistries and mixing conditions. They used a series of A-poly(AAm)s with the same ionic charges but varying molecular weights. The authors did not report the average molecular weight, only the intrinsic viscosity of the A-poly(AAm) flocculants, which ranged from 9 to 20 $dL.g^{-1}$. They used a continuous Couette system (shear vessel) to test the effect of varying A-poly(AAm) molecular weights, mixing conditions, and water chemistry. Interestingly, the authors found that if the mixing intensity was low enough to limit the breakage of weakly polymer-bridged aggregates, then below a certain dosage, low molecular weight A-poly(AAm) produced larger and denser aggregates than high

molecular weight A-poly(AAm). This effect was attributed to the higher number of (shorter) chains in the low molecular weight polymers, which promoted more aggregation events in starving dosages.[65] As seen in Figure 2.14, the implication of their results is that depending on the desired range of settling rates or dewatering (reflected in aggregate density), one could decide whether to choose high or low molecular weight polymers for a particular solid-liquid separation. It is important to emphasize that their conclusion goes against a common assumption in solid-liquid flocculation that "the higher the polymer molecular weight, the better the flocculation". They also observed that the water chemistry (ionic strength) affect flocculation less as the molecular weight of the flocculant decreased. This observation was mostly attributed to ions having a higher shielding effect on longer chains than on shorter chains.

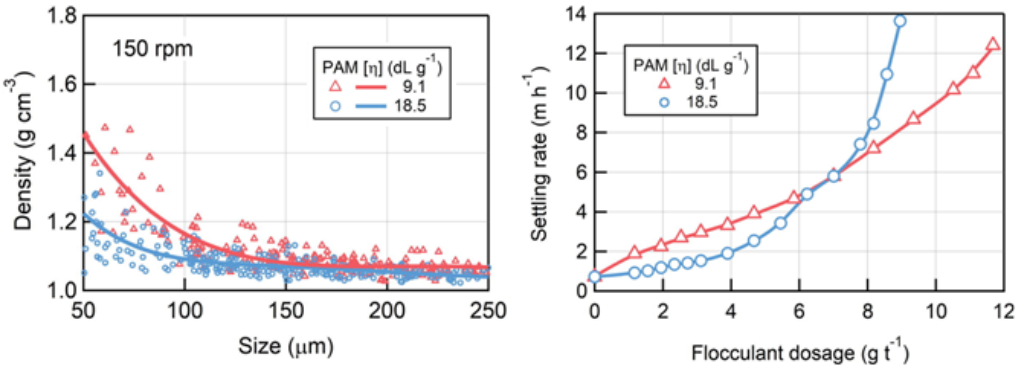

Figure 2.14: Influence of polymer molecular weight on aggregate density and settling rate profiles of kaolin slurries[65]

Chapter 3

Dewatering Oil Sands Mature Fine Tailings (MFT) with Cationic Flocculants : Impact of Polymer Microstructure

Copolymers of acrylamide and cationic comonomers such as diallyldimethylammonium chloride can effectively dewater solid suspensions containing negatively charged fine particles. A good example of such suspensions is oil sands mature fine tailings (MFT). However, little is known about the impact of flocculant microstructure in flocculation/dewatering performance. In this study, a surface response methodology was used to systematically assess the impact of chemical composition and average molecular weight of poly(acrylamide-*co*-diallyldimethylammonium chloride) in dewatering MFT. The chemical composition and average molecular weight of the copolymers were controlled by changing the feed monomer/comonomer ratios and initiator concentration.

A version of this chapter has been published as V. Vajihinejad, R. Guillermo, J. Soares, "dewatering oil sands mature fine tailings (MFTs) with poly(acrylamide-*co*-diallyldimethylammonium chloride): Effect of average molecular weight and copolymer composition" Industrial & Engineering Chemistry Research, 2017, vol. 56, pp 1256-1266 and presented as V. Vajihinejad, J. Soares "Impact of polymer microstructure on flocculation and dewatering: Case of Canadian oil sands tailings" in ACS Fall 2019 National Meeting & Expo, San Diego, August 2019.

Both copolymer composition and molecular weight averages were statistically significant variables for the initial settling rate and supernatant turbidity of the flocculated MFT. However, capillary suction time and resistance to filtration depended only on copolymer composition and polymer dosage, but not significantly on average molecular weight. Depending on the polymer dosage, the optimum chemical composition varies between 0 to 60 mol% of acrylamide in the chain.

In addition to the average microstructure properties, we were also interested in exploring whether the flocculant microstructure distributions affected flocculation, in particular the effect of the chemical composition distribution on aggregate formation and dewatering of MFT. Polymer reaction engineering tools were used to make two series of poly(acrylamide-*co*-vinylbenzyl trimethylammonium chloride) having the same average composition and molecular weight, but one series had narrow CCD, while the other had broad CCD. Surprisingly, the flocculation/dewatering responses of the two series depended on their dosage. The series with broad CCD consistently showed better results in terms of aggregate formation and dewatering in low (starving) dosages, while narrow CCD outperformed it in higher dosages. These results should be of interest to polymer producers trying to tailor-make their products for oil sands tailings or any other wastewater system.

3.1 Introduction

Oil sands mature fine tailings (MFT) are stable slurries of water ($\sim$ 60 wt%), fine particles ($\sim$ 35 wt%), residual bitumen, and other organics ($\sim$ 5 wt%), that form over time after waste streams of the oil sands extraction process is released into tailing ponds. Tailing ponds have polluted an area in Canada as large as 1.5 times the size of the city of Vancouver (176 km^2). To put things into perspective, this area is equivalent to approximately 111 000 hockey rinks. It may take up to 150 years for MFT to consolidate in the settling ponds, due to the presence of very small negatively charged particles (mainly clay), that does not separate from the liquid phase by gravity.[66] Current commercial

methods, such as paste technology, use very high molecular weight anionic polyacrylamide for dewatering MFT. Unfortunately, strong hydrogen bonds due to the amide groups on the poly(AAm) backbone, along with the presence of positive ions in the slurry, form a gel-like structure that retains considerable amounts of water.[10] Copolymerizing acrylamide (AAm) with positively charge comonomers, such as diallydimethylammonium chloride (DADMAC) or [2-(acryloyloxy)ethyl]trimethylammonium chloride, has helped reach higher dewatering efficiencies in MFTs.[67, 68, 69]

In a recent patent on filtration of oil sands tailings, the authors claimed that copolymers of acrylamide and DADMAC having at least 50 mol% of cationic comonomer and molecular weight less than 1 million dewatered MFT well, but no information on the influence of polymer microstructure on the dewatering performance of these copolymers was provided by the inventors.[69] Polymers affects most of their application properties, and dewatering performance is no exception. The number of studies evaluating the influence of copolymer microstructure on MFT flocculation and dewatering is quite limited, although a few studies have been published for other similar systems such as pulp and paper mills wastewater treatment, sludge dewatering, model clays, silica and titanium oxide particles.[70, 71, 72, 73, 64, 60, 61] For instance, Gill and Herrington investigated the impact of the molecular weight of copolymers of acrylamide and [2-(acryloyloxy)ethyl]trimethylammonium chloride on the flocculation of kaolin suspensions in water.[60] They kept the composition constant and varied the molecular weight of the copolymers from 1×10^6 to 10×10^6 g.mol^{-1}. They found that supernatant clarity and settling rate improved by increasing polymer molecular weight. In another study by the same authors, they flocculated kaolin suspensions with cationic copolymers of the same molecular weight but with different compositions.[61] They tested three cationic copolymers of acrylamide with 15, 31, and 44% [2-(acryloyloxy)ethyl]trimethylammonium chloride and same molecular weight of about 2.7×10^6. Surprisingly, they found no correlation between copolymer composition, settling rate and supernatant turbidity. Since in both studies the authors used copolymers with very high range of molecular weights and small range of chemical compositions,

we cannot confidently extrapolate their results to wider polymer microstructural ranges, even for model tailings (i.e. kaolinite suspensions). Another work on the effect of molecular weight, charge density, and polymer dosage of cationic copolymers of acrylamide on flocculation of kaolinite suspensions was published by Nasser and James, where they found that the supernatant turbidity did not improve notably when they changed the charge density of the cationic polyacrylamide from 10% to 35%, while keeping the molecular weight constant.[64] Their results also suggested that settling rates (at the optimum dosage) decreased slightly when the charge density was increased and when the polymer molecular weight was reduced.

In another interesting study, Subramanian et al. compared the flocculation performance of graft and random AAm and DADMAC in a dilute model tailing of TiO_2.[62] Their results showed that grafted microgels performed better than random microgels (at optimum conditions), as indicated by the size of aggregates and the turbidity of the supernatant. They also showed that both linear and random microgels performed better than linear random copolymer of acrylamide and DADMAC. The authors, however, did not attempt to match the molecular weights of the three products they compared, which may affect the generality of their results. In another study, O'Shea et al. showed the advantage of using block structure in thermo-responsive flocculants in dewatering model tailings of silica. The authors made a series of cationic random and block copolymers of poly(NIPAM-b-DQA) by free radical and reversible addition-fragmentation chain-transfer (RAFT) polymerization, respectively.[47] They observed, in contrast to random charged copolymers, block copolymers induced secondary consolidation below the LCST. The block copolymers, also, formed micellar structure above the LCST, promoting more effective adsorption by charge-neutralization and forming larger aggregates.

In a detailed study, Costine et al. investigated the effect of molecular weight of anionic polyacrylamide on flocculation, aggregate properties and sedimentation behavior of kaolin suspensions under various water chemistry and mixing conditions. They used a series of anionic polyacrylamide of the same chemical compositions but varying molecular weights. Interestingly, the authors

found that if the mixing intensity was low enough to limit the breakage of weakly polymer-bridged aggregates, then below a certain dosage, low molecular weight A-poly(AAm) produced larger and denser aggregates than high molecular weight A-poly(AAm). This effect was attributed to the higher number of (shorter) chains in the low molecular weight polymers, which promoted more aggregation events in starving dosages.[65]

The work discussed in this chapter quantifies the impact of average copolymer composition and molecular weight, as well as chemical composition distribution, on the dewatering of MFT with cationic copolymers of acrylamide. The study is divided in two parts:

i) The first part explores the impact of average molecular weight and average chemical composition of a series of cationic copolymers of acrylamide, poly(AAm-*co*-DADMAC), through a response surface method (RSM). A central composite design was chosen for the RSM and flocculation/dewatering responses (settling rate, turbidity of supernatant, capillary suction time (CST), and resistance to filtration) were simulated with a multiple linear regression model.

ii) The second part of the study examines whether the chemical composition distribution affects the flocculation/dewatering of MFT. Polymer flocculants are usually made by free radical polymerization in batch reactors, in which a significant amount of comonomer composition drift may take place depending on the reactivity ratios of the monomers, ultimately producing copolymers with broad chemical composition distribution (CCD). To examine the effect of flocculant CCD on flocculation/dewatering, two series of cationic copolymers of acrylamide, poly(acrylamide-*co*-vinylbenzyl trimethylammonium chloride), poly(AAm-*co*-VBTMAC), were synthesized, with the same average chemical composition and molecular weight, but different (broad or narrow) CCD.

3.2 Experimental section

3.2.1 Materials

Acrylamide (AAm), diallydimethylammonium chloride (DADMAC) and vinylbenzyl trimethylammonium chloride, initiator, 2,2′-azobis(2-methylpropionamidine) dihydrochloride (V-50), were purchased from Sigma-Aldrich. Coanda Research & Development Corporation in Alberta, Canada, supplied the MFT samples used in this research.

3.2.2 Polymerization

This section discusses the polymerization of the two copolymer systems investigated in this chapter, poly(AAm-*co*-DADMAC) and poly(AAm-*co*-VBTMAC). Poly(AAm-*co*-DADMAC) was used to study the effect of average molecular weight and average copolymer composition of cationic flocculants. To be able to use the literature kinetic data for controlling the composition of poly(AAm-*co*-DADMAC) copolymer by controlling the monomer/comonomer ratios in the feed, and to be able to finish polymerization within the life time of the initiator, all poly(AAm-*co*-DADMAC)s were polymerized to small conversions, to avoid composition drift. However, to study the effect of CCD on flocculation, we replaced DADMAC with VBTMAC. The main reason for this was the slow kinetics of DADMAC. In other words, it was not possible to polymerize a system of AAm/DADMAC to full conversion (to make copolymers with broad CCD) in the life time of the initiator. However, VBTMAC allowed as to reach full conversion (to get broad CCD) within a reasonable amount of time with reasonably large overall molecular weight.

Poly(AAm-*co*-DADMAC)

Poly(AAm-*co*-DADMAC), was made by free radical polymerization at 50 °C in a 0.5 L glass polyclave reactor (büchiglasuster®, Switzerland) equipped with a jacket, a mixer, and a nitrogen line for purging oxygen. Initially, the monomer solutions were added to the reactor and bubbled with nitrogen for about 1 hour while increasing the reactor temperature to 50 °C. Initiator, previously

purged with nitrogen, was then added to the reactor. The average comonomer fraction in the copolymer was controlled by varying the comonomer composition in the feed. After a certain time, estimated based on previously published polymerization kinetics data, the polymerizations was stopped by adding 0.1 ml of 1 wt% hydroquinone solution to every 10 ml of the reaction mixture.[74] Separation of the poly(AAm-*co*-DADMAC) from unreacted monomers was done by precipitating the reaction solution in acetone. Since the conversions were small (to avoid composition drift), the mass of polymer produced was little, making it important to recover all polymer from the reaction mixture. To meet this end, following purification procedure was used:

Small volumes of the reaction mixture were mixed with about 10-15-fold (by volume) of acetone in centrifugation tubes. After shaking, the mixture became a cloudy suspension, indicating that the polymer had precipitated from solution. The mixture was then placed in a centrifuge for about a minute at high speed to separate the polymer from the solution. The resulting polymer was then washed multiple times with acetone for further purification. The purified polymer was frozen with liquid nitrogen and dried in a freeze-dryer for at least 4 days to remove any remaining solvent and water.

Equations (3.1) to (3.3) show how the cumulative copolymer composition is related to the initial feed composition, monomers conversion, monomers reactivity ratios, and instantaneous monomers compositions[75, 76]

$$\overline{F}_1 = \frac{f_{10} - f_1(1-x)}{x} \tag{3.1}$$

$$\frac{df_1}{dx} = \frac{f_1 - F_1}{1-x} \tag{3.2}$$

$$F_1 = \frac{r_1 f_1^2 + f_1 f_2}{r_1 f_1^2 + 2 f_1 f_2 + r_2 f_2^2} \tag{3.3}$$

where $\overline{F}_1$ and F_1 are the cumulative and instantaneous molar fraction of monomer 1 in the copolymer, respectively; f_{10} and f_1 are the initial and in-

stantaneous molar fraction of monomer 1 in the reactor, respectively; r_1 and r_2 are the reactivity ratios of monomers 1 and 2, respectively; and x is total molar conversion. To control the copolymer composition, the conditions were kept the same for all the polymerizations, except the feed composition. Reactivity ratios for AAm and DADMAC reported in the work of Brand et al. (r_{AAm}= 5.7± 0.5 and r_{DADMAC}= 0.03± 0.001) were used.[74] Since the authors reported that the reactivity ratios changed as a function of the total concentration of the monomers in the solution, the total monomer concentration were kept the same as reported by them, 1.5 mol.L^{-1}, for all polymerizations. More information on how conversions and cumulative copolymer compositions were calculated is available in the Appendix D.[74, 75, 76, 77, 78]

The average molecular weight of the copolymers can be controlled by varying the initial concentration of initiator added to the polymerization reactor. Equation (3.4) shows how the instantaneous number average chain length of polymers made by free radical polymerization are related to initial initiator concentration at low conversions. All polymerizations were run well below 10% molar conversion to avoid substantial composition drift and the consequent broadening of the molecular weight distribution of the polymer.

$$\frac{1}{r_n} = \frac{\frac{k_t^{0.5}}{k_p}(2fk_I[I]_0)^{0.5}}{[M]_0(1-x_n)} + \frac{k_f}{k_p} \tag{3.4}$$

In Equation (3.4), $\overline{r}_n$ is the instantaneous number-average chain length of the polymer; k_p, k_t, and k_f are the rate constants for propagation, termination and transfer to monomer, respectively.[79]

Poly(AAm-*co*-VBTMAC)

Poly(AAm-*co*-VBTMAC) was made in the same reactor following similar procedures used to synthesize poly(AAm-*co*-DADMAC). DAMDAC was replaced with VBTMAC because the kinetics of DADMAC polymerization was too slow to allow a full conversion within the life time of the initiator used in these polymerizations. VBTMAC is much more reactive than DADMAC and can

be used to produce polymers of higher molecular weights. Chapter 4 compares these two compolymers in more details. Interestingly, VBTMAC was found to be even more reactive than AAm (please see Appendix D). For our purposes, we made two groups of copolymers: i) group A (broad CCD) was copolymers made in batch reactors where the reaction proceeded to full conversion, and group B (narrow CCD) was the copolymers made in batch reactors where the reaction proceeded to only small conversions ($\sim 3\%$). More on the chemical composition drift in batch reactors will be discussed in Section 3.3.3.

3.2.3 Copolymer Characterization

Proton nuclear magnetic resonance (^{1}HNMR) was used to measure copolymer composition, which were also estimated according to the kinetics model. D_2O was used as the solvent and ^{1}HNMR was performed at 27 °C using a Varian Mercury 400 MHz instrument. Peak identification and integration procedure were based on Suresha et al.[78] Copolymer molecular weights were measured by gel permeation chromatography (GPC, Agilent 1260 Infinity, equipped with 2 TSKgel G6000PW$_{XL}$ columns). The solvent (mobile phase) was an aqueous solution of 0.2 M $NaNO_3$. Polyethylene oxide standards with narrow molecular weight distribution, ranging from 580 to 5×10^6 g.mol^{-1} , were used to calibrate the GPC column. The GPC flow rate was 1.0 ml.min^{-1}, the injection volume was 100 μL and the sample concentration was 4 mg.ml^{-1}.

3.2.4 MFT Characterization

Dean-Stark extraction was used to quantify the solids fraction, moisture content, and bitumen in the MFT sample. In a typical experiment, a MFT was placed in a thimble on top of a boiling toluene in a round flask, connected to a condenser. The vapors of boiling toluene vaporized the water in MFT and then both got condensed in a condenser and fell into a trap with water on bottom and toluene on top. When the trap became full the remaining toluene would flow back through the thimble dissolving the bitumen down to the round flask. The process usually goes over night until the drops of toluene coming out of the thimble seems clear, which is an indication of complete separation of bitumen

from MFT. The MFT water is collected from the trap and weighted, the solids in the thimble was dried (to get rid of the remaining toluene) and weighted to calculate the solids content. The known volume of bitumen/toluene mixture was poured to a filter paper to measure the amount of bitumen, after drying the filter paper in vacuum oven to vaporize the toluene.

Atomic absorption spectroscopy (AAS) (VARIAN 220 FS) was used to quantify the concentration of major ions in MFT (Na^+, K^+, Ca^{2+}, Mg^{2+}).

3.2.5 Flocculation/Dewatering Test Methods

Before testing different polymer flocculants, the MFT needed to be diluted because its gel-like texture made it difficult to disperse the polymer in the suspension and might mask the effect of distinct polymer microstructures on flocculation and dewatering. The dilution method is important since it may affect water chemistry, which plays an important role in the colloidal stability of tailings. Unfortunately, there is no single accepted dilution method in the literature. The dilution water may be deionized water, process water, obtained by pressure filtering or centrifuging MFT, or pressure filtering the process water. For instance, Alamgir et al. obtained the dilution water by pressure filtering MFT, Klein et al. used process water,[80] Xu et al. pressure-filtered the process water,[9] and Rooney et al. and Reis et al. used deionized water.[10, 81] Since the objective of this study was to solely investigate the impact of polymer microstructure on MFT flocculation, not the effect of water chemistry on flocculation, a dilution method that was consistent, reproducible and did not change the pH of the MFT significantly was required. Deionized water was the option that best met these requirements.

The following polymer/MFT mixing procedure was used for all tests:

1) 100 g of MFT slurry (diluted to 5 wt% solids in deionized water for samples treated with poly(AAm-*co*-DADMAC) samples, and 3 wt% solids for those treated with poly(AAm-*co*-VBTMAC)) was added to a 250 ml glass beaker.

2) While the slurry was being mixed at 200 rpm or 400 rpm using a three-blade

impeller (5 cm diameter), the required amount of polymer was added to the beaker and the slurry was kept under mixing until the aggregates were formed.

3) At the end of this period, the sample was divided in two fractions: *i*) A small 7-ml aliquot of the mixed slurry was poured into a capillary suction time (CST) unit- using a Triton Electronics meter (Type 319 multi-CST) equipped with Triton filter paper 7 cm $\times$ 9 cm. The unit recorded the time taken for the sample to release water through designated points on the filter paper. *ii*) The remaining polymer/MFT suspension (93 mL) was transferred to a 100 ml graduated glass cylinder, and the change in height of the mudline was recorded over time. The initial slope of the mudline height versus time graph was recorded as the initial settling rate (ISR).

4) The slurry was allowed to consolidate in the cylinder for 24 hours, and a sample of the supernatant was taken for turbidity measurements by a Hach 2100 AN turbidimeter.

5) The same mixing procedure was repeated before measuring the specific resistance to filtration (SRF). First, the slurry was transferred to a 0.2-L pressure filtration apparatus equipped with a 12 cm^2 Triton filter paper. Filtration took place under an applied air pressure of 5 psig for 10 minutes. The mass of released water was recorded every 10 seconds using an analytical balance connected to a computer. The specific resistant to filtration is calculated using Equation (3.5),[8]

$$SRF = \frac{2\Delta P A^2}{c\mu_f} b \tag{3.5}$$

where ΔP is the applied pressure in Pa, A is the filter medium area in m^2, b is the slope of t/V against V (t is time and V is the volume of the collected water) in $s.m^{-6}$, c is solid concentration in the slurry in $kg.m^{-3}$, and μ_f is the filtrate viscosity in Pa.s.

Finally, aggregate formation was monitored by focused beam reflectance measurement (FBRM). Details of this technique are given in Chapter 5.

3.3 Results and Discussion

3.3.1 MFT Composition

Table 3.1 quantifies the composition of the MFT sample characterized by Dean-Stark and atomic absorption spectroscopy. The particle size distribution of the MFT sample is represented in Figure 3.1. A detailed description of MFT particle size measurement is given in Chapter 5. The pH of undiluted MFT and diluted MFT (with deionized water) was measured to be approximately 8. This shows that MFT is a relatively strong buffer system, and dilution with deionized water does not significantly affect its colloidal stability.

Table 3.1: Undiluted MFT sample composition

Analysis method	compound	value
Major ions (ppm)	Na^+	248.3
	K^+	18.4
	Ca^{2+}	11
	Mg^{2+}	22.1
Dean-Stark (wt%)	Water	59.8
	Solids	35.2
	Bitumen	2.9

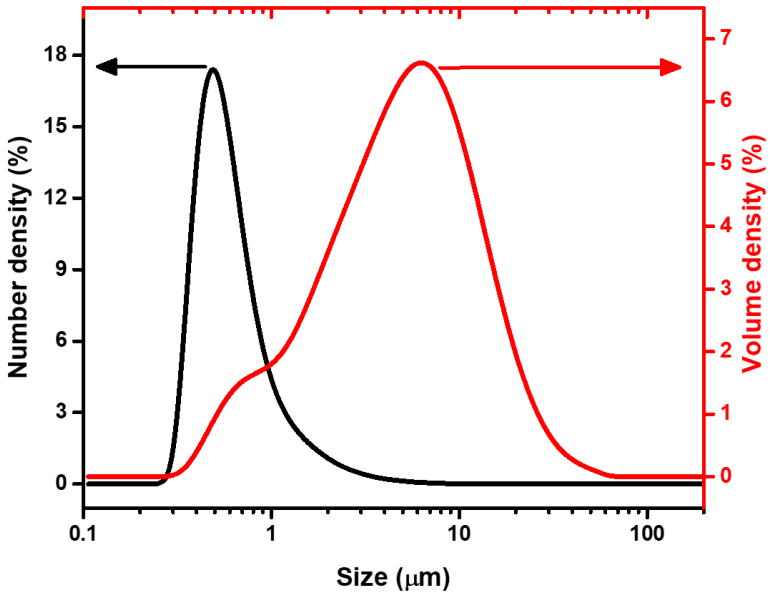

Figure 3.1: MFT particle size distribution

3.3.2 Poly(AAm-co-DADMAC): Average Chemical Composition and Molecular Weight Effect

Design of Experiment

A central composite design (Table 3.2) was selected to investigate the effect of average copolymer composition, molecular weight, and polymer dosage on MFT flocculation with copolymers of AAm and DADMAC. Since the central composite design needs the input variables to be independent of each other, copolymer molecular weight and composition could not be selected as input variables simultaneously because the molecular weight of a copolymer depends on its composition. Therefore, the initial initiator concentration (which affects copolymer molecular weight) was selected as the independent input variable in place of the average molecular weight. Equation (3.4) and data on Table 3.3 show the correlation between number average molecular weight and the initiator concentration. The output variables (responses) were initial settling rate (ISR), capillary suction time (CST), supernatant turbidity, and specific resistance to filtration (SRF). The resulting experimental data was analyzed with TIBCO Statistica Ultimate Academic Bundle (TIBCO® Data Science).

Table 3.2: Indepent variables in central composite design

Independent variables	Levels of coded variables				
	$-\alpha$	-1	0	1	$+\alpha$
	-1.68	-1	0	1	1.68
$\overline{F}_{AAm}$ (X_1)	0	0.24	0.5	0.83	0.99
$log[I]_0$ (X_2)	-4.15	-3.6	-2.8	-2	-1.45
dosage (X_3)	1.27	4	8	12	14.73

$[I]_0$: mol.L^{-1} & dosage: kppm (kilo parts per million)

A multiple linear regression model with quadratic and interaction terms correlated the behavior of the responses to the input variables,[82]

$$y_i = b_0 + \sum_{1}^{n} b_i X_i + \sum_{1}^{n} b_{ii} X_i^2 + \sum_{1}^{n-1} \sum_{i+1}^{n} b_{ij} X_i X_j \tag{3.6}$$

where y_i is the i^{th} predicted response, b_0 is a constant coefficient, b_i, b_{ii}, and b_{ij} are coefficients for linear, quadratic, and interaction terms, respectively, and X_i and X_j are the independent variables.

Table 3.3 lists the sequence of runs performed in this investigation based on a central composite design. It includes observations for all experiments, as well as molecular weights of copolymers made at different monomer fractions and initiator concentrations. Note that the tested copolymers cover a wide range of comonomer composition (0 to 0.99) and molecular weights (90 to 1819 kg.mol^{-1}), covering a much wider range of microstructures than done in previous studies.

Table 3.3: Design of experiment matrix

Run#	$\overline{F}_{AAm}$	$log[I]_0$	*dosage* (*kppm*)	ISR ($cm\ h^{-1}$)	CST (s)	turbidity (NTU)	b($s\ g^{-2}$)	SRF ($m\ kg^{-1}$)	M_n ($kg\ mol^{-1}$)
1	0.50	-1.45	8.00	19.65	8.6	0.593	0.339	7.3×10^{11}	185
2	0.24	-2.00	4.00	12.56	9.2	1.01	0.278	5.9×10^{11}	94
3	0.99	-2.80	8.00	148.51	84.4	18296	12.470	2.7×10^{13}	1819
4	0.83	-2.00	4.00	33.30	85	5993	1.790	3.8×10^{12}	1050
5	0.83	-2.00	12.00	51.87	10.7	72.7	0.041	8.8×10^{10}	1050
6	0.83	-3.60	4.00	78.62	76	5640	1.847	4.0×10^{12}	1450
7	0.24	-3.60	12.00	7.09	9.7	103	0.189	4.1×10^{11}	200
8	0.24	-3.60	4.00	24.02	9	3.47	0.298	6.4×10^{11}	200
9	0.83	-3.60	12.00	95.00	15.2	66.7	0.025	5.4×10^{10}	1450
10	0.50	-2.80	1.27	44.22	51.3	7776	4.530	9.7×10^{12}	280
11	0.50	-4.15	8.00	30.03	7.7	0.902	0.064	1.4×10^{11}	1324
12	0.00	-2.80	8.00	6.22	9.8	32.7	0.246	5.3×10^{11}	90
13	0.50	-2.80	8.00	26.97	7.8	29.4	0.064	1.4×10^{11}	280
14	0.50	-2.80	14.73	12.56	8.8	130	0.281	6.0×10^{11}	280
15	0.50	-2.80	8.00	13.10	6.4	3.26	0.077	1.7×10^{11}	265
16	0.50	-2.80	8.00	25.12	7.3	6.81	0.120	2.6×10^{11}	340
17	0.24	-2.00	12.00	7.64	6.4	345	0.333	7.2×10^{11}	94

Initial Settling Rate (ISR)

Model Development

A model based on only significant predictors was obtained after dropping out insignificant predictors through an analysis of variance study. The residuals were also analyzed to confirm the adequacy of the model according to the regression assumptions. To eliminate non-normality in the residuals, ISR was raised to the power of 0.25 ($ISR^{0.25}$) in Equation (3.6). Similar transformations were needed in the other responses. This is a common practice in regression analysis to find a function that satisfies the assumptions of the regression model.[82] Residuals were plotted versus predicted values to detect non-linearities and to examine the assumption of equal variances. Residuals were also plotted versus runs number (run sequence plot) to detect any systematic non-random pattern and to validate the condition of independency. Finally, normal probability plots of the residuals were inspected to check the normality of the residuals. These plots and the ANOVA analysis is available in D. Equation (3.7) is the final equation relating ISR to the statistically significant factors,

$$y_{ISR} = 2.237 + 0.52X_1 - 0.125X_2 - 0.10X_3 + 0.16X_2X_3 + 0.11X_1^2 \qquad (3.7)$$

where X_1 is $\overline{F}_{AAm}$, X_2 is $log[I]_0$ (X_2), and X_3 is polymer dosage.

Figure 3.2 shows the output of the ISR model. The initial settling rate increases when lower concentrations of the initiator are used (higher polymer molecular weights, all other factors being the same) for any given copolymer composition. In other words, copolymers with the same chemical composition but higher average molecular weights (see Equation (3.4)) settle MFT faster. This agrees with our understanding of the flocculation mechanism: the longer the polymer chains, the larger aggregates, and the faster their settling rates due to gravity. In addition, ISR increases for copolymers with higher fractions of acrylamide.

Is this increase in ISR due to changes in copolymer composition or in molecular weight? It is hard to decouple the two effects, since when the concentration of AAm in the copolymer increases, the polymer molecular weight also increases, even when the same initiator concentration is used (refer to Table 3.3). To understand the effect that the AAm fraction has in the settling rate of MFT independently of copolymer molecular weight, a regression model for ISR based on copolymer composition and the molecular weights of each copolymer at a given copolymer dosage was developed. Figure 3.3 illustrates how the initial settling rate depends on both variables. It may be proposed that polymers with higher AAm fractions and molecular weights capture large clay particles via the bridging mechanism, creating heavier aggregates that settle faster. One could conclude, therefore, that pure poly(AAm) would be the best flocculant for MFT. However, how one defines "best" is important. As it will be shown in the next section, copolymers with higher fractions of AAm produce supernatants with higher turbidities because many fines that are not captured by the high AAm-content copolymers. Similar conclusions can be drawn for CST and SRF, as will be described later.

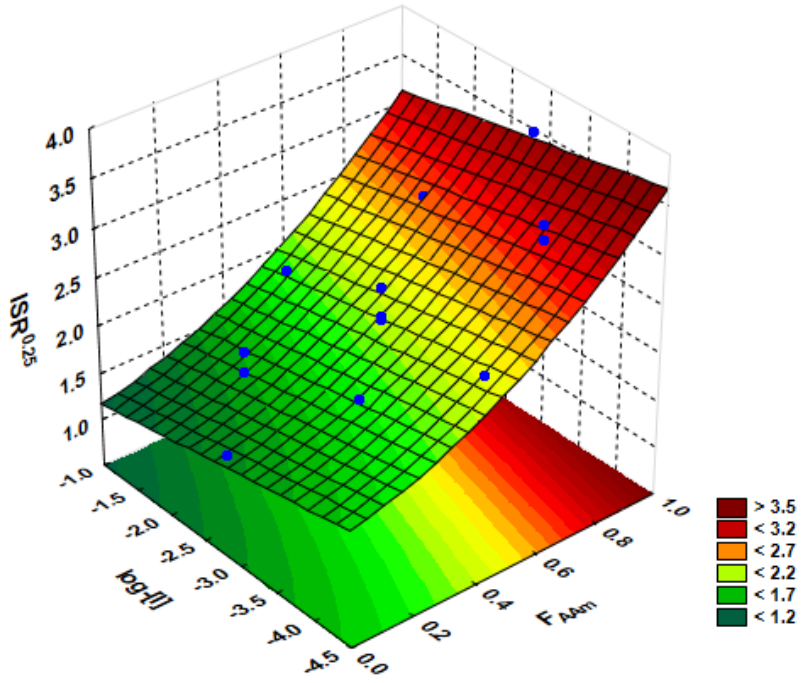

Figure 3.2: Surface response of ISR as a function of compolymer composition and initiator concentration- dosage= 4 kppm. ISR values are in cmh^{-1}

Capillary Suction Time (CST)

CST measurements needed to be modeled as $\frac{1}{\sqrt{CST}}$ to address non-normality in the model defined by Equation (3.6). The analysis of variance results showed that initiator concentration was *not* a significant variable in CST measurements. Since initiator concentration is related to the average copolymer molecular weight - see Equation (3.4) - we conclude that molecular weight does affect CST within the range of values covered in this study.

After rearranging the model based only on significant variables, CST becomes a function of dosage and copolymer composition as shown in Figure 3.4. Equation (3.8) is the final equation relating CST to the statistically significant factors,

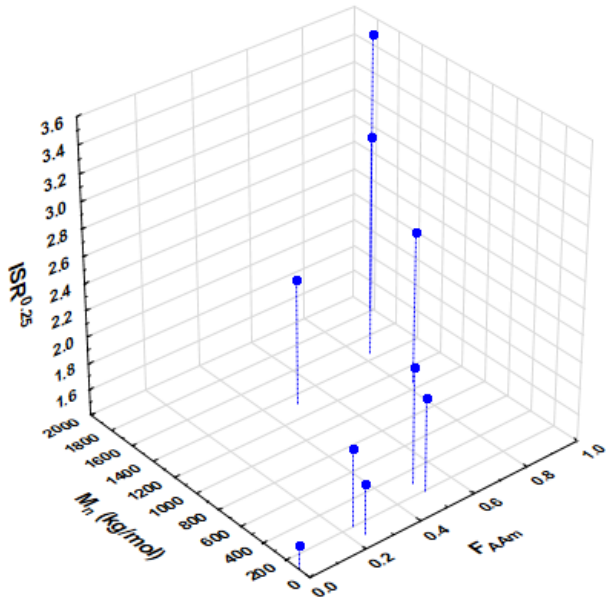

Figure 3.3: Scatter plot of ISR as a function of compolymer composition and number average molecular weight- dosage= 8 kppm. ISR values are in cmh^{-1}

$$Y_{CST} = 0.356 - 0.07X_1 + 0.05X_3 + 0.05X_1X_3 - 0.05X_1^2 - 0.04X_3^2 \qquad (3.8)$$

Figure 3.4 shows that, as one moves towards the center of response surface, the CST values decrease (faster MFT dewatering). Interestingly, when the AAm fraction in the copolymer increases, higher dosage are required to keep the CST low. This behavior suggests that charge density and copolymer hydrophobicity (explained by the fraction of AAm) is a dominant factor in determining the dewaterability of the aggregates, as opposed to a bridging mechanism imposed by the size of the polymer chains.

Supernatant Turbidity

The supernatant was separated from the flocculated MFT after it was allowed to settle for 24 hours. Analysis of variance initially showed that initiator concentration was not a significant predictor for supernatant turbidity. This conclusion was based on comparing calculated and tabulated F values (low p

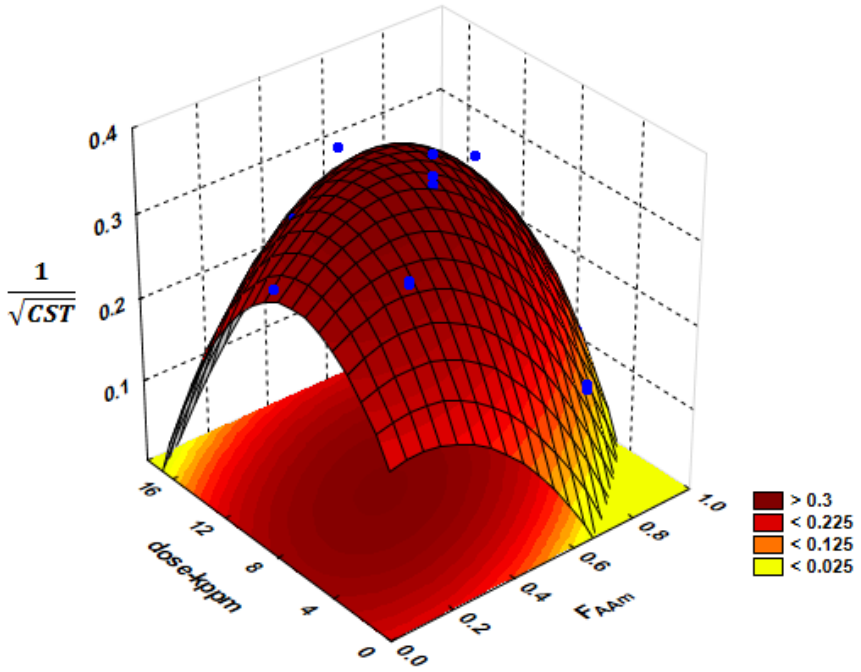

Figure 3.4: Surface response of CST as a function of compolymer composition and dosage. CST values are in sec

values, see Appendix D). When initiator concentration was dropped from the model, however, the residuals became non-normal and violated the regression assumptions. Therefore, the initiator concentration was reintroduced in the model. Such behavior may happen when the variable of interest (initiator concentration) is not an explanatory variable (molecular weight), but is rather correlated with it. Residual plots are shown in Figure 3.5a to 3.5d. Equation (3.9) is the final equation for turbidity as a function of the statistically significant coded factors,

$$\begin{aligned} Y_{turbidity} =& 1.517 + 0.70X_1 + 0.01X_2 - 0.35X_3 - 0.69X_1X_3 + 0.50X_1^2 \\ & - 0.21X_2^2 + 0.49X_3^2 \end{aligned} \tag{3.9}$$

Figure 3.6 shows how turbidity changes as a function of copolymer compo-

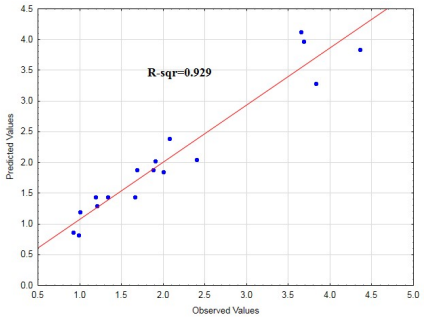

Figure 3.5a: Predicted vs. observed values for supernatant turbidity model

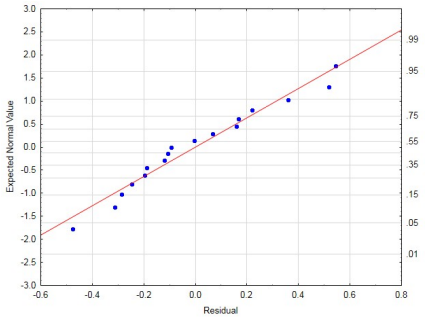

Figure 3.5b: Normal probability plot for supernatant turbidity model

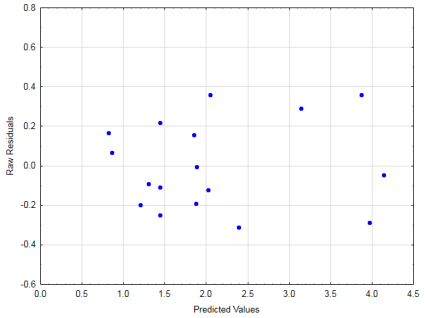

Figure 3.5c: Residuals vs. predicted values for supernatant turbidity model

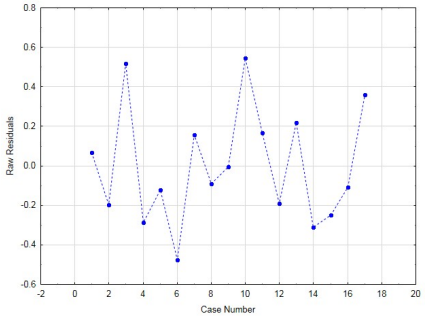

Figure 3.5d: Run sequence plot for supernatant turbidity model

sition at different polymer dosages. At low AAm fraction in the copolymer, the copolymer tends to capture more of the negatively charged fine particles, mainly due to charge neutralization, whereas in very high fractions of acrylamide (low DADMAC composition), the supernatant becomes highly turbid.

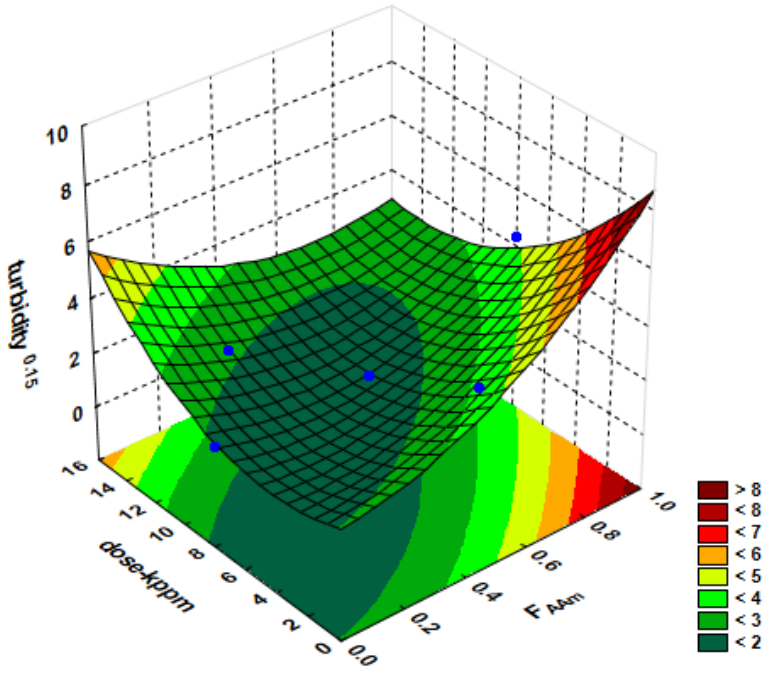

Figure 3.6: Surface response of turbidity as a function of compolymer composition and dosage

Specific Resistant to Filtration (SRF)

The resistant of the flocculated MFT to pressure filtration was also measured. According to Equation (3.5), the slope of t/V vs V (= b) was modeled based on the input variables, since all the other parameters are the same for all the runs. This parameter quantifies how fast aggregates dewater under pressure. The lower this value, the lower the specific resistant to filtration. Not surprisingly, the filtration experiment results followed the trends seen for the CST experiments: the initiator concentration (copolymer molecular weight) was not a statistically significant variable, and the SRF was mainly controlled by copolymer composition and polymer dosage. Equation (3.10) is the final empirical equation relating SRF to the statistically significant factors,

$$Y_{SRF} = 1.039 - 0.63X_1 + 0.56X_3 + 0.57X_1X_3 - 0.19X_1^2 - 0.2X_3^2 \qquad (3.10)$$

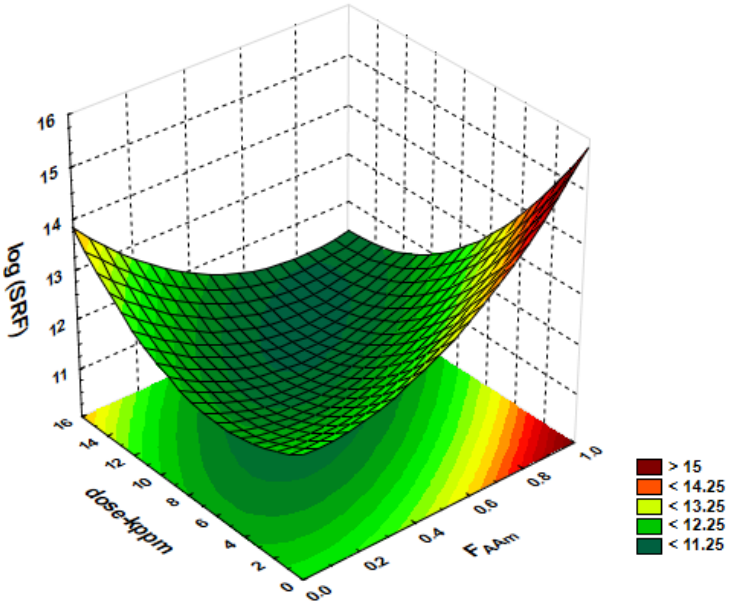

Figure 3.7: Surface response of SRF as a function of copolymer composition and dosage

As observed in Figure 3.7, as more AAm is present in the copolymer chain,

more water is retained in the aggregates, reducing water release and increasing SRF values. Not surprisingly, CST with SRF follow similar trends: in the CST experiments, the water trapped in the sediments flows out through capillary forces in the filter paper, whereas in the filtration experiment, air pressure is the driving force for sediment dewatering.

Table 3.4 summarizes how each copolymer property, and their interactions, affect flocculation/dewatering performance measured by different metrics.

Table 3.4: Significance levels

#	Predictors	ISR	CST	SRF	Turbidity
1	Copolymer composition	significant	significant	significant	significant
2	Average molecular weight	significant	—	—	significant
3	Polymer dosage	significant	significant	significant	significant
4	1 by 2	significant	—	—	—
5	1 by 3	significant	significant	significant	significant
6	2 by 3	—	—	—	—

3.3.3 Poly(AAm-*co*-VBTMAC): Chemical Composition Distribution Effect

Flocculants Design: Measurement and Simulation of Copolymer Microstructure

Table 3.5 lists the polymerization conditions used to make the two series of AAm/VBTMAC copolymers. Series A has a narrow CCD and Series B has a broad CCD.

The polymerization conditions listed in Table 3.5 were found based on changes of monomer/comonomer feed ratio and the initiator concentration until adequate values were obtained for molecular weight and chemical composition. Appendix D shows more characterization details for these copolymers. After finding the polymerization conditions that would make copolymers with identical average compositions and molecular weights in both series, the polymeriza-

Table 3.5: Polymerization conditions for narrow CCD samples (Series A) and broad CCD samples (Series B)

Polymerization conditions	Series A	Series B
Feed composition (f_{AAm})	0.8	0.59
Monomer concentration [M]/molL^{-1}	1	0.8
Initiator concentration [I]/molL^{-1}	2×10^{-3}	1.2×10^{-3}
Reaction time	5 min	20 h
Conversion (%)	$\sim$3	$\sim$99
Copolymer composition ($\overline{F}_{AAm}$)	60-62	60-62

tions for each series were replicated at least four times to exclude the possible errors from polymerization/polymer properties into our flocculation/dewatering experiments. Table 3.6 shows the properties of the copolymer flocculants made in these replicate polymerizations.

Table 3.6: Polymer properties obtained for narrow CCD samples (Series A) and broad CCD samples (Series B) in different replicates

Series - replicate no.	$\overline{F}_{AAm}$	M_w	PDI
A-1	0.61	1071000	2.8
A-2	0.60	1211000	3.8
A-3	0.60	1107000	3.6
A-4	0.62	1144000	3.4
B-1	0.61	1152000	3.9
B-2	0.63	1031000	4.1
B-3	0.60	1072000	4.7
B-4	0.61	1019000	4.2

Flocculants in Series B have slightly larger polydispersity indices (PDI) since these polymerizations proceeded to full conversions. The concentrations of the two comonomers decrease continuously with increasing conversion, leading to

the formation of shorter chains that broaden the MWD of the copolymer. In matching the weight average molecular weights (M_w) of the polymers in the Series A and B, we tried to approximate the high end of their MWDs (see Figure 3.8), since the flocculation process is mostly affected by the longer chains.

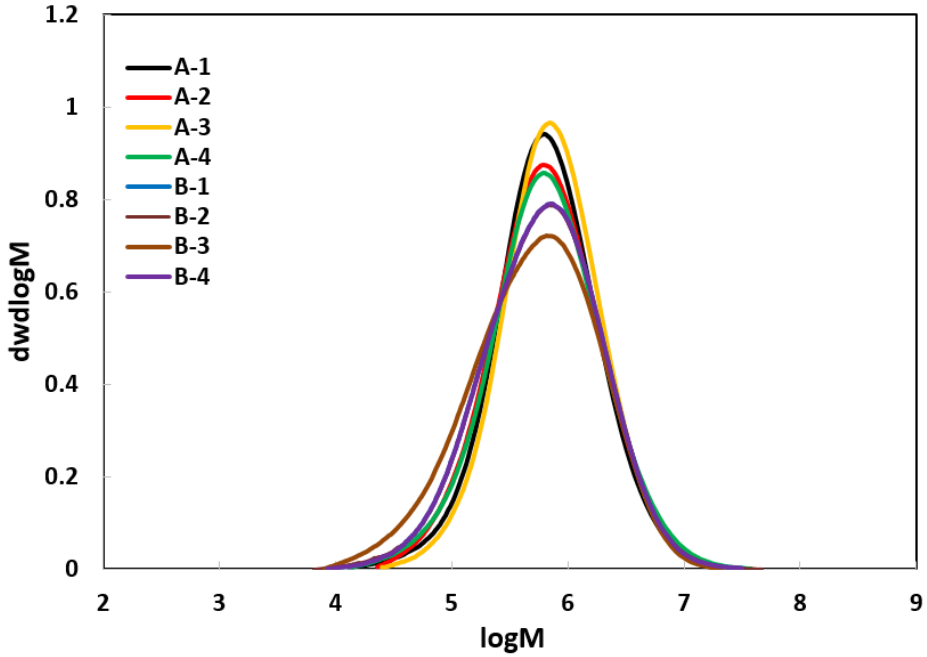

Figure 3.8: Molecular weight distribution of flocculants of Series A and Series B at different polymerization replicates

The reactivity ratios for the AAm/VBTMAC system was found to be r_{AAm}= 0.46 and r_{VBTMAC}= 2.48. The details of reactivity ratio estimation are given in Appendix D. Using these values and Equation (3.1) to Equation (3.3), one can simulate how the average chemical composition is changing in a batch reactor as a function of conversion (Figure 3.9). Polymerizations for both series started with 60 mol% AAm and 40 mol% VBTMAC. At the beginning of the polymerization, the fraction of VBTMAC in the copolymer was higher than 60 mol% because VBTMAC is more reactive than AAm. As a consequence, the *instantaneous* fraction of VBTMAC in the reator (f_{VBTMAC}) drops rapidly (composition drift), and the copolymer chains made at increasingly higher conversions (higher polymerization times) have lower and lower fractions of

VBTMAC (F_{VBTMAC}). Finally, the *cumulative* fraction of VBTMAC in the copolymer chains ($\overline{F}_{VBTMAC}$) is the fraction for the whole copolymer made after a given polymerization time.[83]

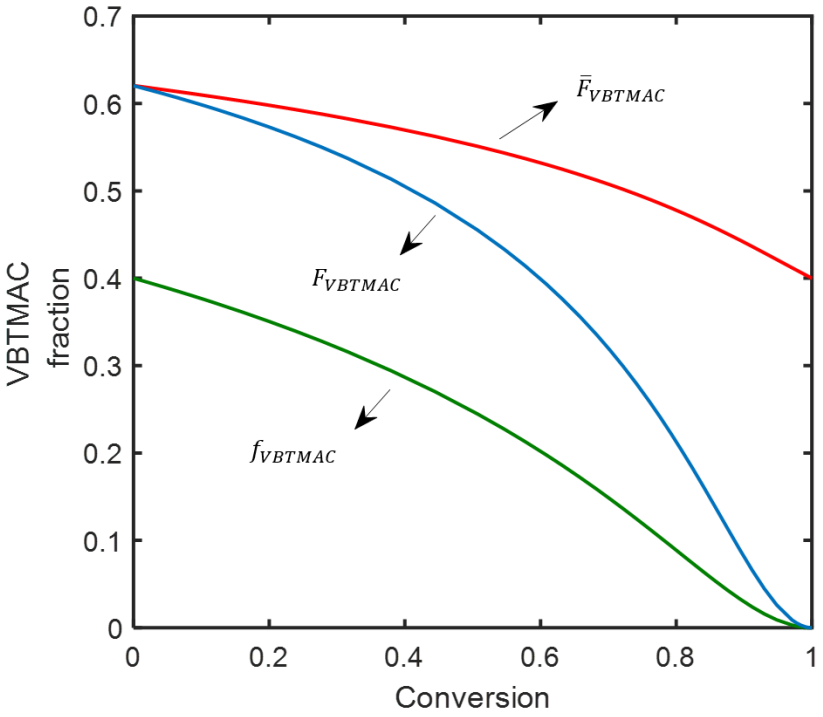

Figure 3.9: Simulation of chemical composition for poly(AAm-*co*-VBTMAC). VBTMAC fraction in the monomers mixture (green line), in the polymer chains produced at a given instance of time (blue line), and the cumulative fraction of VBTMAC in the whole polymer chains produced in the reactor until a given conversion x (red line)

To visualize the microstructural differences of the polymers in Series A and B, and how composition drift affects their distributions of chemical composition, the copolymerization of AAm/VBTMAC was modeled using the method of population balances [84]. Please see Appendix C.

Figure 3.10 to Figure 3.14 shows how the breadth of chemical composition distribution changes with conversion. Figure 3.10 represents the microstructure of a copolymer made after only 5% conversion, similar to that expected for copolymers made in Series A. As the conversion increases, both distributions broaden (Figure 3.10 to 3.12) due to composition drift and decreasing

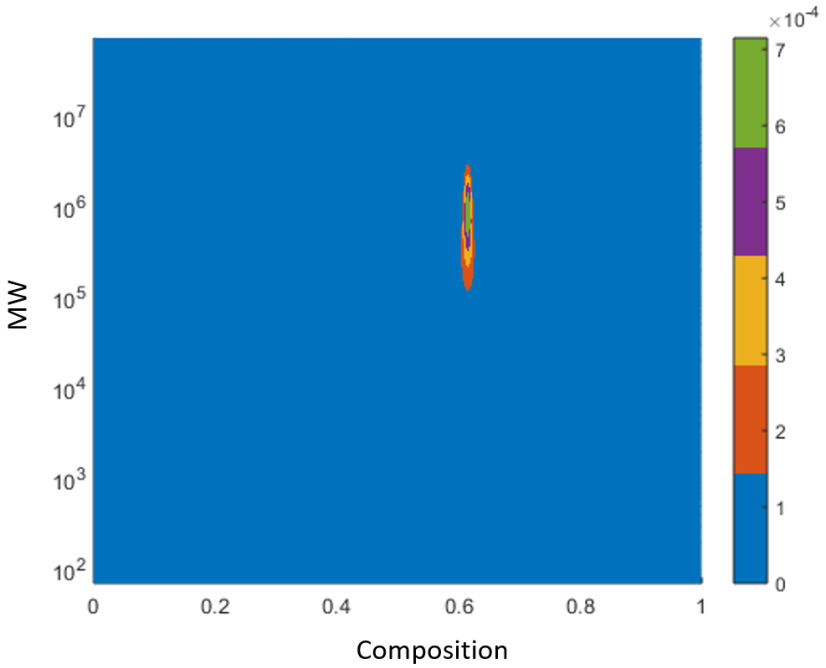

Figure 3.10: Example of a simulated bivariate distribution of molecular weight and chemical composition in a batch reactor at 5% conversion, $\overline{F}_{VBTMAC}$= 0.61, feed composition= 40% VBTMAC

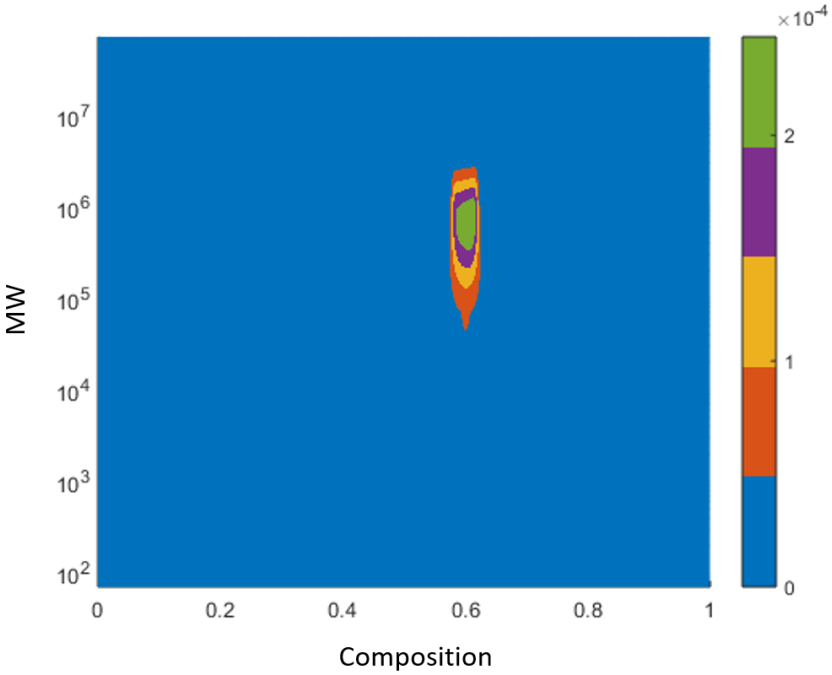

Figure 3.11: Example of a simulated bivariate distribution of molecular weight and chemical composition in a batch reactor at 18% conversion, $\overline{F}_{VBTMAC}$= 0.60, feed composition= 40% VBTMAC

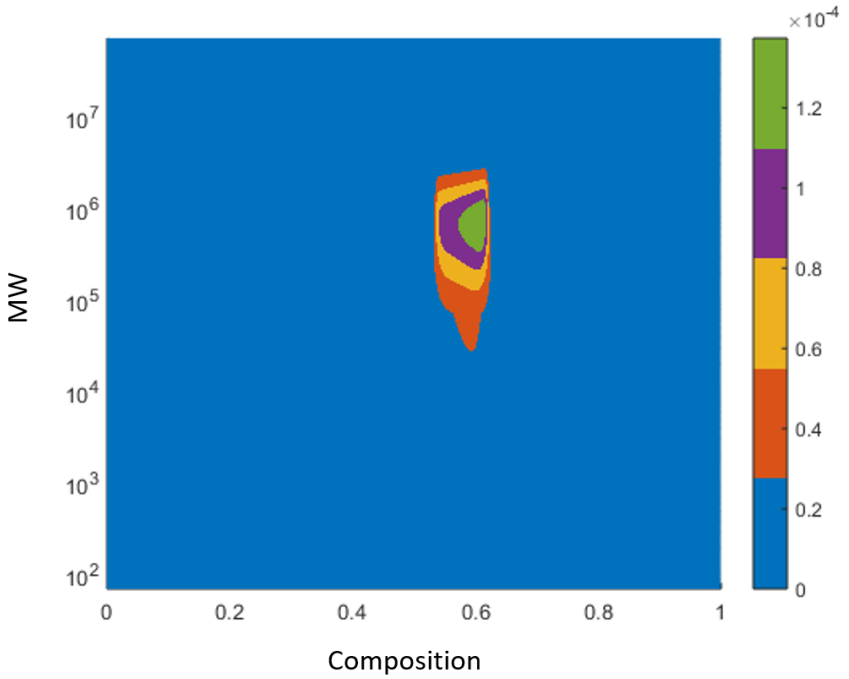

Figure 3.12: Example of a simulated bivariate distribution of molecular weight and chemical composition in a batch reactor at 32% conversion, $\overline{F}_{VBTMAC}$= 0.58, feed composition= 40% VBTMAC

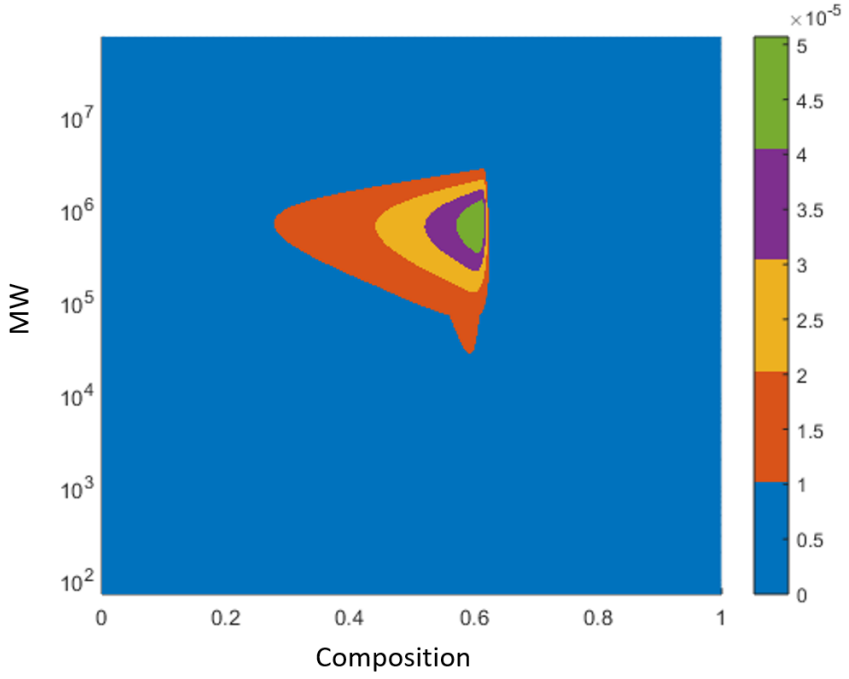

Figure 3.13: Example of a simulated bivariate distribution of molecular weight and chemical composition in a batch reactor at 87% conversion, $\overline{F}_{VBTMAC}$= 0.45, feed composition= 40% VBTMAC

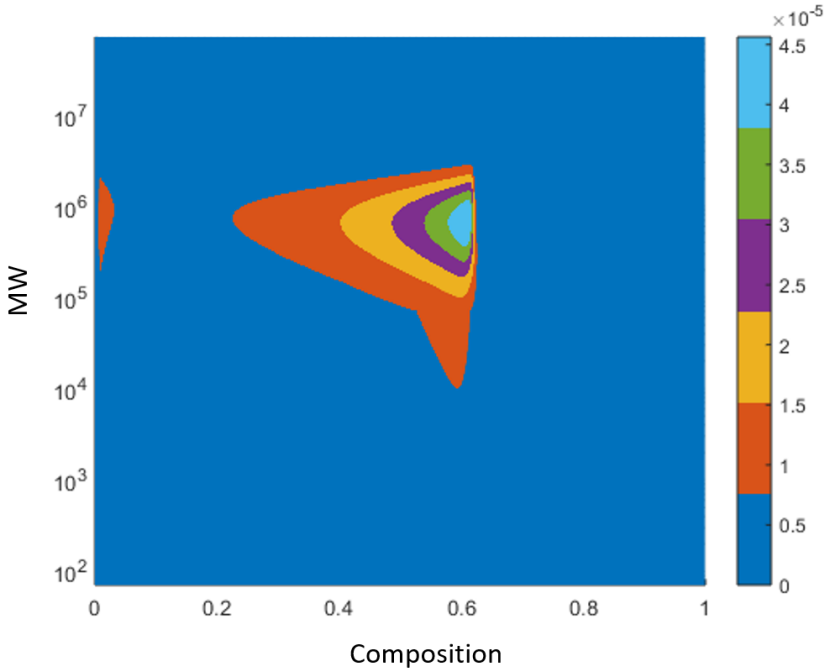

Figure 3.14: Example of a simulated bivariate distribution of molecular weight and chemical composition in a batch reactor at 99% conversion, $\overline{F}_{VBTMAC}$= 0.4, feed composition= 40% VBTMAC

comonomer concentrations. Finally, when the conversion approaches 100% in Figure 3.14, a separate population of pure polyacrylamide is formed, indicating that the more reactive comonomer, VBTMAC, was completely consumed during the copolymerization.

Settling Rate and Dewatering

Diluted MFT samples were treated with polymers from both series under mild mixing conditions to magnify the differences between the two flocculant series. Figure 3.15 and Figure 3.16 compares settling rates and CST measurements for MFT treated with flocculants from Series A and B. The reported results are averages of all replicates (i.e. A-1/A-2/A-3/A-4 for Series A).

At low (starving) dosages, flocculants from Series B (broad CCD, full conversion) led to the highest settling rates. It seems that at low dosages, in which case only a small fraction of the particle surfaces are covered with poly-

mer, chains with higher AAm fraction had a better chance of bridging the suspended particles. Although the overall charge of polymers in both series were the same, those with broader CCD containing chains with higher AAm fractions (compare Figure 3.9 with Figure 3.13) were more efficient in forming aggregates by the bridging mechanism.

Interestingly, flocculants in Series A outperformed those in Series B as the dosage was increased over 4,000 ppm. It may be hypothesized that for higher dosages, most of the particle surfaces are covered with polymer chains. Under these conditions, the AAm-rich chains that exist in Series B but not in Series A do not influence the formation of aggregates, and consequently the flocculation rates. For Series A (narrow CCD), all polymer chains have about the same chemical composition and help flocculate the sediments by a combined mechanism of charge neutralization and bridging , thus increasing the settling rate.

Figure 3.16 compares the CST of the samples flocculated with both polymer types. In low dosages, Series B led to faster dewatering (smaller CST values), which agrees with the formation of larger aggregates inferred from Figure 3.14. At higher dosages, however, both polymers in both series perform similarly. Thise may be attributed to the high dilution levels of the MFT samples: that is because the system was dilute and the aggregates were much larger than in the case of low dosages, the water was escaping the inter-aggregate structure with no restriction so any moderate difference in size would not make a difference in the final CST value.

Figure 3.17 compares the size (chord length) distributions of the aggregates formed after adding flocculants from Series A and B. These plots show the square-weighted chord length distribution when the largest aggregates were formed for each flocculant samples at different dosages. To ensure the accuracy of the results, FBRM tests were repeated for all four replicates in each series. Figure 3.17, however, only shows one representative example from each series and dosage. The FBRM plots confirm our hypothesis that at low dosages, polymers in Series B (broad CCD) formed larger aggregates, but this trend was reversed for dosages higher than 4,000 ppm, for which flocculants in Series

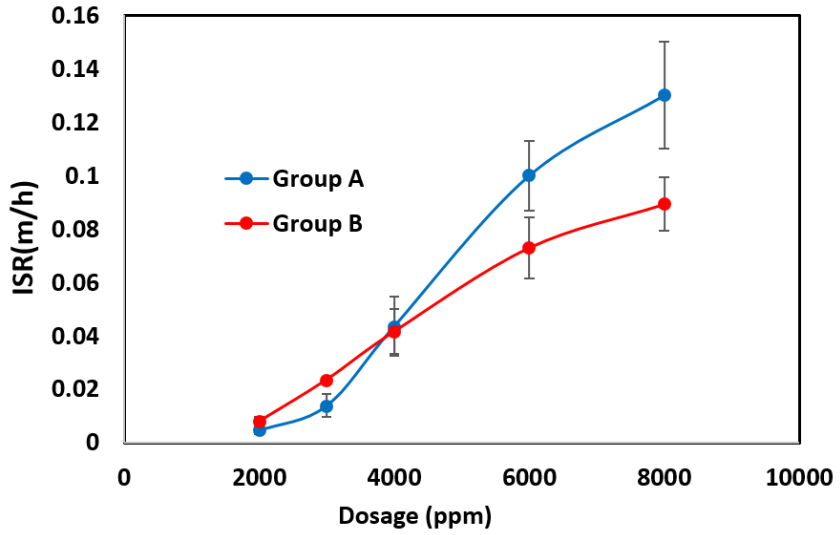

Figure 3.15: ISR of Series A (narrow CCD) and Series B (broad CCD) after flocculation of diluted MFT samples

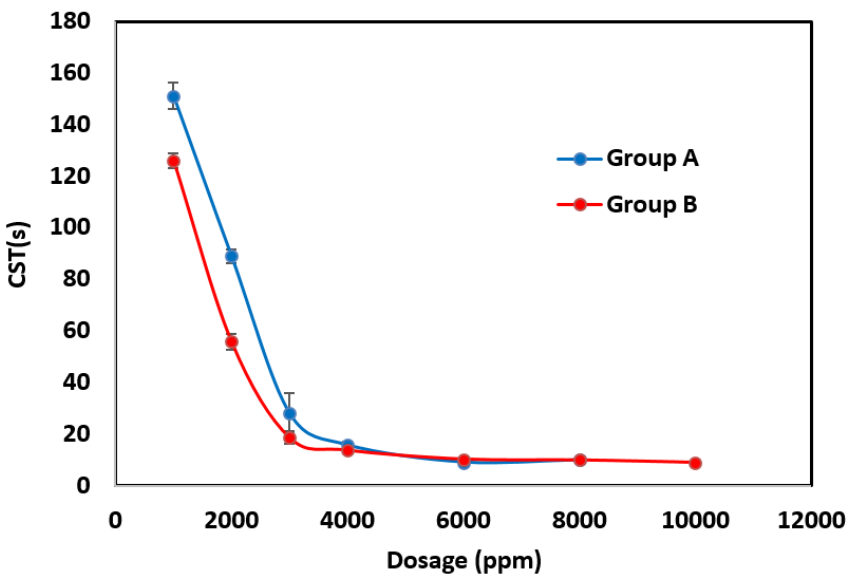

Figure 3.16: CST of Series A (narrow CCD) and Series B (broad CCD) after flocculation of diluted MFT samples

A (narrow CCD) made larger aggregates.

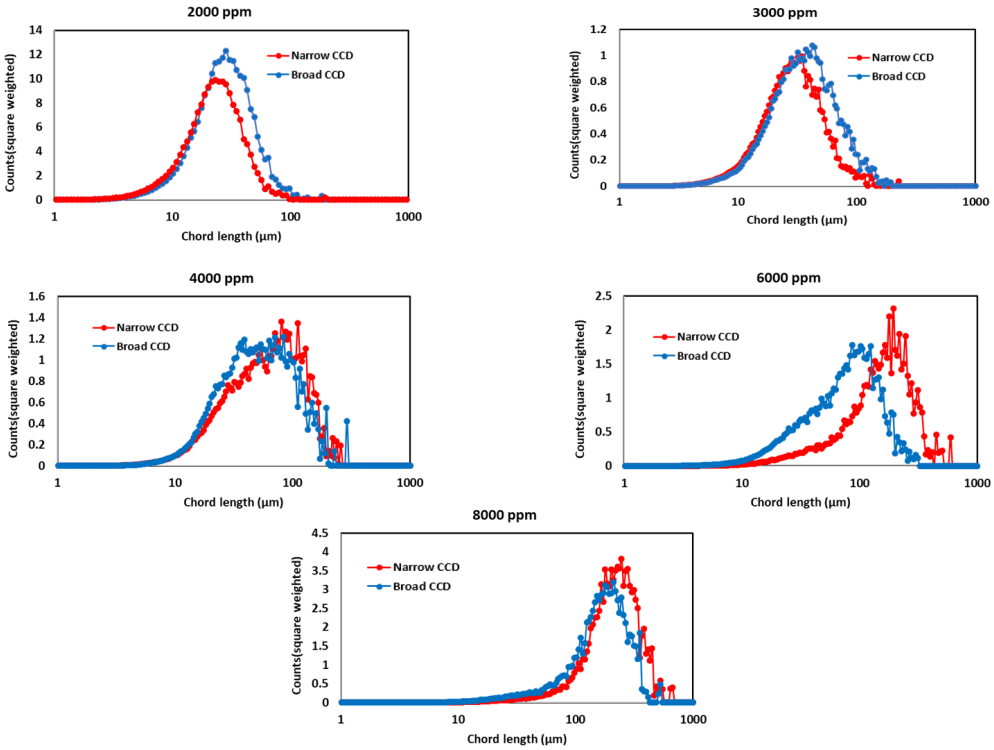

Figure 3.17: Chord length distribution of aggregates formed by flocculating MFT with Series A (narrow CCD) and Series B (broad CCD) at different dosages, measured by FBRM

3.4 Conclusions

Two cationic acrylamide copolymers were used to study the effect of average molecular weight, average chemical composition, and chemical composition distribution on the flocculation and dewatering of MFT. The average chemical composition was the microstructural property which significantly affected how the polymer interacted with the MFT particles in all methods used to assess flocculant performance.

The average molecular weight, however, did not significantly affect CST and SRF values (within the relatively wide range examined herein, 90 000 to 1 450 000 g·mol^{-1}, but it is conceivable that it would become a factor for much

lower molecular weights). The chemical composition distribution of the flocculants did not have a significant influence on their performance, but the small observed differences were, interestingly, dosage-dependent. Our results suggest that, depending on the polymer dosage and target settling rate, a narrow CCD polymer may be preferred or vice-versa. It is important to note that these findings should not be generalized to other flocculants (such as anionic or graft copolymers) without further investigation.

Chapter 4

Enhanced Dewatering of Oil Sands Tailings by a Novel Water-Soluble Cationic Polymer

This work investigates how poly(vinylbenzyl trimethylammonium chloride) (poly(VBTMAC)) flocculates oil sands mature fine tailings (MFT). The chains of this water-soluble cationic polymer contain pendant benzene rings that make them partially hydrophobic. The positive charges on the poly(VBTMAC) backbone neutralize the negatively charged MFT clays, while the hydrophobic benzene rings expel the water entrapped in the aggregates. VBTMAC can be polymerized to produce long chains (comparable to the anionic polyacrylamide) with fast polymerization rates. Focused beam reflectance measurement (FBRM) experiments showed that larger aggregates were formed using higher molecular weight poly(VBTMAC), which is an evidence of the bridging mechanism. The flocculation performance of poly(VBTMAC) was tested against commercially available anionic polyacrylamides for undiluted MFT by measuring the extent of dewatering in filtration tests and the rheological prop-

A version of this chapter has been submitted as V. Vajihinejad, S. Gumfekar, J. Soares, "Enhanced dewatering of oil sands tailings by a novel water-soluble cationic polymer" Environmental Science: Water Research & Technology, 2019

erties of the sediments. Our results showed that poly(VBTMAC) is a better flocculant in terms of ease of production, fast dewatering rate, and formation of sediments with high shear strength, but required substantially higher dosages to perform better than commercially available anionic polyacrylamides.

4.1 Introduction

Canada has the third largest oil sands deposits in the world, from which bitumen is extracted using large amounts of hot water and caustic. This extraction process generates fluid wastes called oil sands tailings.[85] Although oil sands deposits are a great energy resource, tailings pose serious environmental concerns for Canada. Typically, mature fine tailings (MFT) contain fine negatively charged clays (33 wt%), water (65 wt%), and fugitive bitumen (2-5 wt%).[86] Mature fine tailing ponds in Alberta occupy an area over 176 km^2, and this area continues to expand with the further exploration of oil sands.[9] Its water chemistry and solid components make it difficult for MFT to consolidate to levels required for land reclamation even after decades.

The main goals associated with MFT treatment are: *i*) to enhance the settling of solids, and *ii*) to recover the water trapped in the tailings. Over the last couple of decades, oil sands companies used technologies such as composite tailings, polymer-assisted flocculation, centrifugation, and freeze-thaw to address the issues associated with MFT treatment.[87] Polymer flocculants can destabilize clays in MFT using mechanisms such as bridging, charge patching, and charge neutralization, depending on their composition and physical properties.[87] Commercial flocculants are water soluble polymers, such as poly(AAm) and its ionic copolymers. Although ionic copolymers of acrylamide initiate the solid-liquid separation effectively, they generate sediments that retain a significant amount of water within their loose network, perhaps due to the limited adsorption of amide and carboxylic groups on the partially bitumen-coated clays. The hydrophilic chemistry of these groups makes the dewatering even harder. The majority of the existing commercial polymer flocculants cannot effectively promote fast release of clear water upon flocculation.

A recent review article has described the merits of combining chemical and mechanical dewatering techniques that include polymer-assisted flocculation plus filtration or centrifugation.[88]

Some researchers have addressed this limitation by copolymerizing hydrophilic with hydrophobic monomers, hoping that the hydrophobic groups incorporated into the copolymer backbone would cause the sediments to hold less water.[89, 90, 91, 92] Botha et al. modified polyethylene, a completely hydrophobic polymer, with polar functional groups to reach a balance between hydrophilicity and hydrophobicity in their novel flocculant.[11] Although the performance of this novel flocculant was adequate, the synthesis route to make functionalized hyperbranched polyethylene is complex and unlikely to be scaled up effectively. Thermosensitive polymers such as poly(N-isopropylacrylamide), poly(NIPAM), and its derivatives, have also been used to treat MFT.[47, 12, 93] By increasing the temperature, the conformation of poly(NIPAM) in aqueous solution changes from hydrophilic to hydrophobic. Although researchers obtained compact sediments with poly(NIPAM) by heating them above the hydrophilic-hydrophobic transition temperature, the cost involved in heating large volumes of MFT limits the use of these polymers.[94] Taking a different look at this problem, some researchers recently proposed a method to increase polymer hydrophobicity by degrading the flocculant within the sediments after flocculation.[81, 15] The synthesis steps to make these polymers, however, are complex and time-consuming.

Inspired by the positive effect of adding hydrophobic groups to the flocculant, and according to the results of our previous study,[86] we decided to use VBTMAC, to produce cationic partially hydrophobic homopolymers of with high molecular weight. This cationic polymer is soluble in water in the range of working concentrations for flocculation but also contains hydrophobic pendant benzene rings. The monomer, VBTMAC, also polymerizes faster than currently used similar cationic monomers such as DADMAC. Although poly(DADMAC) produces compact sediments with good dewaterability due to its charge density and partial hydrophobicity, propagation to higher molecular weights (in the range of millions) is limited because DADMAC polymerizes

comparatively slowly and is prone to chain transfer and termination reactions.[95, 96]To produce high molecular weight poly(DADMAC) at reasonable polymerization rates, DADMAC must be copolymerized with monomers such as acrylamide, which increase its hydrophilicity and leads to higher water retention in the sediments, as shown by our own previous results and results of other researchers.[97, 98]

To the best of our knowledge, this is the first time poly(VBTMAC) is used to flocculate oil sands tailings. In the present investigation, the molecular weight of poly(VBTMAC) and its dosage were varied to study their effects on the dynamics of aggregate formation and aggregate size. The ultimate dewatering and sediment shear strength of undiluted MFT was also tested. Our results support our hypothesis that poly(VBTMAC) is an effective flocculant for treating MFT.

4.2 Materials and Methods

Vinylbenzyl trimethylammonium chloride (VBTMAC) and initiators, 2,2′-Azobis(2-methylpropionamidine) dihydrochloride (V-50) and potassium persulfate (KPS), were purchased from Sigma-Aldrich and used as received. Coanda Research and Development Corporation in Alberta, Canada, supplied the MFT sample.

4.2.1 Synthesis of Poly(VBTMAC)

All poly(VBTMAC) samples were synthesized using homogeneous aqueous free radical polymerization at 50 °C in a 0.5 L glass polyclave reactor (büchiglasuster®) equipped with a temperature-controlled jacket, impeller, and a nitrogen inlet. In free radical polymerization, polymer molecular weight is inversely proportional to initiator concentration. The concentration of VBTMAC was kempt constant at 0.5 M for all the polymerizations but initiator concentration was changed to make poly(VBTMAC) flocculants of different molecular weights. Table 4.1 lists initiator concentrations and the corresponding poly(VBTMAC) molecular weights. Figure 4.1 shows our polymerization setup and the chemical structure of the repeating unit of the polymer.

In a typical polymerization, a 2 M stock VBTMAC solution of monomer was prepared with deionized (DI) water at room temperature. The initiator solution was also prepared with deionized water in small vials and purged with nitrogen. A volume of 150 ml of 0.5 M monomer solution in DI water was introduced in the reactor; the reactor was purged with nitrogen for 45 min and then heated to 50 °C by circulating hot water into the jacket. While the reactor was still being purged for additional 15 minutes, the desired amount of initiator solution was added to the reactor, and the polymerization was allowed to proceed for at least 20 hours to ensure full monomer conversion.

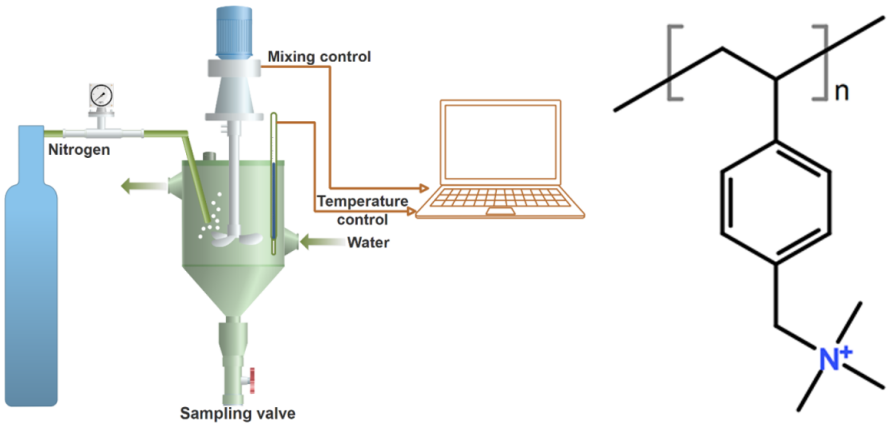

Figure 4.1: Experimental polymerization setup for VBTMAC and chemical structure of the repeating unit of poly(VBTMAC)

4.2.2 Characterization of Poly(VBTMAC) and MFT

The molecular weight of all polymers were measured by gel permeation chromatography (GPC) (1260 Infinity Multi-Detector GPC/SEC System, Agilent Technologies). The GPC system includes three detectors: viscosity, refractive index, and light scattering. Two columns (TKS gel G6000PW XL-CP, designed for cationic polymers) connected in series were used for better resolution. The GPC was calibrated using polyethylene oxide standards provided by Agilent Technologies. Water containing 0.3 M sodium nitrate and 0.01 M monosodium phosphate was used as a mobile phase for the analyses. Table

4.1 shows the molecular weight analyses of poly(VBTMAC) synthesized in this study. The letters L, M, H refer to low, medium, and high molecular weight samples respectively.

Table 4.1: Molecular weight analyses of poly(VBTMAC)

Polymer	[M]/molL^{-1}	[I]/molL^{-1}	M_w/gmol^{-1}
poly(VBTMAC)-L	0.5	0.036	250000
poly(VBTMAC)-M	0.5	0.001	750000
poly(VBTMAC)-H	0.5	0.000028	1700000

The molecular weight distribution of the high molecular weight anionic polyacrylamide was measured by field flow fractionation (FFF) instead of GPC to obtain a better separation resolution. The experimental setup for the FFF consisted of an AF4 instrument (AF2000, Postnova Analytics, Landsberg, Germany), and a multi-angle light scattering detector and a refractive index detector. The experiments were performed at room temperature. The mobile phase was a 0.1 M NaCl solution. The detectors were calibrated using bovine serum albumin (BSA) with molecular weight of 63900 and then tested using two PEO standards with molecular weights of 2×10^5 and 4×10^6.

Coanda Research provided the MFT analysis (Table 4.2). Focused beam reflectance measurement (FBRM) quantified the size of aggregates by measuring their chord length. More details of the FBRM analyses are given in Chapter 5.

Table 4.2: MFT sample composition

Analysis method	compound	value
Major ions (ppm)	Na^+	938
	K^+	16.1
	Ca^{2+}	24.4
	Mg^{2+}	10.6
Dean-Stark (wt%)	Water	65.5
	Solids	33.3 (82.3% clays)
	Bitumen	1.2

4.2.3 MFT flocculation and Dewatering Tests

Low Solids (Diluted) MFT

Focused beam reflectance measurement was used to measure the size of MFT aggregates treated with poly(VBTMAC)s of different molecular weight, to understand the flocculation mechanism, and the quantify the impact of mixing on dewatering metrics. FBRM experiments were carried out in diluted MFT to avoid fouling of the FBRM probe by bitumen (which often happens in high solids MFT is analyzed with this method), and to minimize the polymer dispersion effect in the suspension.[99] Each flocculation used 200 mL of a 5 wt% solids slurry, made by diluting MFT with deionized water. The MFT suspension (in the presence of the FBRM probe) was mixed at 300 rpm using a 45 degree pitched blade impeller (4 blades, 4.8 cm diameter) and the desired amount of the flocculant was added to the suspension at once.

A light microscope (ZEISS AXIO Scope A1) measured the fractal dimension of aggregates at different stages of flocculation. A small aliquot of flocculated MFT was diluted in water (about 25 times dilution), and upon a gentle mixing, a small droplet was placed onto the microscope slide for observation. A minimum of 50 magnified screen shots (in 5 different batches) were captured.

The area (A) and perimeter (P) of the aggregates were measured by an image analysis software (Image J) to calculate the perimeter fractal dimension, d_{PF}, using the following relation, [100]

$$A \propto P^{(2/d_{PF})} \tag{4.1}$$

High Solids (Undiluted) MFT

The primary objective of this set of experiments was to find the ultimate dewatering of MFT using a poly(VBTMAC) flocculant selected from the low solids tests and to compare the results on a fair basis with results obtained with a commercially available anionic polyacrylamide flocculant. The polymer solutions were prepared using pond effluent water received from our industry partner, to ensure it had the same water chemistry of the MFT. Polymer solutions were prepared so that their viscosities matched that of the MFT to maximize mixing efficiency. To reach this specification, the poly (VBTMAC) solution concentration was 0.5 wt% and that of anionic polyacrylamide (A-poly(AAm)) was 0.1 wt%. To facilitate the flocculation by A-poly(AAm), Ca^{2+} was added to MFT from a calcium chloride solution in pond effluent water prior to flocculation.

The flocculation was carried out in a 250 ml glass beaker stirred with a T-shape overhead mixer. The polymers were added drop-wise to better disperse in MFT, and the mixing continued until the largest aggregates were formed, as determined by visual assessment. This dosing method allowed for the simultaneous determination of the optimum dosage and optimum mixing time. The flocculated MFT was then transferred to an air-pressurized filtration cell (Figure 4.2) and allowed to dewater for 4 minutes under 5 psig. After that the solids content of the cake was measured by drying it in an oven. This procedure was repeated four times to determine the experimental error. All the four cakes were then combined in a single mass and transferred back to the filtration cell, which was exposed to an air pressure of 5 psig for another 4 minutes. The resulting thick cake was tested for its shear strength using a rheometer (Brookfield Rheometer) or a vane shear apparatus, depending on

its strength.

Figure 4.2: The impeller and the air-pressurized filtration unit used for mixing and dewatering of MFT.

4.3 Results and Discussion

4.3.1 Polymerization Kinetics

The polymerization kinetics of VBTMAC and DADMAC were compared to demonstrate the advantages of replacing the more commonly used DADMAC with VBTMAC. Both poly(VBTMAC) and poly(DADMAC) have similar cationicities. Abdollahi et al. had previously reported on the polymerization kinetics DADMAC. Therefore, the polymerization kinetics of VBTMAC were measured for the exact same conditions used by Abdollahi et al.[101]

Figure 4.3 shows that the polymerization rate of VBTMAC is significantly faster than DADMAC. At low conversions (about 20%), we also compared the

molecular weight of poly(DADMAC) and poly(VBTMAC), synthesized under the same conditions, to be 2.5×10^5 and 1×10^6, respectively.

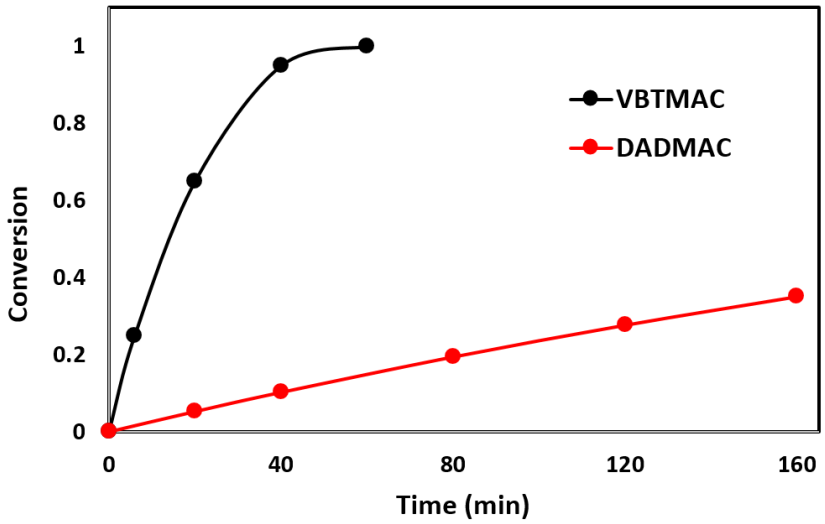

Figure 4.3: Kinetics of VBTMAC (T=50 °C, [M]=1.0 M, [I]/KPS= 0.03 M), and DADMAC (T=50 °C, [M]=1.0 M, [I]/KPS= 0.03 M). DADMAC kinetics results is obtained from the work of Abdollahi et al.[101]

4.3.2 Aggregate Formation and Dewatering

Figure 4.4 shows the real-time evolution of aggregate size at different dosages of poly(VBTMAC)-M. As the dosage increased, the aggregates formed quickly, grew to their largest size, and subsequently approached their final size. Increasing the dosage of poly(VBTMAC)-M up to 7000 ppm increased the maximum aggregate size, but substantially higher dosages (i.e 11000 ppm) reduced their maximum size. This observation is attributed to polymer overdosing causing steric and electrostatic repulsion among the aggregates, as reflected by ISR and CST measurements discussed in the next section.

The inset graph of Figure 4.4 magnifies the first 20 seconds after the polymer was added to the MFT, revealing how the polymer flocculates MFT at different dosages. The curves become steeper as the polymer dosage increases, except at 11000 ppm. The slopes of these curves are proportional to the rate of adsorption of polymer onto clay surfaces, leading to aggregate formation. This

process involves neutralizing the negative charges on the clay surfaces with the cationic charges on the polymer chains, and then bridging clays as the non-adsorbed polymer segments (loops and tails) attach to the bare surfaces of other colliding clay particles.

When the polymer dosage was raised to 11000 ppm, however, the cation density around the clay particles increased and hindered further electrostatic attraction between clays and polymer chains. A similar behavior was observed for the high and low molecular weight poly(VBTMAC) samples. Adsorption of polymer onto clays in a sheared suspension is a transport-limited process wherein the adsorption time decreases as the polymer dosage increases, provided that the surface coverage is low and that polymer-clay collisions are not hindered by the presence of excess polymers (such as overdosing at 11000 ppm in these experiments).[102]

According to Gregory and Barany, the adsorption rate of polymer onto clays can be viewed as the rate of loss of polymer from the bulk phase.[28] Equation (4.2) quantifies the characteristic adsorption time at a given concentration of solid particles,

$$t_{ads} = \frac{-ln(1-\psi)}{k \times N} \tag{4.2}$$

where ψ is the fraction of total polymer needed to adsorb onto the clay surface to induce the flocculation, k is the collision rate coefficient between polymer molecules and clay particles per unit time, and N is the initial number of particles per unit volume in the suspension. It is evident from the inset graph of Figure 4.4 that increasing polymer dosage decreased the characteristic adsorption time, which is explainable by Equation (4.2). The required polymer fraction, ψ, decreases with increasing polymer dosage, while the collision rate coefficient k remains practically constant because the viscosity of suspension does not change significantly with polymer dosage.

Figure 4.5 shows the evolution of aggregates size at a constant dosage of 7000 ppm for poly(VBTMAC) flocculants with different molecular weights. The dosage of 7000 ppm was chosen because it was the best dosage of all poly(VBTMAC) experiments. The time required for the sharp increase in

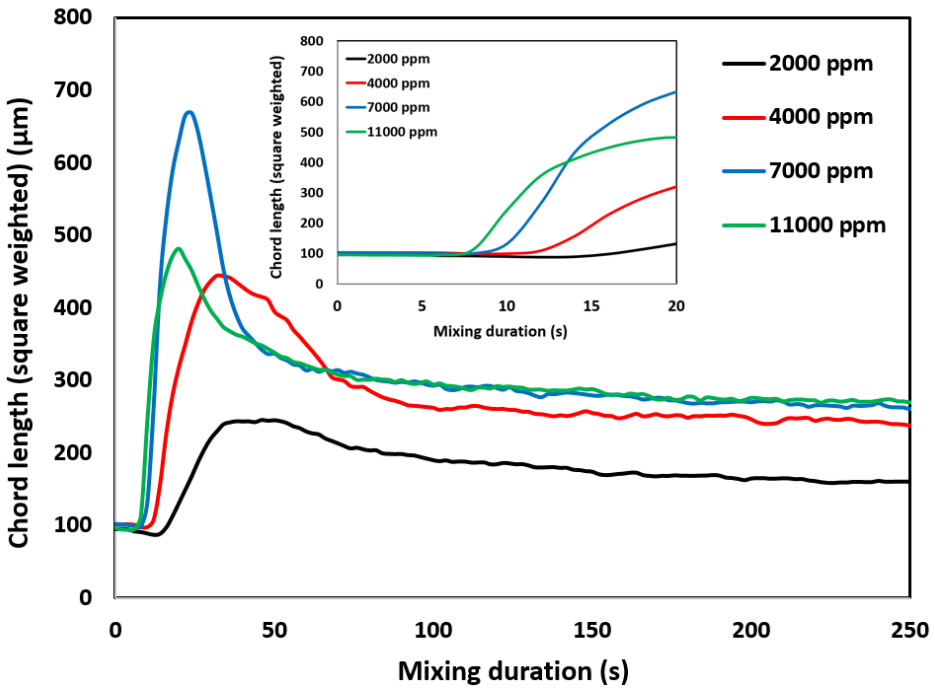

Figure 4.4: Real-time evolution of floc size measured using different dosages of poly(VBTMAC)-M. The insert of the figure shows the response up to 20 seconds

aggregate size (t_{ads}) increased for polymers with higher molecular weight, implying that shorter chains are easier to adsorb on particles than longer chains (likely due to mass transfer limitations). The increase in aggregate size with polymers of higher molecular weights shows that the flocculation of MFT by poly(VBTMAC) occurs due to a combination of charge neutralization and bridging mechanism.

To further prove that the bridging mechanism was important in this system, MFT was flocculated with pure VBTMAC (MW= 211.73 g.mol^{-1}) using a dosage of 7000 ppm (same cationic density as the poly(VBTMAC) experiments). Much smaller aggregates were formed when the polymer was replaced by its monomer because the monomer could only neutralize the clay charges, but not bridge the clay particles (4.5). It is likely that when poly(VBTMAC)-H (the flocculant with the highest molecular weight) is added to the MFT, it neutralizes the negative charges on the clay particles via electrostatic interac-

tions within a short time interval, but the polymer chains do not completely flatten/relax onto the clay surface; they rather extend part of their segments into the solution, making loops and tails. These positively charged loops and tails attract and bridge other negatively charged clay particles in their surroundings.

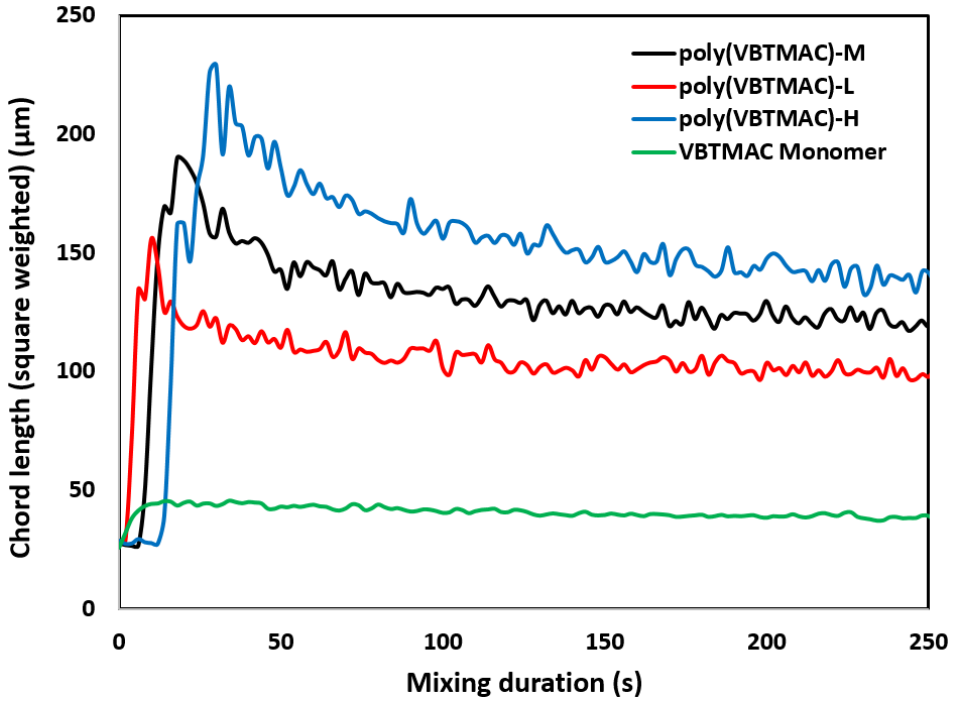

Figure 4.5: Real-time evolution of average aggregate size measured using 7000 ppm of poly(VBTMAC)-H, poly(VBTMAC)-M, poly(VBTMAC)-L, and VBTMAC monomer.

It is also important to understand the reason behind the gradual drop in aggregate size after reaching its largest peak value. This behavior is observed when bridging flocculation is involved and commonly attributed to several reasons: *i)* restructuring of aggregates, induced by repeated aggregation/fragmentation imposed by hydrodynamic shear forces, which leads to aggregates having the same number of primary particles but a less porous and more compact structure (lower effective hydrodynamic size), *ii)* irreversible aggregate fragmentation due to polymer chain scission at very high shear rates, and *iii)* polymer chain reconformation and relaxation on the surface of the particles, leading to

less available surface area and less effective bridging.[103, 104, 105]

It is unlikely that chain scission happens to any appreciable degree in this system because of the low shear rates of 300 s^{-1} used to mix MFT and polymer flocculants. Aggregate restructuring is also improbable as the size of the aggregates decreased within a short period of time.

The fractal dimension at different times during flocculation was measured to confirm aggregate restructuring was negligible, since restructuring is associated with an increase in fractal dimension over time.[104, 105] Table 4.3 shows 2D fractal dimensions measured by image analysis at different times during MFT flocculation with poly(VBTMAC)-H dosed at 7000 ppm. The fractal dimension does not change significantly. Therefore, it seems that polymer chain reconfirmation and relaxation on the surface of particles was responsible for the observed change in aggregate size. As shown in Figure 4.5, aggregates formed by VBTMAC do not change sizes after reaching their largest size, which further supports this hypothesis.

Table 4.3: Perimeter fractal dimension of aggregates in time (7000 ppm poly(VBTMAC)-H)

Flocculation time	6 s	12 s	18 s	60 s	240 s
D_{fp}	1.24	1.45	1.21	1.21	1.35

4.3.3 Ultimate Dewatering: A Comparison with Anionic Polyacrylamide

A series of experiments was designed to compare the ultimate dewatering of high-solids MFT flocculated with poly(VBTMAC) and a typical industrial standard linear anionic polyacrylamide (Ref-PAM). Figure 4.6 depicts the molecular weight distribution of poly(VBTMAC) and Ref-PAM. Field flow fractionation (FFF) had to be used for these analyses because GPC cannot accurately measure the molecular weight distribution of Ref-PAM. More de-

tailed discussion on the limitations of GPC and on the working principles of FFF can be found elsewhere.[27]

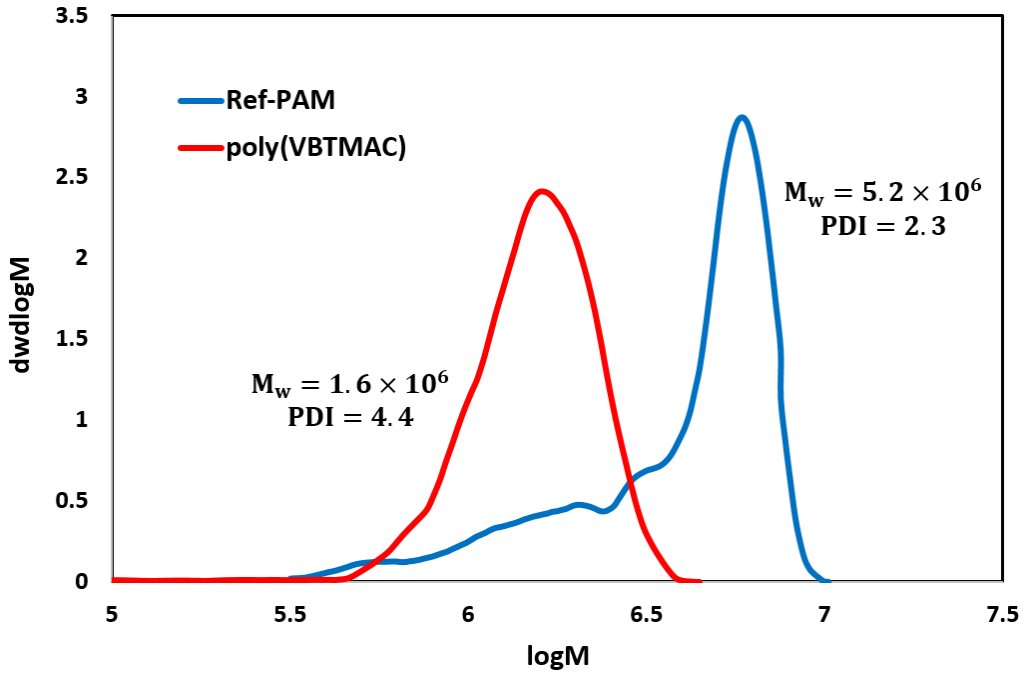

Figure 4.6: Molecular weight characterization of poly(VBTMAC) and Ref-PAM, measured by field flow fractionation.

Capillary suction time was not used to measure the dewatering of these high-solids tests its reading was affected by the large size of the formed aggregates, especially when Ref-PAM was used. Large aggregates are difficult to place uniformly in the CST cell, which gives erroneous readings. Therefore, filtration was selected as the alternative metric. In all flocculation tests, the mixing intensity was kept as low as possible to generate uniform mixing while minimizing aggregate breakage. The mixing rate for poly(VBTMAC) was 200 rpm and for Ref-PAM was 300 rpm. Mixing continued until the largest aggregates were formed for each flocculant. This is a common practice in field trial tests of flocculants.

The results depicted in Table 4.4 shows the best performance of each flocculant at their corresponding optimum dosage and mixing conditions.

Table 4.4: Dewatering performance for the flocculation of whole MFT using poly(VBTMAC)(PVB) and Ref-PAM

Flocculant	Dosage/ppm (Ca^{2+}+polymer)	Final solid%	Shear strength/kPa
poly(VBTMAC)	1400 + 8000	50.5±1.6	19.7±2.6 (55% solids)
Ref-PAM	1400 + 1000	42.5±3.8	4.2±0.8 (56% solids)
Ref-PAM + poly(VBTMAC)	1400 + 450 + 1900	53.9±0.9	10±0.7 (57% solids)

Sediments flocculated with poly(VBTMAC) had higher solid contents and significantly higher shear strength. The optimum dosages leading to such enhanced performance, however, is notably higher for poly(PVBTMAC), which may make this polymer less attractive for dewatering tailings at large scales. Lu et al. showed that combining cationic and anionic flocculants enhanced the flocculation of tailings.[7] Inspired by their work, and hoping to reduce the poly(VBTMAC) dosage, a dual system was used where the Ref-PAM was added first, followed by poly(VBTMAC). In this case, the final solids content of the sediments was higher than when either flocculant was used alone, and the dosages of both flocculants were reduced substantially. It may be argued that the overall polymer dosage of the dual flocculant (2350 ppm) is still higher than for the Ref-PAM (1000 ppm), but this slight increase in dosage may be worthwhile considering that the solids content increases from 42.5% to 53.9% and the shear strength of the sediments more than doubles, changing from 4.2 kPa to 10 kPa.

Figure 4.7 shows a photo of the MFT cakes made with different flocculants after being filtered for only 4 minutes at 10 psig. The photos show the marked difference between the sediments generated only with Ref-PAM and those using poly(VBTMAC). Tailings treated with Ref-PAM have a gel-like texture, while the those treated with poly(VBTMAC), alone or in combination with Ref-PAM, exhibit a much more compact, dry, and soil-like texture.

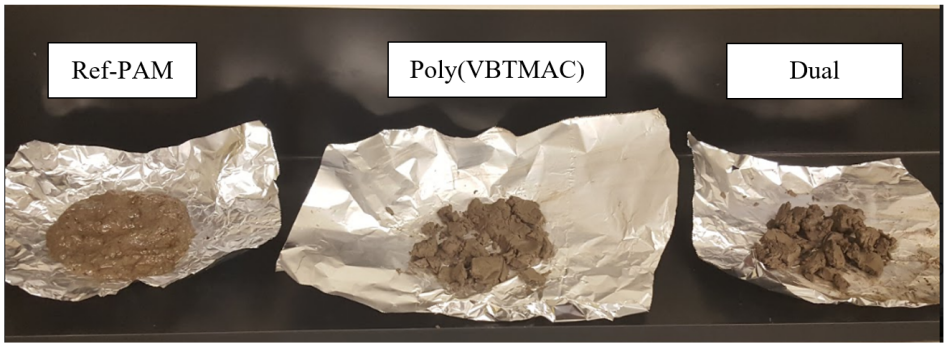

Figure 4.7: Flocculated MFT cakes by different polymers after being filtered for 4 minutes at 10 psig

4.4 Conclusion

This investigation introduced a new polymer flocculant for the enhanced dewatering of oil sands mature fine tailings. The monomer VBTMAC polymerizes rapidly in aqueous free radical polymerization to produce relatively high molecular weight poly(VBTMAC) that appears to be a good candidate for the flocculation of MFT. Focused beam reflectance measurement investigations showed that the flocculation mechanism was bridging induced by charge neutralization of VBTMAC on clay surfaces.

Poly(VBTMAC) flocculate undiluted MFT more effectively than an industrial high molecular weight anionic polyacrylamide, consistently producing more compact aggregates that dewatered faster in a filtration apparatus to generate sediments of higher shear strength. The only drawback of using poly(VBTMAC) was the higher required dosages compared to the anionic polyacrylamide. However, the combination of the two polymers led to a synergistic dewatering effect while substantially reducing the required dosage of poly(VBTMAC).

Chapter 5

Monitoring Polymer Flocculation in Oil Sands Tailings: A Population Balance Model Approach

Oil sands mature fine tailings are stable suspensions of clay particles and residual bitumen in an alkaline aqueous medium. They are formed when bitumen is extracted from oil sands using the Clark hot water process. Polymer flocculants are widely used to flocculate and subsequently dewater these tailings, but our knowledge is limited to empirical observations on how they work. A fundamental mathematical model would help monitor and design flocculation and dewatering processes more efficiently. In this study, a population balance model to describe the flocculation of mature fine tailings with novel poly(vinylbenzyl trimethylammonium chloride) was used. A time varying function was defined to account for the aggregate size evolution during MFT flocculation induced by polymer chains relaxation and rearrangement on the particle surfaces. The

A version of this chapter has been published as V. Vajihinejad, J. Soares, "Monitoring polymer flocculation in oil sands tailings: A population balance model approach" Chemical Engineering Journal, 2018, vol. 346, pp. 447-457.

validity of the model was tested by varying the shear rate, mixing time and flocculant dosage using focused beam reflectance measurements. The proposed model is a first step towards a more rational and quantitative approach to monitor and control treatment processes for oil sands tailings.

5.1 Introduction

Population balances are used to describe how the size and distribution of particles in a population change as a function of time.[106] Marian von Smoluchowski, the godfather of stochastic physics, was the first to describe the aggregation of monodisperse colloidal particles using population balances approximately 100 years ago.[107, 108, 109] Since then, population balances have been used to describe processes such as crystallization,[110, 111] polymerization,[112, 113] granulation,[114, 115] coagulation and flocculation.[116, 117]

Flocculation is a process in which large aggregates are formed from fine particles with the help of long polymer chains (flocculant). Light weight fine particles (in the range of micrometers) in wastewater or mineral processing (waste streams) usually carry surface charges that significantly delay (or even prevent) the aggregation and settling of the particles. Polymer chains adsorb onto particle surfaces and accelerate the aggregation process, forming aggregates up to a few millimeters in size, through bridging, induced by van der Waals forces or by charge neutralization. Mixing promotes the flocculation by enhancing the flocculant dispersion, adsorption, and not the least, the collision rates between particles and polymer molecules. Therefore, flocculation is governed by two events: 1) aggregation due to contact of particles, and 2) fragmentation (breakage) due to fluid shear forces. To model the flocculation, population balances must account for aggregation and fragmentation events during flocculation processes. No general explicit solution exists for these population balance equations, although some analytical solutions have been proposed under simplifying assumptions.[106] The two numerical methods widely used to solve population balances involve discretization (Hounslow et al.,[118] Kumar and Ramkrishna,[119] Spicer and Pratsinis[120]), and the

method of moments (McGraw,[121] and Fox et al.[122]).

Several researchers have used population balances to describe the flocculation of real or synthetic colloidal systems. For instance, Ding et al. used population balances to describe activated sludge flocculation,[123] Ahmad et al. modeled the flocculation of palm oil mil effluents,[124] and Heath et al. adapted population balances to describe calcite flocculation in turbulent pipe flow.[103] Our work is the first attempt to model the flocculation of oil sands tailings.

Canada's oil sand deposits are the third largest oil reserves in the world. The heavy crude oil (bitumen) they contain is extracted using large volumes of warm water. The net water consumption (after subtracting the water recycled back to the process) varies depending on the method of extraction. For instance, every barrel of bitumen produced by surface mining consumes about 3 barrels of fresh water.[1] Since the first commercial production of bitumen by surface mining in a Suncor mine in 1967, close to 600 km^2 of land have been affected by oil sands mining, 180 km^2 of which are currently occupied by tailing ponds. This area, more than 1.5 times the size of city of Vancouver, continues to grow, posing considerable environmental concerns.[2]

Tailings are pumped to ponds, where sand settles quickly and is used to build containment dikes. The solids suspended in fluid fine tailings (containing mineral particles with characteristic dimensions below 44 μm) remain in slurry for as long as five years of gradual sedimentation, and eventually form a mud-like slurry (30-40% solids by weight) called mature fine tailings (MFT). The volume of MFT generated in this process is approximately 1.5 times larger than the volume of bitumen extracted from oil sands.[2]

MFT is identified by its suspended minerals and water chemistry, which vary depending on geological location and process. A typical MFT is a suspension of fine mineral particles (mostly clays, 30-40% by weight), water (60-70%), and residual bitumen (2-5%). MFT clays are mostly kaolinite and interlayered kaolinite-smectite (35% by weight, 10-20 $m^2.g^{-1}$), and illite and interlayered illite-smectite (60-65%, 65-100 $m^2.g^{-1}$), chlorite (3-5%) and swelling clays (such as montmorillonite, 1-2%, 700-840 $m^2.g^{-1}$).[4, 5] MFT water contains in-

organic ions, and has a typical pH of about 8. The suspended particles have net negative surface charges that prevent them from aggregating and settling.

Oil sands producers treat MFT with technologies such as thin lift, rim ditching, consolidated/composite tailings, and centrifugation. Each has their own advantages and disadvantages. For example, thin lift drying, where flocculated tailings are spread and allowed to dewater over an area with shallow slope, is a relatively inexpensive practice but requires large land area, while centrifugation or filtration of flocculated tailings may be effective dewatering methods that do not require much space, but are also more expensive.[2]

Regardless of what method is used, polymer flocculants are the basis of most of these treatment technologies. Polymer flocculants destabilize MFT particles via bridging, charge patching, and/or charge neutralization. Current commercial flocculants are designed to treat a variety of wastewater types, and are highly soluble in water. They generally belong to the polyacrylamide family and its ionic copolymers. When polyacrylamide-based flocculants are used to treat MFT, they produce a loose cake with a gel-like structure that is hard to dewater.[87]

Currently, the leading researchers in this field are trying to develop new polymer flocculants designed to work in the challenging MFT environment. Most of their effort, however, has been spent on evaluating potential flocculants through indirect performance indicators such as settling rate, supernatant water clarity, sediment solids content, dewaterability through capillary suction time, shear monitoring, sieve testing, or pressure filtration.[125, 8, 126, 127, 128, 129, 88]

Several operating conditions, however, influence MFT flocculation: 1) flocculant dosage, 2) flocculant microstructure (molecular weight, charge density, comonomer composition, branching density, grafting frequency, polydispersity), 3) water chemistry (pH, ion strength), 4) mixing time, pattern and intensity, and 5) primary particle size and concentration of the suspended solids.[28, 65, 130, 131, 132] All these variables affect the dynamics of aggregate formation, flocculation mode, aggregate size, density, dewaterability, and

compressibility. These conditions are key to evaluate the performance of new flocculants, and the subsequent dewatering and consolidation of the sediments. One of the crucial steps in the efficient design of dewatering processes is controlling the flocculation process by polymers. Faced with so many variables, we are convinced that a mathematical model that could quantify the effect of *at least* some of these conditions on tailings flocculation would be extremely useful to develop new flocculants and tailings treatment processes. Population balance models can predict the size of aggregates, which is directly linked to their settling velocities, this information is essential to determine the size and efficiency of a treatment process, such as large scale thickeners. More importantly, population balances can be integrated with computational fluid dynamics (CFD) models to predict a full spectrum of aggregate size and concentration within a large-scale treatment unit experiencing large variations in fluid mixing conditions.[133]

This chapter proposes an approach that may help fill this need: a population balance model to describe MFT aggregate formation using the novel flocculant poly(vinylbenzyl trimethylammonium chloride), poly(VBTMAC). This approach, however, is not limited to poly(VBTMAC), but could be used with other flocculants. Experimental MFT batch flocculation data obtained by in-situ focused beam reflectance measurement (FBRM) was used to train the population balance model and validate its predictions considering three industrially relevant variables: shear rate, mixing time, and flocculant dosage. This is the first step in a long-term research effort to establish quantitative methods to correlate polymer type and treatment conditions to MFT flocculation and dewatering performance.

5.2 Experimental

5.2.1 Materials

Vinylbenzyl trimethylammonium chloride (VBTMAC) and initiator, 2,2'-Azobis(2-methylpropionamidine) dihydrochloride (V-50) were purchased from Sigma-Aldrich. Shell Canada supplied the MFT sample.

5.2.2 Flocculant Synthesis and Characterization

A partially hydrophobic cationic flocculant, poly(VBTMAC), was synthesized by aqueous free radical solution polymerization at 50 °C in a 0.5 L glass polyclave reactor (büchiglasuster®, Switzerland) equipped with a temperature-controlled jacket, impeller, and a purging line. A 0.5 M VBTMAC solution was introduced into the reactor and purged with nitrogen for 45 min at room temperature followed by 10 min at 50 °C. The initiator (0.001 M) was transferred from a previously purged solution into the reactor using a transfer needle. The polymerization was allowed to proceed for 3 hr. After that, polymer was purified by precipitating it in acetone. The product was dried overnight in a vacuum oven at 50 °C. Gel permeation chromatography (GPC, Agilent 1260 Infinity) measured the molecular weight distributions of the poly(VBTMAC) samples. The GPC system included three detectors (viscosity, refractive index, light scattering) and two columns (TKS gel G6000PW XL-CP, designed for cationic polymers) connected in series for higher resolution. The GPC was calibrated using PEO standards provided by Agilent Technologies. An aqueous solution of 0.3 M sodium nitrate and 0.01 M monosodium phosphate in deionized water was used as the mobile phase for the analyses.

5.2.3 MFT Characterization

Content Analysis

Solid, water and fugitive bitumen contents were measured by Dean-Stark extraction.[134] Atomic absorption spectroscopy (AAS) quantified the concentration of major ions (Na^+, K^+, Ca^{2+}, Mg^{2+}) in MFT. The original MFT had about 35% solid, 62% water and 3% residual bitumen. Deionized water was used to dilute the MFT sample when necessary. The detail results for the MFT analysis were presented in a previous work.[86]

Particle Size Analysis

A laser diffraction particle size analyzer (Mastersizer 3000, Malvern Instruments Ltd, UK) was used to quantify the particle size distribution in the

MFT sample. The Mastersizer tank was filled with deionized water and the mixer speed was set to 2500 rpm without sonication. A few drops of diluted MFT (2 wt%), previously mixed and sonicated to ensure full dispersion, was added to the Mastersizer tank until obscuration came in the range (2-5%). For the software calculations, the particle absorption index, particle refractive index, and density were set to the following values: MFT: 1.0, 1.526, and 2.6 g.cm^{-3}, respectively, and the model clay (illite): 0.1, 1.55, and 2.75 g.cm^{-3}, respectively. The same analysis was performed at least 3 times to ensure reproducibility, and a weighted residual below 1% was chosen to verify good results in each scan.

5.2.4 Flocculation Monitoring - Focused Beam Reflectance Measurement (FBRM)

Flocculation experiments were performed on MFT diluted to 3 wt% solid in deionized water in a 400 ml batch stirred beaker under different flocculant dosages and shear rates. An FBRM probe (FBRM G400, Mettler Toledo, USA) monitored the dynamics of aggregate formation. Figure 5.1 shows the geometry of the flocculation vessel. Optics elements in the FBRM probe are used to focus the laser beam (791 nm- near infrared) through the sapphire window. The optic elements rotate, causing the laser beam to rapidly (2 to 8 ms^{-1}) scan across aggregates flowing in suspension close to the sapphire window. When the laser beam hits the edge of an aggregate, part of the light is backscattered. The backscattered beam is converted to a signal, and the instrument measures the time taken for the beam to pass another edge of the aggregate. Multiplying this time by the speed of the laser beam gives a distance called *chord length.*[135] FBRM makes no assumption about the shape of aggregates, but it might misinterpret their number. For example, an aggregate with irregular shape could be counted twice, or two aggregates in close vicinity could be counted as one. The latter is a concern in highly concentrated slurries, which is not a major problem in this study. The FBRM signal processing unit classifies the edges of an aggregate, where a discrimination circuit measures the intensity decay rate of a reflected beam and decides whether or not

it is sufficient to define an edge on the aggregate.[136] There are two modes for signal processing: coarse (macro) and fine (primary). Deciding which mode to use comes down to the process under study. In flocculation kinetics, where the main interest is measuring the formation of aggregates, the coarse mode is recommended if the solids concentration is low enough to minimize the overlapping of aggregates. Alternatively, the fine mode is favored if one needs to track the population of fine particles.[137] External measurements, such as image analysis or settling rates of aggregates, can provide additional insights as to which signal-processing mode is favored for a given investigation.

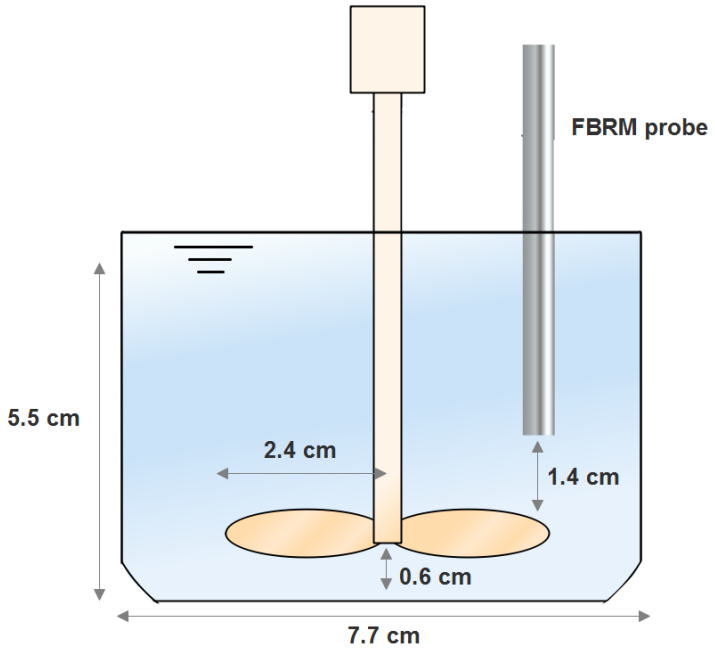

Figure 5.1: Geometry of the flocculation vessel. The mixer was a 45 degree pitched blade turbine impeller

FBRM Data Calibration

Population balances keep track of how the average aggregate size changes during the flocculation. Since the proposed model assumes that the colliding aggregates are spherical, the FBRM data needed to be correlated with the sphere-equivalent diameter of the aggregates. In addition, to model any

post flocculation process, such as the settling rate of aggregates, the sphere-approximate diameter of the aggregates needed to be estimated. Unlike other particle size measurement techniques, such as laser diffraction, FBRM measures the average chord lengths of the aggregates, not their sphere-equivalent diameters. Aggregates counts measured by the FBRM probe are proportional to the number of aggregates in the system, but do not represent their true number. FBRM uses different averaging methods (mode, mean, and median), and assigns several weighting moments to the chord length distribution (unweighted, square-weighted, cube weighted, etc.). The higher moments of the aggregate size distribution, such as square-weighted or cube-weighted, are more sensitive to large particles, and thus are favored for studying aggregation processes. Fawell and his team studied the correlation between the average particle size of a series of sieved calcite and aluminum particles with different average chord lengths measured by FBRM. They found out that the mean square-weighted chord length (2^{nd} moment of chord length distribution) correlated best with the average aggregate size measured with conventional techniques (such as sieving or laser diffraction) in the range of 50-400 μm. The 2^{nd} moment was also unaffected by the focal position of the beams, and valid for a wide range of particle concentrations (0.1-20% by weight).[138]

Based on these findings, the FBRM average chord data was calibrated with sphere-equivalent average diameters measured with the laser diffraction. Correlating chord lengths of the flocculated MFT aggregates with their sizes measured by laser diffraction was not satisfactory because the large aggregates settled to the bottom of the Mastersizer tank, fragmented due to dilution and mixing, and some adhered to the Mastersizer tank walls, perhaps due to the presence of bitumen. To overcome this experimental difficulty, illite clays were used for FBRM calibration. A piece of illite rock from the Clay Mineral Society was first grounded, passed through multiple sieves, and subsequently rinsed with water to wash out any fines that may had remained on the surface of the larger particles. The clay fractions were then dispersed in 200 ml deionized water to generate suspensions of 2 wt%. It was not possible to use other abundant clays in MFT, such as kaolinite, because after grounding

the frail kaolinite rock sample and dispersing its fractions in water, almost no particles with sizes higher than 100 μm were recovered. The illite fractions were analyzed using laser diffraction and FBRM under agitation. The mixing speed should not affect the FBRM results appreciably since the laser beam scanning speed is far larger than the velocity of the particles in suspension, as confirmed in the work of Heath et al.[138] Two hundred channels (bins used to generate the particle size distribution) were used by the FBRM software and mean square weighted chord length data was collected in 1 to 4000 μm range. Figure 5.2 shows the resulting calibration curve. The coarse mode correlation in our model provided a better fit to the experimental data and a more realistic aggregate size as confirmed by image analysis (see Figure 5.7).

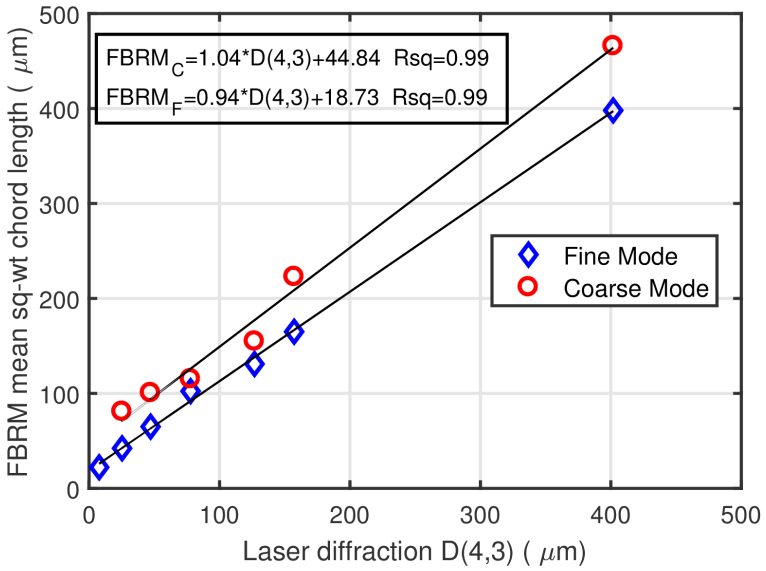

Figure 5.2: Calibration curve of FBRM mean square-weighted chord length against sphere-equivalent diameter by laser diffraction data

Image Analysis

Different techniques may be used to measure mass or 2D fractal dimension of aggregates. The most common methods are static light scattering, settling velocity, and image analysis.[139] Image analysis was chosen because static light scattering only works well with small particles (for our system, the light scattering equations are not valid because the size of MFT primary particles

is comparable to the wavelength of the incident light),[100] and the settling velocity method gave erroneous results because samples needed to be taken in short time intervals, which could not be done easily in a batch system like the one used in this study. A light microscope (ZEISS AXIO Scope A1) was used to examine restructuring (change in aggregate fractal dimension) in the flocculation experiments. In a typical experiment, the mixing was stopped at random times (from 6 s to 4 min) in several batches. Then a small aliquot of the aggregate (2 ml) was diluted in water (50 ml). After gentle mixing, a small drop of the suspension was placed onto the microscope slide for observation. A minimum of 10 magnified screenshots were captured and processed by an image analysis software (Image J), where the area and perimeter of individual aggregates were measured to estimate the perimeter fractal dimension (two-dimensional) using Equation (5.1).[100] The same procedure was repeated at least 5 times for each sampling time to ensure good statistics a minimum of 50 images from each sample). The correlation provided by Lee and Kramer was used to estimate the mass fractal dimension using the perimeter fractal dimension.[140]

$$A \propto P^{(2/d_{PF})} \tag{5.1}$$

where A, P, and d_{PF} are aggregate projected surface area, perimeter and perimeter fractal dimension, respectively.

5.3 Model Development

5.3.1 Population Balance Equation

Flocculation involves the simultaneous aggregation and breakage of aggregates. Equation (5.2) is the population balance for an aggregate of size v[119]

$$\frac{\partial n(v,t)}{\partial t} = \frac{1}{2}\int_0^v Q(v-v',v')n(v-v',t)n(v',t)dv' + \int_v^\infty \Gamma(v,v')S(v')n(v',t)dv' - \int_0^\infty Q(v,v')n(v,t)n(v',t)dv' - S(v)n(v,t) \tag{5.2}$$

where $n(v,t)$ and $n(v',t)$ are number of aggregates of size v and v' in unit volume at time t, respectively, $Q(v,v')$ is the aggregation kernel, $S(v)$ is the breakage kernel, and $\Gamma(v,v')$ is the breakage distribution function. The kinetic terms Q, S and Γ will be defined in the next section. Equation (5.2) tracks the change in the number concentration of aggregates (or particles) with size v in the system. The first two terms in Equation (5.2) quantify the rate of the events leading to the formation of aggregates of size v; the first term is the rate of formation of aggregates of size v due to aggregation between aggregates of smaller size v and $v-v'$, and the second term is the rate of formation of aggregates of size v due to breakage of larger aggregates of size v'. The two last terms quantify the rate of the events leading to disappearance of aggregates of size v; the third term is the rate of disappearance of aggregates of size v due to aggregating with all other aggregates (particles) in the system, and the last term is the rate of disappearance of aggregates of size v due to breakage.

Equation (5.2) was solved using the discretized form of population balance proposed by Spicer and Pratsinis,[120] which is a combination of discretization framework proposed by Hounslow et al.[118] for aggregation events and Kusters et al.[141] for breakage events. The mathematical framework begins with discretizing the aggregate size distribution into a known number of numerical channels (as many channels as needed to cover the size of all aggregates) in such a way that the i^{th} channel contains aggregates ranging from size (volume) v_i to v_{i+1}, where $\frac{v_{i+1}}{v_i} = 2$. If the minimum size among primary particles in the initial distribution ($t = 0$) is v_1, then an aggregate of size v_i contains $2^{(i-1)}$ smallest primary particles ($v_i = 2^{(i-1)}v_1$). Equation 5.3 is the discretized form of Equation (5.2)

$$\frac{dN_i}{dt} = \sum_{j=1}^{i-2} 2^{j-i+1} Q_{i-1,j} N_{i-1} N_j + \frac{1}{2} Q_{i-1,i-1} N_{i-1}^2 - N_i \sum_{j=1}^{i-1} 2^{j-i} Q_{i,j} N_j - N_i \sum_{j=i}^{i_{max,1}} Q_{i,j} N_j - S_i N_i + \sum_{j=i}^{i_{max,2}} \Gamma_{i,j} S_j N_j \tag{5.3}$$

where N_i is the number concentration of aggregates with size (volume) v_i at time t, $N_i = \int_{v_i}^{v_{i+1}} n(v,t)dv$.

5.3.2 Aggregation Kernel

Aggregation kernel, Q, is a kinetic term that contains collision frequency and capture efficiency

$$Q_{i,j} = \beta_{i,j} \times \alpha_{i,j} \tag{5.4}$$

where $\beta_{i,j}$ is the collision frequency, and $\alpha_{i,j}$ is the capture efficiency.

The collision frequency between aggregates from the i^{th} channel and the j^{th} channel can result from Brownian motions, shear flow, or differential settling (larger aggregates capture smaller aggregates as they settle to the bottom of the tank). In a stirred tank, differential settling may be considered negligible. In the presence of shear flow (mixing), Brownian motion may also be neglected. Saffman and Turner proposed the following equation for shear-induced (orthokinetic) collision frequency in isotropic turbulent flow[142]

$$\beta_{i,j} = 0.162 G (d_i + d_j)^3 \tag{5.5}$$

where d_i is the effective collision diameter of an aggregate that contains $2^{(i-1)}$ primary particles. Usually, aggregates are not compact spheres, but rather porous fractal objects. Therefore, their effective collision diameters will be larger than for spheres. The diameter d_i, assuming unity packing density, is

defined as[143]

$$d_i = d_1(2^{i-1})^{1/d_F} \tag{5.6}$$

where d_F is mass fractal dimension of aggregates ($1.0 \leq d_F \leq 3.0$).

In Equation (5.4), G is average turbulent shear rate (velocity gradient)[144]

$$G = (\frac{\epsilon \times \rho_{sus}}{\mu_{sus}})^{1/2} \tag{5.7}$$

where ϵ is the average energy dissipation rate in a stirred vessel[145]

$$\epsilon = \frac{N_p \Omega^3 D^5}{V} \tag{5.8}$$

and N_p, Ω and D are the impeller power number, rotation speed, and diameter, respectively. V is the working volume of the vessel. Finally, ρ_{sus} and μ_{sus} are density and viscosity of the flocculating suspension[146]

$$\rho_{sus} = \rho_s \phi + \rho_w (1 - \phi) \tag{5.9}$$

where ρ_s, ρ_w and ρ_{sus} are the densities of the primary solid particles, water and slurry, respectively. ϕ is the volume fraction of primary particles in suspension

$$\phi = \frac{w \rho_{sus}}{\rho_s} \tag{5.10}$$

and w is weight fraction of solids in slurry.

In the flocculating suspension, the volume fraction of solids (aggregates) is larger than the volume fraction of the primary solids, since the aggregates are porous. Therefore, the effective volume fraction of the aggregates in the suspension can be described by the fractal geometry of the aggregates[147, 148, 103]

$$\frac{\phi_{eff}}{\phi} = (\frac{\bar{d_{agg}}}{\bar{d_s}})^{3-d_F} \tag{5.11}$$

where $\bar{d_s}$ and $\bar{d_{agg}}$ are average size of primary particles and aggregates, respectively.

The viscosity of flocculating suspension can be then calculated using Equation (5.12),[103, 149]

$$\mu_{sus} = \mu_0(1 - \frac{\phi_{eff}}{\phi_{max}})^{-2} \tag{5.12}$$

where μ_0 is the viscosity of the suspending liquid (water in this investigation), and ϕ_{max} is the maximum solid fraction (0.6 - 0.7).

Due to hydrodynamic forces and electrostatic repulsion, not every collision between aggregates leads to further aggregation. The capture efficiency is the probability of aggregation upon collision. Hogg derived a mathematical relationship to estimate the capture efficiency for polymer-induced flocculation. Using probability theory, Hogg showed that if n_i and n_j are the number of adsorption sites on the surface of particles i and j, and θ is the fraction of surface covered with polymer, the capture efficiency between particles i and j can be expressed as[150]

$$\alpha_{i,j} = 1 - \theta^{n_i+n_j} - (1-\theta)^{n_i+n_j} \tag{5.13}$$

Although the size of colliding bodies is considered in Hogg's treatment of capture efficiency, he did not include the effect of hydrodynamic forces. Kusters used trajectory analysis proposed by Adler to define a capture efficiency function that considers hydrodynamic interaction as well as sizes of colliding bodies. Selomulya et al. adopted Kusters's treatment to define an equation for capture efficiency in discretized population balance models[104]

$$\alpha_{i,j} = \frac{exp(-x(1-\frac{i}{j})^2)}{(i \times j)^y}\alpha_{max} \tag{5.14}$$

where x and y are fitting parameters, i and j are numerical channel numbers, and α_{max} is the maximum capture efficiency, which is usually treated as a tuning parameter. Runkana et al. estimated the capture efficiency as a function of interaction forces between polymer-coated particles undergoing Brownian (perikinetic) collision, which is not adequate for our experiments.[116] Figure 5.3 is a typical FBRM response of MFT flocculation induced by poly(VBTMAC). The initial lag time before aggregation takes place is the time the polymer chains need to disperse through the slurry, reach and adsorb onto the surface of the particles. Since the physical adsorption of the polymer chains is relatively fast, the process is limited by the mass transfer rate of the polymer chains through the slurry, which is a function of shear rate, polymer solution viscosity, slurry viscosity, and number concentration of particles. After the polymer has adsorbed enough to start forming aggregates, their sizes grow quickly up to a maximum size, after which aggregate size drops until eventually reaching a steady-state value. This trend is typical of flocculation induced by bridging, and researchers have used different approaches to address this trend in their models. For example, Jeldres et al. attributed this trend to the restructuring of aggregates stemmed from shear-induced aggregation, fragmentation, elongation and compaction of aggregates.[105] They used Equation (5.14), and introduced a restructuring term in their population balance model by defining a time-varying function for fractal dimension (the aggregate fractal dimension increased as a function of time due to restructuring).

Heath et al. observed the same trend (initial increase in aggregate size, followed by a gradual drop before attaining a steady-state size) for the flocculation of calcite with high molecular weight anionic flocculants in turbulent pipe flow.[103] To address this behavior, they considered a constant fractal dimension for the aggregates, attributed the size drop to polymer degradation (due to carbon chain scission or rearrangement), and defined a degradation term in the breakage kernel to take into account this phenomenon. It is, however,

unlikely that shear-induced chain scission is appreciable in our system because the drop would happen even at relatively low shear rates and short times.

It can be hypothesized that this phenomenon could be explained by polymer rearrangement, that is, chain relaxation on the surface of the particles and subsequent reduction in the number of surface active sites and shortening of the length of polymer chains dangling into the liquid phase, as shown in Figure 5.3.

To test this hypothesis, a series of poly(VBTMAC) flocculants of different molecular weights were used as flocculants, at their optimum dosages. The results show that bridging (induced by charge neutralization) was the main flocculation mechanism in the system. Polymers with different molecular weight averages were synthesized, and MFT flocculation was monitored by FBRM (please see 4 for more discussions). Polymers of higher molecular weights needed longer times to reach steady state, an indication of the dynamics of polymer chains rearrangement. Since the mentioned deteriorated bridging mainly affects the aggregation process, such deterioration effect was included in the aggregation kernel by defining an empirical time-varying function for the capture efficiency

$$f(\alpha) = (\alpha_{max} - \alpha_{min})e^{-k_d t} + \alpha_{min} \tag{5.15}$$

where α_{max} is maximum capture efficiency, α_{min} is minimum capture efficiency (after reaching steady state size), k_d is capture efficiency decay constant (s^{-1}).

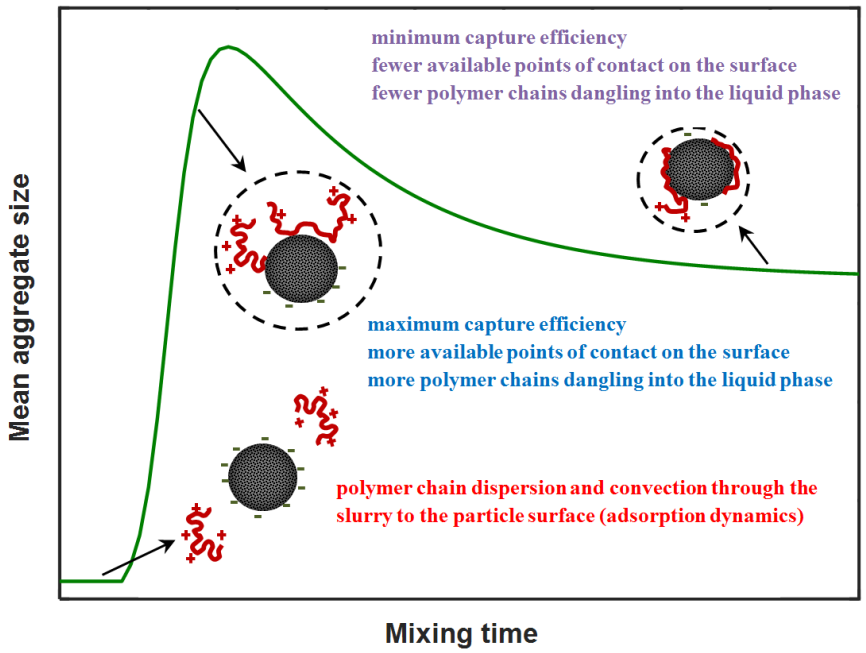

Figure 5.3: Typical FBRM response of MFT flocculation by poly(VBTMAC)

5.3.3 Breakage Kernel

The breakage kernel (breakage rate coefficient) for shear-induced breakage of aggregates suggested by Pandya and Spielman was used in the proposed model[151]

$$S_i = s_1 G^{s_2} d_i \tag{5.16}$$

where s_1 and s_2 are system-specific constants. For simplicity, binary breakage was assumed, so the breakage distribution function reduced to the simpler form. Spicer and Pratsinis showed that the choice of breakage distribution function does not appreciably affect the final aggregate size distribution.[120]

$$\Gamma_{i,j} = \frac{v_j}{v_i} \tag{5.17}$$

5.3.4 Model Solution and Parameter Estimation

The population balance in Equation (5.3) was solved using a variable-step, variable-order solver based on numerical differentiation formula (NDFs) for stiff ODEs (ode15s in MATLAB). The model parameters were estimated by minimizing the objective function given in Equation (5.18) using particle swarm global optimization (PSO)

$$F(\alpha_{max}, .., s_2) = \sum_{t=0}^{max} (d_{exp.} - d_{model})^2 \tag{5.18}$$

$$d_{model} = \frac{\sum_{i=1}^{max} N_i d_i^4}{\sum_{i=1}^{max} N_i d_i^3} \tag{5.19}$$

where F(α_{max},...,s_2) is the objective function for parameter estimation, and d is volume-average diameter of aggregates.

The following quantitative criteria were used to validate model fit and predictions:[82]

i) Coefficient of determination (R^2, $0 \leq R^2 \leq 1.0$): to examine how close model predictions were to experimental measurements

$$R^2 = 1 - \frac{\sum_{j=1}^{j_{max}} (d_{exp,j} - d_{model,j})^2}{\sum_{j=1}^{j_{max}} (d_{exp,j} - \bar{d}_{exp,mean})^2} \tag{5.20}$$

ii) Pearson correlation coefficient (PCC, $-1.0 \leq PCC \leq 1.0$): to quantify the linear correlation between model responses and experimental measurements (how well the model captures the trends in aggregate size evolution)

$$PCC = \frac{\sum_{j=1}^{j_{max}} (d_{exp,j} - d_{exp,mean})(d_{model,j} - d_{model,mean})}{(\sum_{j=1}^{j_{max}} (d_{exp,j} - d_{exp,mean})^2 \sum_{j=1}^{j_{max}} (d_{model,j} - d_{model,mean})^2)^{1/2}} \tag{5.21}$$

iii) Mean absolute percentage error ($MAPE$): to measure the prediction ac-

curacy of the model

$$MAPE = \frac{100}{j_{max}} \sum_{j=1}^{j_{max}} |\frac{d_{exp,j} - d_{model,j}}{d_{exp,j}}| \tag{5.22}$$

where j_{max} is the size of data set.

Table 5.1 summarizes the model equations, values and solution steps.

Table 5.1: Model summary

Model terms	**Reference**
Population balance (PB)	
$\frac{dN_i}{dt} = \sum_{j=1}^{i-2} 2^{j-i+1} Q_{i-1,j} N_{i-1} N_j + \frac{1}{2} Q_{i-1,i-1} N_{i-1}^2 - N_i \sum_{j=1}^{i-1} 2^{j-i} Q_{i,j} N_j$ $- N_i \sum_{j=i}^{i_{max,1}} Q_{i,j} N_j - S_i N_i + \sum_{j=i}^{i_{max,2}} \Gamma_{i,j} S_j N_j$	[120]
Aggregation kernel	
$Q_{i,j} = [0.162 G (d_i + d_j)^3] \times [(\alpha_{max} - \alpha_{min}) e^{-k_d t} + \alpha_{min}]$	[142], this study
Breakage kernel	
$S_i = s_1 G^{s_2} d_i$	[151]
Breakage distribution function	
$\Gamma_{i,j} = \frac{v_j}{v_i}$	[120]
Definitions and initial values	
$d_i = d_1 (2^{i-1})^{1/d_F}, d_1 = 0.27 \mu m$	[143]
$G = (\frac{\epsilon \times \rho_{sus}}{\mu_{sus}})^{1/2}$	[144]
$\epsilon = \frac{N_p N^3 D^5}{V}, N_p = 1.27, D = 4.8cm, V = 0.2L$	[145], this study
$\rho_{sus} = \rho_s \phi + \rho_w (1 - \phi), \phi = \frac{w \rho_{sus}}{\rho_s}, w = 0.03, \rho_s = 2.60 \mathrm{gcm}^{-3}$	[146, 21], this study
$\frac{\phi_{eff}}{\phi} = (\frac{\bar{d_{agg}}}{d_s})^{3-d_F}, d_s = 16.5 \mu m$	[103],[147], [148], this study
$\mu_{sus} = \mu_0 (1 - \frac{\phi_{eff}}{\phi_{max}})^{-2}, \phi_{max} = 0.65$	[103], [149]
Unknown parameters	
$\alpha_{max}, \alpha_{min} \in [0, 0.6], k_d, s_1, (s_2 > 1.0), d_F \in [1, 3]$	
PB solution with known parameters	
variable-step, variable-order solver based on numerical differentiation formula (NDFs) for stiff ODEs (ode15s in MATLAB)	
$d_{model} = \frac{\sum_{i=1}^{max} N_i d_i^4}{\sum_{i=1}^{max} N_i d_i^3}$	
PB paremeter estimation	
objective function: $F(\alpha_{max}, .., s_2) = \sum_{t=0}^{max} (d_{exp.} - d_{model})^2$	
minimization was done by MATLAB PSO tool box	
Validating model fit and prediction	
coefficient of determination : $R^2 = 1 - \frac{\sum_{j=1}^{j_{max}} (d_{exp,j} - d_{model,j})^2}{\sum_{j=1}^{j_{max}} (d_{exp,j} - \bar{d}_{exp,mean})^2}$	[82]
Pearson correlation coefficient : $\rho = \frac{\sum_{j=1}^{j_{max}} (d_{exp,j} - d_{exp,mean})(d_{model,j} - d_{model,mean})}{(\sum_{j=1}^{j_{max}} (d_{exp,j} - d_{exp,mean})^2 \sum_{j=1}^{j_{max}} (d_{model,j} - d_{model,mean})^2)^{1/2}}$	
mean absolute percentage error : $MAPE = \frac{100}{j_{max}} \sum_{j=1}^{j_{max}} |\frac{d_{exp,j} - d_{model,j}}{d_{exp,j}}|$	

5.4 Results and Discussion

5.4.1 Initial Population of MFT Particles and Conversion of FBRM Data

The solution of Equation (5.3) requires the initial size and number density distribution of particles in the MFT before the flocculation begins. The volume-based particle size distribution (PSD) data obtained by laser diffraction was used to generate the initial population of primary particles. Figure 5.4 shows PSD of MFT obtained by the Mastersizer laser diffraction instrument.

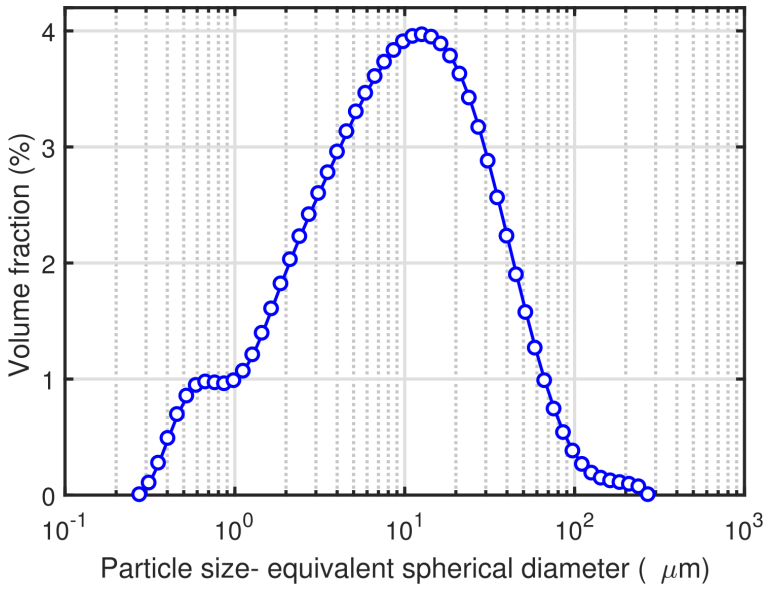

Figure 5.4: MFT initial PSD

The following set of equations were used to generate the number density distribution of primary particles from experimental PSD, satisfying the relation $\frac{V_{i+1}}{V_i} = 2$:

$$N_{0,i} = \frac{\phi \times v(d_{0,i})}{V_{0,i}} \tag{5.23}$$

$$V_{0,i} = 2^{(i-1)} V_1 \tag{5.24}$$

where $N_{0,i}$ and $V_{0,i}$ are the number concentration and volume of primary particles of size d_i registered in the i^{th} channel, respectively. The parameter V_1 is the volume of the smallest primary particle in the population (0.27 μm), ϕ is the volume fraction of primary particles in the MFT sample calculated using Equation (5.10), $v(d_{0,i})$ is the volume fraction of primary particles of size d_i estimated by linear interpolation using initial PSD data in Figure 5.4

$$v(d_{0,i}) = \frac{v(d_{i+1}^{exp}) - v(d_{i-1}^{exp})}{d_{i+1}^{exp} - d_{i-1}^{exp}}(d_{0,i} - d_{i-1}^{exp}) + v(d_{i-1}^{exp}) \tag{5.25}$$

and d_{i-1}^{exp} and d_{i+1}^{exp} are the experimental volume fraction of primary particles appearing immediately before and after $d_{0,i}$, respectively. Figure 5.5 shows the number concentration distribution (m^{-3}) of primary particles assigned to 31 numerical channels containing MFT particles ranging from 0.27 μm to 270 μm (full size range), with the majority of them being sub-micron. The values in Figure 5.5 are used as initial conditions in the solution of population balances, any generated aggregates are then assigned to one of these channels.

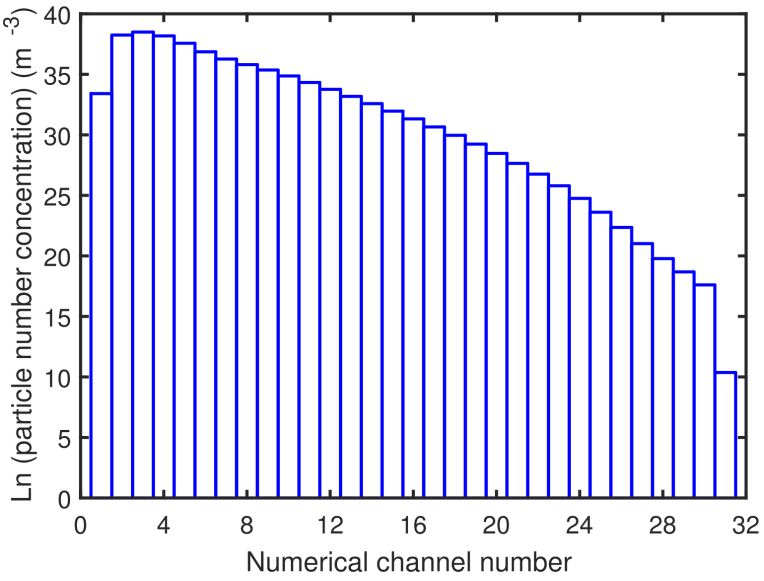

Figure 5.5: Distribution of number concentration of primary particles registered in 31 channels

The method explained in Section 5.2.4 was used to estimate the size of aggre-

gates over time using FBRM data.

5.4.2 Fractal Dimension

Figure 5.6 shows the estimated mass fractal dimension from the calculation of perimeter fractal dimension using image analysis as explained in Section 5.2.4. Given the analysis error, the fractal dimension did not change appreciably (no aggregate restructuring) during the short period of flocculation, and could not explain the considerably large drop in aggregate size before reaching steady state sizes (Figure 5.3). Figure 5.7 shows a typical screenshot of MFT aggregates flocculated by the partially hydrophobic flocculant used in this study.

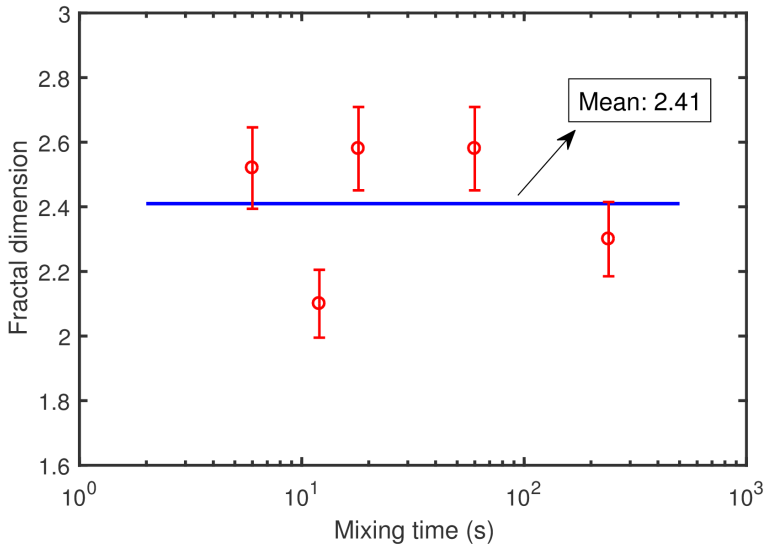

Figure 5.6: Estimated mass fractal dimension by image analysis for different mixing times. This set of data is for G= 390 s^{-1} and dosage= 5000 ppm

5.4.3 Fitting the Model to Experimental Data

The solution of the population balance model, Equation (5.3), was fitted to the flocculation experimental data obtained from FBRM. Figure 5.8 shows the experimental data and the fitted model. Table 5.2 shows the estimated model parameters and the model statistics for the fit present in Figure 5.8.

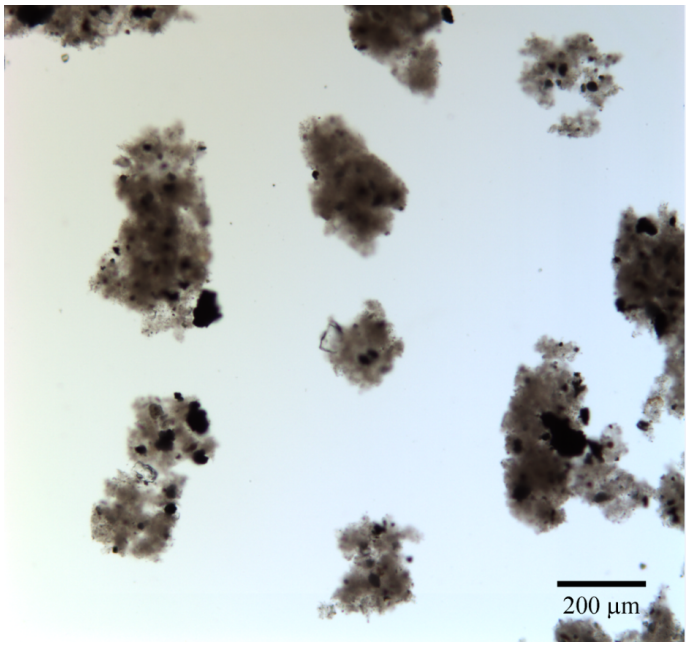

Figure 5.7: A typical image of MFT aggregates flocculated by poly(VBTMAC). This image is for condition of G= 390 s^{-1} and dosage= 5000 ppm

It is worth mentioning that use of the fractal dimension estimated in Section 5.4.2, did not allow for a good fit between the model and experimental data. To estimate the fractal dimension that would fit the model to experimental data, the fractal dimension was treated as a tuning parameter and the particle swarm global optimization (PSO) algorithm was used to fit the model to the experimental data. Surprisingly, the fractal dimension estimated by PSO was 2.96 (very close to sphere fractal dimension). We attribute this discrepancy to the inaccuracies in the value of the shear rate given to the model as an input. The shear rate given in Equation (5.7) is a good estimate of the average shear rate for the whole system, but the FBRM probe is located in a stream of flow close to the tip of the impeller, where the shear rate could be 5 to 10 times higher than the average shear rate defined in Equation (5.7).[152] A higher fractal dimension (in this case 2.96) would correct for the difference between estimated and true average shear rates. Another minor discrepancy is that the fractal dimension estimated by image analysis underestimates the actual fractal dimension mainly due to the dilution effect on the structure

of aggregates. Figure 5.9 shows how peak aggregate size depends on shear rate and fractal dimension in our model (keeping all other parameters fixed at some arbitrary values). The plot shows that, to obtain the same aggregate size range, one needs to decrease the value of the fractal dimension when increasing the shear rate. It is also worthy to note that there is a distribution of flocculation responses within our system, the magnitude of which depends on the mixing conditions. In other words, different aggregation states exist within the tank due to the turbulent shear distribution (the shear is maximum at the tip of the impeller, leading to maximum breakage, and minimum near the vessel walls). One may observe different flocculation responses by probing at different locations in the flow stream within the vessel. Our model, on the other hand, uses the average shear rate in the system to find average aggregate sizes as a function of mixing time. Therefore, the distribution of shear rates is "lumped" into a single average shear rate value. Provided that the model parameters are estimated for a given system, the distribution of shear rates should not affect the model predictions, and the model could be useful for quantifying the effect of different conditions.

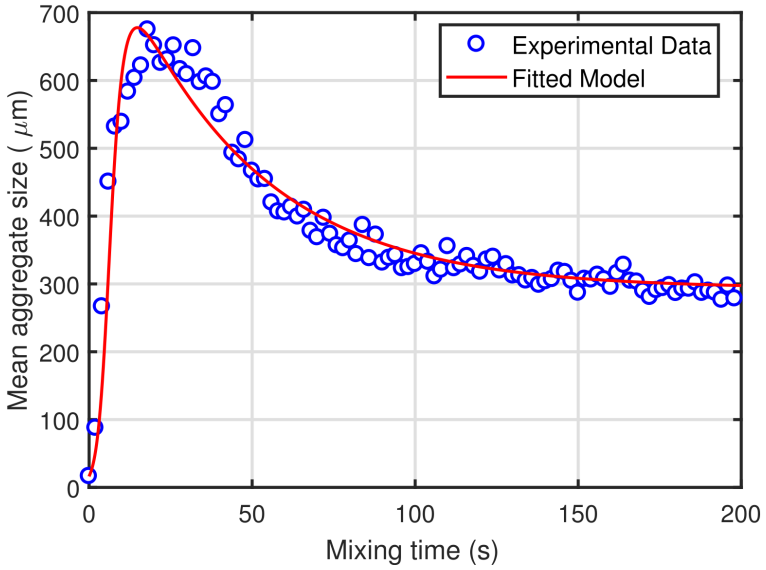

Figure 5.8: Model (continuous line) fitted to experimental data (circles) of the evolution of mean aggregate size of MFT particles (3wt.%) over time flocculated with a partially hydrophobic cationic flocculant (poly(VBTMAC)) (batch flocculation, G= 310 s^{-1} (235 rpm), flocculant dosage= 5000 ppm (mg polymer/kg dry particle), pH=8.6)

Table 5.2: Estimated model parameters and statistics (G= 310 s^{-1} (235 rpm), 3 wt% MFT, 5000 ppm flocculant)

α_{max}	α_{min}	k_d	s_1	s_2
0.0049	0.0016	0.018	0.22	1.73
	R^2	PCC	$MAPE$	
	0.88	0.94	7.3	

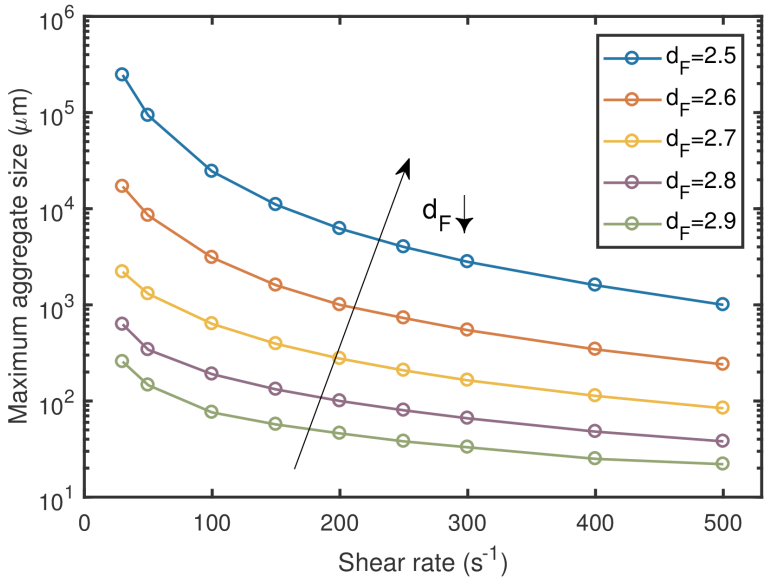

Figure 5.9: Simulation of aggregate peak size as a function of shear rate and fractal dimension- all other variables were kept constant at some arbitrary values in the model. The same aggregate size range could be achieved by decreasing shear rate while increasing fractal dimension and vice versa

Given the relatively large number of parameters that need to be estimate, the stability, computation time, and accuracy of the population balance solution and parameter estimation are influenced by the boundaries on the tuning parameters. The upper limit on α_{max} could be estimated from trajectory analysis of particles by Van de Ven and Mason, where they derived an empirical expression for the capture efficiency in the presence of hydrodynamic interactions, and absence of electrostatic repulsion for the colliding particles of the same size (i.e. maximum probability)[153]

$$\alpha_{max,limiting} = f(\lambda/a)(\frac{A}{36\pi\mu G a^3})^{0.18} \tag{5.26}$$

where $f(\lambda/a)$ represents retardation effects, a is particle size, A is the Hamaker constant of the system. Plugging appropriate values for our MFT system, the limiting capture efficiency was estimated to be 0.06. As such, the lower limit of s_2 is 1.0 since in flocculation, breakage is more sensitive to shear than aggregation.

5.4.4 Effect of Shear Rate

To verify whether the model could quantify the effect of changing the average shear rate during flocculation, flocculations at different shear rates were performed by varying the mixing rate while keeping all other conditions the same. Figure 5.10 compares model predictions and experimental results at different shear rates using the parameters in Table 5.2.

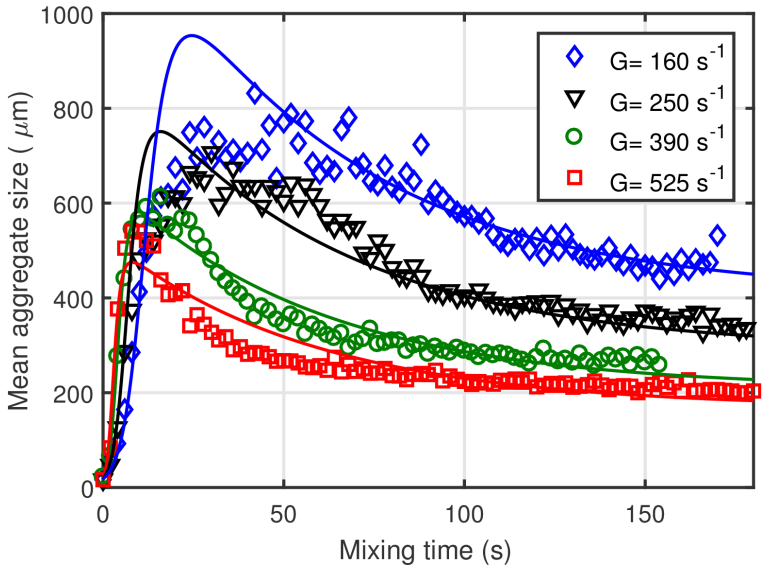

Figure 5.10: Effect of shear rates on the evolution of mean aggregate size of MFT particles (3wt.%) over time flocculated with a partially hydrophobic cationic flocculant (poly(VBTMAC)) (batch flocculation, flocculant dosage= 5000 ppm (mg polymer/kg dry particle), pH= 8.6). Model is continuous line and experimental data are symbols

Table 5.3: Model prediction statistics in different shear rates (3 wt.% MFT, 5000 ppm flocculant)

Average shear rate	R^2	PCC	$MAPE$
160 s^{-1}(150 rpm)	0.62	0.91	10.6
250 s^{-1}(200 rpm)	0.80	0.91	8.9
390 s^{-1}(275 rpm)	0.93	0.97	7.9
525 s^{-1}(340 rpm)	0.86	0.93	10.7

Figure 5.10 and Table 5.3 show that the proposed model quantifies well the effect of mixing rate on aggregate formation without the need to readjust any model parameter. When the shear rate increases, the flocculation starts earlier (due to the enhanced adsorption rate of polymer on the suspended solid particles), but the average aggregate size is smaller because the breakage rate increases more than the aggregation rate (i.e. exponent 1.7 vs. 1.0). The model did not describe well the size of aggregates around the peak position for a shear rate of 160 s^{-1}, and to a lesser extent for 250 s^{-1}, but described the approach to steady-state sizes adequately for all mixing rates. We argue that this deviation does not point to a model deficiency, but rather to the fact that at relatively low mixing rates larger (heavier) aggregates settled to the bottom of the beaker and were not detected by the FBRM probe. Lower mixing rates are normally preferred because they consume less energy and form larger aggregates (lower breakage rate). Excessively low mixing rates, however, disperse polymer flocculants and solids nonuniformly in the slurry. Consequently, an optimum mixing rate must be found, depending on which particular performance response (sediment dewatering or aggregates settling velocity) one is trying to optimize by mixing conditions at a given solids concentration, polymer flocculant type and microstructure.

5.4.5 Effect of Flocculant Dosage

When more flocculant is added to the suspension, the capture efficiency increases because a higher number of cationic chains become available to neutralize the surface of the suspended particles and link them via the bridging mechanism. However, if too much flocculant is added (>11,000 ppm in our case) the charge of the system is reversed and the suspension becomes stable again. A good indication of overdosing is the change in supernatant turbidity. The turbidity of MFT supernatants depends on flocculant dosage. The turbidity initially decreases, as more polymers chains were available to capture suspended particles, but after a certain point the clarity of the supernatant starts to decline (deteriorated fine capture capacity) due to excessive polymer coverage of the particle surface and restabilization of the system

The capture efficiency function in the model includes three parameters, the maximum probability of aggregation, a decay constant (a function of polymer chain relaxation on the particle surface), and the minimum probability of aggregation that is reached after chain relaxation dynamic has reached steady state on the particles (fewer points of contact). Since flocculant chain relaxation on the surface of the particle is mainly affected by the nature of polymer chains and the electrostatic charges of the particles (in a moderate window of flocculant concentration), the capture efficiency decay was assumed to be constant and independent of dosage. Flocculations were performed at several dosages to construct a correlation between capture efficiency and flocculant dosage (Figure 5.11), while keeping all other parameters in the model constant (k_d, s_1, s_2, dF).

The model predicted well the impact of flocculant dosage on aggregate formation as shown in Figure 5.12. Higher dosages increased the average aggregate size mainly due to enhanced charge neutralization of the polymer in the suspension that increased the capture efficiency of the colliding particles. Adding more flocculant increased the average aggregate size, mainly due to enhanced charge neutralization by the polymer.

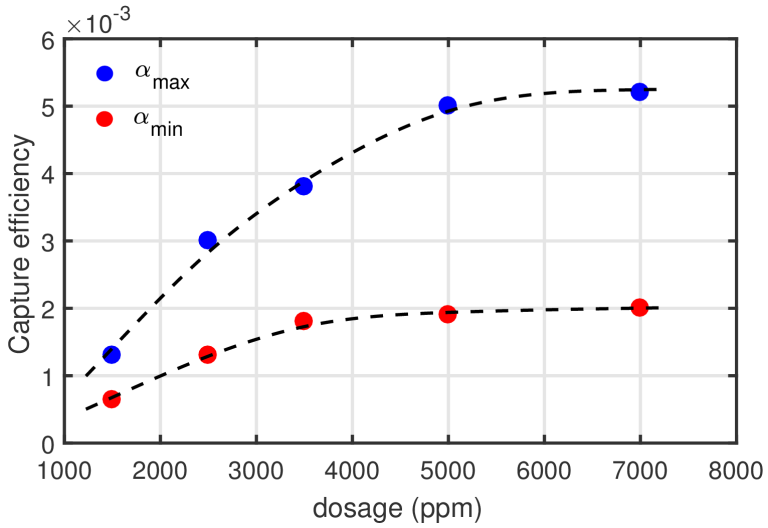

Figure 5.11: Effect of flocculant dosage on the capture efficiency. Data is for MFT particles (3wt.%) flocculated with a partially hydrophobic cationic flocculant (poly(VBTMAC)) (batch flocculation, shear rate= 340 s^{-1} (mg polymer/kg dry particle), pH= 8.6).

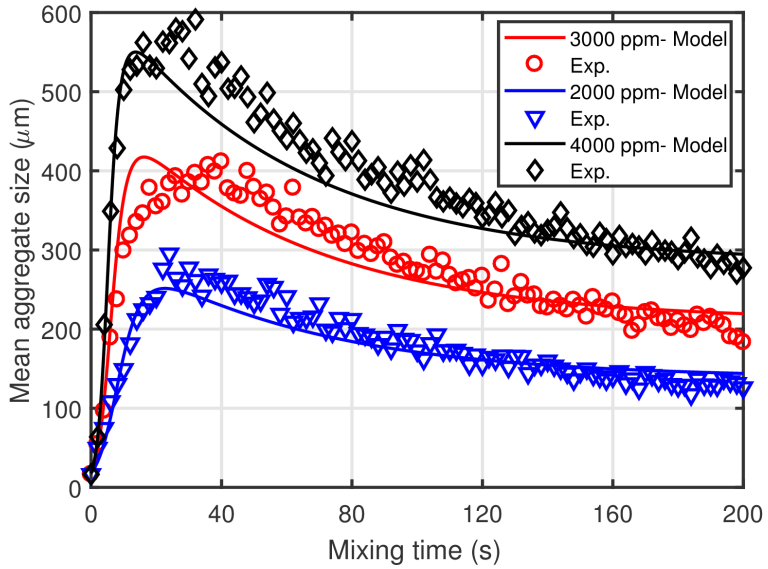

Figure 5.12: Effect of flocculant dosage on the evolution of mean aggregate size of MFT particles (3wt.%) over time flocculated with a partially hydrophobic cationic flocculant (poly(VBTMAC)) (batch flocculation, shear rate= 340 s^{-1} (mg polymer/kg dry particle), pH= 8.6). Model is continuous line and experimental data are symbols

The population balances model in this work was applied to describe flocculation of tailings with low solids content. In field applications, however, tailings with higher solids concentration (at least above 15%) are normal. Increasing solids concentration substantially increases the viscosity of the suspension. As Heath et al. showed for calcite treatment,[103] this would also increase the breakage rate of aggregates, but our preliminary unpublished studies indicate that their proposed model does not work well for MFT. Therefore, a new function would need to be included in the population balance model to account for the effect of high solids concentration. Therefore, upon generating sufficient data at increasing solids concentration, the population balance model proposed herein could be modified to describe the flocculation of more concentrated slurries.

Two main challenges are associated with modeling tailings with high solids content:

1) Conventional batch stirred tank experiments may not be suitable set-ups for high solids, mainly because the nonuniform mixing of high-viscosity slurries generates substantial shear gradients in the system. The latter may be taken into account by coupling the proposed population balance model with a CFD model,[133] at the expense of generating a rather complex model. An alternative system, such as a turbulent pipe flow or a stirred tank with multiple baffles, may solve this problem to some extent.

2) Our experiments showed that at high solids MFT (e.g. 20%), the FBRM probe is rapidly covered with bitumen/organics present in MFT, leading to inaccurate readings of the probe. One needs to solve this operational problem in order to collect reliable data for the model at high solids content. One way to minimize this limitation would be to clean the sapphire window periodically without significantly perturbing aggregate formation.

5.5 Conclusion

This study was the first effort to model polymer-promoted flocculation in oil sands tailings. Population balances were developed and online in-situ FBRM experimental data were used to model polymer flocculation of oil sands mature fine tailing (MFT) in a batch stirred tank set-up. The population balances were developed according to the successful mathematical framework proposed by Hounslow et al.[118] and modified by Spicer and Pratsinis.[120] Focused beam reflectance measurements responses of MFT flocculated with a partially hydrophobic cationic flocculant showed a sharp increase to maximum aggregate size and were followed by a reduction in the aggregate size until a steady state was reached. In the absence of appreciable restructuring, this behavior was attributed to the dynamics of chain relaxation on the surface, thus reducing the probability of aggregation. A new decay capture efficiency function, defined in Equation (5.15), was included in the population balance model to account for this behavior.

Nonuniform shear in the mechanically-stirred batch set-up invalidated the use of aggregates fractal dimensions obtained from external experiments, thus a particle swarm optimization technique was used to extract the mass fractal dimension according to FBRM responses, correcting for the inaccuracies in the application of a mean-shear value in the model. The proposed model could successfully predict the effect of the three most relevant parameters for industrial applications on aggregate formation: shear rate, mixing time, and flocculant dosage.

Chapter 6

Conclusions and Recommendations

6.1 Conclusions

The main objective of this thesis was to study the treatment of oil sands tailings using different polymer flocculants. Investigation of the effect of polymer microstructure on flocculation and dewatering oil sands tailings. A system of cationic copolymers was chosen to accomplish this objective. Polymer reaction engineering tools were used to make a series of cationic copolymers of acrylamide with different molecular weight and chemical composition. Design of experiments and concepts of polymer reaction engineering allowed for a meaningful investigation over the impact of average molecular weight, average chemical composition, and chemical composition distribution of cationic copolymers of acrylamide, DADMAC and VBTMAC on flocculation, aggregate formation, and dewatering of oil sands tailings.

The results showed that for the design of an "optimum" polymer flocculant, one must bear in mind the flocculation/dewatering metrics used to measure its performance. For instance, when producing (at least) cationic copolymers, if the metric of interest is how fast a sediment dewater, then one may not be concerned with the molecular weight of the flocculant, provided that the

average molecular weight does not limit handling and mixing of the polymer solution with tailings. This was evident in CST and SRF tests, where these metrics were shown to be a strong function of flocculant chemical composition but not of flocculant molecular weight. In contrast, if the metrics of interest is how large the aggregate become (the case of settling in thickeners), then polymer molecular weight takes a decisive role in flocculant design.

It was also observed that CST and SRF tests consistently produced similar trends in terms of polymer properties effects. This may suggest the use of the faster CST method over the more time-consuming and tedious SRF method whenever possible, at least for performance characterization of low solids tailings. In terms of the effect of chemical composition distribution (CCD) of polymer flocculants, experimental results show that the CCD of flocculants indeed affected the flocculation results, specifically the formation of aggregates. More interestingly, this effect was found to be different depending on the dosage of the flocculant. For instance, flocculants with broader CCD form larger aggregates compared to flocculants with narrower CCD in low (starving) dosage ranges. These conclusions are likely not restricted to oil sands tailings, and could be applied to similar low solids wastewater systems.

Based on the results summarized above, a new cationic homopolymer flocculant was synthesized. This novel flocculant could effectively place cationic copolymers of acrylamide, while imparting partial hydrophobicity to the flocculant to enhance dewatering of oil sands tailings. The novel flocculant, poly(VBTMAC), contains a quaternary ammonium cation with a pendant benzene ring in its repeating unit. Poly(VBTMAC) homopolymers with molecular weight over one million could be produced within a short conversion time using free radical polymerization.

Focused beam reflectance measurements were used to track down aggregate formation using poly(VBTMAC) of different molecular weights, showing that the underlying flocculation mechanism was bridging induced by charge neutralization. It may be hypothesized that presence of benzene rings on the backbone would enhance the dewatering of tailings using poly(VBTMAC). The ultimate performance of this polymer for dewatering was tested using

undiluted MFT against an industrial standard flocculant, anionic polyacrylamide. Poly(VBTMAC) consistently made sediments with higher dewatering rates and, more interestingly, much higher shear strengths in the sediments compared to anionic polyacrylamide. One limitation in replacing anionic polyacrylamid with poly(VBTMAC) is the substantially higher dosage required to obtain the optimum performance with the latter. However, combining poly(VBTMAC) with anionic polyacrylamid kept the same performance and reduced the required dosages of the flocculants.

The development of a mathematical model to describe the kinetics of aggregate formation in tailings with poly(VBTMAC) was also the subject of this research. Population balances were used to describe this process, and FBRM measurements were used to collect experimental data and train the proposed model. A time-dependent function was proposed and introduced in the model to account for the poly(VBTMAC)-promoted aggregate size dynamics in low solids tailings. The validity of the model was tested by varying the relevant operating parameters including shear rates, mixing time, and polymer dosages. The proposed model is the first of its kind towards a more rational and quantitative approach to control flocculation in oils sands tailings.

In addition to the core work done in this thesis, a few side studies were also performed, as described below:

i) A radically different approach in dealing with oil sands tailings was proposed in which the clays suspended in MFT were used as reinforcement agents for the in-situ production of polyurethane composites. Results showed that composites with similar, and sometimes better properties than those obtained with commercial clay fillers, could be produced out of MFT. Details are discussed in Appendix A.

ii) The effect of the microstructure of copolymers of acrylamide and poly(ethylene oxide methyl ether methacrylate) in flocculation/dewatering of oil sands tailings was also investigated, specifically the effect of comonomer composition, hydrophobic chain length, and molecular weight. A detailed study is described in Appendix B.

iii) Polymer reaction engineering concepts were employed to model the polymerization process of an industrial standard flocculant, poly(AAm-*co*-AAc) (the anionic polyacrylamide), in batch reactors. This polymer is commonly used to treat oil sands tailings. The effect of reactor operating conditions on final product microstructure were simulated in details, as described in Appendix C.

6.2 Recommendations

The findings of this thesis gave rise to several areas that need further investigation:

i) One of the areas that have not been systematically studied yet is how the molecular weight distribution of a flocculant would affect aggregate formation and dewatering performance. Controlled radical polymerization (CRP) techniques could be used to produce polymers with narrow molecular weight distributions. The challenge, however, would remain in obtaining acrylamide polymers with high molecular weights (in the range of millions) with narrow distributions using CRP. Several groups have recently attempted to produce high molecular weight water soluble polymers while maintaining the living character of the polymerization. The typical molecular weight range achieved (maximum of a few 100 000), unfortunately, is still beyond what is easily produced by conventional free radical polymerization and typically recommended for tailings flocculants.[154, 155, 156, 157]

ii) The addition of an optimum amount of polymer in large scale flocculation of tailings in the field is often achieved by observing the onset of flocculation by an operator, in a way that is very similar to what is done in laboratory scale flocculation of tailings. Although this method is reliable, it would be costly to manually monitor the addition of polymers on a continuous basis. In addition, a marginal reduction on the polymer dosage could add a considerably large dollar value in large scale tailings treatment operations. One relatively straightforward solution could be to develop image-processing techniques that, when coupled with data analysis, could determine and control the addition of

the optimum amount of flocculant to a specific tailinga stream. Such soft sensors could be tuned for inclusion of larger operating parameters such as the clay or bitumen content of the tailing streams or effect of water chemistry.

iii) Similar to the idea above, and with a more sophisticated approach, one could further develop the mathematical model proposed in this thesis to account for the effect of other operating conditions such as water chemistry, solids/bitumen contents, or even flocculant microstructure. In large scale, such models should be integrated with CFD models to account for the differences in flow regimes.[133]

Bibliography

[1] Babkir Ali and Amit Kumar. "Development of life cycle water footprints for oil sands-based transportation fuel production". In: *Energy* 131 (2017), pp. 41–49.

[2] Kim L Kasperski and Randy J Mikula. "Waste streams of mined oil sands: characteristics and remediation". In: *Elements* 7.6 (2011), pp. 387–392.

[3] Jacob Masliyah et al. "Understanding water-based bitumen extraction from Athabasca oil sands". In: *The Canadian Journal of Chemical Engineering* 82.4 (2004), pp. 628–654.

[4] Linda Botha and joão BP Soares. "The Influence of Tailings Composition on Flocculation". In: *The Canadian Journal of Chemical Engineering* 93.9 (2015), pp. 1514–1523.

[5] Randy J Mikula et al. "Nature and fate of oil sands fine tailings". In: ACS Publications, 1996.

[6] M Gräfe, A McFarlane, and Craig Klauber. "Clays and the minerals processing value chain (MPVC)". In: *Clays in the Minerals Processing Value Chain*. Cambridge University Press, 2017, pp. 1–80.

[7] Qiuyi Lu et al. "A two-step flocculation process on oil sands tailings treatment using oppositely charged polymer flocculants". In: *Science of the Total Environment* 565 (2016), pp. 369–375.

[8] Aurangzeb Alamgir et al. "Al-PAM assisted filtration system for abatement of mature fine tailings". In: *Chemical engineering science* 80 (2012), pp. 91–99.

[9] Chen Wang et al. “Role of preconditioning cationic zetag flocculant in enhancing mature fine tailings flocculation”. In: *Energy & Fuels* 30.7 (2016), pp. 5223–5231.

[10] Leidiane G Reis et al. “Using acrylamide/propylene oxide copolymers to dewater and densify mature fine tailings”. In: *Minerals Engineering* 95 (2016), pp. 29–39.

[11] Linda Botha et al. “Flocculation of oil sands tailings by hyperbranched functionalized polyethylenes (HBfPE)”. In: *Minerals Engineering* 108 (2017), pp. 71–82.

[12] Dan Zhang, Thomas Thundat, and Ravin Narain. “Flocculation and dewatering of mature fine tailings using temperature-responsive cationic polymers”. In: *Langmuir* 33.23 (2017), pp. 5900–5909.

[13] Atreya K Nittala, Sarang P Gumfekar, and João BP Soares. “Multifunctional CO2-switchable polymers for the flocculation of oil sands tailings”. In: *Journal of Applied Polymer Science* (2019), p. 47578.

[14] Leonardo Pennetta de Oliveira et al. “Dewatering of oil sands tailings with novel chitosan-based flocculants”. In: *Energy & Fuels* 32.4 (2018), pp. 5271–5278.

[15] Sarang P Gumfekar et al. “Dewatering Oil Sands Tailings with Degradable Polymer Flocculants”. In: *ACS applied materials & interfaces* 9.41 (2017), pp. 36290–36300.

[16] Randy Mikula. “Trading water for oil: Tailings management and water use in surface-mined oil sands”. In: (2013).

[17] RJ Mikula, O Omotoso, et al. “Predicting Oil Sands Tailings Behaviour From Clay Content and Water Chemistry”. In: *Canadian International Petroleum Conference*. Petroleum Society of Canada. 2002.

[18] RJ Mikula et al. “Commercial implementation of a dry landscape oil sands tailings reclamation option: consolidated tailings”. In: *Proceedings 7th UNITAR Conference*. 1998.096. 1998, pp. 907–921.

[19] MAURICE B DUSSEAULT and J Don Scott. “Tailings pond behavior and characterization of oil sand tailings sludge”. In: *Particulate Science and Technology* 1.3 (1983), pp. 295–309.

[20] William R Bryant and Richard H Bennet. "Origin, physical, and mineralogical nature of red clays: the Pacific Ocean Basin as a model". In: *Geo-Marine Letters* 8.4 (1988), pp. 189–249.

[21] Jacob Masliyah, Jan Czarnecki, and Zhenghe Xu. "Handbook on theory and practice of bitumen recovery from Athabasca oil sands". In: *Theoretical Basis* 1 (2011).

[22] Koffi Léon Konan et al. "Surface properties of kaolin and illite suspensions in concentrated calcium hydroxide medium". In: *Journal of colloid and interface science* 307.1 (2007), pp. 101–108.

[23] Phillip Fawell. "Solid–Liquid Separation of Clay Tailings". In: *Clays in the Minerals Processing Value Chain*. Ed. by Markus Gräfe et al. Cambridge University Press, 2017, 327–380. DOI: 10.1017/9781316661888.010.

[24] YUANMO WANG. "Development of Ultra-fast Biosensors for Detection of Non-electroactive Neurotransmitters". In: (2017).

[25] v N Fuchs. "Über die stabilität und aufladung der aerosole". In: *Zeitschrift für Physik* 89.11-12 (1934), pp. 736–743.

[26] Venkataramana Runkana, P Somasundaran, and PC Kapur. "Mathematical modeling of polymer-induced flocculation by charge neutralization". In: *Journal of colloid and interface science* 270.2 (2004), pp. 347–358.

[27] Vahid Vajihinejad et al. "Water Soluble Polymer Flocculants: Synthesis, Characterization, and Performance Assessment". In: *Macromolecular Materials and Engineering* (2018), p. 1800526.

[28] John Gregory and Sandor Barany. "Adsorption and flocculation by polymers and polymer mixtures". In: *Advances in colloid and interface science* 169.1 (2011), pp. 1–12.

[29] LT Lee et al. "Adsorption of polyacrylamides on the different faces of kaolinites". In: *Journal of colloid and interface science* 147.2 (1991), pp. 351–357.

[30] Lahcen Nabzar and Emile Pefferkorn. "An experimental study of kaolinite crystal edge-polyacrylamide interactions in dilute suspensions". In: *Journal of colloid and interface science* 108.1 (1985), pp. 243–248.

[31] Mehmet Ali Yukselen and John Gregory. "The reversibility of floc breakage". In: *International Journal of Mineral Processing* 73.2-4 (2004), pp. 251–259.

[32] Matthew L Taylor et al. "Kinetics of adsorption of high molecular weight anionic polyacrylamide onto kaolinite: the flocculation process". In: *Journal of colloid and interface science* 250.1 (2002), pp. 28–36.

[33] Anne-Gwenaelle Guezennec et al. "Transfer and degradation of polyacrylamide-based flocculants in hydrosystems: a review". In: *Environmental Science and Pollution Research* 22.9 (2015), pp. 6390–6406.

[34] AF Horn and EW Merrill. "Midpoint scission of macromolecules in dilute solution in turbulent flow". In: *Nature* 312.5990 (1984), p. 140.

[35] Theo GM Van De Ven. "Kinetic aspects of polymer and polyelectrolyte adsorption on surfaces". In: *Advances in colloid and interface science* 48 (1994), pp. 121–140.

[36] Wei Sung Ng et al. "In situ study of aggregate sizes formed in chalcopyrite-quartz mixture using temperature-responsive polymers". In: *Advanced Powder Technology* 29.8 (2018), pp. 1940–1949.

[37] Maria G Rasteiro et al. "Correlation between flocculation and adsorption of cationic polyacrylamides on precipitated calcium carbonate". In: *Chemical Engineering Research and Design* 95 (2015), pp. 298–306.

[38] Menachem Elimelech, John Gregory, and Xiadong Jia. *Particle deposition and aggregation: measurement, modelling and simulation*. Butterworth-Heinemann, 2013.

[39] Donald H Napper. *Polymeric stabilization of colloidal dispersions*. Vol. 3. Academic Pr, 1983.

[40] Menglian Wei et al. "Stimuli-responsive polymers and their applications". In: *Polymer Chemistry* 8.1 (2017), pp. 127–143.

[41] Fang Liu and Marek W Urban. "Recent advances and challenges in designing stimuli-responsive polymers". In: *Progress in polymer science* 35.1-2 (2010), pp. 3–23.

[42] Yasushi Maeda, Tomomi Higuchi, and Isao Ikeda. "Change in hydration state during the coil- globule transition of aqueous solutions of

poly (N-isopropylacrylamide) as evidenced by FTIR spectroscopy". In: *Langmuir* 16.19 (2000), pp. 7503–7509.

[43] Ipsita Chakraborty et al. "Monitoring Coil–Globule Transitions of Thermoresponsive Polymers by Using NMR Solvent Relaxation". In: *The Journal of Physical Chemistry B* 122.22 (2018), pp. 6094–6100.

[44] Avraham Halperin, Martin Kroeger, and Francoise M Winnik. "Poly (N-isopropylacrylamide) phase diagrams: fifty years of research". In: *Angewandte Chemie International Edition* 54.51 (2015), pp. 15342–15367.

[45] Vitaly J Klenin and Sergei L Shmakov. "Features of phase separation in polymeric systems: cloud-point curves (discussion)". In: *Univers. J. Mater. Sci* 1.2 (2013), pp. 39–45.

[46] M Constantin et al. "Lower critical solution temperature versus volume phase transition temperature in thermoresponsive drug delivery systems". In: *Express Polym Lett* 5.10 (2011), pp. 839–848.

[47] John-Paul O'Shea, Greg G Qiao, and George V Franks. "Temperature-responsive solid–liquid separations with charged block-copolymers of poly (N-isopropyl acryamide)". In: *Langmuir* 28.1 (2011), pp. 905–913.

[48] Wei Sung Ng et al. "In situ investigation of aggregate sizes formed using thermo-responsive polymers: Effect of temperature and shear". In: *Journal of colloid and interface science* 494 (2017), pp. 139–152.

[49] Han Lu et al. "Temperature-and pH-responsive benzoboroxole-based polymers for flocculation and enhanced dewatering of fine particle suspensions". In: *ACS applied materials & interfaces* 7.49 (2015), pp. 27176–27187.

[50] Haihong Li et al. "Enhancing treatment and geotechnical stability of oil sands fine tailings using thermo-sensitive poly (n-isopropyl acrylamide)". In: *The Canadian Journal of Chemical Engineering* 93.10 (2015), pp. 1780–1786.

[51] Sarang P Gumfekar, Vahid Vajihinejad, and João BP Soares. "Advanced Polymer Flocculants for Solid–Liquid Separation in Oil Sands Tailings". In: *Macromolecular rapid communications* 40.1 (2019), p. 1800644.

[52] Behnaz Bazoubandi. "Synthesis and Characterization of Amylopectin-grafted Polyacrylamide (AP-g-PAM) Flocculants for Dewatering of Oil Sands Mature Fine Tailings (MFT)". In: (2018).

[53] WY Yang, JW Qian, and ZQ Shen. "A novel flocculant of Al (OH) 3–polyacrylamide ionic hybrid". In: *Journal of colloid and interface science* 273.2 (2004), pp. 400–405.

[54] Xiaoyan Wang et al. "Polymer aids for settling and filtration of oil sands tailings". In: *The Canadian Journal of Chemical Engineering* 88.3 (2010), pp. 403–410.

[55] Wei Sun et al. "Study of Al (OH) 3- Polyacrylamide-Induced Pelleting Flocculation by Single Molecule Force Spectroscopy". In: *Langmuir* 24.24 (2008), pp. 14015–14021.

[56] FA Benn et al. "Sedimentation and consolidation of different density aggregates formed by polymer-bridging flocculation". In: *Chemical Engineering Science* 184 (2018), pp. 111–125.

[57] Allan D Costine et al. "Aggregate structures formed by hyperbranched functionalized polyethylene (HBfPE) treatment of oil sands tailings". In: *The Canadian Journal of Chemical Engineering* 97.1 (2019), pp. 99–102.

[58] J Farrow and L Warren. "Measurement of the size of aggregates in suspension". In: *SURFACTANT SCIENCE SERIES* (1993), pp. 391–391.

[59] Allan D Costine et al. "Aggregate structures formed by hyperbranched functionalized polyethylene (HBfPE) treatment of oil sands tailings". In: *Manuscript submitted for publication in Canadian Journal of Chemical Engineering* (2018).

[60] RIS Gill and TM Herrington. "The flocculation of kaolin suspensions with cationic polyacrylamides of varying molar mass but the same cationic character". In: *Colloids and surfaces* 22.1 (1987), pp. 51–76.

[61] RIS Gill and TM Herrington. "The flocculation of kaolin suspensions using polyethylenimine and cationic polyacrylamides of the same molar mass but different charge density". In: *Colloids and surfaces* 28 (1987), pp. 41–52.

[62] R Subramanian, S Zhu, and RH Pelton. "Synthesis and flocculation performance of graft and random copolymer microgels of acrylamide and diallyldimethylammonium chloride". In: *Colloid and Polymer Science* 277.10 (1999), pp. 939–946.

[63] Kun Xu et al. "A Novel Hyperbranched Polymeric Flocculant for Wastewater Treatment". In: *Journal of Polymers and the Environment* 26.7 (2018), pp. 2782–2792.

[64] MS Nasser and AE James. "The effect of polyacrylamide charge density and molecular weight on the flocculation and sedimentation behaviour of kaolinite suspensions". In: *Separation and purification technology* 52.2 (2006), pp. 241–252.

[65] Allan Costine et al. "Variations in the molecular weight response of anionic polyacrylamides under different flocculation conditions". In: *Chemical Engineering Science* 176 (2018), pp. 127–138.

[66] Phillip M Fedorak et al. "Methanogenic potential of tailings samples from oil sands extraction plants". In: *Canadian Journal of Microbiology* 48.1 (2002), pp. 21–33.

[67] Barry Bara et al. *Oil sands fine tailings flocculation using dynamic mixing*. US Patent App. 13/620,121. 2013.

[68] George Vincent Franks and Haihong Li. *Flotation aids and processes for using the same*. US Patent 8,915,374. 2014.

[69] C Steven Sikes, T Daniel Sikes, and Mark A Hochwalt. *Flotation and separation of flocculated oils and solids from waste waters*. US Patent 9,321,663. 2016.

[70] Haijing Ren et al. "Effect of hydrophobic group on flocculation properties and dewatering efficiency of cationic acrylamide copolymers". In: *Reactive and functional polymers* 67.7 (2007), pp. 601–608.

[71] Ying Zhou and George V Franks. "Flocculation mechanism induced by cationic polymers investigated by light scattering". In: *Langmuir* 22.16 (2006), pp. 6775–6786.

[72] M Ma and S Zhu. "Grafting polyelectrolytes onto polyacrylamide for flocculation 2. Model suspension flocculation and sludge dewatering". In: *Colloid and Polymer Science* 277.2-3 (1999), pp. 123–129.

[73] Haihong Li, John-Paul O'Shea, and George V Franks. "Effect of molecular weight of poly (N-isopropyl acrylamide) temperature-sensitive flocculants on dewatering". In: *AIChE journal* 55.8 (2009), pp. 2070–2080.

[74] Fabien Brand et al. "Polyelectrolytes with various charge densities: Synthesis and characterization of diallyldimethylammonium chloride-acrylamide copolymers". In: *Die Angewandte Makromolekulare Chemie* 248.1 (1997), pp. 41–71.

[75] Niousha Kazemi et al. "Reactivity ratio estimation in radical copolymerization: from preliminary estimates to optimal design of experiments". In: *Industrial & Engineering Chemistry Research* 53.18 (2014), pp. 7305–7312.

[76] Victor E Meyer and George G Lowry. "Integral and differential binary copolymerization equations". In: *Journal of Polymer Science Part A: General Papers* 3.8 (1965), pp. 2843–2851.

[77] Calista Preusser et al. "Modeling the radical batch homopolymerization of acrylamide in aqueous solution". In: *Macromolecular Reaction Engineering* 10.5 (2016), pp. 490–501.

[78] PR Suresha, Manohar V Badiger, and Bernhard A Wolf. "Polyelectrolytes in dilute solution: viscometric access to coil dimensions and salt effects". In: *RSC Advances* 5.35 (2015), pp. 27674–27681.

[79] SM Shawki and AE Hamielec. "Estimation of transfer constants in the aqueous solution polymerization of acrylamide with potassium persulfate initiator". In: *Journal of Applied Polymer Science* 23.11 (1979), pp. 3341–3354.

[80] Colin Klein et al. "Impact of fugitive bitumen on polymer-based flocculation of mature fine tailings". In: *The Canadian Journal of Chemical Engineering* 91.8 (2013), pp. 1427–1432.

[81] Thomas R Rooney et al. "Cationic hydrolytically degradable flocculants with enhanced water recovery for oil sands tailings remediation". In: *Macromolecular Materials and Engineering* 301.10 (2016), pp. 1248–1254.

[82] John Neter, William Wasserman, and Michael H Kutner. "Applied linear statistical models: regression, analysis of variance, and experimental designs". In: *Irwin, Boston* (1990).

[83] João BP Soares. "The use of instantaneous distributions in polymerization reaction engineering". In: *Macromolecular Reaction Engineering* 8.4 (2014), pp. 235–259.

[84] Tuyu Xie and Archie E Hamielec. "Modelling free-radical copolymerization kinetics—evaluation of the pseudo-kinetic rate constant method, 1. Molecular weight calculations for linear copolymers". In: *Macromolecular Theory and Simulations* 2.3 (1993), pp. 421–454.

[85] KA Clark and DS Pasternack. "Hot water seperation of bitumen from Alberta bituminous sand". In: *Industrial & Engineering Chemistry* 24.12 (1932), pp. 1410–1416.

[86] Vahid Vajihinejad, Rina Guillermo, and João BP Soares. "Dewatering Oil Sands Mature Fine Tailings (MFTs) with Poly (acrylamide-co-diallyldimethylammonium chloride): Effect of Average Molecular Weight and Copolymer Composition". In: *Industrial & Engineering Chemistry Research* 56.5 (2017), pp. 1256–1266.

[87] Diógenes RL Vedoy and Joao BP Soares. "Water-soluble polymers for oil sands tailing treatment: A Review". In: *The Canadian Journal of Chemical Engineering* 93.5 (2015), pp. 888–904.

[88] Chen Wang et al. "Current state of fine mineral tailings treatment: A critical review on theory and practice". In: *Minerals Engineering* 58 (2014), pp. 113–131.

[89] Huaili Zheng et al. "UV-initiated polymerization of hydrophobically associating cationic flocculants: Synthesis, characterization, and dewatering properties". In: *Chemical engineering journal* 234 (2013), pp. 318–326.

[90] Shuji Sakohara et al. "Consolidation of suspended particles by using dual ionic thermosensitive polymers with incorporated a hydrophobic component". In: *Separation and purification technology* 106 (2013), pp. 90–96.

[91] Haijing Ren et al. “Flocculation of kaolin suspension with the adsorption of N, N-disubstituted hydrophobically modified polyacrylamide”. In: *Colloids and Surfaces A: Physicochemical and Engineering Aspects* 317.1-3 (2008), pp. 388–393.

[92] Rhys Hripko et al. “Enhanced Flocculation of Oil Sands Mature Fine Tailings Using Hydrophobically Modified Polyacrylamide Copolymers”. In: *Global Challenges* 2.3 (2018), p. 1700135.

[93] Hongjun Li et al. “Flocculation of kaolinite clay suspensions using a temperature-sensitive polymer”. In: *AIChE journal* 53.2 (2007), pp. 479–488.

[94] Sarang P Gumfekar and João BP Soares. “A novel hydrophobically-modified polyelectrolyte for enhanced dewatering of clay suspension”. In: *Chemosphere* 194 (2018), pp. 422–431.

[95] M Hahn and W Jaeger. “Kinetics of the free radical polymerization of dimethyl diallyl ammonium chloride, 5. Kinetic model with persulfate as initiator”. In: *Die Angewandte Makromolekulare Chemie: Applied Macromolecular Chemistry and Physics* 198.1 (1992), pp. 165–178.

[96] Ch Wandrey, J Hernandez-Barajas, and D Hunkeler. “Diallyldimethylammonium chloride and its polymers”. In: *Radical polymerisation polyelectrolytes*. Springer, 1999, pp. 123–183.

[97] Vahid Vajihinejad, Sarang P Gumfekar, and JBP Soares. “Floc formation in oil sands tailings induced by a water-soluble cationic polymer with hydrophobic groups”. In: *Manuscript submitted for publication* (2017).

[98] Xiuju Yang and Liang Ni. “Synthesis of hybrid hydrogel of poly (AM co DADMAC)/silica sol and removal of methyl orange from aqueous solutions”. In: *Chemical engineering journal* 209 (2012), pp. 194–200.

[99] Colin Saraka et al. “Effective sapphire repellency treatment to reduce fouling of a focused beam reflectance measurement (FBRM) probe in bituminous systems”. In: *The Canadian Journal of Chemical Engineering* 97.6 (2019), pp. 1949–1952.

[100] M Soos et al. “Dynamic response studies on aggregation and breakage dynamics of colloidal dispersions in stirred tanks”. In: *Journal of dispersion science and technology* 29.4 (2008), pp. 605–610.

[101] Mahdi Abdollahi et al. “A comprehensive study on the kinetics of aqueous free-radical homo-and copolymerization of acrylamide and diallyldimethylammonium chloride by online 1 H-NMR spectroscopy”. In: *Journal of Polymer Research* 20.10 (2013), p. 239.

[102] John Gregory. “Monitoring particle aggregation processes”. In: *Advances in colloid and interface science* 147 (2009), pp. 109–123.

[103] Alex R Heath et al. “Polymer flocculation of calcite: Population balance model”. In: *AIChE Journal* 52.5 (2006), pp. 1641–1653.

[104] Cordelia Selomulya et al. “Understanding the role of restructuring in flocculation: the application of a population balance model”. In: *Chemical Engineering Science* 58.2 (2003), pp. 327–338.

[105] Ricardo I Jeldres, Fernando Concha, and Pedro G Toledo. “Population balance modelling of particle flocculation with attention to aggregate restructuring and permeability”. In: *Advances in colloid and interface science* 224 (2015), pp. 62–71.

[106] Doraiswami Ramkrishna. *Population balances: Theory and applications to particulate systems in engineering*. Academic press, 2000.

[107] Peter Hänggi. “Smoluchowski’s Oeuvre: Its Impact for Physics and Chemistry”. 4-th Conference on Statistical Physics: Modern Trends and Applications. 2012.

[108] Marian Von Smoluchowski. “Drei vortrage uber diffusion. Brownsche bewegung und koagulation von kolloidteilchen”. In: *Z. Phys.* 17 (1916), pp. 557–585.

[109] M v Smoluchowski. “Versuch einer mathematischen Theorie der Koagulationskinetik kolloider Lösungen”. In: *Zeitschrift für physikalische Chemie* 92.1 (1918), pp. 129–168.

[110] Caliane Bastos Borba Costa, Maria Regina Wolf Maciel, and Rubens Maciel Filho. “Considerations on the crystallization modeling: Population balance solution”. In: *Computers & chemical engineering* 31.3 (2007), pp. 206–218.

[111] Hecham M Omar and Sohrab Rohani. "Crystal population balance formulation and solution methods: A review". In: *Crystal Growth & Design* (2017).

[112] Costas Kiparissides et al. "Population balance modeling of particulate polymerization processes". In: *Industrial & engineering chemistry research* 43.23 (2004), pp. 7290–7302.

[113] Daniele Semino and W Harmon Ray. "Control of systems described by population balance equations—II. Emulsion polymerization with constrained control action". In: *Chemical Engineering Science* 50.11 (1995), pp. 1825–1839.

[114] Anwesha Chaudhury et al. "Population Balance Models for Pharmaceutical Processes". In: *Process Simulation and Data Modeling in Solid Oral Drug Development and Manufacture* (2016), pp. 43–83.

[115] Charles David Immanuel and Francis Joseph Doyle. "Solution technique for a multi-dimensional population balance model describing granulation processes". In: *Powder Technology* 156.2 (2005), pp. 213–225.

[116] Venkataramana Runkana, P Somasundaran, and PC Kapur. "A population balance model for flocculation of colloidal suspensions by polymer bridging". In: *Chemical Engineering Science* 61.1 (2006), pp. 182–191.

[117] PTL Koh, JRG Andrews, and PHT Uhlherr. "Modelling shear-flocculation by population balances". In: *Chemical engineering science* 42.2 (1987), pp. 353–362.

[118] MJ Hounslow, RL Ryall, and VR Marshall. "A discretized population balance for nucleation, growth, and aggregation". In: *AIChE Journal* 34.11 (1988), pp. 1821–1832.

[119] Sanjeev Kumar and D Ramkrishna. "On the solution of population balance equations by discretization—I. A fixed pivot technique". In: *Chemical Engineering Science* 51.8 (1996), pp. 1311–1332.

[120] Patrick T Spicer and Sotiris E Pratsinis. "Coagulation and fragmentation: universal steady-state particle-size distribution". In: *AIChE journal* 42.6 (1996), pp. 1612–1620.

[121] Robert McGraw. "Description of aerosol dynamics by the quadrature method of moments". In: *Aerosol Science and Technology* 27.2 (1997), pp. 255–265.

[122] Daniele L Marchisio, R Dennis Vigil, and Rodney O Fox. "Quadrature method of moments for aggregation–breakage processes". In: *Journal of colloid and interface science* 258.2 (2003), pp. 322–334.

[123] A Ding, MJ Hounslow, and CA Biggs. "Population balance modelling of activated sludge flocculation: Investigating the size dependence of aggregation, breakage and collision efficiency". In: *Chemical Engineering Science* 61.1 (2006), pp. 63–74.

[124] AL Ahmad, MF Chong, and S Bhatia. "Population Balance Model (PBM) for flocculation process: Simulation and experimental studies of palm oil mill effluent (POME) pretreatment". In: *Chemical Engineering Journal* 140.1 (2008), pp. 86–100.

[125] Rosalynn Loerke, Xiaoli Tan, and Qi Liu. "Dewatering of Oil Sands Mature Fine Tailings by Dual Polymer Flocculation and Pressure Plate Filtration". In: *Energy & Fuels* (2017).

[126] Alebachew Demoz and Randy J Mikula. "Role of mixing energy in the flocculation of mature fine tailings". In: *Journal of Environmental Engineering* 138.1 (2011), pp. 129–136.

[127] Chandra W Angle and Sameh Gharib. "Effects of sand and flocculation on dewaterability of kaolin slurries aimed at treating mature oil sands tailings". In: *Chemical Engineering Research and Design* 125 (2017), pp. 306–318.

[128] Paul C Painter, Bruce G Miller, and Aron Lupinsky. *Oil sands tailings treatment*. US Patent App. 15/370,479. 2016.

[129] Ying Zhu, Xiaoli Tan, and Qi Liu. "Dual polymer flocculants for mature fine tailings dewatering". In: *The Canadian Journal of Chemical Engineering* 95.1 (2017), pp. 3–10.

[130] Wen-zheng Yu et al. "The role of mixing conditions on floc growth, breakage and re-growth". In: *Chemical Engineering Journal* 171.2 (2011), pp. 425–430.

[131] Sudip K Pattanayek and Vinay A Juvekar. "Adsorption of polymer from solution to solid surface: Effect of polydispersity". In: *Macromolecules* 36.3 (2003), pp. 956–960.

[132] YD Yan et al. "The flocculation efficiency of polydisperse polymer flocculants". In: *International Journal of Mineral Processing* 73.2 (2004), pp. 161–175.

[133] Alex R Heath and Peter TL Koh. "Combined population balance and CFD modelling of particle aggregation by polymeric flocculant". In: *Proceedings of the 3rd International Conference on CFD in the Minerals and Process Industries*. CSIRO Melbourne, Australia. 2003, pp. 10–12.

[134] Syncrude Research. *Determination of bitumen, water and solids content of oil sand, reject and slurry samples (Classical). Method 2.7. Syncrude analytical methods for oil sand and bitumen processing*. Report. Version 1979. Canada: Syncrude Canada Limited, Syncrude Research, 1979.

[135] Jörg Worlitschek and Marco Mazzotti. "Choice of the focal point position using Lasentec FBRM". In: *Particle & Particle Systems Characterization* 20.1 (2003), pp. 12–17.

[136] Douglas J Turner. "Clathrate hydrate formation in water-in-oil dispersions". PhD thesis. Colorado School of Mines. Arthur Lakes Library, 2005.

[137] R Hecker et al. "Focused beam reflectance measurement for the continuous assessment of flocculant performance". In: *Polymers in Mineral Processing*. Canad. Inst. Mining, Metall. Petrol Montreal, Quebec, 1999, pp. 91–105.

[138] Alex R Heath et al. "Estimating average particle size by focused beam reflectance measurement (FBRM)". In: *Particle & Particle Systems Characterization* 19.2 (2002), pp. 84–95.

[139] GC Bushell et al. "On techniques for the measurement of the mass fractal dimension of aggregates". In: *Advances in Colloid and Interface Science* 95.1 (2002), pp. 1–50.

[140] Chunwoo Lee and Timothy A Kramer. "Prediction of three-dimensional fractal dimensions using the two-dimensional properties of fractal ag-

gregates". In: *Advances in colloid and interface science* 112.1 (2004), pp. 49–57.

[141] Karl A Kusters et al. "Ultrasonic fragmentation of agglomerate powders". In: *Chemical engineering science* 48.24 (1993), pp. 4119–4127.

[142] PGf Saffman and JS Turner. "On the collision of drops in turbulent clouds". In: *Journal of Fluid Mechanics* 1.1 (1956), pp. 16–30.

[143] Jürgen C Flesch, Patrick T Spicer, and Sotiris E Pratsinis. "Laminar and turbulent shear-induced flocculation of fractal aggregates". In: *AIChE journal* 45.5 (1999), pp. 1114–1124.

[144] Thomas R Camp and Philip C Stein. "Velocity gradients and internal work in fluid motion". In: *Journal of the Boston Society of Civil Engineers* 85 (1943), pp. 219–37.

[145] D Cory Hopkins and Joel J Ducoste. "Characterizing flocculation under heterogeneous turbulence". In: *Journal of Colloid and Interface Science* 264.1 (2003), pp. 184–194.

[146] Massimo Poletto and Daniel D Joseph. "Effective density and viscosity of a suspension". In: *Journal of Rheology* 39.2 (1995), pp. 323–343.

[147] Karl A Kusters, Johan G Wijers, and Dirk Thoenes. "Aggregation kinetics of small particles in agitated vessels". In: *Chemical Engineering Science* 52.1 (1997), pp. 107–121.

[148] Qing Jiang and Bruce E Logan. "Fractal dimensions of aggregates determined from steady-state size distributions". In: *Environmental Science & Technology* 25.12 (1991), pp. 2031–2038.

[149] S Liu and JH Masliyah. "Suspensions: fundamentals and applications in the petroleum industry". In: *Advances in Chemistry (American Chemical Society, Washington, DC, 1996)* 251 (1996).

[150] R Hogg. "Collision efficiency factors for polymer flocculation". In: *Journal of colloid and interface science* 102.1 (1984), pp. 232–236.

[151] JD Pandya and LA Spielman. "Floc breakage in agitated suspensions: theory and data processing strategy". In: *Journal of Colloid and Interface Science* 90.2 (1982), pp. 517–531.

[152] Alex Heath. "The simulation of polymer aggregation/breakage at high solid fraction in turbulent flow by population balance". PhD thesis. Murdoch University, 2002.

[153] TGM Van de Ven and SG Mason. "The microrheology of colloidal dispersions VII. Orthokinetic doublet formation of spheres". In: *Colloid & Polymer Science* 255.5 (1977), pp. 468–479.

[154] Eric A Appel et al. "High molecular weight polyacrylamides by atom transfer radical polymerization: Enabling advancements in water-based applications". In: *Journal of Polymer Science Part A: Polymer Chemistry* 50.1 (2012), pp. 181–186.

[155] Wen-Jun Wang et al. "Synthesis and characterization of hyperbranched polyacrylamide using semibatch reversible addition- fragmentation chain transfer (RAFT) polymerization". In: *Macromolecules* 43.9 (2010), pp. 4062–4069.

[156] Mathias Destarac et al. *Preparation of hydrophilic polymers of high mass by controlled radical polymerization.* US Patent 9,975,980. 2018.

[157] R Nicholas Carmean et al. "Ultra-high molecular weights via aqueous reversible-deactivation radical polymerization". In: *Chem* 2.1 (2017), pp. 93–101.

[158] Donald R Paul and Lioyd M Robeson. "Polymer nanotechnology: nanocomposites". In: *Polymer* 49.15 (2008), pp. 3187–3204.

[159] Xia Cao et al. "Polyurethane/clay nanocomposites foams: processing, structure and properties". In: *Polymer* 46.3 (2005), pp. 775–783.

[160] Fengge Gao. "Clay/polymer composites: the story". In: *Materials today* 7.11 (2004), pp. 50–55.

[161] Pravakar Mondal and DV Khakhar. "Regulation of cell structure in water blown rigid polyurethane foam". In: *Macromolecular Symposia*. Vol. 216. 1. Wiley Online Library. 2004, pp. 241–254.

[162] Tomy Widya and Christopher W Macosko. "Nanoclay-modified rigid polyurethane foam". In: *Journal of Macromolecular Science, Part B: Physics* 44.6 (2005), pp. 897–908.

[163] Biqiong Chen et al. "A critical appraisal of polymer–clay nanocomposites". In: *Chemical Society Reviews* 37.3 (2008), pp. 568–594.

[164] Zhen-Guo Yang et al. "Study on the mechanical properties of hybrid reinforced rigid polyurethane composite foam". In: *Journal of Applied Polymer Science* 92.3 (2004), pp. 1493–1500.

[165] G Harikrishnan, T Umasankar Patro, and DV Khakhar. "Polyurethane foam- clay nanocomposites: nanoclays as cell openers". In: *Industrial & engineering chemistry research* 45.21 (2006), pp. 7126–7134.

[166] MC Saha, Md E Kabir, and S Jeelani. "Enhancement in thermal and mechanical properties of polyurethane foam infused with nanoparticles". In: *Materials Science and Engineering: A* 479.1-2 (2008), pp. 213–222.

[167] Zhongbin Xu et al. "Novel preparation and mechanical properties of rigid polyurethane foam/organoclay nanocomposites". In: *Journal of applied polymer science* 106.1 (2007), pp. 439–447.

[168] Liliana Madaleno et al. "Processing and characterization of polyurethane nanocomposite foam reinforced with montmorillonite–carbon nanotube hybrids". In: *Composites Part A: Applied Science and Manufacturing* 44 (2013), pp. 1–7.

[169] Umme Salma Rima. "Characterization and centrifuge dewatering of oil sands fine tailings". PhD thesis. Faculty of Graduate Studies and Research, University of Regina, 2013.

[170] M Thirumal et al. "Effect of foam density on the properties of water blown rigid polyurethane foam". In: *Journal of applied polymer science* 108.3 (2008), pp. 1810–1817.

[171] Susmita Sengupta, Eric L Tollefson, and Ajay K Dalai. "Recovery, characterization and conceptual modelling of Non-Bituminous organic materials from oil sands". In: *The Canadian Journal of Chemical Engineering* 75.2 (1997), pp. 379–390.

[172] Shau-Tarng Lee and Natarajan S Ramesh. *Polymeric foams: mechanisms and materials*. CRC press, 2004.

[173] Stanislav R Stoyanov, Feng Lin, and Yuming Xu. "Solvent-kaolinite interactions investigated using the 3D-RISM-KH molecular theory of solvation". In: *Clays and Clay Minerals* 66.3 (2018), pp. 286–296.

[174] RJ Mikula, VA Munoz, O Omotoso, et al. "Centrifugation options for production of dry stackable tailings in surface-mined oil sands tailings management". In: *Journal of Canadian Petroleum Technology* 48.09 (2009), pp. 19–23.

[175] Hongzhou Shang et al. "Synthesis, characterization, and flocculation properties of poly (acrylamide-methacryloxyethyltrimethyl ammonium chloride-methacryloxypropyltrimethoxy silane)". In: *Journal of Applied Polymer Science* 111.3 (2009), pp. 1594–1599.

[176] Lana Alagha et al. "Probing adsorption of polyacrylamide-based polymers on anisotropic basal planes of kaolinite using quartz crystal microbalance". In: *Langmuir* 29.12 (2013), pp. 3989–3998.

[177] Wilhelm E Walles. "Role of flocculant molecular weight in the coagulation of suspensions". In: *Journal of Colloid and Interface Science* 27.4 (1968), pp. 797–803.

[178] JM Henderson and AD Wheatley. "Factors affecting the efficient flocculation of tailings by polyacrylamides". In: *Coal Perparation* 4.1-2 (1987), pp. 1–49.

[179] Shulei Li et al. "Flocculating and dewatering performance of hydrophobic and hydrophilic solids using a thermal-sensitive copolymer". In: *Water Science and Technology* 76.3 (2017), pp. 694–704.

[180] Alberta Energy Regulator. "Directive 085". In: *Fluid Tailings Management for Oil Sands Mining Projects* (2016).

[181] Nicholas Beier et al. "Impact of flocculation-based dewatering on the shear strength of oil sands fine tailings". In: *Canadian Geotechnical Journal* 50.9 (2013), pp. 1001–1007.

[182] S KY Gawu and AB Fourie. "Assessment of the modified slump test as a measure of the yield stress of high-density thickened tailings". In: *Canadian geotechnical journal* 41.1 (2004), pp. 39–47.

[183] D Lorne Ball et al. "A rapid method for the determination of bitumen, water, and solids in oil sands". In: *Canadian Journal of Chemistry* 59.10 (1981), pp. 1527–1530.

[184] Huining Xiao, Robert Pelton, and Archie Hamielec. "Preparation and kinetic characterization of copolymers of acrylamide and poly (ethy-

lene glycol)(meth) acrylate macromonomers". In: *Polymer* 37.7 (1996), pp. 1201–1209.

[185] Alberta Energy Regulator. "Directive 085: Fluid tailings management for oil sands mining projects". In: *Alberta Energy Regulator: Alberta, AB, Canada* (2017).

[186] Marc A Dubé et al. "Mathematical modeling of multicomponent chain-growth polymerizations in batch, semibatch, and continuous reactors: a review". In: *Industrial & Engineering Chemistry Research* 36.4 (1997), pp. 966–1015.

[187] Jose Asua. *Polymer reaction engineering*. John Wiley & Sons, 2008.

[188] WH Stockmayer. "Distribution of chain lengths and compositions in copolymers". In: *The Journal of Chemical Physics* 13.6 (1945), pp. 199–207.

[189] TY Xie et al. "Experimental investigation of vinyl chloride polymerization at high conversion: molecular-weight development". In: *Polymer* 32.6 (1991), pp. 1098–1111.

[190] Marzieh Riahinezhad et al. "Optimal estimation of reactivity ratios for acrylamide/acrylic acid copolymerization". In: *Journal of Polymer Science Part A: Polymer Chemistry* 51.22 (2013), pp. 4819–4827.

[191] Nils FG Wittenberg et al. "Modeling acrylic acid radical polymerization in aqueous solution". In: *Macromolecular Reaction Engineering* 10.2 (2016), pp. 95–107.

[192] Jiangyan Feng et al. "In-Situ NMR Measurement of Reactivity Ratios for Copolymerization of Methyl Methacrylate and Diallyl Dimethylammonium Chloride". In: *Industrial & Engineering Chemistry Research* 57.46 (2018), pp. 15654–15662.

[193] Calista Preusser and Robin A Hutchinson. "An In-Situ NMR Study of Radical Copolymerization Kinetics of Acrylamide and Non-I onized Acrylic Acid in Aqueous Solution". In: *Macromolecular Symposia*. Vol. 333. 1. Wiley Online Library. 2013, pp. 122–137.

[194] Danilo Cuccato, Giuseppe Storti, and Massimo Morbidelli. "Experimental and Modeling Study of Acrylamide Copolymerization with Qua-

ternary Ammonium Salt in Aqueous Solution". In: *Macromolecules* 48.15 (2015), pp. 5076–5087.

[195] Ming S Liu et al. "Conformational transitions and dynamics of thermal responsive poly (N-isopropylacrylamide) polymers as revealed by molecular simulation". In: *European Polymer Journal* 55 (2014), pp. 153–159.

[196] Irmgard Bischofberger et al. "Hydrophobic hydration of poly-N-isopropyl acrylamide: a matter of the mean energetic state of water". In: *Scientific reports* 4 (2014), p. 4377.

[197] J Pillai. "Flocculants and coagulants: The keys to water and waste management in aggregate production". In: *Stone review* (1997), pp. 1–6.

[198] Han Lu et al. "Molecular weight dependence of synthetic glycopolymers on flocculation and dewatering of fine particles". In: *Langmuir* 32.44 (2016), pp. 11615–11622.

[199] O Sawalha and M Scholz. "Assessment of capillary suction time (CST) test methodologies". In: *Environmental technology* 28.12 (2007), pp. 1377–1386.

[200] Alexander Senaputra et al. "Focused beam reflectance measurement for monitoring the extent and efficiency of flocculation in mineral systems". In: *AIChE Journal* 60.1 (2014), pp. 251–265.

[201] S Proskin, D Sego, and M Alostaz. "Freeze–thaw and consolidation tests on Suncor mature fine tailings (MFT)". In: *Cold Regions Science and Technology* 63.3 (2010), pp. 110–120.

[202] Vahid Vajihinejad and Joao BP Soares. "Monitoring polymer flocculation in oil sands tailings: A population balance model approach". In: *Chemical Engineering Journal* 346 (2018), pp. 447–457.

[203] Zhen Yang et al. "Synthesis of amphoteric starch-based grafting flocculants for flocculation of both positively and negatively charged colloidal contaminants from water". In: *Chemical Engineering Journal* 244 (2014), pp. 209–217.

[204] Yinan Wang et al. “Temperature-responsive hyperbranched amine-based polymers for solid–liquid separation”. In: *Langmuir* 30.9 (2014), pp. 2360–2368.

[205] Veronica Czitrom. “One-factor-at-a-time versus designed experiments”. In: *The American Statistician* 53.2 (1999), pp. 126–131.

[206] Vahid Vajihinejad and João BP Soares. “Can we make better polyurethane composite foams with oil sands mature fine tailing?” In: *Macromolecular Materials and Engineering* 301.4 (2016), pp. 383–389.

[207] ASTM. “Standard test method for methylene blue index of clay”. In: (2009).

[208] Heather AW Kaminsky et al. “Characterization of heavy minerals in the Athabasca oil sands”. In: *Minerals Engineering* 21.4 (2008), pp. 264–271.

[209] Robert B Jackson et al. “Trading water for carbon with biological carbon sequestration”. In: *science* 310.5756 (2005), pp. 1944–1947.

[210] Adrian Peter Revington et al. *Process for Flocculating and Dewatering Oil Sand Mature Fine Tailings*. US Patent App. 13/496,176. 2010.

[211] Leticia Pérez et al. “Study of influence of pH and salinity on combined flocculation of Chaetoceros gracilis microalgae”. In: *Chemical Engineering Journal* 286 (2016), pp. 106–113.

[212] Mehmet Ali Yukselen and John Gregory. “The effect of rapid mixing on the break-up and re-formation of flocs”. In: *Journal of Chemical Technology and Biotechnology* 79.7 (2004), pp. 782–788.

[213] Doraiswami Ramkrishna and Alan W Mahoney. “Population balance modeling. Promise for the future”. In: *Chemical Engineering Science* 57.4 (2002), pp. 595–606.

[214] AF Grabsch et al. “The impact of achieving a higher aggregate density on polymer-bridging flocculation”. In: *International Journal of Mineral Processing* 124 (2013), pp. 83–94.

**

Appendix A

Can We Make Better Polyurethane Composite Foams with Oil Sands Mature Fine Tailing?

In this study, we produced rigid polyurethane/mature fine tailings (PU/MFT) foam composites with good mechanical and thermal properties by in-situ polymerization. MFT contains inorganic fillers and water, which is the chemical blowing agent for PU reactive foam polymerization. The novel PU/MFT composites have similar compression and tension properties, and improved thermal properties, compared to those of PU/Cloisite Na^+ and PU/ Cloisite 30B composites. Adding 2 pphp (parts per hundred parts of polyol by weight) of MFT particles decreased the thermal conductivity of rigid PU foam by 10%, while adding Cloisite Na^+ or Cloisite 30B caused a reduction of only 6% and 5%, respectively. This apparently small difference in thermal conductivity would result in considerable energy saving in large-scale insulation applications. Fur-

A version of this appendix has been published as V. Vajihinejad, J. Soares "Can We Make Better Polyurethane Composite Foams with Oil Sands Mature Fine Tailing?" Macromolecular Materials and Engineering, 2016, vol. 301, pp 383-389.

thermore, adding from 0 to 20 pphp of fillers caused the specific compressive and tensile strengths to increase initially, but then fall for all filler types. However, PU/MFT foams could sustain about the same compressive strength and modulus even when loaded up to 20 pphp MFT. These results are important for oil sands industries trying to decrease the environmental footprint of their operations and for polyurethane-producing companies attempting to improve properties of their products and contribute to environmental cleanup.

A.1 Introduction

When the waste stream of an oil sands extraction process is released into tailing ponds, a stable mixture of water (about 65% by mass), fine particles (30-35%), small amount of residual bitumen and other minerals (about 2-5%) forms over time. We call this mixture mature fine tailings (MFT).[4] Oil sands tailing ponds cover an area 1.5 times the size of the city of Vancouver (176 km^2); this area is equivalent to about 33,000 football fields, including the two end zones. Not surprisingly, tailing ponds are among the most challenging environmental problems in Canada. Because small charged particles (smaller than 44 μm) do not allow MFTs to settle on their own, many groups in academia and industry have proposed methods to dewater tailings, so the industry can solidify the remaining waste and reclaim the land.[87]

A radically different approach is to consider MFT as valuable materials rather than wastes. Since MFT is a source of organically-modified fine particles such as quartz and clays (kaolinite, illite, and montmorillonite), it may be used as a reinforcing material in polymer composites and nanocomposites. Polymer nanocomposites are polymers filled with particles that have at least one dimension in the range of 1-100 nm.[158] Since nanoparticles have high surface energy, they interact with polymer chains at the molecular level more effectively, improving their mechanical, thermal, and barrier properties.[159] Polymer-clay nanocomposites were firstly used by Toyota Motor Co. in the 90s, when the company used nylon-clay nanocomposites to obtain better thermal and mechanical properties in timing belt cover and other components of car

engines.[160]

One of the widely used matrices in the area of polymer nanocomposites is polyurethane (PU), accounting for the highest supply in the global foam market. Polyurethanes can be tailored to fulfill many applications such as cushioning, thermal insulation, footwear, buoyancy applications, and packaging. Polyurethanes are the products of catalyzed polyaddition reactions between polyols and isocyanates, and PU foam is made when a blowing agent, such as distilled water, is added to the reaction mixture. The reaction between isocyanate and water molecules generates carbon dioxide bubbles that form the cellular structure of the foam. Different fillers such as nanoclays, graphene, titanium dioxide, and carbon nanofibers have been used to make PU nanocomposites foams.[161, 159]

Several researchers have studied the effect of clays on mechanical, thermal, and barrier properties of rigid or flexible PU foams. Clays could be pure or treated with organic compounds (e.g. alkyl ammonium salts).[162, 163, 164, 165] Among pure clays, montmorillonite is usually the choice because it has cations in its crystal galleries that are exchangeable with other cations of similar charge to form organically-modified clays. Among them, we may mention Cloisite 15A, 25A, and 30B, among others. For example, Cloisite 15A is a montmorrillonite (MMT) modified with ditallow dimethylammonium salts. Cao et al. found that adding 5% of organically-modified clay significantly enhanced the specific compressive strength and thermal properties of PU foams with higher molecular weight polyols (M_n = 500), while observing slightly negative effects in the case of highly crosslinked PU foams.[159, 166] In another study by Xu et al., the tensile and compression strengths increased by a maximum of 154% and 118%, respectively, when the authors added 2% clay to PU.[167] However, we cannot confidently judge these results because the authors did not show how the foam density changed as a function of clay content. In another work by Saha and his team, addition of 1% MMT considerably improved mechanical and thermal properties of rigid PU foams.[166] In this work, we made rigid PU foams filled with inorganic solids from oil sands mature fine tailings (MFTs) using an in-situ polymerization technique

(PU/MFT), and compared their mechanical and thermal properties with those of PU composites made with pristine and organically-modified clays. Surprisingly, we found the properties of our PU/MFT composites to be equivalent, and often better, than the properties of PU composites using regular clays. This initial research results may open new directions for the disposal and use of oil sands mature fine tailings.

A.2 Experimental Section

A.2.1 Materials

Suncor's Oil Sands plant in Alberta, Canada, supplied the mature fine tailings (MFT) samples used in this research. Cloisite Na^+ (pure MMT) and Cloisite 30B (MMT modified by methyl tallow bis-2-hydroxyethyl ammonium) were purchased from Southern Clay, USA. Huntsman Polyurethanes generously supplied polyol and isocyanate monomers. The polyol was a blend of JEFFOL SD-361 (OH value: 360, M_n= 690, viscosity at 25°C: 5500 cP) and JEFFOL SD-441 (OH value: 400, M_n= 550, viscosity at 25°C: 2500 cP). The isocyanate was RUBINATE M MDI (a diphenylmethane diisocyanate, NCO equivalent weight: 133, viscosity at 25°C: 180 cP). The catalyst (pentamethyldiethylenetriamine) was supplied by Sigma-Aldrich, and Evonik Canada Inc. generously provided the surfactant (TEGOSTAB 8404). The blowing agent was deionized water.

A.2.2 Polymerization of Rigid Polyurethane Foams

For comparison purposes, we firstly removed the water in the MFT samples by placing them in a vacuum oven at 100°C. Then, we ground Cloisite Na^+, Cloisite 30B, and MFT particles for 5 minutes in an automatic Mortar Grinder (RM 200, Retsch Technology) and dehydrated the remaining moisture in a vacuum oven at 100°C. We mixed Cloisite Na^+, Cloisite 30B, or MFT particles in desired proportions with the polyol in a vessel under magnetic stirring for 24 hours at 65°C, cooled the polyol/particles mixtures to room temperature

(21 ± 0.5°C), and then added 0.8 pphp (parts per hundred parts of polyol by weight) of catalyst, 1.5 pphp of blowing agent, and 0.8 pphp of surfactant, and stirred the resulting blend for 15 seconds at 2500 rpm. After that, we added the isocyanate and stirred the reactive mixture for 7 seconds at 3000 rpm. Immediately after, we poured the reactive mixture into an open-top wood mold covered with aluminum foil (19 cm × 19 cm × 8 cm) and left it for about 10 minutes until the polymerization was completed. Finally, we demolded the foam composites and kept them for about 2 days at room temperature to cure completely. We adopted our synthesis procedure from Khakhar et al.[165]

A.2.3 Measurements and Characterization

The microstructure of PU foams with and without fillers was analyzed with a XL30 scanning electron microscope (SEM) and a Morgagni 268 Philips-FEI transmission electron microscope (TEM). We cut the samples for SEM analysis using a sharp razor, and after coating with Au/Pd using a Hummer 6.2 Sputter Coater, we mounted them into SEM sample holders for observations. To obtain average cell size, we carried out image analysis on SEM micrographs using Scandium 5.0 imaging software. We prepared samples for TEM according to the procedure in Madaleno et al.[168] Compression and tension tests were performed using a 5943 Instron machine with 1 KN load cell. We cut the specimens using a band saw machine (9-in Bandsaw, Mastercraft) and performed tensile tests according to ASTM 638-14 with type I specimens at a crosshead speed of 2.25 mm min^{-1}. We performed compression tests according to ASTM D1621, and measured compressive strength and modulus in the rising direction of the foam, with specimens with dimensions of 25.4 mm × 25.4 mm × 12.7 mm. The crosshead speed of the compression test was 1.2 mm min^{-1}. We tested a minimum of eight specimens. The thermal conductivity of foams was measured with a Hot Disk thermal constants analyzer (TPS 2500S) with sample sizes of 35 mm × 35 mm × 8 mm. We tested a minimum of three specimens. The apparent density of foams was measured according to D1622/D1622M–14. We cut the samples in cubes with a volume of 16.4 cm^3, and tested a minimum of five specimens. The particle size distribution

of fillers was measured with a Mastersizer 3000 laser diffraction particle size analyzer (Malvern Instrument Ltd.). Deionized water was used as dispersant and obscuration was set in the range of 4-5%.

A.3 Results and Discussion

A.3.1 Characteristics of MFT

Mature fine tailings are mixtures of about 30-35% solid and 65-70% water by mass. The solid in MFT consists of about 50% quartz (SiO_2), 45% clays (35% kaolinite, 60% illite, and other clay minerals), 5% bitumen, and other organic and mineral compounds. The cation exchange capacity of MFT has been estimated to be 29 cmol(+) kg^{-1}. A typical MFT has Na^+ (776 mg cm^{-3}), HCO^{3-} (679 mg cm^{-3}), Cl^{-1} (518 mg cm^{-3}), and $SO_2{}^{2-}$ (377 mg cm^{-3}), with a pH of about 8.5.[169] Figure A2 compares the particle size distribution of an MFT sample with those of a commercial Cloisite Na^+. The distribution of the MFT particle size has a longer tail of larger particles, but a less pronounced shoulder in the small particle size range. Figure A1 compares the SEM micrographs of MFT particles and commercial Cloisite Na^+. The Cloisite Na^+ particles have smoother surfaces than MFT particles. MFT particles also appear to be thicker than the commercial clay, forming broken structures with irregular shapes. MFT particles also have a broader particle size distribution, as shown in Figure A2.

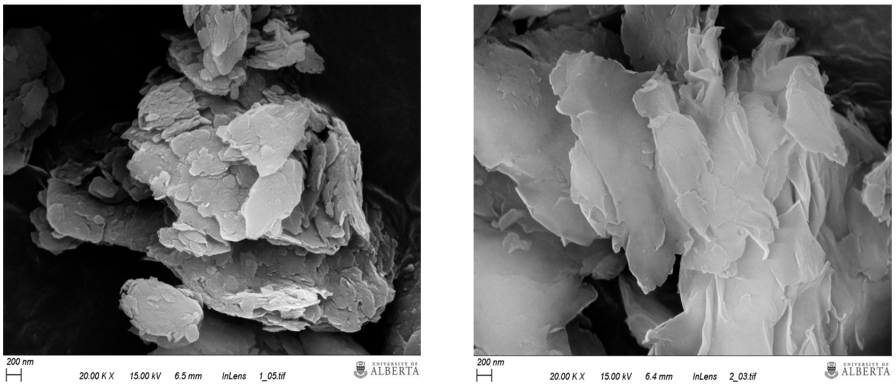

Figure A1: SEM micrographs of particles in MFT and commercial clay. Left micrograph is MFT particles and the right micrograph is Cloisite Na^+.

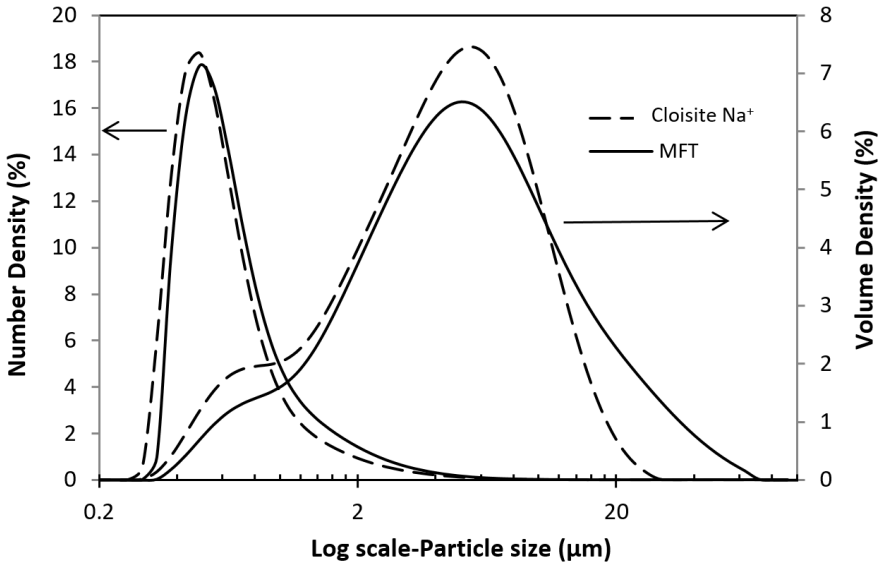

Figure A2: Volume-density and number-density particle size distribution of MFT and Cloisite Na^+.

A.3.2 Mechanical Properties of PU Foam Composites

Figure A5a - A5b compare the compression and tensile properties of PU/MFT, PU/Cloisite Na^+, and PU/Cloisite 30B composites. Since the mechanical properties of foams depend on their densities, we needed to correct for differences in apparent density among these samples to reach a meaningful conclu-

sion when comparing the properties of these composites. We accounted for density effects using the results reported by Thirumal et al.[170] We divided the measured compressive strength, compressive modulus, tensile strength, and tensile modulus by the apparent density raised to the power of 1.5, 1.72, 1.48, or 1.48, respectively. The Table shown in Figure A3 represents the apparent density of the foams, the observed, and the specific values for both tensile and compression tests. The specific compressive and tensile strength and modulus of the foam composites initially increase as fillers are added, but decrease after reaching a maximum value. Macosko et al. suggested that clay initiates a competition between two effects: a positive effect due to clay reinforcement, and a negative effect caused by the disruption of hydrogen bonds between polymer chains.[159] Our observations corroborate this explanation: the first upward trend on mechanical properties is dominated by the reinforcement effect, but eventually the negative effect on H-bonding suppression predominates.

Composites made with MFT had relatively better properties than the other two composite foams. We suggest that bitumen and other organic compounds found on the surface of MFT particles enhance their dispersion in the polyol mixture by van der Waals and ionic interactions. Understanding the roots of these interactions is difficult because MFT is composed of many mineral particles with different structures and relatively unknown interactions. Sengupta and Tollefson, however, proposed a conceptual model for oil sand tailings that simplifies understanding the interaction between the constituents of MFT.[171] Figure A6 illustrates how the organic constituents in MFT act as compatibilizers between particles and polymer chains. Bitumen and non-bituminous compounds form van der Waals interactions with the organic polymer (red arrows), and with the help of cations form ionic interactions with clay particles (blue arrows).

Figure A7 presents TEM micrographs of PU composites filled with 3 pphp Cloisite Na^+ and MFT. MFT particles are relatively better dispersed than Cloisite Na^+, since the clay stacks in the MFT composite do not agglomerate as much as in the case of Cloisite Na^+. This observation tells us there is

a stronger interaction between filler and the polymer in the case of MFT, suggesting bitumen and organics in MFT play a positive role in the structural reinforcement of the polymer composites.

Composite type	Apparent density (kg m^{-3})	Observed compressive modulus (MPa)	Specific compressive modulus (MPa g^{-1} cm^3)	Observed compressive strength (MPa)	Specific compressive strength (MPa g^{-1} cm^3)	Observed tensile modulus (MPa)	Specific tensile modulus (MPa g^{-1} cm^3)	Observed tensile strength (MPa)	Specific tensile strength (MPa g^{-1} cm^3)
Pure PU	71.1 ± 1.7	12.36 ± 0.22	8.08 ± 0.14	0.38 ± 0.01	0.64 ± 0.01	7.26 ± 0.18	13.20 ± 0.34	0.48 ± 0.02	0.88 ± 0.04
1 pphp Cloisite 30B	57.3 ± 0.4	9.44 ± 0.23	8.92 ± 0.22	0.31 ± 0.02	0.71 ± 0.01	6.09 ± 0.16	15.21 ± 0.39	0.38 ± 0.02	0.94 ± 0.07
2 pphp Cloisite 30B	56.1 ± 0.7	9.68 ± 0.30	9.52 ± 0.29	0.31 ± 0.02	0.75 ± 0.01	5.20 ± 0.21	13.45 ± 0.54	0.34 ± 0.01	0.89 ± 0.03
3 pphp Cloisite 30B	55.9 ± 1.6	9.99 ± 0.31	9.84 ± 0.31	0.31 ± 0.04	0.75 ± 0.03	5.33 ± 0.03	13.79 ± 0.07	0.30 ± 0.01	0.78 ± 0.02
5 pphp Cloisite 30B	68.9 ± 2.1	12.33 ± 0.34	8.48 ± 0.23	0.40 ± 0.02	0.69 ± 0.01	7.21 ± 0.23	13.70 ± 0.45	0.34 ± 0.03	0.64 ± 0.06
10 pphp Cloisite 30B	70.7 ± 1.1	11.64 ± 0.26	7.66 ± 0.17	0.35 ± 0.01	0.60 ± 0.01	7.60 ± 0.05	13.91 ± 0.08	0.36 ± 0.02	0.66 ± 0.03
20 pphp Cloisite 30B	75.7 ± 2.6	11.59 ± 0.24	6.78 ± 0.14	0.35 ± 0.02	0.54 ± 0.01	8.45 ± 0.16	13.97 ± 0.27	0.36 ± 0.02	0.60 ± 0.03
1 pphp MFT	45.1 ± 1.3	7.47 ± 0.15	10.65 ± 0.08	0.24	0.79	4.15 ± 0.29	14.76 ± 0.46	0.29 ± 0.04	1.05 ± 0.06
2 pphp MFT	46.2 ± 1.1	7.79 ± 0.11	10.68 ± 0.05	0.25	0.79 ± 0.01	3.88 ± 0.30	13.33 ± 0.46	0.28 ± 0.01	0.97 ± 0.02
3 pphp MFT	53.3 ± 1.3	9.35 ± 0.10	10.01 ± 0.04	0.29 ± 0.03	0.76 ± 0.03	4.58 ± 0.17	12.74 ± 0.21	0.33 ± 0.02	0.92 ± 0.04
5 pphp MFT	65.7 ± 1.2	11.95 ± 0.28	8.93 ± 0.08	0.37 ± 0.01	0.71 ± 0.01	6.54 ± 0.10	13.35 ± 0.09	0.36 ± 0.01	0.73 ± 0.01
10 pphp MFT	66.5 ± 1.1	11.76 ± 0.31	8.61 ± 0.08	0.35 ± 0.01	0.66 ± 0.01	6.87 ± 0.04	13.78 ± 0.03	0.35 ± 0.01	0.71
20 pphp MFT	67.3 ± 1.8	11.43 ± 0.24	8.21 ± 0.06	0.36	0.65	6.83 ± 0.05	13.46 ± 0.04	0.31 ± 0.01	0.62 ± 0.01
1 pphp Cloisite Na$^+$	55.9 ± 0.2	9.56 ± 0.15	9.42 ± 0.06	0.31 ± 0.02	0.75 ± 0.02	5.32 ± 0.09	13.78 ± 0.11	0.35 ± 0.03	0.90 ± 0.07
2 pphp Cloisite Na$^+$	53.0 ± 0.9	9.17 ± 0.43	9.91 ± 0.17	0.30 ± 0.02	0.77 ± 0.02	4.75 ± 0.02	13.33 ± 0.03	0.27 ± 0.01	0.77 ± 0.02
3 pphp Cloisite Na$^+$	61.1 ± 5.1	10.98 ± 0.09	9.29 ± 0.03	0.35 ± 0.02	0.73 ± 0.01	5.73 ± 0.07	13.01 ± 0.07	0.34 ± 0.02	0.77 ± 0.06
5 pphp Cloisite Na$^+$	62.8 ± 0.9	10.73 ± 0.20	8.67 ± 0.06	0.34 ± 0.03	0.68 ± 0.02	6.05 ± 0.09	13.22 ± 0.09	0.33 ± 0.01	0.73 ± 0.03
10 pphp Cloisite Na$^+$	68.2 ± 2.3	11.01 ± 0.36	7.71 ± 0.09	0.36 ± 0.02	0.65 ± 0.01	7.19 ± 0.04	13.88 ± 0.03	0.34 ± 0.01	0.67 ± 0.02

Figure A3: Observed and specific values for mechanical properties of PU foam composites with different fillers.

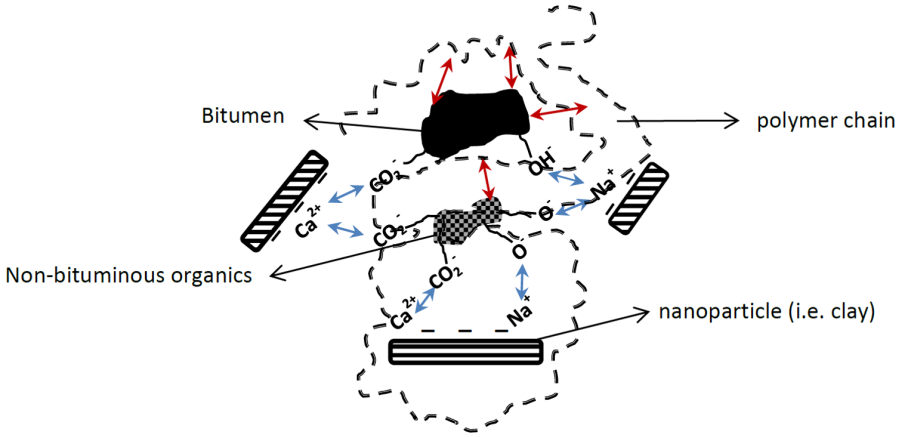

Figure A6: Schematic model showing how polymer chains and MFT particles interact in a MFT/polyol mixture. Red and blue arrays indicate polymer-MFT interactions and interactions between particles of MFT, respectively.

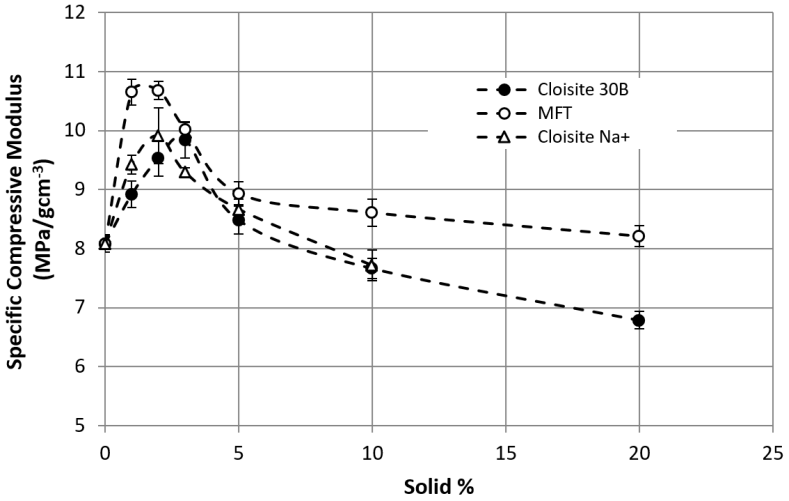

Figure A4a: Specific compressive modulus of PU composite foams. Error bars represent the standard error of these measurements

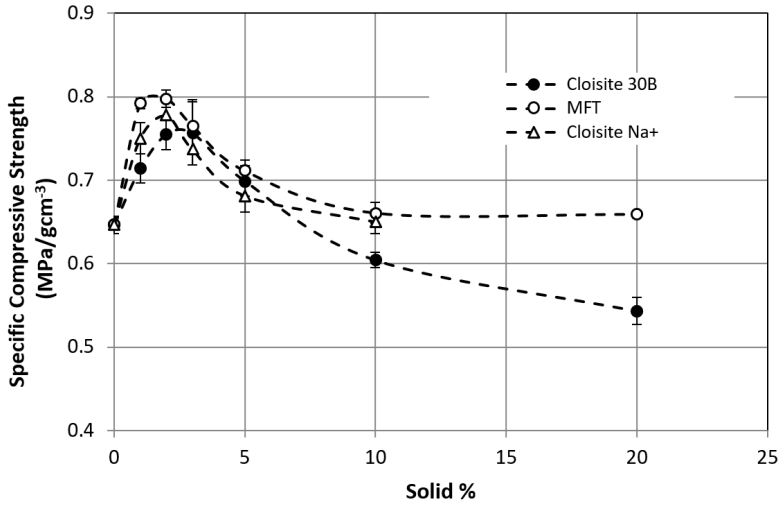

Figure A4b: Specific compressive strength of PU composite foams. Error bars represent the standard error of these measurements

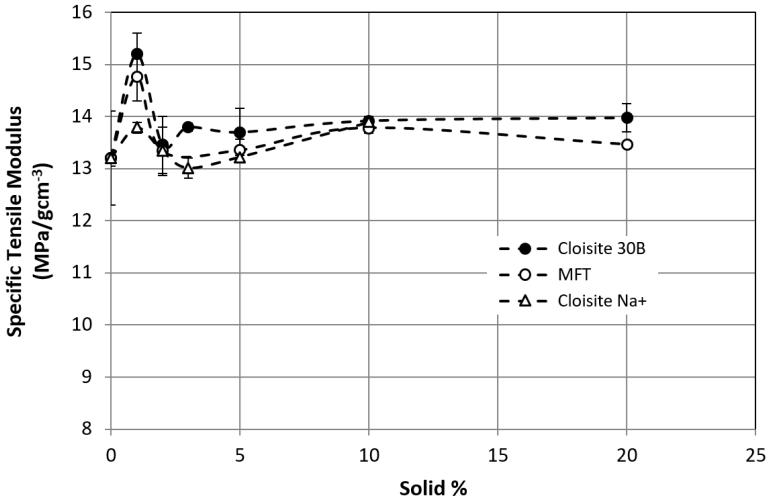

Figure A5a: Specific tensile modulus of PU composite foams. Error bars represent the standard error of these measurements

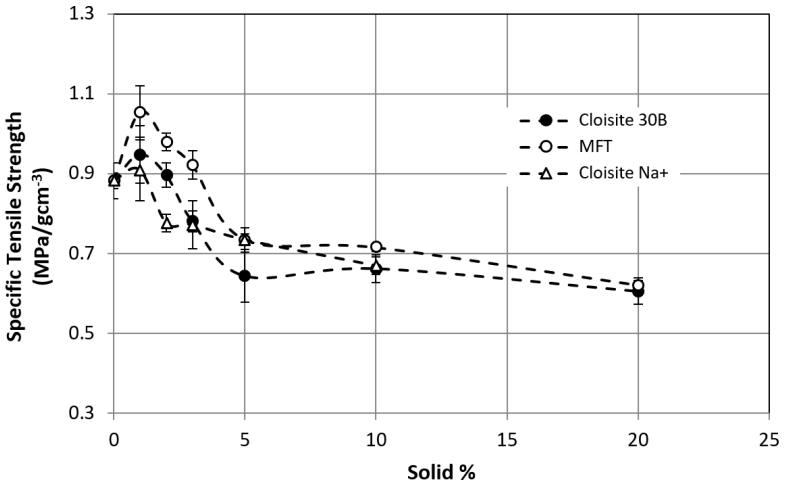

Figure A5b: Specific tensile strength of PU composite foams. Error bars represent the standard error of these measurements

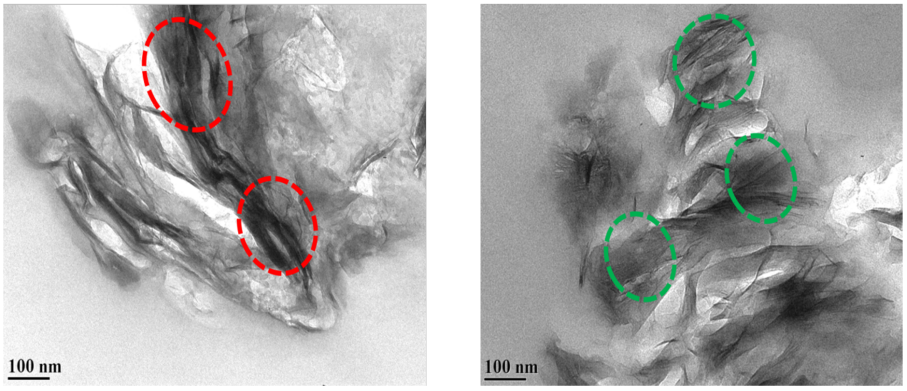

Figure A7: TEM micrographs of PU foam composites. Left micrograph is PU filled with 3 pphp Cloisite Na^+ and the right micrograph is PU filled with 3 pphp MFT. Circles in red and green compare dispersion of particles of each filler in the polymer. PU/MFT is better dispersed in the PU medium.

A.3.3 Thermal Conductivity

Figure A8 shows the thermal conductivity of PU composite foams infused with various amounts of different clay types. The thermal conductivity of rigid PU foams is an essential property for thermal insulation applications. Heat transfer in foams occurs by three mechanisms: conduction through the solid (polymer) phase, radiation, and gas conduction. In the range of our foams density, polymer conduction, gas conduction, and radiation contribute about 50%, 40%, and 10% to the total heat transferred, respectively.[172] Since density has a negligible influence on thermal conductivity in the density range of this study (50-70 kg m^{-3}),[172] we did not correct the observed values to account for density differences. The thermal conductivity drops when we added relatively small amounts of clays because the average cell size also decreases (Figure A9 and Table A1). When we increased the clay loading, however, the thermal conductivity started increasing because more broken cells are formed, more bubbles coalesce, and the contribution of solid conduction grows due to the addition of clays to the polymer. In low to moderate clay loadings, the thermal conductivity is mostly a function of the average cell size. Table A1 lists apparent densities and average cell sizes of all PU foams composites. The smallest average cell size was measured for the PU/MFT composite with 1

pphp of MFT particles. Clay particles promote the formation of smaller CO2 bubbles because they provide nucleation sites when the foam is expanding in the mold. On the other hand, too much clay reduces van der Waals forces (mainly hydrogen bonds) between polymer chains, weakens cell structures, and cause them to break, forming cells with larger diameter.

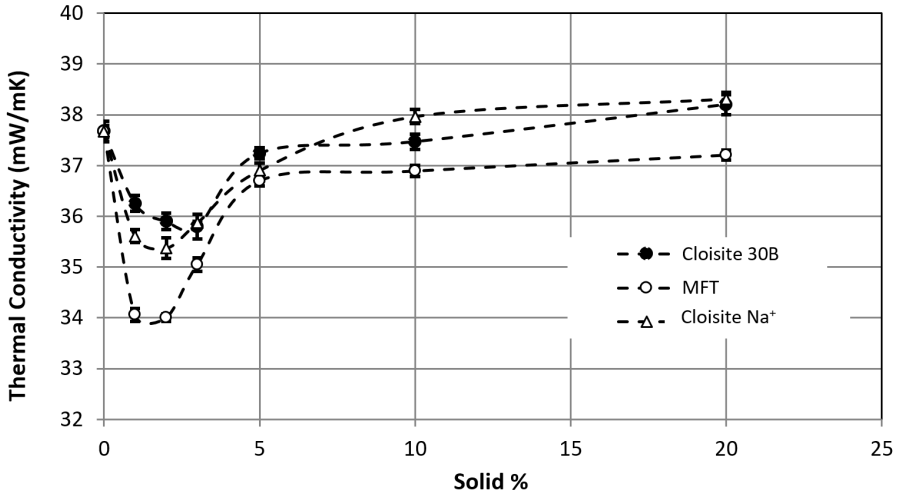

Figure A8: Thermal conductivity of PU composite foams. Error bars represent the standard error of the measurements.

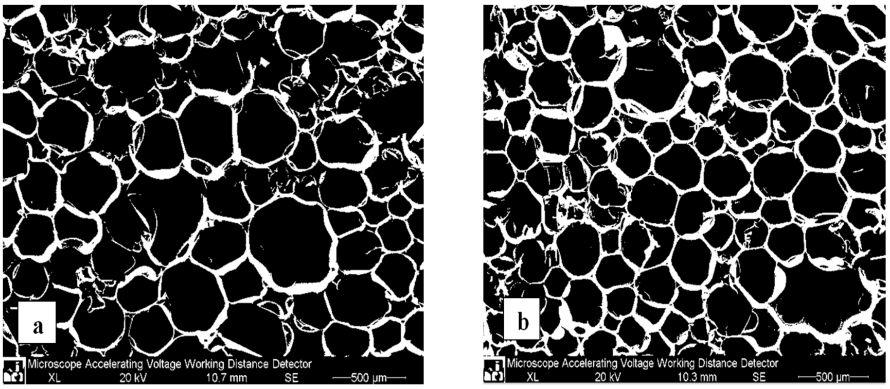

Figure A9: Thermal conductivity of PU composite foams. Error bars represent the standard error of the measurements.

Table A1: Apparent density and average cell size of PU nanocomposites infused with different nanoparticles at different concentrations.

Foam type	Apparent density (kg m^{-3})	Average cell size (mm)
Pure	71.1 ± 1.7	0.248 ± 0.023
1 pphp Cloisite 30B	57.3 ± 0.4	0.238 ± 0.017
2 pphp Cloisite 30B	56.1 ± 0.7	0.234 ± 0.032
3 pphp Cloisite 30B	55.9 ± 1.6	0.250 ± 0.027
5 pphp Cloisite 30B	68.9 ± 2.1	0.242 ± 0.026
10 pphp Cloisite 30B	70.7 ± 1.1	0.244 ± 0.024
20 pphp Cloisite 30B	75.7 ± 2.6	0.250 ± 0.024
1 pphp MFT particles	45.1 ± 1.3	0.187 ± 0.027
2 pphp MFT particles	46.2 ± 1.1	0.200 ± 0.031
3 pphp MFT particles	53.3 ± 1.3	0.205 ± 0.028
5 pphp MFT particles	65.7 ± 1.2	0.217 ± 0.026
10 pphp MFT particles	66.5 ± 1.1	0.234 ± 0.026
20 pphp MFT particles	67.3 ± 1.8	0.225 ± 0.028
1 pphp Cloisite Na^+	55.9 ± 0.2	0.219 ± 0.026
2 pphp Cloisite Na^+	53.0 ± 0.9	0.197 ± 0.029
3 pphp Cloisite Na^+	61.1 ± 5.1	0.222 ± 0.030
5 pphp Cloisite Na^+	62.8 ± 0.9	0.237 ± 0.022
10 pphp Cloisite Na^+	68.2 ± 2.3	0.239 ± 0.021
20 pphp Cloisite Na^+	71.4 ± 1.8	0.230 ± 0.026

A.4 Conclusion

We used mixtures of organically modified fine particles present in oil sands mature fine tailing (MFT) to make rigid polyurethane (PU) composite foams. Polyurethane foams filled with MFT particles had better mechanical and thermal properties than pure polyurethane or polyurethane foams filled with commercial clays (Cloisite Na^+ and Cloisite 30B). We attribute this enhancement to bitumen and other organic compounds present on the surface of MFT particles, which act as compatibilizers between polymer chains and clay particles. Furthermore, MFT particles may reduce the thermal conductivity of PU foams by about 10%, by providing nucleation sites that reduced the average cell size of the CO_2 bubbles. Polyurethane foam composites with lower thermal conductivities can save a substantial amount of energy in large-scale applications. For instance, if we consider a building with 100 units, with each unit using about 50 m^2 $\times$ 10 cm insulation panel to maintain a steady state temperature, we would prevent an energy loss about 300 MW.hr throughout a year with only 10% reduction in thermal conductivity of insulating foams

Appendix B

Enhanced Dewatering of Oil Sands Mature Fine Tailings by Use of Hydrophobically-Modified Polyacrylamide Copolymers

Hydrophobically-modified acrylamide copolymers dewater oil sands tailings more effectively than A-poly(AAm), but the root causes for this enhanced performance have not been investigated systematically. We synthetized polyacrylamide-poly(ethylene oxide methyl ether methacrylate) copolymers with different comonomer compositions, hydrophobic chain lengths, and molecular weights to map out these effects systematically. Through a statistical design of experiments, we found out that all three variables above significantly affected flocculation performance, and that certain combinations achieved optimal results. We also investigated the effect of centrifugation on the flocculation and dewatering

A version of this appendix has been published as R. Hripko, V. Vajihinejad, J. Soares "Enhanced flocculation of oil sands mature fine tailings using hydrophobically modified polyacrylamide copolymers" Global Challenges, 2018, vol. 2, p. 1700135.

performance of these polymers.

B.1 Introduction

There is a stigma surrounding the Alberta Oil Sands in terms of environmental hazards. One of the main contributors to this stigma is the generation of large volumes of waste stored in tailings ponds. Tailings ponds are composed of water, residual bitumen, fine mineral particles, and organic compounds, covering an area more than 175 km^2.[4] Masliyah et al. stated that this problem is getting worse – for every barrel of crude bitumen extracted, 3.3 m^3 of tailings are discharged in the environment.[21] This problem is not going away any time soon, since the negatively charged fine particles (mostly clays) suspended in the tailings prevent the suspension from settling.[173] To wait many decades for the tailings ponds to consolidate naturally is unacceptable not only for the oil sands processing companies, but also for the Canadian society. Many researchers are trying to find solutions to this problem, and several are investigating novel water-soluble polymers to achieve rapid flocculation and dewatering.[87, 10, 88] Increasing the efficiency of tailings separation would be immediately beneficial to oil sands processing companies, as it would significantly lower both the volume of tailings creation and costs of operation.[88]

The industry has practiced several technologies to dewater and consolidate tailings. Thin lift and freeze-thaw drying, centrifugation, and composite tailing are examples of some of these practices.[2] In thin lift drying, for example, a thin layer of polymer-flocculated tailings is spread over a land area with small slope, and allowed to dewater until the remaining sediments are ready for land-reclamation. The method is easy and relatively inexpensive, but requires a large land area. Another technology is composite tailing, where fluid fine tailings are mixed with sands and are flocculated using polymers or chemical additives such as gypsum. The sands helps aggregate dewater more rapidly by making channels in the sediments, and it also strengthens the sediments. One drawback of this method is the use of large amounts of sand, which

otherwise could be used to build storage containment dikes for tailings.[2] Centrifugation is also a technology that may be used for the densification of sediments after flocculation, if run under conditions that are economically viable. Mikula et al. concluded that centrifugation of MFT could drastically reduce the water loss per barrel of bitumen, and also eradicate any possible need for the storage of tailings in fluid form, reducing the time elapsed between mining and reclamation.[174] All the mentioned technologies have one thing in common: they all use polymer flocculant to aggregate fines in tailings.

The industry standard flocculant is ultra-high molecular weight (a few millions) A-poly(AAm), but the sediments from A-poly(AAm)-induced flocculation are loosely packed and have a gel-like structure because they trap water in their matrix via hydrogen bonding among polymer chains and water molecules. If the sediments shear strength is too low, the tailings ponds will not be reclaimable, since it is not possible to build or walk on top of sediments that have weak mechanical properties. Adding comonomers with different functional groups to poly(AAm) may allow for the optimization of the copolymer properties in order to achieve better flocculation results. Some previous investigations have shown that copolymerizing acrylamide with hydrophobic monomers lowers the content of water retained in the flocs, and therefore increases the solids content of the sediments.[10, 88, 93, 175]

Though some research groups have tested acrylamide copolymers as flocculants for oil sands tailings, to the best of our knowledge there are only few studies that have performed a systematic study of the causes for improved dewatering and consolidation of oil sands tailings in the open literature.[10, 70, 88, 176, 175] For example, Reis et al. varied the copolymer composition and molecular weight of a polyacrylamide-graft-poly(propylene oxide) (poly(AAm)-g-PPO) copolymer, but only compared the data points in terms of flocculation performance, and did not inquire into the reason for differing results at different copolymer compositions.[10] They compared two different lengths of the poly(propylene oxide) (PPO) grafts, using either 300 $gmol^{-1}$ or 1000 $gmol^{-1}$ macromonomers, but with only two different values it is not possible to determine a correlation between graft size and flocculation/dewatering performance.

Their results did show that the PPO graft with the lowest molecular weight (300 $gmol^{-1}$) achieved better results, such as lower turbidity and faster settling rate, which was a unique outcome, since most tests ascertain the opposite: higher molecular weight polymers usually performs better than lower molecular weight ones.[64, 177, 178] The authors attributed this effect to the higher hydrophobicity of the PPO grafts. A relationship between different copolymer compositions and hydrophobic group size was not obtained, as they instead focused on optimizing the dosage and performance of the most promising poly(AAm)-g-PPO flocculant. Ren et al. flocculated kaolin suspensions with poly(AAm), polydiallyldimethylammonium chloride (poly(DADMAC)), and 3-acrylamido-2-hydroxypropyltrialkylammonium chloride copolymers, where the alkyl group was ethyl, butyl, or octyl.[70] They noticed that the hydrophobic groups enhanced dewatering ability and reduced turbidity, in comparison to poly(AAm) and poly(DADMAC). Ren et al. stated that the hydrophobically-modified polymers were likely able to form bridges with the suspended kaolin particles, since the long alkyl chains might adsorb onto more sites on the particles.[70] Indeed, most researchers agree that a better bridge between the polymer and suspended solids will lead to stronger flocs and better flocculation performance. Ren et al. observed that the addition of hydrophobic groups onto an acrylamide backbone increases settling rates and decreases both water retention and supernatant turbidity. Although the effect of hydrophobic chains on the polyacrylamide backbone has been recognized,[10, 179] we have been unable to find a study assessing the relationship between the size of hydrophobic chain, amount of hydrophobic chain in the copolymer, polymer molecular weight, and its performance on mature fine tailings flocculation and dewatering.

Laboratory scale screening of polymer flocculants for oil sands tailings is still controversial, mainly because of the lack of clear procedures and accepted values to quantify flocculation and dewatering, as well as different performance metrics required by different dewatering technologies. For example, a high settling rate of 20 mh^{-1}, sought in gravity thickeners, may not be as important if dewatering is done by post-flocculation centrifugation or by thin lift

drying. The Alberta Energy Regulator, however, has approved Directive 085 for fluid tailings management for oil sands mining projects, where it states some minimum acceptable criteria for treated tailings before they are ready to be reclaimed (such as minimum undrained shear strength, solids content, and sand to fines ratio), which is not helpful for flocculation performance characterization.[180] In the open literature, researchers use different performance indicators to characterize their flocculants and flocculation process for oil sands tailings, most of which were adapted from wastewater treatment and other mining applications. Among them are aggregate hindered settling rate, capillary suction time, specific resistant to filtration, turbidity of supernatant, fine residues in the supernatant, shear strength of the sediment, gravity dewatering by sieve test, yield strength of sediment by slump test, solid content after centrifugation, and solid content after 24 h jar settling.[87, 10, 88, 127, 181, 7, 182]

In this study, we used a central composite rotatable design of experiment to analyze our results and evaluated the performance of our novel copolymers through capillary suction time (CST), supernatant turbidity, initial settling rate (ISR), and solid content of sediments. To observe the effect of centrifugation on flocculation performance, we also tested the turbidity, solid content, and CST after centrifugation. By studying the cause of this increased flocculation performance, we will be able to understand the reason for improvement and tailor polymers for optimal performance during oil sands tailings flocculation and dewatering. It is worth noting that the intention of this study was not to optimize the proposed flocculant composition for what are arbitrarily selected conditions or a particular MFT concentration, but rather to study how certain polymer microstructure properties (MW, macromonomer size, comonomer composition) affected their performance in small-scale tests under controlled conditions.

B.2 Materials and Methods

Monomers (acrylamide, 99.9% pure, and poly(ethylene oxide) methyl ether methacrylate (PEOMA)), initiator (2,2′Azobis(2-methylpropionamidine) dihydrochloride (V-50)), and organic solvents (acetone, toluene) were purchased from Sigma Aldrich. Coanda Research and Development supplied the mature fine tailings used in this investigation. A Dean Stark apparatus was used to determine the amount of solids, water, and bitumen in the tailings we used for testing. The Dean Stark apparatus comprises of a trap, round bottom flask, and reflux condenser.[183] To begin the analysis, 140 g of MFT was placed into the trap, and 200 mL of toluene was added into the round bottom flask, where it was heated up to its boiling point. Once boiling, the vapors, consisting of water and toluene, travelled to the condenser where they condensed into the trap. Since the liquids are immiscible, the toluene, less dense than water, separated on top, and water on the bottom. Once the water level had stabilized, the water was drained and the weight of water inside of the MFT was measured. Since bitumen and toluene were mixed together, we evaporated the toluene to determine the amount of toluene and bitumen. After the process was completed, the amount of solids left from the beginning were dried and weighed to obtain the solid content of the sample. We performed this process twice to ensure accuracy of results. In addition to the Dean Stark analysis, we measured the major ion concentrations through Atomic Absorption Spectroscopy (AAS) using a VARIAN 220FS Atomic Absorption Spectrophotometer. Table B1 lists the composition of MFT use in this work.

Table B1: MFT sample composition

Analysis method	compound	value
Major ions (ppm)	Na^+	248.3
	K^+	18.4
	Ca^{2+}	11
	Mg^{2+}	22.1
Dean-Stark (wt%)	Water	59.8
	Solids	35.3
	Bitumen	3.28

B.2.1 Polymerization

The copolymers were synthesized by free radical polymerization at 40 °C in a batch reactor. The reagents were added to the reactor in the following order: deionized water, acrylamide, and then PEOMA. Once in the reactor, the solution was purged with nitrogen for one hour to ensure a complete nitrogen atmosphere. After that, the initiator, also purged with nitrogen, was added to begin the polymerization. The polymerization was left to run for 24 hours to obtain high monomer conversion for all experiments. The total monomer concentration was kept constant at 0.1 $molL^{-1}$ for all polymerizations. Once the reaction had finished, the polymer, whose structure is shown in Figure B1, was precipitated in a 90:10 acetone:toluene mixture, rewashed in acetone for purification for at least three times, then dried for 24 hours in a vacuum oven at 50 °C.

B.2.2 Molecular Weight Measurement

The molecular weights of all copolymers were measured by gel permeation chromatography using an Agilent 1260 Infinity GPC and PL aquagel-OH Mixed-H 8 μm columns. PEO standard samples with narrow molecular weight

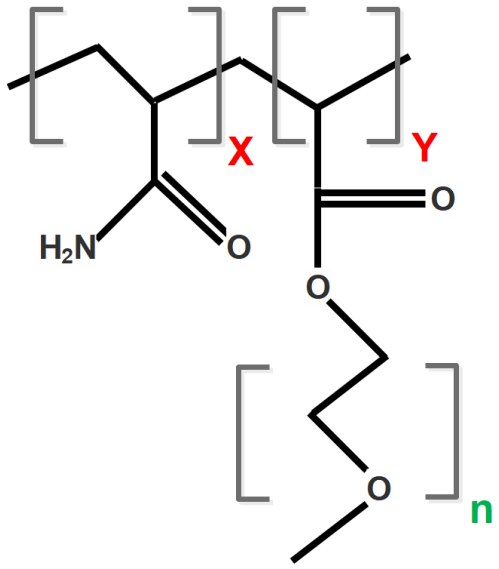

Figure B1: Poly(AAm)-*g*-PEOMA copolymer structure, where 'X', 'Y', and 'n' refer to the repeating units of the portion in parentheses.

were used for the column calibration. The concentration of all samples was 3.6 $\mathrm{mgml^{-1}}$, diluted in an aqueous solution containing 0.2 M $NaNO_3$, and injected at a volume of 100 μL. The analysis was performed at a flow rate of 1 $\mathrm{mLmin^{-1}}$ and at a temperature of 30 °C.

B.2.3 Design of Experiments

Using a central composite rotatable design allows us to compare the effects of macromonomer size, copolymer composition, and molecular weight as a function of flocculation performance. Macromonomer refers to a macromolecule with a functional group to allow further polymerization. As per the design, there were five different coded values for each variable, where 15 unique combinations and an additional three repetitions of the center point to ensure reproducibility were tested, allowing us to create a surface to map the effects of the design variables shown in Table B2.

Although Table B2 specifies negative and positive alpha values being ±1.68, the analysis may still be performed if the true values are reasonably close to the theoretical value. As the molecular weight of the copolymer cannot be precisely

controlled, the initiator concentration, [I], was varied to obtain a range of copolymer molecular weights.[86] We analyzed all data through Statistica 13 (StatSoft Inc.). In Table B2, PEOMA chain length and wt% are independent variables that can be changed without altering each other. Note that the full performance optimization of our copolymer would require testing it at different dosages, shear rates, solids contents, and water chemistries. Such an extensive study, however, would substantially add to the complexity of the process, and likely make the regression analysis unreliable. Therefore, we narrowed down the flocculation window by fixing these additional variables and concentrating on the impact of three main microstructural features: average PEOMA length, PEOMA composition, and copolymer average molecular weight.

Table B2: Indepent variables in central composite design

Independent variables	Levels of coded variables				
	$-\alpha$	-1	0	1	$+\alpha$
	-1.68	-1	0	1	1.68
Average PEOMA length (n)	1	9.1	19.3	31.8	43.13
Wt% PEOMA	5	14.12	27.5	40.88	50
Log([I])	-5	-4	-3	-2	-1

$[I]_0$: mol.L^{-1} & wt% is g-basis

B.2.4 MFT Flocculation and Dewatering Tests

In order to create the MFT slurry for testing, the MFT sample was diluted to 5 wt% solids in 160 g of slurry, using deionized water. We used diluted solid concentration to obtain as uniform mixing as possible when testing different polymers, and to maximize our ability to observe performance differences upon addition of polymers with different microstructures. The slurry was mixed at 610 rpm for 30 seconds to obtain a homogeneous distribution of solids in the slurry. At that point, 1000 ppm of a Ca^{2+} solution was added and mixing continued for an additional minute. The addition of calcium is necessary as the neutral polymer flocculants we used were unable to form bridges with the suspended particles without the charge neutralization effect obtained by

calcium ions. The polymer dosage was kept constant at 10,000 ppm (mg polymer per kg of dry solid) for all experiments, and the polymer mixed with the slurry at 610 rpm. The dosage of 10,000 ppm in our study was chosen based on preliminary tests with our polymers (from the highest MW to the lowest MW), and we found out that this dosage is not too far from the working window of our polymers. It is true that 10,000 ppm would be considered a high dosage in practical application (as opposed to 1000-1500 ppm dosages used for commercial A-poly(AAm));[86] however, it was not the intention of this study to optimize the polymer microstructure according to dosage.

Once aggregates formed, the mixing speed was reduced to 300 rpm and stirring continued for another two minutes. After flocculation was done, while the flocculated suspension was still under gentle mixing (to achieve uniform solid concentration upon sampling), we used a large pipet (0.5 cm diameter) and separated the flocculated suspension into 3 different portions: (1) A volume of 10 mL was used for testing capillary suction time (CST) with a Triton Electronics Meter (Type 319 multi-CST) with Triton filter paper (7 cm by 9 cm); (2) An aliquot of 50 mL was transferred to a Corning centrifuge tube for centrifugation purposes; and (3) The remaining 100 mL of sample was poured into a graduated cylinder so the change in mudline level could be recorded as a function of time.

After the slurry had settled in the graduated cylinder for 24 hours, the supernatant was extracted for turbidity measurement in a Hach 2100 AN Turbidmeter, and additional CST measurements were performed on the solids after settling. We also took 5 mL of settled solids and calculated the solids content by weighing the sample before and after 24 hours drying in an oven at 60 °C. The solids content is calculated by the following formula, where weight was measured in grams.

$$SC\% = (\frac{dryweight - aluminumfoilweight}{wetweight - aluminumfoilweight}) * 100\% \tag{B1}$$

B.3 Results and Discussion

In this study, we will classify PEOMA by length only, and when 'polymer molecular weight' is referred to, we refer to the molecular weight of the entire copolymer. This could be a source of confusion as the PEOMA length influences the copolymer molecular weight, but they are two separate entities. For simplicity, all the ANOVA and residual analysis were transfered to appendix, but the concept and the analysis steps are similar to those discussed in Chapter 3. In the ANOVA tables, we compared the three main variables, both linear (L) and quadratic (Q), and their two factor interaction effects, where the notation used is linear effect by linear effect (for example, 1L by 2L denotes the linear interaction between PEOMA length (1) and PEOMA wt% (2).

Table B3 lists the properties of the synthesized poly(AAm)-*g*-PEOMA flocculants and all observed MFT flocculation/dewatering results. A wide range of polymer properties were considered to obtain useful correlations between polymer structure and flocculation/dewatering performance.

Table B3: Experimental design matrix

Run#	PEOMA length (n)	Wt% PEOMA	[I](molL^{-1})	Turbidity (NTU)	CST (s)	24 h solids (%)	ISR(mh^{-1})	M_n ($kg\ mol^{-1}$)	PDI
1	9.1	14.2	1×10^{-4}	5.44	71.1	16.07	0.092	40	2.4
2	31.8	14.2	1×10^{-4}	1.32	13.1	19.56	0.376	36	2.46
3	9.1	40.88	1×10^{-4}	4.33	5.7	18.76	1.375	76	3.38
4	31.8	40.88	1×10^{-4}	26.4	7.6	16.61	1.23	121	2.7
5	9.1	14.12	1×10^{-2}	2.79	8.3	20	1.288	23	4.24
6	31.8	14.12	1×10^{-2}	0.65	22.8	16.93	0.049	14	2.81
7	9.1	40.88	1×10^{-2}	1.42	20.5	17.58	0.070	33	2.95
8	31.8	40.88	1×10^{-2}	2.04	7.1	17.19	0.070	33	3.95
9	1	27.5	1×10^{-3}	1.08	14.8	20.25	0.070	21	2.21
10	43.1	27.5	1×10^{-3}	1.01	42.1	17.31	0.141	38	2.74
11	19.3	5	1×10^{-3}	22.8	5.5	33.7	1.474	122	2.15
12	19.3	50	1×10^{-3}	10	9.0	18.45	0.862	1473	2.44
13	19.3	27.5	1×10^{-5}	10.5	6.7	16.45	1.092	211	2.17
14	19.3	27.5	1×10^{-1}	0.3	18.9	18.81	0.12	12	3.39
15	19.3	27.5	1×10^{-3}	6.23	9.5	19.09	0.567	79	2.91
16	19.3	27.5	1×10^{-3}	3.21	9.2	20.01	0.453	68	3.51
17	19.3	27.5	1×10^{-3}	0.3	16.1	19.58	0.393	82	3.04
18	19.3	27.5	1×10^{-3}	0.3	13	19.32	0.414	59	2.97

B.3.1 poly(AAm)-*g*-PEOMA Molecular Weight

The molecular weight distribution of all poly(AAm)-*g*-PEOMA flocculants were measured by GPC and the results are displayed in Table B3. Unsurprisingly, the initiator concentration, [I], significantly affected the molecular weight of all poly(AAm)-*g*-PEOMA copolymers, as it is known that the molecular weight of a polymer is controlled by the initiator concentration, and according to Shawki and Hamielec,[79]

$$\frac{1}{r_n} = \frac{\frac{k_t^{0.5}}{k_p}(2fk_I[I]_0)^{0.5}}{[M]_0(1-x_n)} +$$

Interestingly, PEOMA wt% in the copolymer also affected the molecular weight of poly(AAm)-*g*-PEOMA. Figure B2a shows that the molecular weight of poly(AAm)-*g*-PEOMA increases as the PEOMA wt% increases, irrespective of the PEOMA length. The effect of initiator concentration on poly(AAm)-*g*-PEOMA molecular weight is observed in Figure B2b, where lowering [I] increases poly(AAm)-*g*-PEOMA molecular weight, as expected for solution free radical polymerization. Figure B2c combines the effects of [I] and PEOMA wt%, and shows that polymerization with low [I] and high PEOMA wt% will produce poly(AAm)-*g*-PEOMA with the highest molecular weights. There seems to be a trend indicating a slight decrease in poly(AAm)-*g*-PEOMA molecular weight as the length of the PEOMA grafts increases, as shown in Figure B2b. This trend is in agreement with the results by Xiao et al., where they determined the reactivity ratios of Poly(AAm)/PEOMA system and discovered that the reactivity of the macromonomer (PEOMA) decreased as its chain length increased.[184] The lower reactivity of longer PEOMA macromonomers would then lead to a lower overall copolymer molecular weight, and our findings support the similar conclusion. These findings do not imply that long PEOMA macromonomers cannot be used to make poly(AAm)-*g*-PEOMA copolymers with higher molecular weights; it only means that when all other variables are kept constant - namely initiator concentration, monomer (macromonomer) concentration, and temperature - the molecular weight of poly(AAm)-*g*-PEOMA

will decrease as the length of the hydrophobic PEOMA macromonomer increases. One could, evidently, change the polymerization conditions (such as decreasing [I]) to compensate for this effect.

As seen in Table B3, we produced poly(AAm)-*g*-PEOMA copolymers with molecular weights ranging from 12,000 to 1,473,000 $gmol^{-1}$. This wide molecular weight range will help show the effect of poly(AAm)-*g*-PEOMA molecular weight on flocculation/dewatering performance. Compared to most flocculants, the molecular weights of our poly(AAm)-*g*-PEOMA flocculants are relatively low, as it is generally accepted that high molecular weight polymers are more effective flocculants (i.e. in terms of settling rate),[64, 177, 178] but our recent results suggested that higher the molecular weight does not necessarily mean better dewatering in the sediments they generate, as indicated by the independence of slurry CST on MW of the cationic copolymer of acrylamide and DADAMC.[86]

B.3.2 Initial Settling Rate

Our design showed that all the three manipulated variables, PEOMA length, PEOMA wt%, and log[I], are significant factors. Figure B3a shows that poly(AAm)-*g*-PEOMA performs best (high ISR) when the PEOMA length and PEOMA wt% are hight (upper right quadrant), or when the PEOMA length and PEOMA wt% are low (lower left quadrant). Combining this finding with the results shown in Figure B3b and B3c, we conclude that all poly(AAm)-*g*-PEOMA copolymers lead to higher ISR when their molecular weights are increased. This agrees with our knowledge of flocculation mechanism with these polymers, as higher molecular weight poly(AAm)-*g*-PEOMA can create larger aggregates that settle faster.

Figure B3b displays the ISR as a function of initiator concentration and PEOMA wt% for PEOMA length of 40, clearly indicating that high settling rate were achieved when the molecular weight of poly(AAm)-*g*-PEOMA was high and it contained high PEOMA wt%. The higher poly(AAm)-*g*-PEOMA molecular weight and PEOMA wt% allows the polymer to form strong bridges

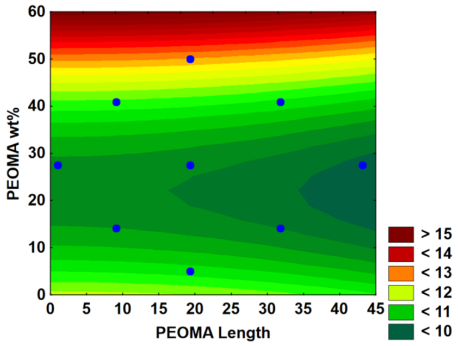

Figure B2a: MW as a function of PEOMA wt% and length

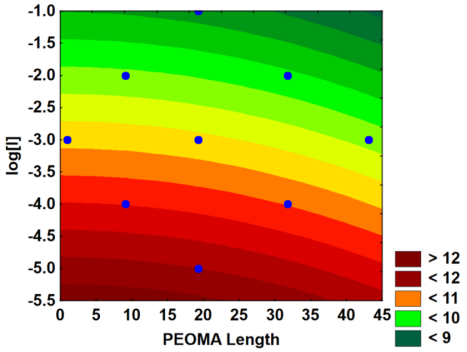

Figure B2b: MW as a function of initiator concentration and PEOMA length

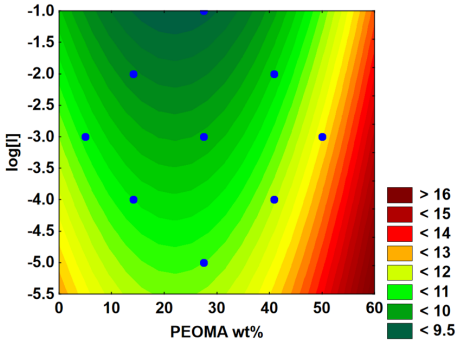

Figure B2c: MW as a function of initiator concentration and PEOMA wt%

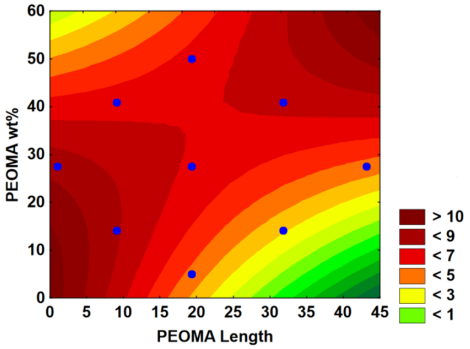

Figure B3a: ISR as a function of PEOMA wt% and length, [I]=10^{-3}

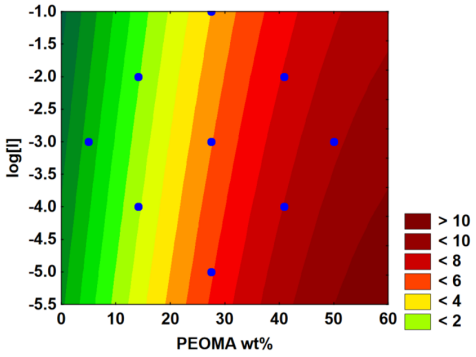

Figure B3b: ISR as a function of initiator concentration and PEOMA wt%, n= 40

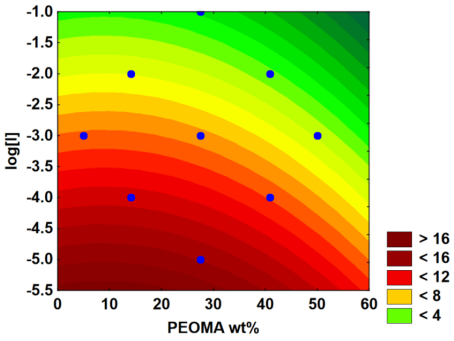

Figure B3c: ISR as a function of initiator concentration and PEOMA wt%, n= 5

with multiple points of contact among the suspended particles, forming large, strong aggregates that settle quicker.

Figure B3c displays similar relationship for a PEOMA length of 5. The correlation between poly(AAm)-*g*-PEOMA molecular weight and ISR is stronger than for the longer PEO unit discussed in Figure B3b. The figure shows that ISR decreases drastically once [I] is lowered below 0.001 molL^{-1}. On the other hand, the weight percent of PEOMA is not as significant of a predictor for ISR, as one may get a high ISR for any PEOMA wt% when molecular weight of poly(AAm)-*g*-PEOMA is high (that is, when [I] is low), although lower PEOMA wt% seems to produce slightly higher ISR values.

B.3.3 Turbidity of Supernatant

Similar to the ISR, the analysis of variance for turbidity values found out that all variables were significant, but we had to take the natural logarithm of the turbidity values in order to obtain a correlation with accurate prediction power. Figure B4a shows that the supernatant reaches the lowest turbidities in two cases: 1) low PEOMA length and high PEOMA wt% (left upper corner), and 2) high PEOMA length and low PEOMA wt% (right lower corner). The poor results (higher turbidity) obtained when poly(AAm)-*g*-PEOMA had a high PEOMA wt% with high length (right upper corner) may be due to steric hindrance among the long partially-hydrophobic PEOMA grafts that lowered the performance of flocculation when there was a high amount of PEOMA in the copolymer. These chains may interact with each other and are unable to trap the finest particles. On the other hand, poly(AAm)-*g*-PEOMA with shorter PEOMA grafts, required a higher PEOMA% on the copolymer to trap all of the fines because PEOMA chains were shorter. Having more frequent, shorter PEOMA side chains increases the surface area of poly(AAm)-*g*-PEOMA and creates more sites onto which flocculant may adsorb to the surface of MFT particles.

Figure B4b illustrates the effect of [I] and PEOMA wt% for a constant length of 40, and confirms our conclusion above: poly(AAm)-*g*-PEOMA with long PEOMA grafts produces supernatant with low turbidity when a low PEOMA% is present in the polymer so that there is no steric hindrance between the hydrophobic groups. Lowering the poly(AAm)-*g*-PEOMA molecular weight for a given PEOMA wt% also helps decrease the turbidity for the same reasons.

These conclusions are different from those observed for ISR, as ISR was the highest when the poly(AAm)-*g*-PEOMA had high PEOMA wt% and high PEOMA length, while the turbidity analysis showed that high PEOMA length and low PEOMA% was ideal. We may suggest an explanation for this observation using the proposed flocculation mechanism for these polymers: When poly(AAm)-*g*-PEOMA polymers trap particles to form aggregates, the larger aggregates are heavier, and thus settle faster, but these polymers may not be able to trap all the fine particles because the larger hydrophobic PEOMA

side groups interact with each other, hindering the ability to adsorb on to the smallest suspended particles. Such copolymers would yield high ISR, but would also produce supernatants with higher turbidity. Notice that this is a discussion relative to the other poly(AAm)-*g*-PEOMA tested in this investigation. The highest turbidity measured with all copolymers was 26 NTU, which is still an acceptable value, even for the poorest performer among the poly(AAm)-*g*-PEOMA listed in Table B3.

B.3.4 Capillary Suction Time (CST)

Figure B5a shows how CST depends on [I] and PEOMA wt%. CST values were slightly lower when poly(AAm)-*g*-PEOMA had a higher molecular weight and much higher when the copolymer had higher PEOMA wt%. These results are easy to explain because the higher the PEOMA%, the higher the hydrophobicity of the copolymer; since CST measures the dewatering ability of aggregates, a more hydrophobic flocculant is expected to retain less water inside the aggregates. By the same token, a higher molecular weight poly(AAm)-*g*-PEOMA flocculant makes larger, more compact aggregates that retain less water, and yield a lower CST. Although the effect of copolymer molecular weight on CST is not very significant, it contradicts the findings of our recent work where the CST of aggregates produced by cationic copolymers of acrylamide and DADMAC did not depend on molecular weight.[86] We believe this discrepancy is due to the fact that the dewaterability of aggregates produced by cationic flocculants are so strongly affected by charge density (copolymer composition) that the little effect of molecular weight was masked.

Figure B5b plots the CST as a function of PEOMA% and length, where the green colored areas near the center of the plot indicate desirable low CST. This trend is almost the exact opposite of that observed for turbidity, and most likely occurs because the combination of high PEOMA length and PEOMA% produces a more hydrophobic flocculant, which retains less water. Comparing Figure B5b to Figure B3a, we notice that the graphs overlap in similar fashion, with red indicating high ISR and green low CST, meaning that a satisfactory performance may be achieved in both tests by the same copolymer. Although

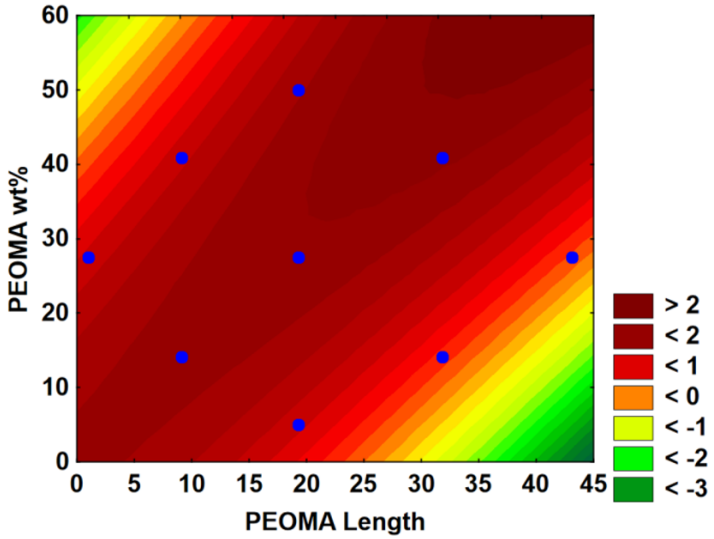

Figure B4a: Ln(turbidity) as a function of PEOMA wt% and length, [I]=10^{-3}

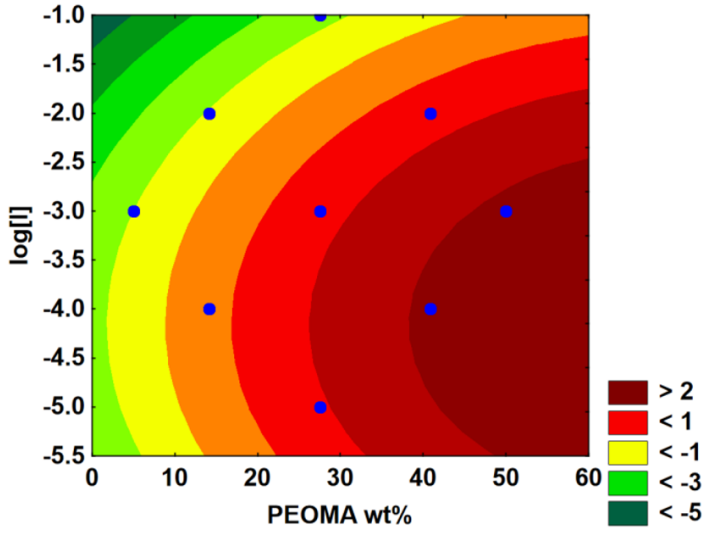

Figure B4b: Ln(turbidity) as a function of initiator concentration and PEOMA wt%, n= 40

not all tests are satisfied by the same flocculant, it shows that there is no 'one size fits all' flocculant for MFT suspensions.

B.3.5 Centrifuge Turbidity

Instead of measuring the turbidity of supernatant after 5, this time we centrifuged the samples after flocculation for 2 minutes under 500 × g.

The supernatant turbidity following centrifugation yields very similar results to the turbidity after 24 hours of settling. Figure B6 shows that poly(AAm)-*g*-PEOMA with long PEOMA side chains requires low PEOMA% to capture all of the fine particles, and that poly(AAm)-*g*-PEOMA with shorter PEOMA grafts needs higher PEOMA% in the copolymer to produce clear supernatant and follows the same pattern for the turbidity without centrifugation - the copolymers with a large percentage of long PEOMA grafts may hinder the entrapment of smaller particles, while the copolymers with a low percentage of short PEOMA grafts are unable to adsorb to all of the particles as there are fewer sites to form a proper bridge. Although we could obtain a strong correlation among these variables, it should be noted that the highest turbidity after centrifugation was only 16.4 NTU, which is still corresponds to a very clear supernatant. For all practical purposes, after centrifugation, all poly(AAm)-*g*-PEOMA flocculants produced supernatants that were essentially free of fine particles. Although the differences are statistically significant and indicate that the polymer microstructure affects turbidity, these differences may have little practical significance, since all of them satisfy the condition of less than 0.5% solid residues in the supernatant indicated by Directive 085.[185]

B.3.6 Further Consolidation through Centrifugation

An interesting observation obtained through this study was the effect of centrifugation on the solids content of the sediments, compared that obtained in settling over a single day. By dividing the solid content of the centrifuged solids by that of the 24 hour settled solids, we were able to compare the increase in solid content by centrifugation. Figure B7a and Figure B7b show the ratio

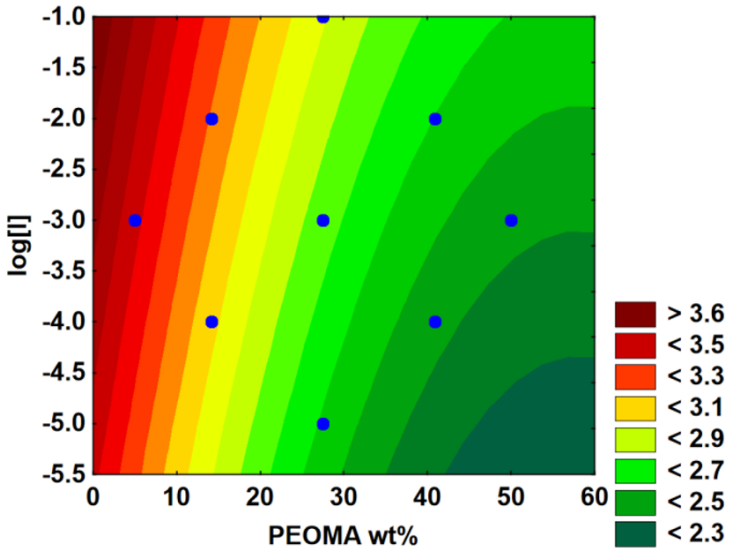

Figure B5a: Ln(CST) as a function of PEOMA wt% and [I]

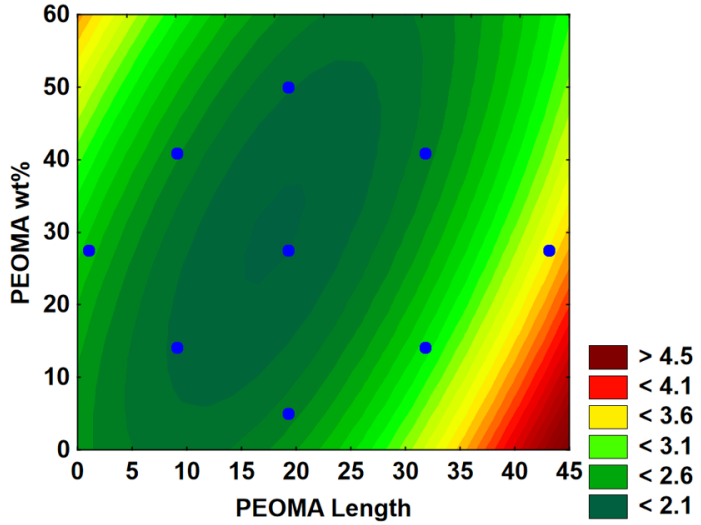

Figure B5b: Ln(CST) as a function of PEOMA length PEOMA wt%

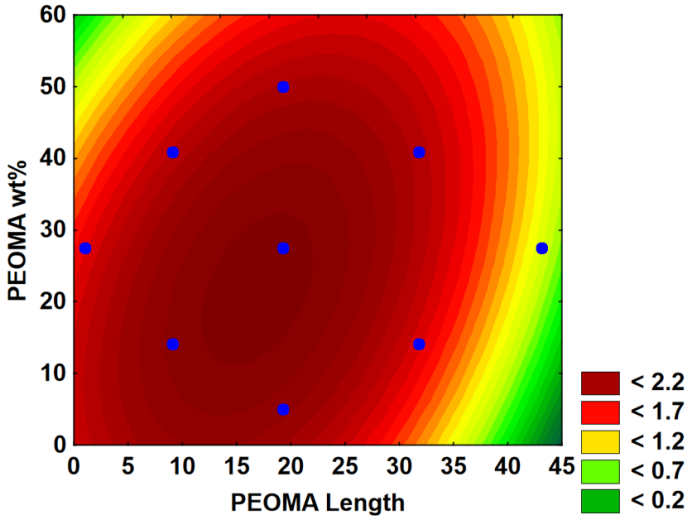

Figure B6: Ln(Turbidity) after centrifugation as a function of PEOMA wt% and [I]

of solid content obtained after 24 h settling to one obtained after centrifuging flocculated samples under 500 × g for 2 minutes.

The higher the PEOMA% in poly(AAm)-*g*-PEOMA, the greater the increase in solids content. The centrifuge increases the g-force on the sample, forcing the aggregates to settle to the bottom of the centrifuge vials, where the high hydrophobic PEOMA groups decrease the amount of water trapped inside of the sediments. Equally important, the lower the [I], the higher the molecular weight of poly(AAm)-*g*-PEOMA, and the greater the effect of centrifugation on the solids content. The impact of poly(AAm)-*g*-PEOMA molecular weight is shown most clearly by Figure B7b, as the area of the graph showing the greatest increase in solids content corresponds to low [I] values and high PEOMA%. As shown by Figure B7b, PEOMA length is not very significant in terms of solids content improvement by centrifugation. This may be because the PEOMA length was not significant in the molecular weight of the copolymer, and thus, the additional g-force did not improve compaction of the sediments based on this variable.

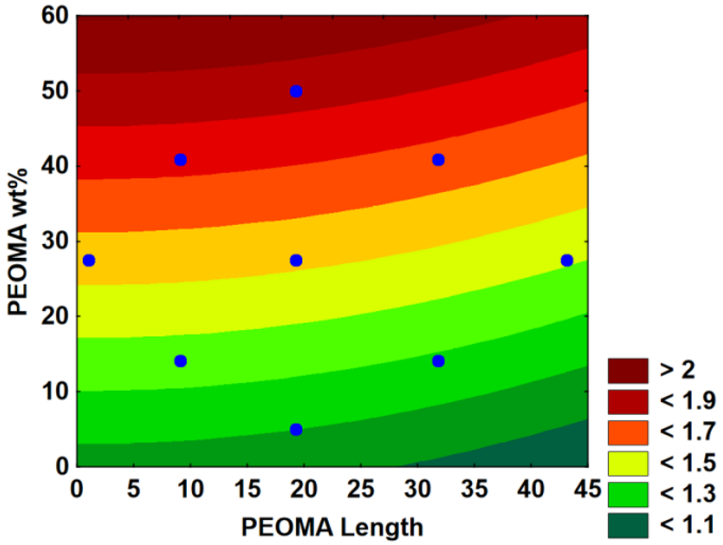

Figure B7a: Solid content increase (upon centrifugation after 24 hr settling) as a function of PEOMA wt% and PEOMA length

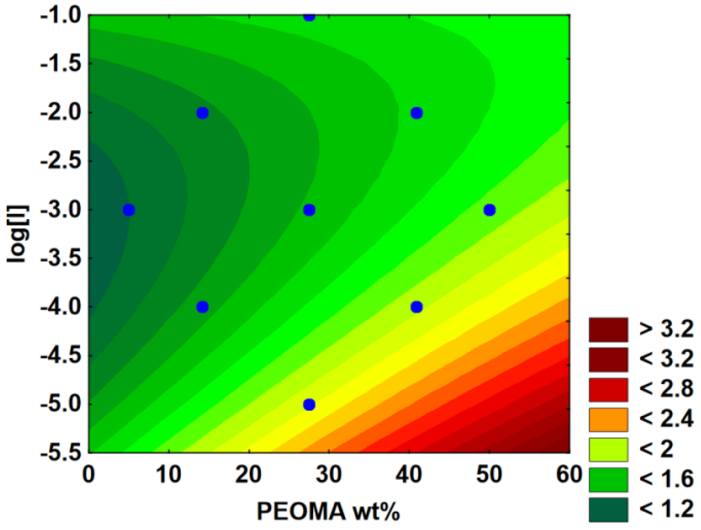

Figure B7b: Solid content increase (upon centrifugation after 24 hr settling) as a function of [I] and PEOMA wt%

B.3.7 Application of our Model to Other Systems

As mentioned in the introduction, Reis et al.[10] explored the addition of hydrophobic groups to an acrylamide backbone. They found similar results with Poly(AAm)-g-PPO (poly(propylene oxide methacrylate)) copolymer, where the shorter length grafts with higher content of grafts performed the best. Also, they found that one of the best copolymers using the longer PPO length (1000 $gmol^{-1}$ macromonomer) was when they used only 5 wt% PPO. The combination hydrophobic chain length and low wt% was required in our model so there was less steric hindrance. The only copolymer with the longer PPO length that performed better in some tests was a 35 wt% PPO, but it performed better in CST, where our model states that the additional hydrophobic groups would expel water faster, producing a lower value. The alignment between their results and our conclusions confirms that our model is applicable in similar polymer systems where a hydrophobic chain is added to acrylamide.

Shang et al. also added hydrophobic groups to acrylamide, making P(AM-DMAC-MAPMS), poly(acrylamide-methacryloyloxy ethyl trimethyl ammonium chloride-methacryloxypropyltrimethoxysilane). The hydrophobic groups are relatively small, only having two and three repeating units for the DMC and MAPMS, respectively. According to our model, the shorter hydrophobic group length would indicate that a larger amount of the DMC and MAPMS would be required in order to achieve optimal effects. Although their flocculation testing was not performed by using MFT, they still concluded that the higher feed ratios of hydrophobic group increased the performance of their flocculant. Their findings also coincide with ours with respect to the ISR and turbidity trends, as the low chain length required higher molecular weight, represented by intrinsic viscosity reported in their work, and a higher percentage of hydrophobic groups to perform well.[175]

B.3.8 Conclusion

As discussed through the different optimal variables for each one of the dewatering tests, there is no 'perfect' polymer for treating MFT; however, it is

possible to tailor a polymer for specific flocculation purposes. Depending on the required characteristics of flocculation, one is able to synthesize a polymer based on a specific set of criteria. This study allowed us to delve deeper into the reasons behind enhanced flocculation performance gained by the addition of hydrophobic chains to an acrylamide backbone. Through the analysis of the effects of initiator concentration, PEOMA length, and PEOMA wt%, we determined the effect of hydrophobic chain addition to acrylamide copolymers. Adding many hydrophobic chains (greater than 30 wt%) can effectively help in the dewatering performance of the flocculant, shown in the ISR and CST tests, but may not capture all of the fine particles, leading to a higher turbidity. A lower initiator concentration (higher molecular weight) was also shown to improve flocculation performance in most categories. The length of hydrophobic chains was observed to be of mild importance – the shorter chains required a larger percentage of hydrophobic groups to achieve the same effects as the larger chains, whereas the longer hydrophobic chains needed a low weight percent of PEOMA to prevent steric hindrance.

Although most poly(AAm)-*g*-PEOMA copolymer molecular weights studied were low (smaller than 200,000), we still observed very good flocculation performances from all polymers tested. This contradicts the most common assumptions about flocculants, but it actually has some advantages as well. There are benefits to having low molecular weights, as high molecular weight flocculants will lead to an increase in viscosity and may cause problems such as non-uniform mixing. Reis et al. also noted that having a lower molecular weight flocculant allows for a wider window of mixing environments in which the flocculant may be used.[10] One should note that the findings of this study are restricted to the conditions we investigated in our experiments and cannot not be extended uncritically to other situations (such as different vessel geometries, shear rates, primary solids contents, and polymer dosages) or even other tailings. Inspired from our study, more research should be conducted to optimize the microstructure of polymer flocculants so they can achieve their optimum performances under a wide range of operating conditions.

Appendix C

Mathematical Modeling of Free Radical Copolymerization

This appendix describes the mathematical modeling of free radical copolymerization and explains the steps taken to construct bivariate distributions of molecular weight and chemical composition, similar to ones shown in Figure 3.10 to Figure 3.14. An example of the microstructure simulation of an important industry standard flocculant, poly(AAm-*co*-AAc), is also discussed to show the effect of polymerization temperature on the properties of the copolymer. The model is based on the pioneer work of Xie and Hamielec,[84] who proposed the method of pseudo kinetics rate constant to model free radical polymerization.

The following mechanism is widely accepted for free radical copolymerization,

Radical formation

$$\mathrm{I} \xrightarrow{\mathrm{k_I}} 2\,\mathrm{f}\mathrm{R}_i^o$$

Chain initiation

$$\mathrm{R}_i^o + \mathrm{M}_1 \xrightarrow{\mathrm{k}_{i1}} \mathrm{R}_{1,0,1}^o$$
$$\mathrm{R}_i^o + \mathrm{M}_2 \xrightarrow{\mathrm{k}_{i2}} \mathrm{R}_{0,1,2}^o$$

Chain propagation

$$\mathrm{R}^o_{m,n,1} + \mathrm{M}_1 \xrightarrow{\mathrm{k}_{11}} \mathrm{R}^o_{m+1,n,1}$$
$$\mathrm{R}^o_{m,n,1} + \mathrm{M}_2 \xrightarrow{\mathrm{k}_{12}} \mathrm{R}^o_{m,n+1,2}$$
$$\mathrm{R}^o_{m,n,2} + \mathrm{M}_1 \xrightarrow{\mathrm{k}_{11}} \mathrm{R}^o_{m+1,n,1}$$
$$\mathrm{R}^o_{m,n,2} + \mathrm{M}_2 \xrightarrow{\mathrm{k}_{11}} \mathrm{R}^o_{m,n+1,2}$$

Chain transfer

To monomer

$$\mathrm{R}^o_{m,n,1} + \mathrm{M}_1 \xrightarrow{\mathrm{k}_{f11}} \mathrm{P}_{m,n} + \mathrm{R}^o_{1,0,1}$$
$$\mathrm{R}^o_{m,n,1} + \mathrm{M}_2 \xrightarrow{\mathrm{k}_{f12}} \mathrm{P}_{m,n} + \mathrm{R}^o_{0,1,2}$$
$$\mathrm{R}^o_{m,n,2} + \mathrm{M}_1 \xrightarrow{\mathrm{k}_{f21}} \mathrm{P}_{m,n} + \mathrm{R}^o_{1,0,1}$$
$$\mathrm{R}^o_{m,n,2} + \mathrm{M}_2 \xrightarrow{\mathrm{k}_{f22}} \mathrm{P}_{m,n} + \mathrm{R}^o_{0,1,2}$$

Chain termination

By combination

$$\mathrm{R}^o_{m,n,1} + \mathrm{R}^o_{r,s,1} \xrightarrow{\mathrm{k}_{\mathrm{tc}11}} \mathrm{P}_{m+r,n+s}$$
$$\mathrm{R}^o_{m,n,1} + \mathrm{R}^o_{r,s,2} \xrightarrow{\mathrm{k}_{\mathrm{tc}12}} \mathrm{P}_{m+r,n+s}$$
$$\mathrm{R}^o_{m,n,2} + \mathrm{R}^o_{r,s,2} \xrightarrow{\mathrm{k}_{\mathrm{tc}22}} \mathrm{P}_{m+r,n+s}$$

By disproportionation

$$\mathrm{R}^o_{m,n,1} + \mathrm{R}^o_{r,s,1} \xrightarrow{\mathrm{k}_{\mathrm{td}11}} \mathrm{P}_{m,n} + \mathrm{P}_{r,s}$$
$$\mathrm{R}^o_{m,n,1} + \mathrm{R}^o_{r,s,2} \xrightarrow{\mathrm{k}_{\mathrm{td}12}} \mathrm{P}_{m,n} + \mathrm{P}_{r,s}$$
$$\mathrm{R}^o_{m,n,2} + \mathrm{R}^o_{r,s,2} \xrightarrow{\mathrm{k}_{\mathrm{td}22}} \mathrm{P}_{m,n} + \mathrm{P}_{r,s}$$

where M_1 and M_2 are monomers 1 and 2, respectively, I is the initiator, R^o_i is primary radicals formed by decomposition of initiator I, $R^o_{m,n,1}$ is polymer radical ending with monomer 1 (the radical head) that has m units of monomer 1 and n units of monomer 2, respectively. In the similar fashion, $R^o_{m,n,2}$ is the polymer radical ending with monomer 2 (the radical head) that has m units of monomer 1 and n units of monomer 2, respectively. $P_{m,n}$ is a dead polymer chain with m units of monomer 1 and n units of monomer 2. The rest are rate constants, for example, k_I is initiator decomposition rate constant, k_{12} is propagation rate constant of radical ending with monomer 1 propagating

with monomer 2, k_{f21} is transfer-to-monomer rate constant of radical ending with monomer 2 transferring to monomer 1, or k_{tc11} is the termination by combination rate constant of radical ending with monomer 1 terminating with monomer 1, while k_{td11} is the termination by disproportionation rate constant of radical ending with monomer 1 terminating with monomer 1. f is fractional initiator efficiency.

The above elementary reactions contain the following assumptions:

- Terminal model (the rate constant only depends on the chain end type, that is the last monomer carrying radical decides the chain reactivity)[186]
- No transfer to polymer (no branching)

If the long-chain approximation is also assumed, that is the rate of propagation, termination and transfer reactions are independent of the chain length, the copolymerization elementary reactions will be reduced to the following:

Radical formation

$$\mathrm{I} \xrightarrow{\mathrm{k_I}} 2\,\mathrm{f}\mathrm{R}_i^o$$

Chain initiation

$$\mathrm{R}_i^o + \mathrm{M}_1 \xrightarrow{\mathrm{k}_{i1}} \mathrm{R}_1^o$$
$$\mathrm{R}_i^o + \mathrm{M}_2 \xrightarrow{\mathrm{k}_{i2}} \mathrm{R}_2^o$$

Chain propagation

$$\mathrm{R}_1^o + \mathrm{M}_1 \xrightarrow{\mathrm{k}_{11}} \mathrm{R}_1^o$$
$$\mathrm{R}_1^o + \mathrm{M}_2 \xrightarrow{\mathrm{k}_{12}} \mathrm{R}_2^o$$
$$\mathrm{R}_2^o + \mathrm{M}_1 \xrightarrow{\mathrm{k}_{11}} \mathrm{R}_1^o$$
$$\mathrm{R}_2^o + \mathrm{M}_2 \xrightarrow{\mathrm{k}_{11}} \mathrm{R}_2^o$$

Chain transfer

To monomer

$$\mathrm{R}_1^o + \mathrm{M}_1 \xrightarrow{\mathrm{k}_{f11}} \mathrm{P}_1 + \mathrm{R}_1^o$$
$$\mathrm{R}_1^o + \mathrm{M}_2 \xrightarrow{\mathrm{k}_{f12}} \mathrm{P}_1 + \mathrm{R}_2^o$$

$$\mathrm{R}_2^o + \mathrm{M}_1 \xrightarrow{\mathrm{k}_{f21}} \mathrm{P}_2 + \mathrm{R}_1^o$$
$$\mathrm{R}_2^o + \mathrm{M}_2 \xrightarrow{\mathrm{k}_{f22}} \mathrm{P}_2 + \mathrm{R}_2^o$$

Chain termination

By combination

$$\mathrm{R}_1^o + \mathrm{R}_1^o \xrightarrow{\mathrm{k}_{\mathrm{tc}11}} \mathrm{P}_{1+1}$$
$$\mathrm{R}_1^o + \mathrm{R}_2^o \xrightarrow{\mathrm{k}_{\mathrm{tc}12}} \mathrm{P}_{1+2}$$
$$\mathrm{R}_2^o + \mathrm{R}_2^o \xrightarrow{\mathrm{k}_{\mathrm{tc}22}} \mathrm{P}_{2+2}$$

By disproportionation

$$\mathrm{R}_1^o + \mathrm{R}_1^o \xrightarrow{\mathrm{k}_{\mathrm{td}11}} \mathrm{P}_1 + \mathrm{P}_1$$
$$\mathrm{R}_1^o + \mathrm{R}_2^o \xrightarrow{\mathrm{k}_{\mathrm{td}12}} \mathrm{P}_1 + \mathrm{P}_2$$
$$\mathrm{R}_2^o + \mathrm{R}_2^o \xrightarrow{\mathrm{k}_{\mathrm{td}22}} \mathrm{P}_2 + \mathrm{P}_2$$

where

$$[R_1^o] = \sum_{r=1}^{\infty} [R_{r,1}^o] \tag{C1}$$

$$[R_2^o] = \sum_{r=1}^{\infty} [R_{r,2}^o] \tag{C2}$$

C.1 Rate of Polymerization

Looking at the elementary reactions above, the total rate of the copolymerization (R_p) is

$$R_p = k_{11}[R_1^o][M_1] + k_{21}[R_2^o][M_1] + k_{12}[R_1^o][M_2] + k_{22}[R_2^o][M_2] \tag{C3}$$

Equation (C3) can be written as (similar to homopolymerization)

$$R_p = \overline{K_p}[M][R^o] \tag{C4}$$

where

$$[M] = [M_1] + [M_2] \tag{C5}$$

$$[R^o] = [R_1^o] + [R_2^o] \tag{C6}$$

$$\overline{K}_p = \sum_{i=1}^{2} \sum_{j=1}^{2} k_{pij} \Phi_i^o f_j \tag{C7}$$

where

$$f_i = \frac{[M_i]}{\sum_{i=1}^{2} [M_i]} \tag{C8}$$

$$\Phi_i^o = \frac{[R_i^o]}{\sum_{i=1}^{2} [R_i^o]} \tag{C9}$$

Similarly, the rate of termination can be written as

$$R_t = K_t [R^o]^2 \tag{C10}$$

where

$$\overline{K}_t = \overline{K}_{tc} + \overline{K}_{td} = \sum_{i=1}^{2} \sum_{j=1}^{2} k_{tij} \Phi_i^o \Phi_j^o \tag{C11}$$

Making the steady state assumption on radicals, the rate of termination equals the rate of radical decomposition,

$$2 f k_I [I] = \overline{K}_t [R^o]^2 \tag{C12}$$

Note that the steady state approximation is only valid considering no gel-effect in the reactor.[187]

Equation (C4) can then be written as

$$R_p = \overline{K}_p[M](\frac{2fk_I[I]}{\overline{K}_t})^{1/2} \tag{C13}$$

Similarly, the pseudo kinetic rate constants for chain transfer to monomer is

$$\overline{K}_{fm} = \sum_{i=1}^{2}\sum_{j=1}^{2} k_{fij}\Phi_i^o f_j \tag{C14}$$

Another good approximation for binary copolymers is that, on average, the probability of monomer 1 following monomer 2 in a chain is approximately equal to the probability of monomer 2 following monomer 1 in the chain with error ± 1 unit,[84] that is

$$k_{21}[R_2^o][M_1] \approx k_{12}[R_1^o][M_2] \tag{C15}$$

Equation (C15) helps calculate Φ_1^o and Φ_2^o as

$$\Phi_1^o = \frac{k_{21}f_1}{k_{21}f_1 + k_{12}f_2} \tag{C16}$$

$$\Phi_2^o = \frac{k_{12}f_2}{k_{21}f_1 + k_{12}f_2} \tag{C17}$$

C.2 Bivariate Distribution of Molecular Weight and Composition

The instantaneous bivariate distribution of chain length and composition is given by [188, 84]

$$W(r,y,t) = [1 + \frac{y.(mw_1 - mw_2)}{F_1 mw_1 + (1-F_1)mw_2}](\tau+\beta)[\tau + \frac{\beta}{2}(\tau+\beta)(r-1)] \\ .r(\frac{1}{1+\tau+\beta})^r \frac{1}{\sqrt{2\pi\sigma^2}} exp(-\frac{y^2}{2\sigma^2}) \tag{C18}$$

where mw_1 and mw_2 are molecular weight of monomer 1 and monomer 2, respectively, F_1 is the average composition of monomer 1 in copolymer chains produced instantaneously. τ and β are defined as

$$\tau = \frac{\overline{K}_{td}[R^o]}{\overline{K}_p[M]} + \frac{\overline{K}_{fm}}{\overline{K}_p} \tag{C19}$$

$$\beta = \frac{\overline{K}_{tc}[R^o]}{\overline{K}_p[M]} \tag{C20}$$

σ^2 is defined as

$$\sigma^2 = \frac{F_1 F_2 \chi}{r} \tag{C21}$$

with

$$\chi = [1 - 4F_1(1-F_1)(1-r_1 r_2)]^{1/2} \tag{C22}$$

where r_1 and r_2 are reactivity ratios of monomer 1 and monomer 2, respectively, y is the composition deviation defined as

$$y = y_1 - F_1 \tag{C23}$$

with y_1 being the composition of monomer 1 in a single given copolymer chain produced instantaneously, while F_1 is the average composition of monomer 1 in copolymer chains produced instantaneously.

Integrating Equation (C18) with respect to y gives the instantaneous molecular weight distribution of the copolymer as

$$W(r,t) = (\tau+\beta)[\tau + \frac{\beta}{2}(\tau+\beta)(r-1)].r.(\frac{1}{1+\tau+\beta})^r \tag{C24}$$

From the instantaneous bivariate distribution, Equation (C18), one can calculate the cumulative bivariate distribution of copolymer and molecular weight (the accumulated copolymer in the reactor after a given conversion) as

$$\overline{W}(r,y,t) = \frac{\int_0^t W(r,y,t)R_p(t)mw_{ave}(F_1,F_2)dt}{\int_0^t R_p(t)mw_{ave}(F_1,F_2)dt} \tag{C25}$$

Integrating Equation (C26) with respect to y, gives the cumulative (accumulated) molecular weight distribution of the copolymer as

$$\overline{W}(r,t) = \int_{-1}^{1} \overline{W}(r,y,t) = \frac{\int_0^t W(r,t)R_p(t)mw_{ave}(F_1,F_2)dt}{\int_0^t R_p(t)mw_{ave}(F_1,F_2)dt} \tag{C26}$$

where

$$mw_{ave}(F_1,F_2) = mw_1(\frac{R_{p1}}{R_p}) + mw_2(\frac{R_{p2}}{R_p}) \tag{C27}$$

In order to calculate the instantaneous and cumulative bivariate distribution of copolymer composition and molecular weight, one needs to know the values for R_p, τ, β, f_1 and f_2, which can be found by solving population balances for the system. The advantage of using the pseudo kinetic constant method is that one can treat the copolymerization as homopolymerization. [189]

For polymer radicals with chain length unity (r=1),

$$\begin{aligned}\frac{d[R_1^o]}{dt} =& 2fk_I[I] + \overline{K}_{fm}[R^o][M] - \overline{K}_p[R_1^o][M] - \overline{K}_{fm}[R_1^o][M] \\ & - \overline{K}_t[R_1^o][R^o]\end{aligned} \tag{C28}$$

For dead polymers with chain length unity (r=1),

$$\frac{d[P_1]}{dt} = \overline{K}_t d[R_1^o][R^o] + \overline{K}_{fm}[R_1^o][M] \tag{C29}$$

For polymer radicals with chain length r (r≠1),

$$\begin{aligned}\frac{d[R_r^o]}{dt} =& \overline{K}_p[R_{r-1}^o][M] - \overline{K}_p[R_1^o][M] - \overline{K}_t[R_r^o][R^o] \\ & - \overline{K}_{fm}[R_r^o][M]\end{aligned} \tag{C30}$$

For dead polymers with chain length r (r≠1),

$$\begin{aligned}\frac{d[P_r]}{dt} =& \overline{K}_{td}[R_r^o][R^o] + \overline{K}_{fm}[R_r^o][M] \\ & - \frac{1}{2}\overline{K}_{tc}\sum_{s=1}^{r-1}[R_{r-s}^o][R_s^o] - \overline{K}_{fm}[R_r^o][M]\end{aligned} \tag{C31}$$

Using the method of moments, the moments for live chains (polymer radicals) and dead chains are defined as

$$Y_i = \sum_{r=1}^{\infty} r^i[R_r^o] \qquad (i = 0, 1, 2, ...) \tag{C32}$$

$$Q_i = \sum_{r=1}^{\infty} r^i[P_r] \qquad (i = 0, 1, 2, ...) \tag{C33}$$

Using the moments definitions, the population balances in Equation (C28) to Equation (C31) become

$$\begin{aligned}\frac{dY_1}{dt} =& 2fk_I[I] + \overline{K}_{fm}[R^o][M] + \overline{K}_p[M][R^o] \\ & - (\overline{K}_t[R^o] + \overline{K}_{fm}[M])Y_1\end{aligned} \tag{C34}$$

$$\frac{dY_2}{dt} = 2fk_I[I] + \overline{K}_{fm}[R^o][M] + \overline{K}_p[M][2Y_1 + [R^o]] - (\overline{K}_t[R^o] + \overline{K}_{fm}[M])Y_2 \tag{C35}$$

$$\frac{dQ_0}{dt} = (\overline{K}_{td} + \frac{1}{2}\overline{K}_{tc})[R^o]^2 + \overline{K}_{fm}[M][R^o] \tag{C36}$$

$$\frac{dQ_1}{dt} = (\overline{K}_t[R^o] + \overline{K}_{fm}[M])Y_1 \tag{C37}$$

$$\frac{dQ_2}{dt} = (\overline{K}_t[R^o] + \overline{K}_{fm}[M])Y_2 + \overline{K}_{tc}Y_1^2 \tag{C38}$$

C.3 Case Study: Mathematical Modeling of Polymerization of Poly(AAm-*co*-AAc)

Table C1 shows the kinetics parameters for the simulation of poly(AAm-*co*-AAc) microstructure.

Table C1: AAm/AAc copolymerization simulation conditions

Parameters	Values
Feed composition ($f_{AAm,0}$)	0.7
Monomer concentration [M]	40 wt%
Initiator concentration [I]	0.001 mol.L^{-1}
r_{AAm} (pH $\leq$6)	2.2
r_{AAc} (pH $\leq$6)[190]	0.58

In industrial batch polymerization of flocculants (with poly(AAm-*co*-AAc) being the industry standard flocculant), often the heat out of the exothermic polymerization reaction is used to carry over the reaction to full conversion. As an example of the effect of operating parameters on final copolymer product, the model above was used to simulate two cases: I) Constant temperature

(isothermal conditions) and II) Varying temperature. In Case I, the temperature was set to 50°C, while in Case II the temperature started at 20°C and then (due to reaction heat) ramped up to 100°C at full monomer conversion.

Targeted properties (model outputs) of the simulation are:

- Polymerization rate (conversion)
- Evolution of average molecular weight with respect to conversion
- Molecular weight distribution of the final product (polymer produced at full conversion)
- Evolution of chemical (comonomer) composition with respect to conversion
- Bivariate distribution of molecular weight and chemical (comonomer) composition

Table C2 shows the rate coefficients used for the simulation of AAm/AAc copolymerization.

Table C2: AAm/AAc kinetics rate coefficients

Rate coefficients	Values
k_I	$9.24 \times 10^{14} e^{(-14915/T)}$[77]
k_{11}	$9.5 \times 10^{7} e^{(-2189/T)} e^{(-w_1(0.0016T+1.015))}$ [77]
k_{22}	$3.2 \times 10^{7} e^{(-1564/T)}(0.11 + 0.89 e^{-3w_2})$ [191]
k_{12}	k_{11}/r_1
k_{21}	k_{22}/r_2
k_{t11}	$2 \times 10^{10} e^{-((1991+1477w_1)/T)}$ [77]
k_{t22}	$9.8 \times 10^{11} e^{-1860/T}(1.56 - 1.77w_2^2) \times 30^{-0.44} \times 10^{-4.5 \times 0.16}$ [191]
k_{tc11}	k_{td11} (assumed)
k_{tc22}	k_{td22} (assumed)
$k_{tc12} = k_{tc21} = k_{td12} = k_{td21}$	$(k_{tc11} + k_{td22})/2$ (assumed)
k_{f11}	$k_{11} \times 0.00118 e^{-(1002/T)}$ [77]
$k_{f22} = k_{f12} = k_{f21}$	k_{f11} (assumed)

Solving the moments equations (Equation (C34) to Equation (C38)) using the given rate coefficients and the method of pseudo kinetic rate constants, we found the targeted outputs as shown in Figure C1 - Figure C8.

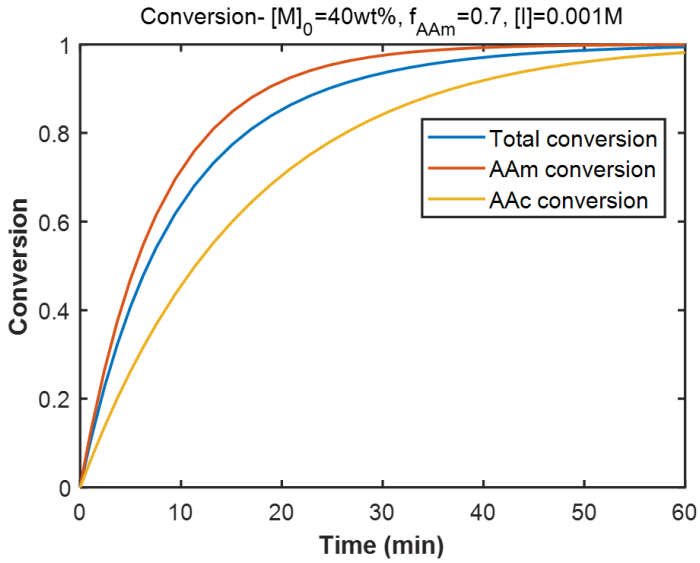

Figure C1: Monomers (total and individual) conversion versus time for the isothermal batch reactor. AAm is used up faster in the reactor.

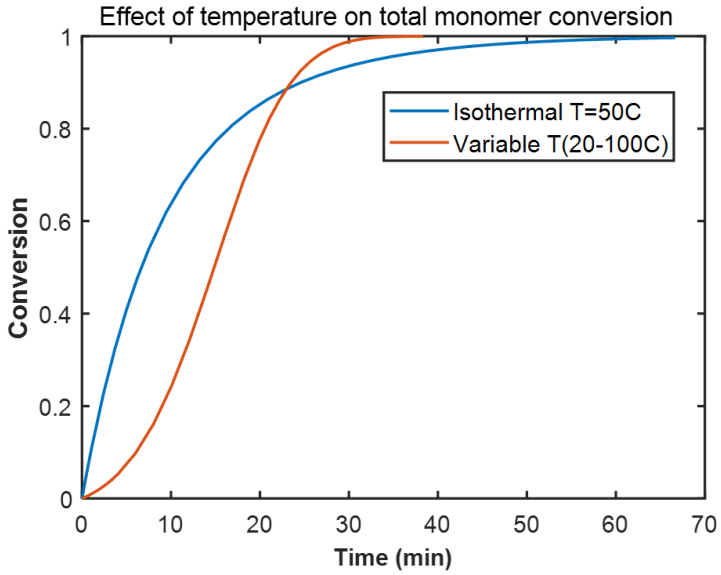

Figure C2: Total monomer conversion with respect to time comparing the effect of thermal condition of the reactor on the rate of polymerization.

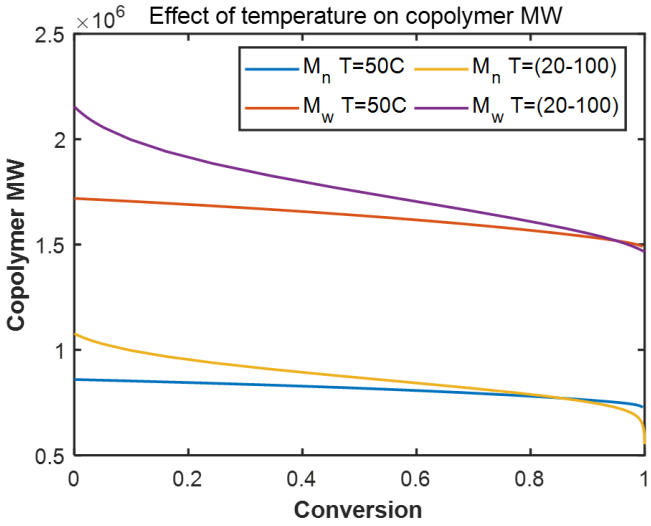

Figure C3: Evolution of the average molecular weight of the copolymer with conversion, comparing two cases of isothermal and non-isothermal conditions.

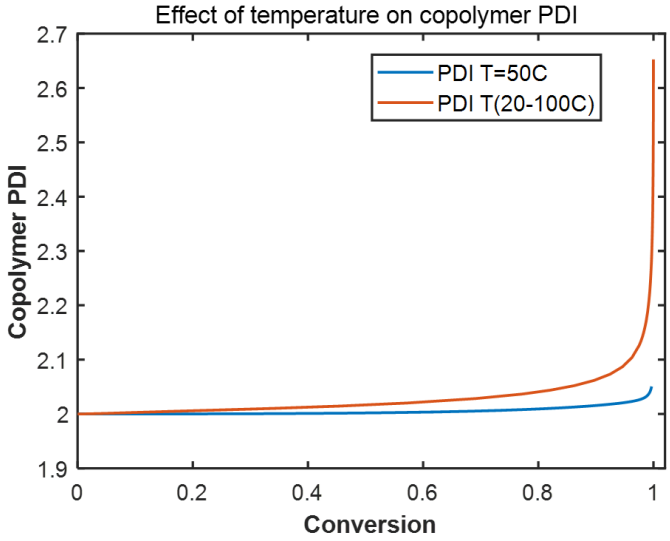

Figure C4: Evolution of polydispersity of the copolymer with conversion, comparing two cases of isothermal and non-isothermal conditions.

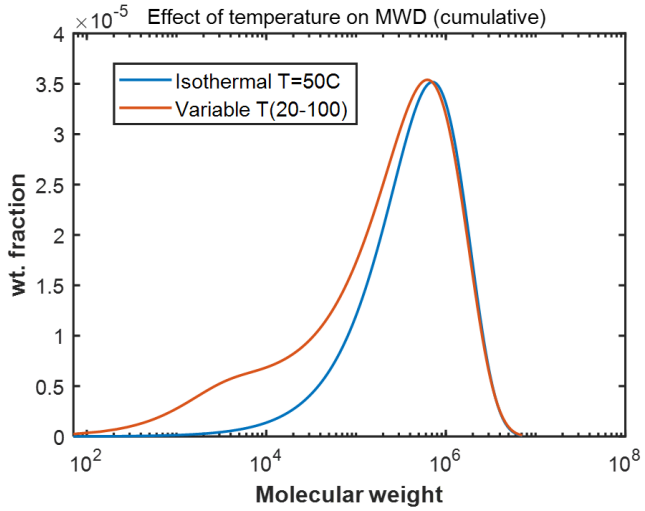

Figure C5: Molecular weight distribution of the copolymer at full conversion (final product), comparison two cases of isothermal and non-isothermal reactions.

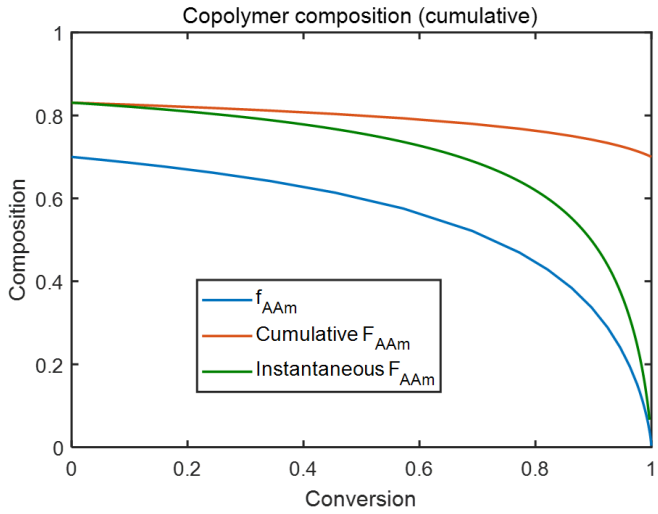

Figure C6: Composition drift in AAm and AAc batch polymerization reactor.

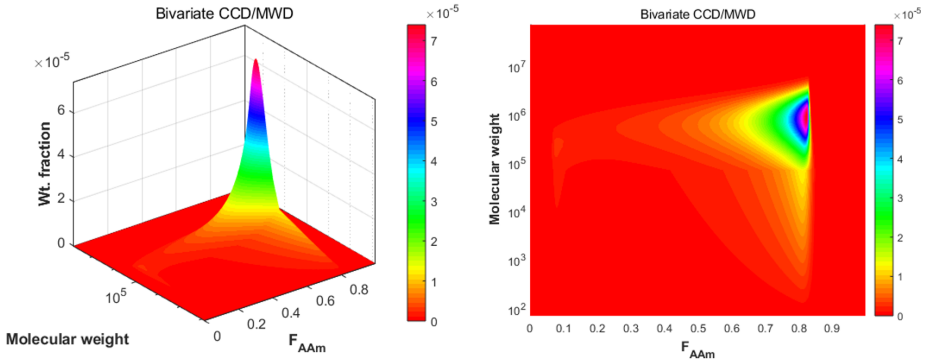

Figure C7: Bivariate chemical composition/molecular weight distribution of the copolymer at full conversion in isothermal condition. The left plot is surface plot and the right graph is top view contour plot.

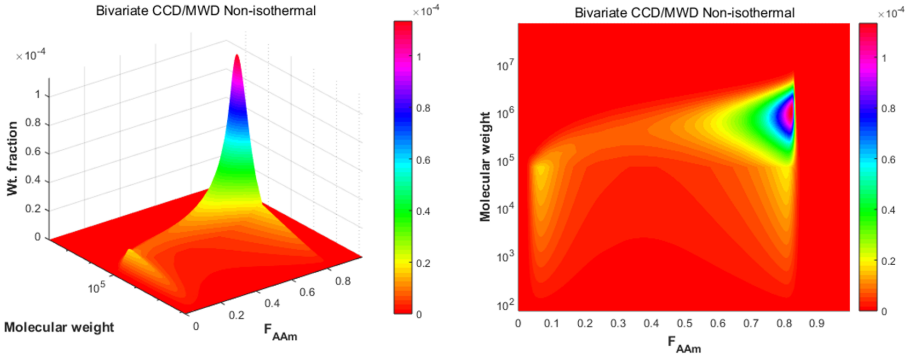

Figure C8: Bivariate chemical composition/molecular weight distribution of the copolymer at full conversion in non-isothermal condition. The left plot is surface plot and the right graph is top view contour plot.

Appendix D

Supplementary Information for Chapter 3

D.1 ANOVA tables

Table C1: ANOVA table- ISR

	Df	SS	MS	F	P	comment
$X_1(L)$	1	3.715	3.715	103.780	0.00002	significant
$X_1(Q)$	1	0.150	0.150	4.131	0.08161	significant
$X_2(L)$	1	0.230	0.230	6.404	0.03919	significant
$X_2(Q)$	1	0.000	0.000	0.0273	0.87354	
$X_3(L)$	1	0.151	0.151	4.220	0.07903	significant
$X_3(Q)$	1	0.001	0.001	0.045	0.83858	
X_1X_2	1	0.069	0.069	1.953	0.20498	
X_1X_3	1	0.021	0.021	5.777	0.04722	significant
X_2X_3	1	0.031	0.031	0.870	0.38208	
Error	7	0.250	0.250			
Total SS	16	4.716				

Table C2: ISR at different M_n and F_{AAm}

$\overline{F}_{AAm}$	M_n ($kg\ mol^{-1}$)	ISR ($cm\ h^{-1}$)	*dosage* (*kppm*)
0	90	6.22	8
0.24	94	10.10	8
0.24	200	15.56	8
0.5	185	19.65	8
0.5	291	26.50	8
0.5	1324	30.03	8
0.83	1050	42.57	8
0.83	1450	86.80	8
0.99	1819	148.51	8
$\overline{F}_{AAm}$ (p value)=0.021	M_n(p value)=0.092	$R^2 = 0.93$	

Table C3: ANOVA table- CST

	Df	SS	MS	F	P	comment
$X_1(L)$	1	0.061	0.061	84.567	0.00004	significant
$X_1(Q)$	1	0.034	0.034	47.559	0.00023	significant
$X_2(L)$	1	0.000	0.000	0.0277	0.87239	
$X_2(Q)$	1	0.000	0.000	0.837	0.39051	
$X_3(L)$	1	0.031	0.031	42.756	0.00032	significant
$X_3(Q)$	1	0.025	0.025	34.432	0.00069	significant
X_1X_2	1	0.000	0.000	1.077	0.33719	
X_1X_3	1	0.018	0.018	24.866	0.00158	significant
X_2X_3	1	0.000	0.000	0.146	0.71348	
Error	7	0.005	0.000			
Total SS	16	0.156				

Table C4: ANOVA table- turbidity of supernatant

	Df	SS	MS	F	P	comment
$X_1(L)$	1	6.717	6.717	34.136	0.00063	significant
$X_1(Q)$	1	2.870	2.870	14.584	0.00655	significant
$X_2(L)$	1	0.001	0.001	0.007	0.93362	
$X_2(Q)$	1	0.513	0.513	2.608	0.15030	
$X_3(L)$	1	1.670	1.670	8.489	0.02254	significant
$X_3(Q)$	1	2.749	2.749	13.972	0.0072	significant
X_1X_2	1	0.002	0.002	0.008	0.92823	
X_1X_3	1	3.927	3.927	19.958	0.00291	significant
X_2X_3	1	0.044	0.044	0.223	0.65081	
Error	7	1.377	0.196			
Total SS	16	19.632				

Table C5: ANOVA table- SRF

	Df	SS	MS	F	P	comment
$X_1(L)$	1	5.344	5.344	142.37	0.00000	significant
$X_1(Q)$	1	0.422	0.422	11.246	0.01219	significant
$X_2(L)$	1	0.004	0.004	0.113	0.74626	
$X_2(Q)$	1	0.001	0.001	0.022	0.88516	
$X_3(L)$	1	4.254	4.254	113.333	0.00001	significant
$X_3(Q)$	1	0.459	0.459	12.245	0.01000	significant
X_1X_2	1	0.010	0.010	0.287	0.60867	
X_1X_3	1	2.646	2.646	70.495	0.00007	significant
X_2X_3	1	0.020	0.020	0.554	0.48084	
Error	7	0.262	0.037			
Total SS	16	12.722				

D.2 Residual Plots

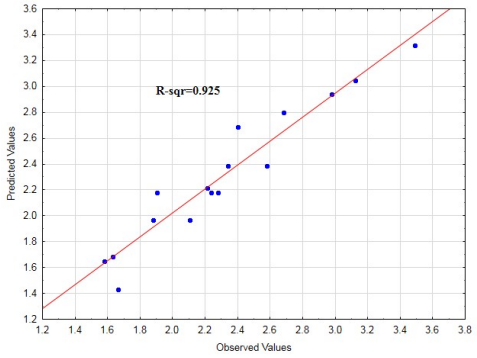

Figure C1a: Predicted vs. observed values for ISR model

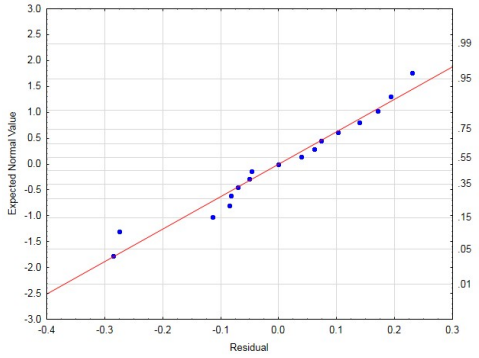

Figure C1b: Normal plot of ISR model

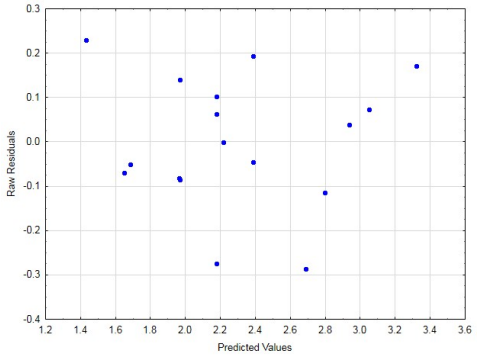

Figure C1c: Residuals vs. predicted values for ISR model

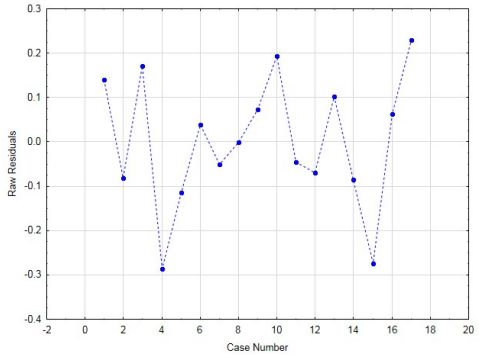

Figure C1d: Run sequence plot of ISR model

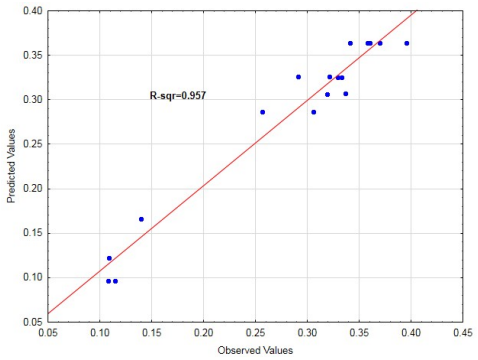

Figure C2a: Predicted vs. observed values for CST model

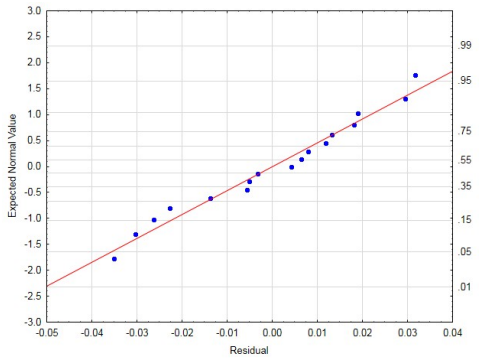

Figure C2b: Normal plot of CST model

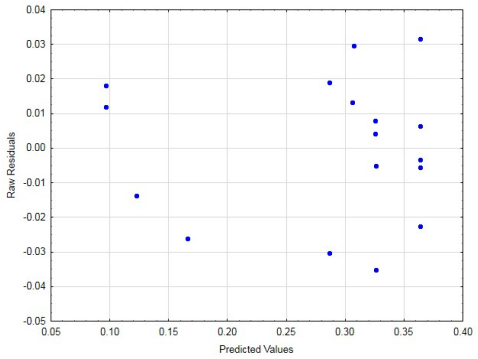

Figure C2c: Residuals vs. predicted values for CST model

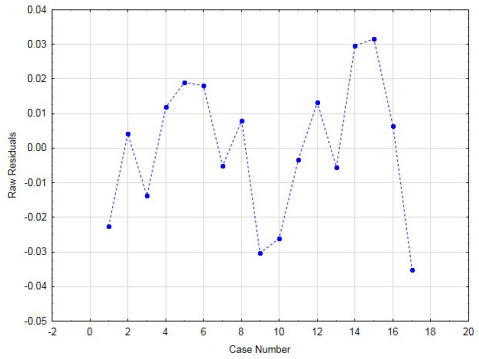

Figure C2d: Run sequence plot of CST model

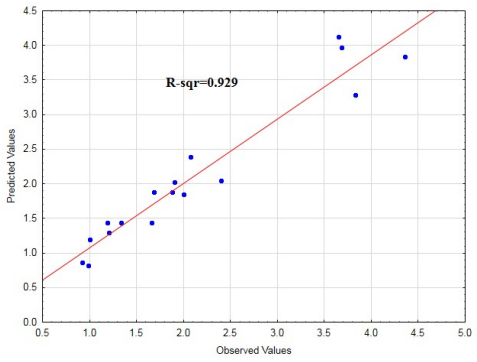

Figure C3a: Predicted vs. observed values for supernatant turbidity model

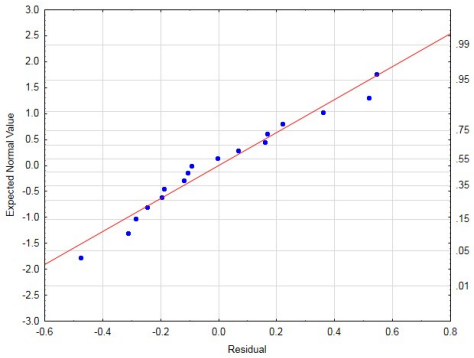

Figure C3b: Normal plot of supernatant turbidity model

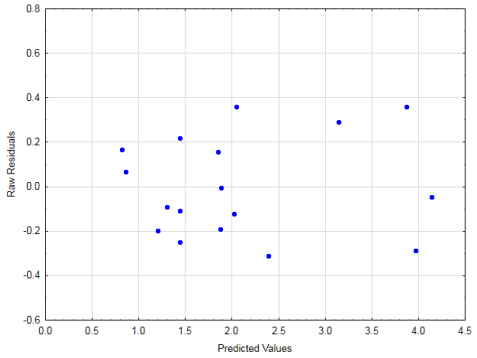

Figure C3c: Residuals vs. predicted values for supernatant turbidity model

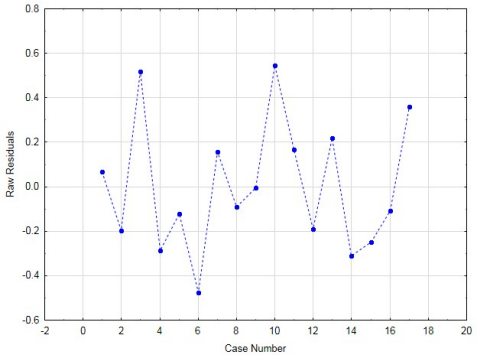

Figure C3d: Run sequence plot of supernatant turbidity model

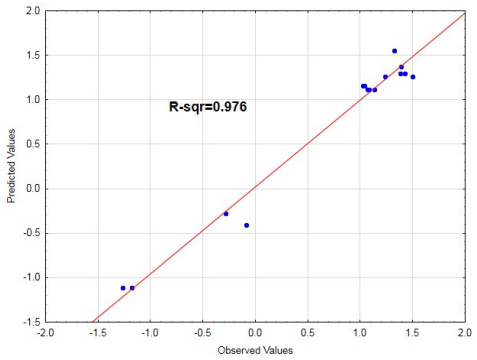

Figure C4a: Predicted vs. observed values for SRF model

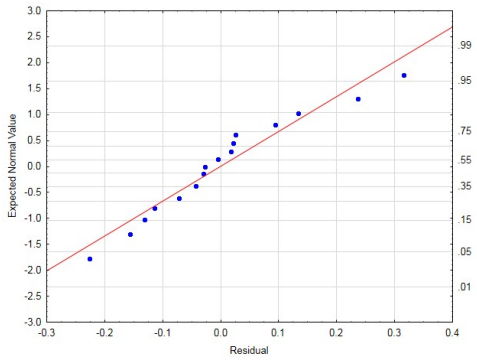

Figure C4b: Normal plot of SRF model

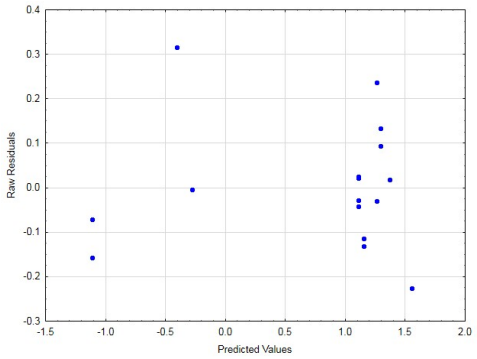

Figure C4c: Residuals vs. predicted values for SRF model

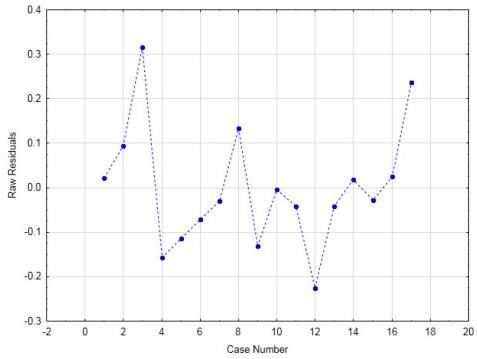

Figure C4d: Run sequence plot of SRF model

D.3 Estimation and Validation of AAm/DADMAC Copolymer Compositions

The following equations were used to estimate copolymer compositions at very low conversions, where the substantial composition drift in the comonomer mixture could be neglected,

$$\overline{F}_1 = \frac{f_{10} - f_1(1-x)}{x} \tag{C1}$$

$$\frac{df_1}{dx} = \frac{f_1 - F_1}{1-x} \tag{C2}$$

$$F_1 = \frac{r_1 f_1^2 + f_1 f_2}{r_1 f_1^2 + 2 f_1 f_2 + r_2 f_2^2} \tag{C3}$$

The following example calculations show how one can estimate $\overline{F}_1$ ($\overline{F}_{AAm}$), at a given conversion (x), as a function of initial feed composition f_{10} ($f_{AAm,0}$). Let r_1= 5.7, r_2= 0.03, and f_{10}= 0.4. If we substitute F_1 in Equation (C2) (Skeist equation) by F_1 from Equation (C3) (instantaneous Mayo-Lewis equation) and numerically solve it for f_1 and x, we get a solution as Figure C5. At 5% conversion f_1 is about 0.38 from Figure C5. Now, by substituting f_1, f_{10}, and x in Equation (C1) (a simple mass balance), we calculate $\overline{F}_1$ to be 0.78. If we do the same for other initial feed composition points, we get Figure C6 that correlates $\overline{F}_1$ as a function of initial feed composition after reaction has proceeded to only very low conversions (i.e. 5%).

The polymerization time needed for 5% conversion were estimated with Equation (C4),

$$Rp = -\frac{d[M]}{dt} = \frac{k_p}{k_t^{0.5}} (2 f k_I)^{0.5} [M]^{\alpha} \tag{C4}$$

where f is the fractional initiator efficiency (f$\approx$ 0.8), k_I is the initiator decomposition rate constant, 8.3×10^{-6} s^{-1}, and $\frac{k_p}{k_t^{0.5}}$ is the lump kinetic constant.

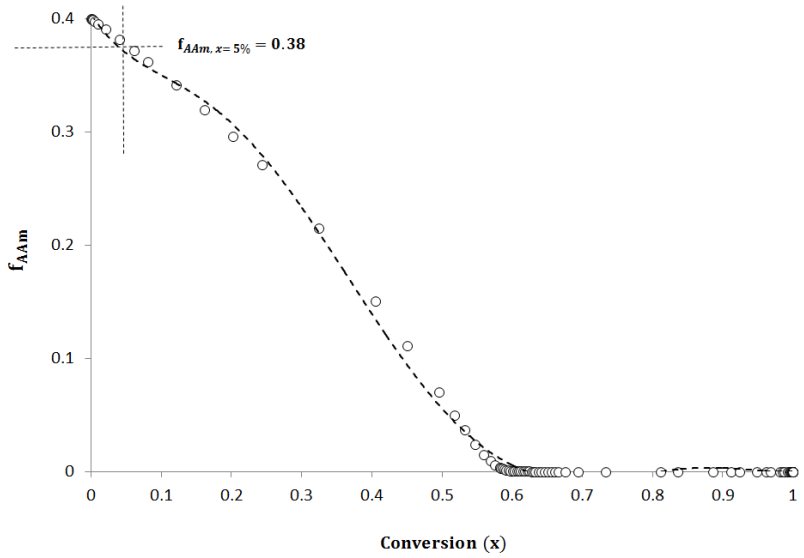

Figure C5: Instantaneous comonomer composition of acrylamide as a function of conversion at initial feed composition of 0.4

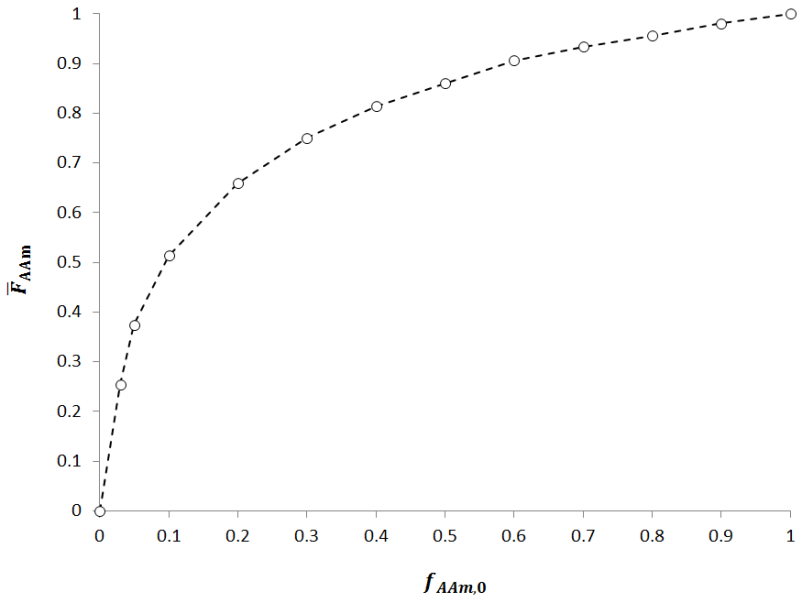

Figure C6: Cumulative copolymer composition of acrylamide after 5% conversion in the reaction as a fucntion of initial acrylamide composition in the comonomer feed

It is known that propagation of radical chains does not follow the classic first order kinetic for the aqueous system of AAm and DADMAC. The propagation rate coefficient changes as a function of monomer/comonomer ratio. The constant α in Equation (C4) shows this proportionality.

Figure C7 shows the lump rate constants, estimated from the kinetic data published in the work of Brand et al., as a function of initial mole fraction for polymerization conditions in this study.[74]

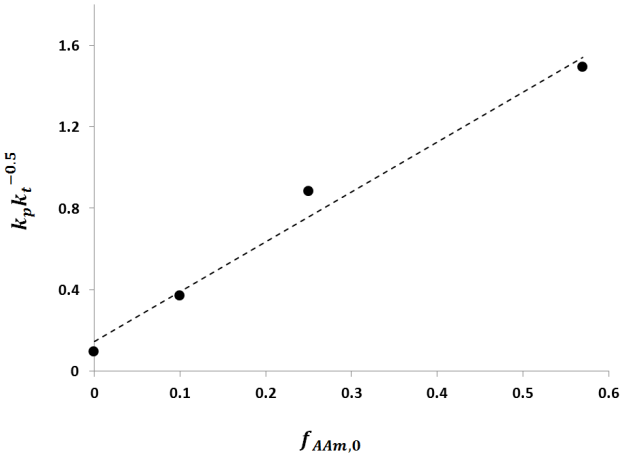

Figure C7: Lump rate constants for aqueous free radical copolymerization of AAm and DADMAC at 50 °C, 1.5 $mol\ L^{-1}$ as a function of initial molar composition of AAm in the feed, estimated from the data published in Brand et al.[74]

Following the the calculations described above, it is easy to find initial feed compositions needed to obtain copolymer compositions suggested by our experimental design for the flocculation. The copolymer compositions were validated using quantitative ^{1}HNMR. Table C6 summarizes these data points.

Table C6: $\overline{F}_{AAm}$ at different initial compositions obtained from the kinetic model versus NMR data

$f_{AAm,0}$	$\overline{F}_{AAm,model}$	$\overline{F}_{AAm,NMR}$
0.03	0.24	0.21
0.1	0.50	0.43
0.39	0.83	0.81
0.95	0.99	0.96

D.4 Estimation of AAm/VBTMAC Copolymer Composition and Reactivity Ratios

Poly(AAm-*co*-VBTMAC) composition was determined by the ratio the VBTMAC peaks to the polymer backbone peaks. VBTMAC repeat unit peaks appear at 6.6 - 7.5 ppm (aromatic H), 4.2 - 4.6 ppm (Ar-CH_2-N), and 2.6 - 3.3 ppm (-$N^+(CH_3)_3$). The polymer backbone peaks appear at 1.0 - 2.0 ppm (-CH_2-) and 2.0 - 2.5 ppm (-CHR-). Smaller peaks from 5.3 - 6.3 ppm, and at 7.5 ppm are signals from residual monomers. The composition of the copolymer was calculated from the area under the curve for the polymer backbone peaks. The area for each peak is normalized to the number of hydrogen atoms in the functional group. The sample spectra in Figure C8 corresponds to copolymers with 50%, 55%, and 65% acrylamide. As seen, by increase of the acrylamide content in the copolymer, the relative area of the VBTMAC peaks decreases compared to the polymer backbone. Equation (C5) calculates the copolymer

The supplementary information given in this appendix for estimation of copolymer composition and reactivity ratios for the system of AAm/VBTMAC is due to Mr. Daniel V. Dixon and will be published in his thesis

composition by averaging over three VBTMAC peaks to minimize integration error compared to using just one peak for the calculation.

$$\overline{F}_{AAm} = 1 - \frac{1/4A_e + 1/2A_f + 1/9A_g}{A_{abcd}} \tag{C5}$$

where A_e, A_f, A_g, A_{abcd} are areas under the curve for peaks e, f, g, and $abcd$, respectively.

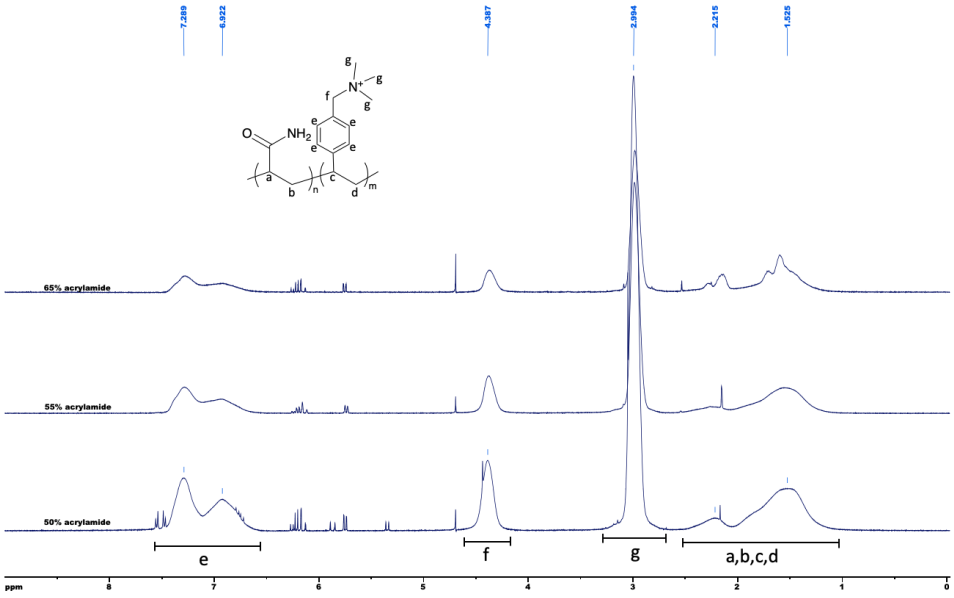

Figure C8: ^{1}HNMR sample spectra of AAm/VBTMAC copolymers. Peaks are labelled with the assigned functional group.

AAm/VBTMAC reactivity ratios were determined using kinetic data obtained from NMR experiments. This technique has been used on a number of copolymer systems including acrylamide, acrylic acid, methyl methacrylate, and diallyldimethylammonium chloride, and 2-(acryloyloxyethyl)trimethylammonium chloride monomers. [192, 101, 193, 194] The free radical polymerization of VBTMAC and AAm were performed in standard 5 mm NMR tubes in an Agilent 400 MHz spectrometer. Total monomer concentration of 0.25 mol.L^{-1} with varying ratios of VBTMAC to AAm were prepared with V-50 (0.0025 mol.L^{-1}) used as the initiator. The solution was prepared in D_2O and purged of air and backfilled with N_2 before being sealed in the NMR tube. NMR

tubes were refrigerated until the NMR spectrometer was ready. The NMR sample chamber in the spectrometer was heated to 50 °C with hot air flowing through the chamber. Once the temperature reached equilibrium, the sample was added and the spectrometer was tuned and shimmed at the reaction temperature. ^{1}HNMR spectra were collected every two minutes for two hours (60 spectra). A set of sample spectra for the copolymerization of VBTMAC and AAm is seen in Figure C9.

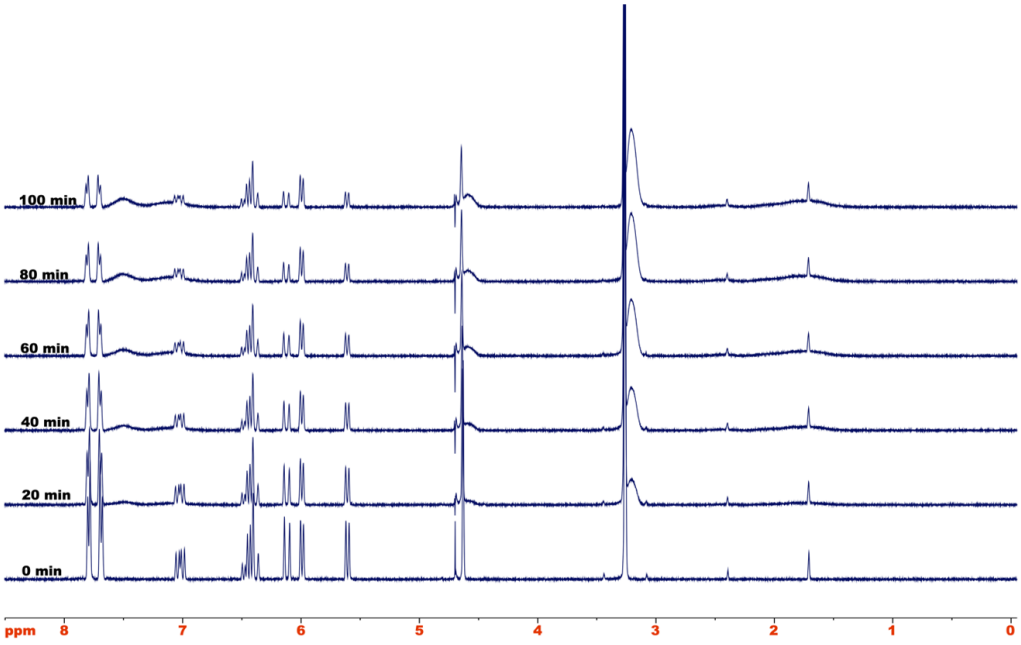

Figure C9: ^{1}HNMR spectra of the polymerization of AAm with VBTMAC over time. Vinyl hydrogen peaks between 5.5 ppm and 7.1 ppm decay over the course of the reaction. Broader polymer peaks begin to form over time.

Monomer concentration over time was calculated from the area under the vinyl hydrogen peaks. Conversion and the monomer molar fraction could be calculated from the concentration. Reactivity ratios for the copolymerization of AAm with VBTMAC were estimated from the comonomer fraction data using a non-linear parameter estimation technique along with direct numerical integration. Figure C10 depicts the change in fraction of acrylamide (f_{AAm}) as a function of conversion. The data was fitted with a model by simultaneously solving the Mayo-Lewis equation (3.3) with the material balance in the form

of Equation (3.2). Reactivity ratios were estimated using orthogonal distance regression and converged when $r_{AAm} = 0.46 \pm 0.03$ and $r_{VBTMAC} = 2.48 \pm 0.09$, where the errors are in 95% confidence intervals.

The reactivity ratios demonstrate that VBTMAC reacts faster than AAm. Similar results have been observed with water soluble ionic monomers when reacting with acrylamide.[193, 194]

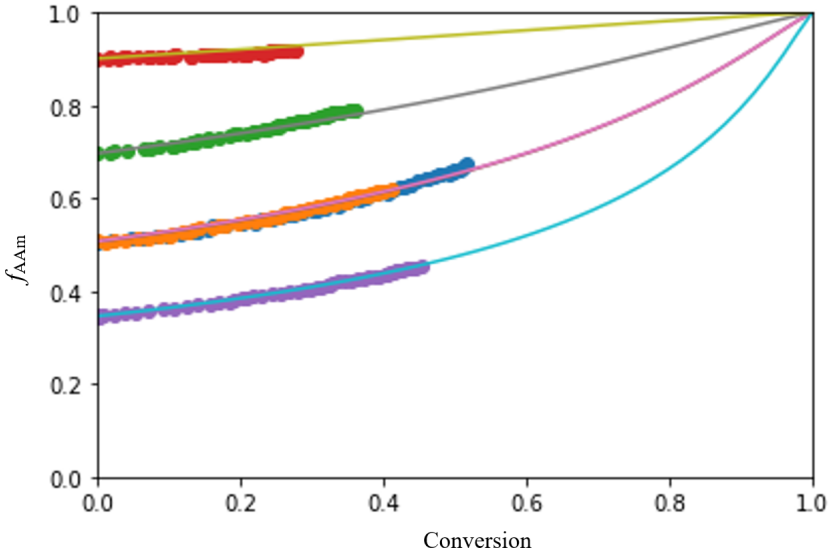

Figure C10: Acrylamide fraction (f_{AAm}) as a function of total conversion. Each color represents an independent reaction monitored by ^{1}HNMR. Solid lines shows the model fitted with reactivity ratios $r_{AAm} = 0.46$ and $r_{VBTMAC} = 2.48$.

The reactivity ratios were validated by experiments done at the bench scale. Samples from reactions were taken at low conversion (below 5%) to ensure no composition drift was occurring. Figure C11 is the Mayo-Lewis plot illustrating how the instantaneous copolymer composition depends on the monomer mole fraction. The composition of the synthesized copolymers was measured by NMR and the results agree with the reactivity ratios calculated from the NMR kinetic experiments.

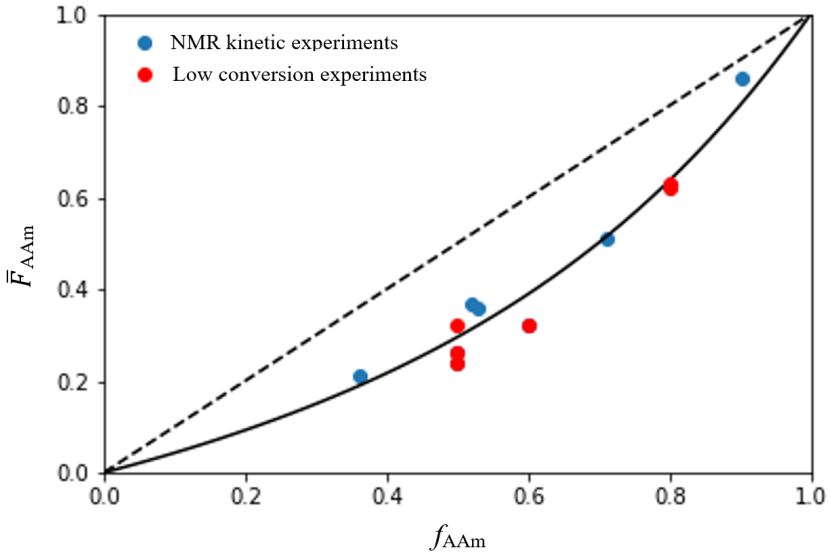

Figure C11: Mayo-Lewis plot of the instantaneous copolymer composition. Blue circles are data collected from NMR kinetic experiments, and red circles are from samples collected at low conversion